



Government of **Western Australia**
Department of **Mines, Industry Regulation and Safety**

RECORD 2018/3

REGOLITH CHEMISTRY OF THE NGURURRPA AREA, NORTHEASTERN WESTERN AUSTRALIA

by
PA Morris, N de Souza Kovacs, and AJ Scheib



Geological Survey of Western Australia

EXPLORATION
INCENTIVE
SHEME





Government of **Western Australia**
Department of **Mines, Industry Regulation and Safety**

RECORD 2018/3

REGOLITH CHEMISTRY OF THE NGURURRPA AREA, NORTHEASTERN WESTERN AUSTRALIA

by
PA Morris, N de Souza Kovacs, and AJ Scheib

PERTH 2018



**Geological Survey of
Western Australia**

MINISTER FOR MINES AND PETROLEUM
Hon Bill Johnston MLA

DIRECTOR GENERAL, DEPARTMENT OF MINES, INDUSTRY REGULATION AND SAFETY
David Smith

DIRECTOR, GEOSCIENCE AND RESOURCE STRATEGY
Jeff Haworth

REFERENCE

The recommended reference for this publication is:

Morris, PA, de Souza Kovacs, N and Scheib, AJ 2018, Regolith chemistry of the Ngururrpa area, northeastern Western Australia: Geological Survey of Western Australia, Record 2018/3, 118p.

ISBN 978-1-74168-806-1



Grid references in this publication refer to the Geocentric Datum of Australia 1994 (GDA94). Locations mentioned in the text are referenced using Map Grid Australia (MGA) coordinates, Zone 52. All locations are quoted to at least the nearest 100 m.

Disclaimer

This product was produced using information from various sources. The Department of Mines, Industry Regulation and Safety (DMIRS) and the State cannot guarantee the accuracy, currency or completeness of the information. Neither the department nor the State of Western Australia nor any employee or agent of the department shall be responsible or liable for any loss, damage or injury arising from the use of or reliance on any information, data or advice (including incomplete, out of date, incorrect, inaccurate or misleading information, data or advice) expressed or implied in, or coming from, this publication or incorporated into it by reference, by any person whosoever.

Published 2018 by the Geological Survey of Western Australia

This Record is published in digital format (PDF) and is available online at <www.dmp.wa.gov.au/GSWApublications>.



© State of Western Australia (Department of Mines, Industry Regulation and Safety) 2018

With the exception of the Western Australian Coat of Arms and other logos, and where otherwise noted, these data are provided under a Creative Commons Attribution 4.0 International Licence. (<http://creativecommons.org/licenses/by/4.0/legalcode>)

Further details of geological products and maps produced by the Geological Survey of Western Australia are available from:

Information Centre
Department of Mines, Industry Regulation and Safety
100 Plain Street
EAST PERTH WESTERN AUSTRALIA 6004
Telephone: +61 8 9222 3459 Facsimile: +61 8 9222 3444
www.dmp.wa.gov.au/GSWApublications

Cover image: Elongate salt lake on the Yilgarn Craton — part of the Moore–Monger paleovalley — here viewed from the top of Wownamina Hill, 20 km southeast of Yalgoo, Murchison Goldfields. Photograph by I Zibra, DMIRS

Contents

Abstract	1
Introduction	1
Location and access	1
Climate	1
Vegetation and soils	5
Geomorphology	5
Paleochannels and paleodrainage	5
Calcrete-filled paleovalleys	5
Magnetic-fill paleochannels	7
Bedrock geology	7
Arunta and Granites–Tanami Orogens, and Murraba Basin	7
Canning Basin	10
Faults	12
Bedrock lithology and chemistry	12
Regolith mapping	12
Distribution of regolith–landform units	16
Residual and relict regolith (<i>R</i>)	17
Regolith in areas of outcrop (<i>X</i>)	18
Transported regolith	18
Regolith thickness	18
Drilling	18
Passive seismic	18
Data acquisition	18
Data analysis	19
Results and data interpretation	19
Control sites — Point Moody well	19
Transect sites	20
Discussion	20
Regolith chemistry	23
Reconnaissance	23
Chemistry of reconnaissance samples	23
Variations with grain size	23
Variations with depth	23
Lag chemistry	23
Discussion	25
Fine-fraction regolith chemistry	25
Statistical treatment of regolith geochemical data	30
Precious metals (Ag, Au, Pd and Pt)	34
Chalcophile elements	34
Rare earth elements	37
Light rare earth elements (LREE; La–Eu)	37
Heavy rare earth elements (HREE: Gd–Yb, Y)	37
Transition elements	37
Lithophile elements	37
Major element oxides	41
Base metals	41
High field strength elements	42
Discussion	42
Bedrock control on regolith composition	42
Regolith–landform unit chemistry	43
Lag chemistry	46
Regolith chemistry along fault transects	46
Stansmore Fault traverses	50
SRT transect	50
SR transect	50
Regolith chemistry	52
Spinifex chemistry	52
Balgo Fault transect	53
SS transect	53
Controls on transect chemistry	53
Fault-controlled fluid flux and composition	54
Spinifex chemistry and plant metabolism	55
Relationship to mineralization	55
Ngurrupa project area — mineralization potential	56
Conclusion	59
Acknowledgements	59
References	60

Appendices*

- 1A. Site information for reconnaissance regolith samples
- 1B. Site observations for Ngururra regional regolith chemistry samples
2. Reconnaissance sample chemistry
- 3A. Sample preparation, analysis and discussion of QA/QC data
- 3B. Sampling form for Ngururra regolith sampling program
- 3C. Explanation of sampling form
- 4A. Regolith sample chemistry
- 4B. Lag sample chemistry
5. Spinifex chemistry
6. Samples with statistically anomalous element concentrations, detectable Ag and Pt, and Au

* Appendices accompany the PDF of this publication online as a digital resource

Figures

1.	Extent of the GSWA regional regolith chemistry programs	2
2.	Geology of Ngururra program area	3
3.	Views of landscape within the Ngururra program area	4
4.	Maps showing relative abundance of vegetation at regolith sample sites	6
5.	Distribution of paleovalleys in the Ngururra area	9
6.	Detailed image of ferruginous and calcrete paleochannel types	10
7.	Gravity and digital elevation images, and location of three sampling transects	11
8.	Simplified regolith–landform map of the Ngururra area	15
9.	Single-station passive seismic site locations, SR transect	20
10.	Stability plot for site SR3A passive seismic	20
11.	Comparison of passive seismic data at control sites	21
12.	H/V vs frequency (Hz) for passive seismic data	22
13.	Contoured passive seismic data (HVSr)	22
14.	Reconnaissance regolith sample site locations	24
15.	Reconnaissance site photographs	25
16.	Spider diagrams for reconnaissance regolith samples	26–30
17.	Variation in Cu and Fe in different grain-size fractions of regolith	30
18.	Screening results for Ngururra regolith samples	31
19.	Comparison of percent <50 µm fraction in parent and site duplicate samples	31

Figures B20–B27 are bubble plot figures — see below

28.	Spider diagram of median values of <50 µm fraction of regolith according to lithological unit	43
29.	Bivariate plot of Fe ₂ O ₃ vs SiO ₂ for analyses of lag samples	46
30.	Bivariate plots of selected elements vs Si/Fe for lag samples	50
31.	Simplified transect maps and sample locations on each transect	51
32.	Concentration of analytes in the fine fraction of regolith from sites on the SRT transect across the Stansmore Fault	51
33.	Concentration of analytes in the fine fraction of regolith from sites on the SR transect across the Stansmore Fault	52
34.	Concentration of analytes in spinifex from on the SR transect across the Stansmore Fault	53
35.	Concentration of analytes in the fine fraction of regolith from sites on the SS transect across the Balgo Fault	54
36.	Chondrite-normalized REE chemistry of host and mineralized rocks from various SEDEX deposits compared to Ngururra transect data	57
37.	Zinc (ppm) in the fine fraction of regolith in relation to known and potential areas of SEDEX mineralization	58

Bubble plot figures

B20.	Bubble plots for Ag, Au and Pt in the fine fraction of regolith	65
B21.	Bubble plots for As, Bi, Cd, Mo, S, Sb, Te and W in the fine fraction of regolith	68
B22.	Bubble plots for La, Ce, Sm, Nd, Eu, Gd, Dy, Er, Yb and Y in the fine fraction of regolith	76
B23.	Bubble plots for Co, Cr, Ni, Sc and V in the fine fraction of regolith	86
B24.	Bubble plots for Ba, Cs, Be, Ga, Hg, In, Li, Rb, Sn, Sr, Th, Tl and U in the fine fraction of regolith	91
B25.	Bubble plots for Al ₂ O ₃ , Fe ₂ O ₃ , MgO, Mn, CaO, Na ₂ O, K ₂ O and P ₂ O ₅ in the fine fraction of regolith	104
B26.	Bubble plots for Cu, Pb and Zn in the fine fraction of regolith	112
B27.	Bubble plots for TiO ₂ , Nb, Hf and Zr in the fine fraction of regolith	115

Tables

1.	Lithostratigraphy and number of regolith samples per lithological unit	8
2.	Whole-rock chemistry of bedrock samples	13
3.	Summary of regolith–landform units for the Ngururrpa area	16
4.	Tromino passive seismic data	19
5.	Fine-fraction regolith geochemistry statistics	32
6.	Statistics for regolith chemistry according to lithological unit	35
7.	Statistics of regolith fine-fraction geochemistry by primary regolith–landform code	39
8.	Results of statistical comparison using the Mann–Whitney U test, exposed regime and eolian regolith	44
9.	Results of statistical comparison using the Mann–Whitney U test, lacustrine and eolian regolith	47
10.	Statistics for analyses of lag	48
11.	Ionic charge (Z), ionic radius (r) and ionic potential (Z/r) for selected elements	55

Plate

1. Interpreted regolith–landform geology of the Ngururrpa area, northeastern Western Australia

Regolith chemistry of the Ngururrpa area, northeastern Western Australia

by

PA Morris, N de Souza Kovacs, and AJ Scheib

Abstract

The silt and clay fraction of 637 regolith samples collected from the Ngururrpa area of northeastern Western Australia has been analysed for 63 elements. The Ngururrpa area, which includes parts of the Proterozoic Granites–Tanami and west Arunta Orogens, the Murraba Basin, and the Paleozoic to Mesozoic Canning Basin, is largely covered by sandplain with less than 14% outcrop, which is dominated by quartz-rich siliciclastic sedimentary rocks. Element variations and statistical analysis show that bedrock control on regolith chemistry is limited to a few units in the Canning Basin. The most marked contrast in chemistry is shown by regolith from lacustrine areas, sandplain, and ferruginized sheetwash. Higher concentrations of Au in the fine fraction (reaching a maximum of 63 ppb) are located on or near to the Granites–Tanami Orogen in the north of the project area. Regolith fine-fraction and spinifex chemistry have been assessed to determine if two regional-scale faults acted as fluid conduits. One fault is shown to be a fluid conduit to buried sediment-hosted exhalative (SEDEX)-style mineralization. This is consistent with the higher Zn content of regolith in an area of bedrock that is being actively explored adjacent to the Ngururrpa area for exhalative-style base metal mineralization.

KEYWORDS: chemical analysis, fluid flow, geochemistry, mapping, mineralization, rare earth elements, regolith

Introduction

In areas of extensive regolith cover, regional-scale geochemistry programs, where samples are collected at densities between 0.01 and 0.1/km² (Salminen, 2011), provide valuable data that can be used to map underlying bedrock and bedrock-hosted mineralization (Morris and Verren, 2001; Morris, 2013). To promote mineral exploration, the Geological Survey of Western Australia's (GSWA) regional regolith geochemistry programs (Fig. 1) have covered a variety of terrains including cratons, craton margins, and intracratonic basins (Kojan and Faulkner, 1994; Morris et al., 1997, 2000; Sanders and McGuinness, 2000; Morris, 2013; Scheib, 2014a; Morris et al., 2015, 2016; Scheib et al., 2016a). This Record extends the intracratonic coverage to regolith over Proterozoic to Paleozoic sedimentary rocks of the Murraba and Canning Basins in the Ngururrpa area of northeastern Western Australia (Figs 1, 2).

The Ngururrpa program area lies directly north of GSWA's west Arunta gravity and regolith geochemistry program (GSWA, 2008; Fig. 1). The results of this program created an increased level of mineral exploration activity, leading to the discovery of several Cu–Au, uranium, base metal and diamond prospects. This prompted the traditional owners of Ngururrpa country (Parna Ngururrpa) to approach GSWA in 2013 to carry out a similar program on their country. Following consultation and on-country heritage assessment in 2013, gravity measurements were made at 4964 stations (2.5 km grid) in May 2014, followed by collection of regolith samples from 637 of the gravity sites in September 2015 (Fig. 2).

Location and access

Most of the Ngururrpa program area is located on LUCAS (SF 52-2) and STANSMORE (SF 52-6) (Fig. 2), but also takes in parts of CORNISH (SF 52-1), HELENA (SF 52-5), WILSON (SF 52-9), and WEBB (SF 52-10) 1:250 000-scale Geological Series map sheets. The northern boundary of the Ngururrpa program area is approximately 250 km south of Halls Creek, and 25 km south of Balgo (Wirrimanu). Access to the program area is via an unsealed road south from the Great Northern Highway to Balgo, then a poorly formed track which bisects the program area, continuing south to Kiwirrkurra. Within the program area, ground access is difficult off this track due to extensive sand cover, and the development of eolian dunes and salt lakes (Fig. 3). Tracks cut for acquisition of seismic data over 40 years ago are visible on imagery (e.g. Google Earth), but are both difficult to identify on the ground and to navigate due to sand drift and revegetation. Aboriginal communities at Yagga Yagga, Yarramurrul, Bibarrd and Lamanbandah (Fig. 2) have been abandoned. During the sampling program, GSWA staff were located at Yagga Yagga, which provided a central location for helicopter-supported operations.

Climate

Climate data are not available for the program area, but Bureau of Meteorology (www.bom.gov.au) records spanning more than 80 years are available for Balgo, approximately 75 km north of Yagga Yagga.

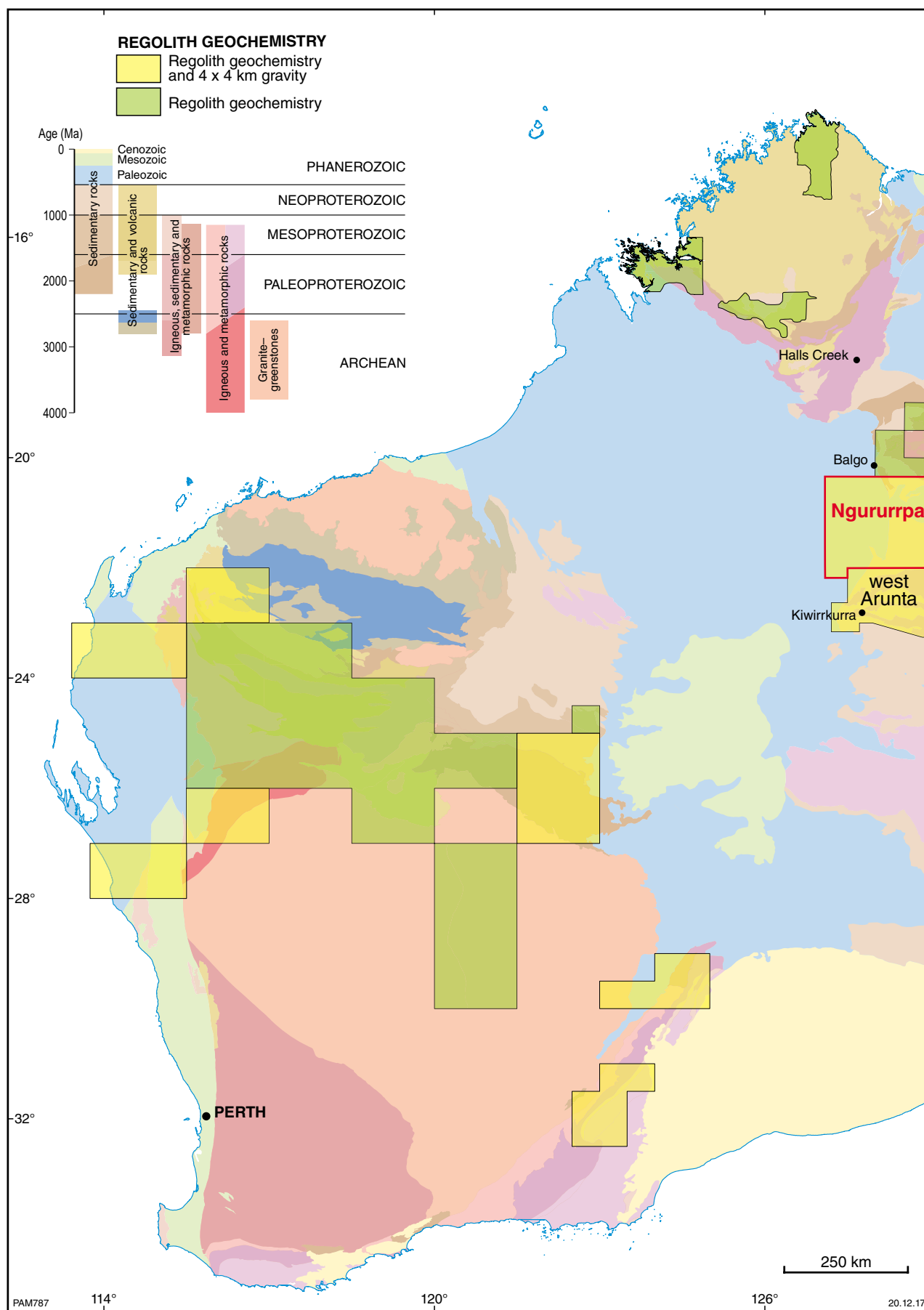


Figure 1. Extent of Geological Survey of Western Australia's regional regolith chemistry programs shown in relation to 1:10 000 000 tectonic subdivisions (Martin et al., 2016)

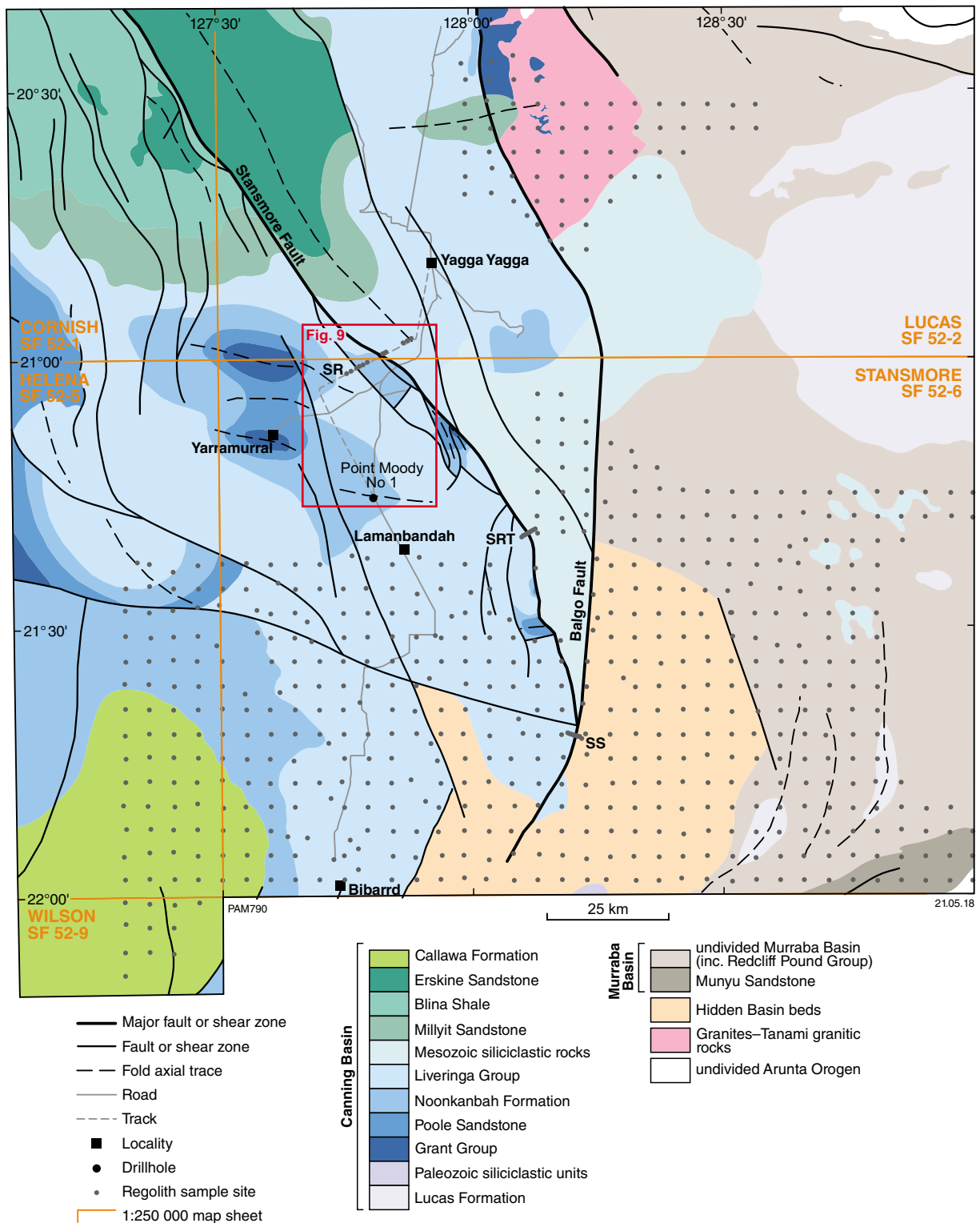


Figure 2. Ngururupa program area, showing interpreted 1:500 000-scale bedrock geology and structures (GSWA, 2016), location of the SR, SRT and SS sample transects (Fig. 31), regolith sample sites, and localities discussed in the text

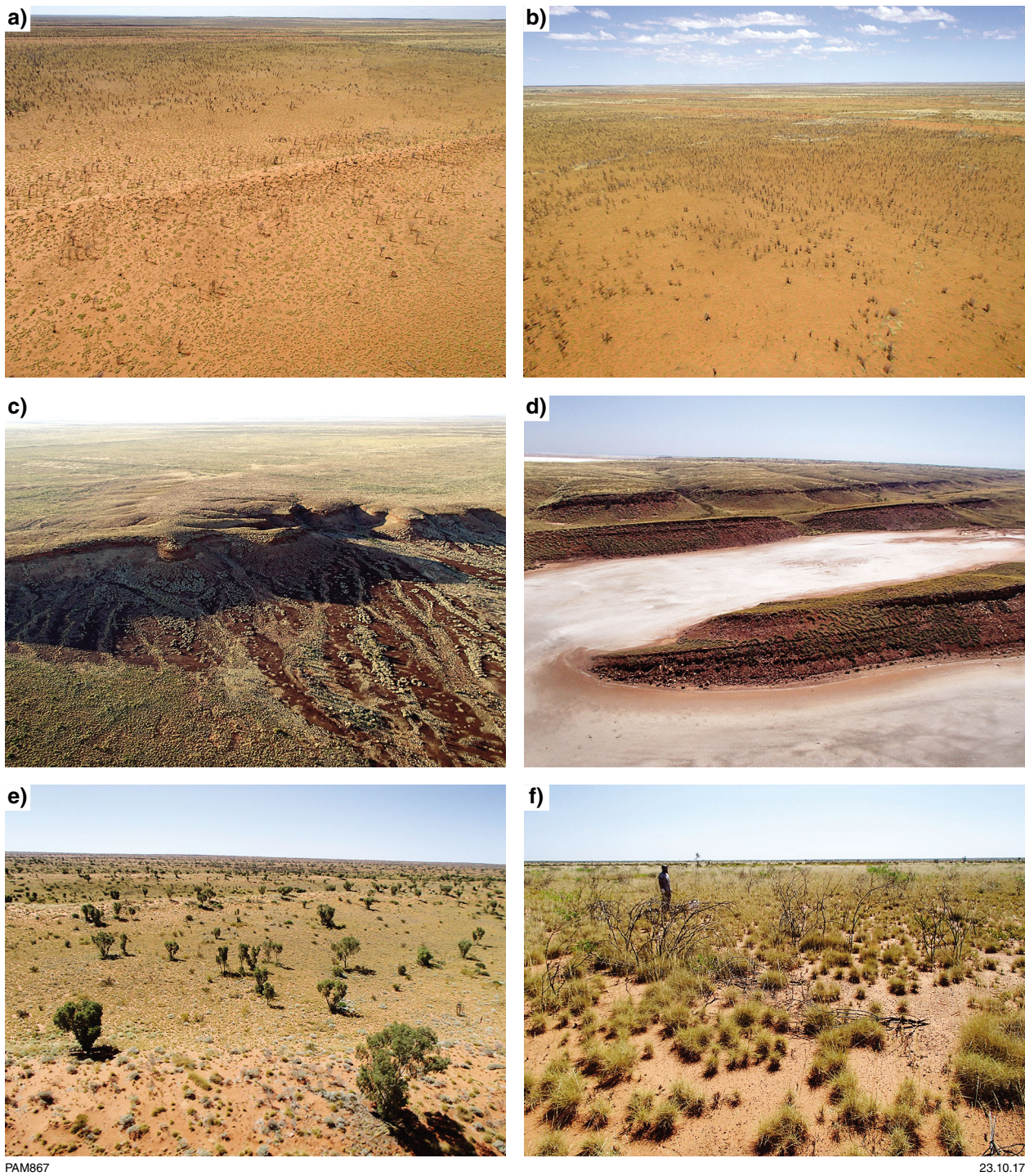


Figure 3. Views of landscape within the Ngururrpa program area: a), b) sandplain with elongate dunes typical of the Ngururrpa program area; c) Canning Basin sedimentary rocks in the Stansmore Range; d) shallow-dipping Murraba Basin sedimentary rocks and salt lakes; e) spinifex cover on sandplain, with less extensive cover on sand dunes (foreground); f) spinifex cover and patches of ferruginous lag on sandplain

The Ngururrpa area is typical of the northern part of the State, characterized by warm to hot and wet summers, and dry and cooler winters. From September to April, the mean maximum monthly temperature exceeds 30°C, with lowest temperatures experienced in June and July, when average monthly temperatures are near 12°C. The annual rainfall is 357 mm, with most precipitation from December to March (>55 mm/month). An average of 3 mm of rain per month is typically recorded for August and September, the time when this sampling program was conducted.

Vegetation and soils

The eastern part of the program area, a part of Beard and Webb's (1974) Great Sandy Desert, has been classified as grasslands, and subdivided into closed grassland communities, and steppe, or open grassland communities. The distinction between the two is based on available moisture, with steppe associations corresponding to areas of lower rainfall. The Ngururrpa program area includes two steppe associations, either mixed shrub steppe on sandplains, or mixed shrub steppe between sand dunes. The vegetation of both associations are similar. Soft spinifex (*Triodia pungens*) is accompanied by wattles (e.g. *Acacia pachycarpa*, *Acacia impressa*), and grevilleas (e.g. *Grevillea wickhamii*, *Grevillea refracta*). Eucalypts are restricted to drainages. Where sand is thicker, such as in areas of mixed shrub steppe between sand dunes, the feather-top spinifex *Plectrachne schinzii* is more common than *Triodia*. Thus, species distribution is in part controlled by regolith composition and thickness. Salt lakes are surrounded by halophytes, including samphire, with salt bush in less saline areas.

During the sampling of regolith, information was recorded at each site on the relative abundance of four vegetation types (spinifex, shrubs, grass, trees). At 93% of sites where data were recorded (630 sites), spinifex is the most common vegetation type (Fig. 4a), and is the only vegetation type recorded at 34 sites. The second most common vegetation type is shrubs (61% of sites; Fig. 4b), and the third most common type of vegetation is trees at 33% of sites (Fig. 4c). These data show that the most common association is spinifex and shrubs, with less common trees and minor grass (not shown). In terms of spatial distribution, the highest concentration of sites where shrubs predominate over spinifex is in the southeast of the program area, with trees more common at sites over the western part of the program area. Thus, there is evidence for some lithological control on vegetation distribution (Fig. 4d).

According to Schoknecht and Pathan (2013), there is a limited range of soil types in the Greater Sandy Desert area. Most common are deep, red, sandy and sandy-earth soils, with less common, highly saline soil and commonly waterlogged soil in and around salt lakes. The deep, red, sandy soils, typical of the arid interior of Western Australia, consist of Fe-stained sand commonly underlain by ferruginous gravel. In parts of the program area, these gravelly layers are exposed as ferricrete. Salt lake soils are commonly water saturated, saline, evaporate rich and locally calcareous. Patches of calcrete are located in low-lying areas between sand dunes. In these areas, carbonate fragments are distributed throughout the regolith.

Geomorphology

The landscape in the Ngururrpa area is flat, with variably weathered, low-lying rock outcrops, and extensive eolian dune fields and sandplain (Fig. 3). The patchy development of ferruginous lag, lateritic residuum, and variably ferruginized lithic fragments at the surface indicates that in some areas, sandplain forms a thin veneer on weathered bedrock, which could therefore have some influence on the composition of regolith nearby (e.g. Fig. 3f). This is consistent with Veevers and Wells (1961), who have argued that although most of the sand is eolian, it is of local origin. Sand dunes, which show a dominant east–west orientation, attain heights of 15 m and can extend over tens of kilometres (Fig. 3a,b,e). The spacing of dunes varies from a few tens of metres to several hundred metres. Prominent saline lakes (Lakes White, Wills and Hazlett) are located in the eastern part of the program area (Fig. 3d), although smaller, unnamed salt lakes are found throughout the program area. Streams draining off areas of outcrop are short, and drainage channels do not extend into the adjacent sandplain (Fig. 3c). Contemporary drainage, where preserved, drains internally into salt lakes and claypans.

One of the most prominent topographic features in the program area is the Stansmore Range, a west-dipping succession of sandstone and siltstone cuestas, which reach heights of up to 510 m above sea level (ASL) and 80 m above the surrounding sandplain (Fig. 3c).

Paleochannels and paleodrainage

Wilford (2005) described a paleovalley network in the Granites–Tanami region as remnants of a river system that developed in a wetter Paleocene to Early Miocene climate. These rivers are now represented by calcrete-filled valleys in the underlying ferricrete-capped and weathered Proterozoic rocks (Figs 5, 6). Some paleovalleys are preserved beneath the early Cambrian Antrim Plateau Volcanics (Magee, 2009). A shallower, less extensive paleovalley succession is identified by material showing a stronger magnetic response (Fig. 6).

Calcrete-filled paleovalleys

These broad paleovalleys are filled with up to 85 m of unconsolidated gypsiferous and calcareous fluvial and lacustrine sediments composed of silt and clay, intercalated sand and gravel, and lenses of calcrete up to 15 m thick (Blake, 1974; Magee, 2009). Groundwater calcrete occupies the central part of the paleovalleys. Replacement of calcrete by opaline and chalcedonic silcrete is common (Magee, 2009). The paleovalleys make up a network that drained into Lake Mackay (Magee, 2009; English, 2016; Fig. 5), now shown as a series of saline lakes and clay pans.

The most conspicuous paleovalley trends southwest from the Granites–Tanami Orogen, across the Canning and Murraba Basins (see Fig. 2), eventually draining into Lake Mackay (paleovalley 1 in Fig. 5). An inferred paleovalley system also drains the Granites–Tanami area north of Lake McKay (paleovalley 4, Fig. 5) This system contains smaller paleochannels filled with more magnetic material bordering its northern margins, but no calcrete at the surface. The second largest paleovalley system (paleovalley 2, Fig. 5)

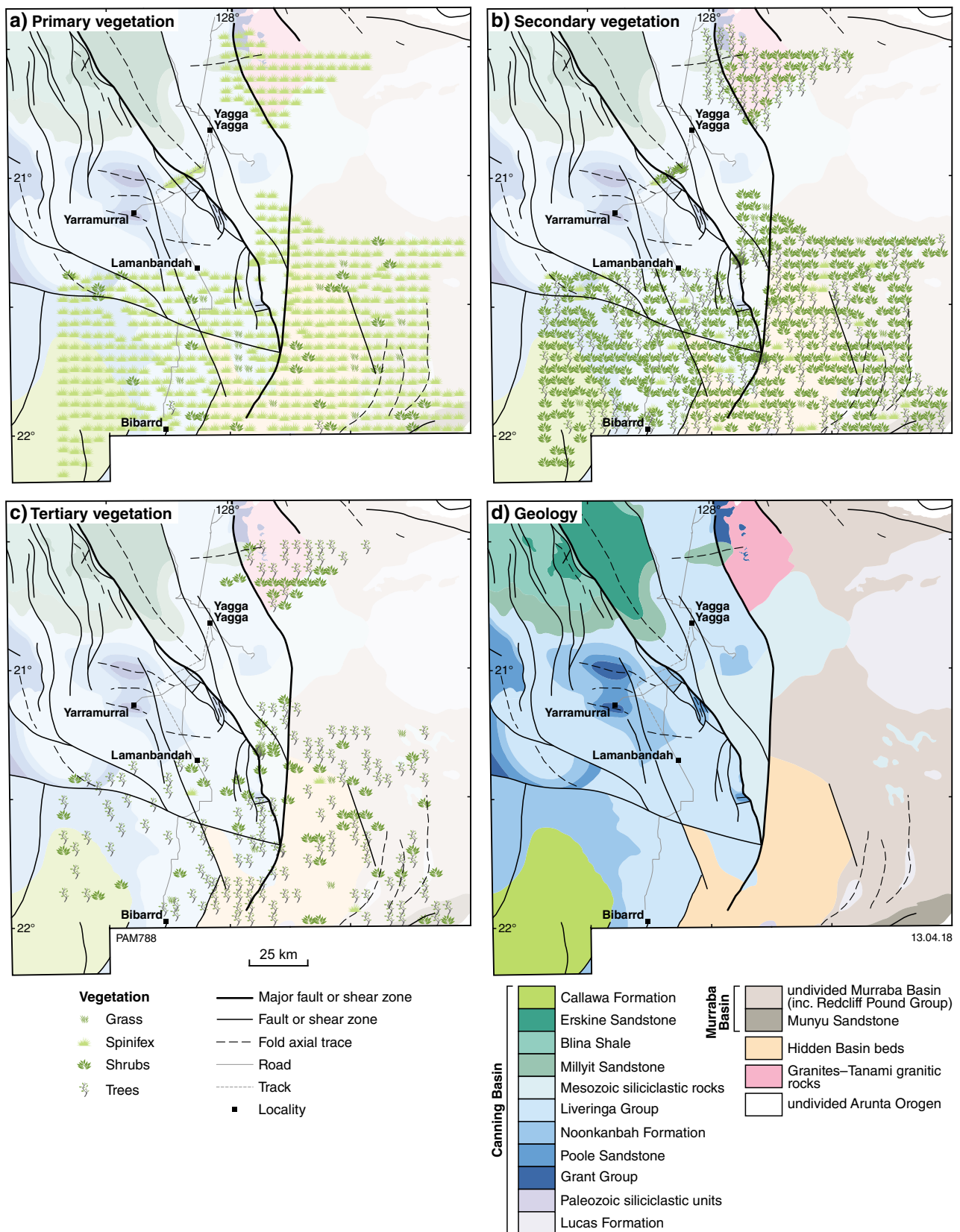


Figure 4. Relative abundance of vegetation at 630 regolith sample sites: a) primary vegetation type; b) secondary vegetation type; c) third most common vegetation type; d) interpreted 1:500 000-scale bedrock geology as a reference for Figures a–c

extends from the northwest over the Canning Basin, along the western side of the Stansmore Range to join up with paleovalley system 1. A less extensive paleovalley system (paleovalley 3, Fig. 5) is located on LUCAS. Stratigraphic drilling (Blake, 1974) shows that paleochannel 3 is >90 m deep in drillhole BMR Lucas 36 (Fig. 5). These paleochannel sediments, which overlie 70 m of mottled grey weathered limestone, consist of 6–24 m of eolian sand overlying 12–15 m of calcrete, and up to 85 m of gypsiferous and calcareous clay with localized dark chert lenses. Potable water was encountered between 14 and 16.5 m in drillholes BMR Lucas 8 and 31, below four metres of calcrete and 10 m of sand.

Magnetic-fill paleochannels

A shallow, dendritic paleochannel network consisting of narrow channels filled with ferruginous magnetic material is visible on a magnetic reduced-to-pole (RTP 1VD) image, where they appear as tributaries of calcrete-filled paleovalleys (Fig. 6). Their aeromagnetic response can be attributed to a high content of maghemite-rich gravel. These paleochannels are present throughout the Ngururupa area, but are especially prominent near the Stansmore Range (Fig. 6). Similar paleochannels described from the Yilgarn Craton are tributaries of the main trunks of paleodrainages. They contain a basal fluvial sand unit overlain by ferruginous gravel, and fragments of ferruginous duricrust probably derived from the weathering and erosion of duricrust and bedrock (Anand and de Broekert, 2005). In addition to aeromagnetic data, the extent of these types of paleochannels can be traced using a variety of imagery. They are evident due to a moderate to high gamma-ray radiometric response for Th and U, indicative of relatively high concentrations of residual minerals. The Advanced Spaceborne Thermal Emission and Reflection Radiometer (ASTER) ferric oxide content image indicates the relative amounts of hematite and magnetite in these channels, whereas on the Landsat AGSO ratio image, paleochannels at the surface appear bright yellow, reflecting higher contents of clay and iron-rich minerals. To be visible in the aeromagnetic images, the maghemite-rich gravel lenses in paleochannels have to be at least 0.4 – 1 m thick at depths between 1.5 and 4.5 m (Mackey et al., 2000; Anand, 2005). In the Stansmore Range area, the surface paleochannels and surrounding ferruginous duricrust are eroding to form Fe-rich sheetwash fans containing magnetic lag, as discussed below.

Bedrock geology

The first comprehensive discussions of the geology of Lucas and Stansmore were provided by Crowe and Muhling (1977) and Blake and Yeates (1976), respectively. A subsequent discussion of the area by Blake et al. (1979) extended over both Western Australia and the Northern Territory, whereas Ahmad (2013) provided a more detailed discussion of the stratigraphy in the Northern Territory. Joly et al. (2013) have discussed the mineralization potential of the west Arunta Orogen, to the south of the Ngururupa program area on WEBB. Stratigraphic revision of parts of the Murraba Basin has been discussed by Haines and Allen (2016, 2017).

Several factors complicate an understanding of bedrock geology of both the Murraba and Canning Basins. Both successions are dominated by patchy and discontinuous outcrops of gently dipping, quartz-rich, siliciclastic sedimentary rocks, with few distinctive marker horizons, limited geochronological data, and rapid lateral facies changes (Yeates et al., 1975; Blake and Yeates, 1976; Crowe and Muhling, 1977; Mory, 2010). The lithostratigraphy of the Canning Basin succession is better understood due to the availability of drillhole data related to petroleum and, less commonly, mineral exploration, more lithological diversity, and better age control afforded by faunal content.

Arunta and Granites–Tanami Orogens, and Murraba Basin

The oldest rocks in the Ngururupa program area form part of the west Arunta Orogen in the south, and the Granites–Tanami Orogen in the north (Fig. 2; Table 1). Metamorphosed siliciclastic and granitic rocks of the west Arunta Orogen are exposed on the northern part of WEBB. They include metasedimentary rocks of the Lander Rock Formation, which contain zircons indicating a maximum depositional age of 1840–1835 Ma (Scrimgeour, 2006). This unit is intruded by 1773 ± 6 Ma granitic rocks (Kirkland et al., 2009c). The overlying Lake McKay Quartzite contains zircons indicating a maximum depositional age of 1750 ± 19 Ma (Kirkland et al., 2009a), whereas the unconformably overlying Munyu Sandstone has a maximum depositional age of 1155 ± 14 Ma (Kirkland et al., 2009b).

Biotite monzogranite of the Granites–Tanami Orogen, which corresponds to the Lewis Granite of Crowe and Muhling (1977), has a U–Pb zircon age of 1825–1719 Ma (Bagas et al., 2010). Granitic rocks intrude sedimentary rocks of the Killi Killi Formation on LUCAS (Crowe and Muhling (1977). Bagas et al. (2009) reported a U–Pb zircon maximum depositional age of 1864 ± 6 Ma for the Killi Killi Formation. The Redcliff Pound Group (Crowe and Muhling, 1977; Blake and Yeates, 1976) to the east of the program area is unconformable on granitic rocks and the Killi Killi Formation.

Crowe and Muhling (1977) and Blake and Yeates (1976) identified the Munyu Sandstone, Lewis Range Sandstone and Muriel Range Sandstone as three stratigraphically equivalent units at the base of the Redcliff Pound Group. The remainder of the Redcliff Pound Group was made up of the overlying Murraba Formation and the Erica Sandstone. A Neoproterozoic age for the Redcliff Pound Group was assigned by Blake et al. (1979) based on correlation with lithologically similar units in the Amadeus Basin, such as the Heavitree Quartzite. They also argued that the Hidden Basin beds (Fig. 2) were younger than the Redcliff Pound Group, although the assertion is tenuous given the limited information available. Haines and Allen (2016, 2017) agreed that the Munyu Sandstone is lithologically similar to the Heavitree Quartzite, but argued for a different provenance and younger age for the Lewis Range Sandstone, based on lithological differences, and SHRIMP U–Pb ages and Hf isotope data for detrital zircons. Despite poor bedrock exposure, the

Table 1. Lithostratigraphy and number of regolith samples per lithological unit, Ngurrupa regolith geochemistry program

Age	Unit	Lithology	Thickness (m)	Regolith samples	Percent total samples (n = 637)	Reference
Canning Basin	Callawa Formation	Sandstone and conglomerate		51	8.0	Middleton (1990)
	Erskine Sandstone	Sandstone, siltstone, minor sandy shale and conglomerate	40	0	0	Yeates et al. (1975); Crowe and Muhling (1977); Mory (2010)
	Blina Shale	Siltstone and shale, claystone, sandstone, minor phosphatic horizons	90	0	0	Yeates et al. (1975); Crowe and Muhling (1977); Mory (2010)
	Millyit Sandstone	Sandstone, siltstone and minor conglomerate	90	5	0.8	Yeates et al. (1975); Crowe and Muhling (1977); Mory (2010)
	undivided Mesozoic	Sandstone, siltstone, claystone and conglomerate		37	5.8	Crowe and Muhling (1977)
	Liveringa Group	Sandstone and siltstone, minor conglomerate and coal	620	168	26.4	Yeates et al. (1975); Crowe and Muhling (1977); Mory (2010)
	Noonkanbah Formation	Mudstone, sandstone, minor sandy carbonate units	640	48	7.5	Yeates et al. (1975); Crowe and Muhling (1977); Mory (2010)
	Poole Sandstone	Sandstone, minor siltstone, thin carbonaceous beds, basal carbonate	160	4	0.6	Yeates et al. (1975); Crowe and Muhling (1977); Mory (2010)
	Grant Group	Sandstone, siltstone, diamictite, conglomerate, shale	1000+	3	0.5	Yeates et al. (1975); Crowe and Muhling (1977); Mory (2010)
	undivided Paleozoic sedimentary rocks	Siliciclastic sedimentary rocks		0	0	
Murrumba Basin	Lucas Formation	Sandstone (partly calcareous), siltstone, mudstone, minor limestone and conglomerate		6	0.9	Blake and Yeates (1976); Crowe and Muhling (1977)
	Redcliff Pound Group*	Sandstone, wacke, minor conglomerate, siltstone, shale, limestone, dolomite, chert, and glauconitic sandstone	2000+	150	23.5	Blake and Yeates (1976); Crowe and Muhling (1977); Blake et al. (1979); Haines and Allen (2016, 2017)
	Munyu Sandstone	Silicified quartz arenite, conglomerate, minor limestone	400+	11	1.7	Blake and Yeates (1976); Crowe and Muhling (1977); Blake et al. (1979); Haines and Allen (2016, 2017)
	Hidden Basin beds	Sandstone, minor siltstone, and shale	3000+	127	19.9	Blake and Yeates (1976); Crowe and Muhling (1977); Blake et al. (1979); Haines and Allen (2016, 2017)
	Granites–Tanami Orogen	Biotite monzogranite		26	4.1	Crowe and Muhling (1977)
	undivided west Arunta Orogen	Quartz–muscovite schist, banded iron-formation, metavolcanic rocks, quartzite, granitic rocks		1	0.2	

NOTE: * Includes undivided Murrumba Formation (Haines and Allen, 2016, 2017)

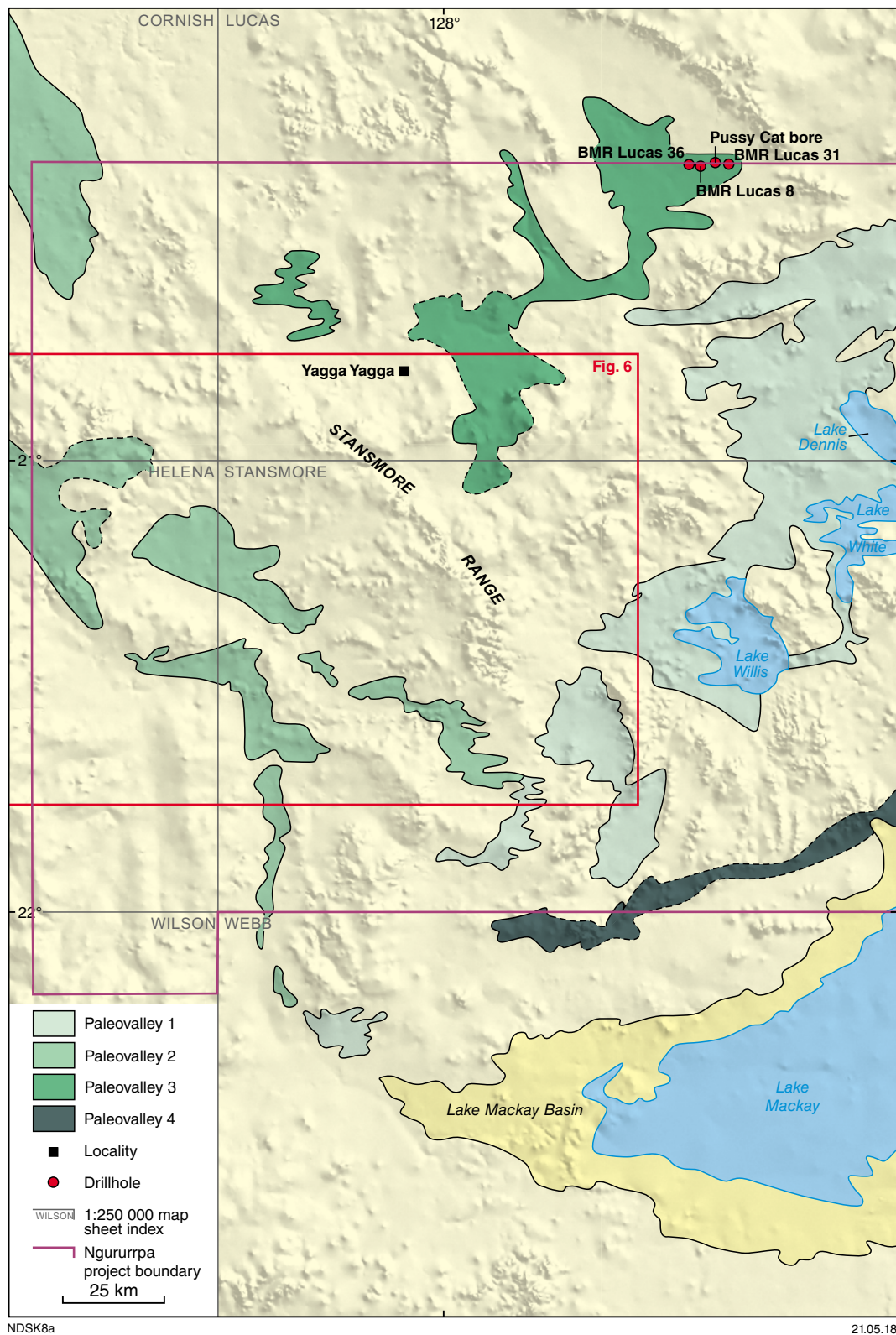


Figure 5. Distribution of paleovalleys in the Ngururrpa area. See text for discussion; rectangle shows location of Figure 6

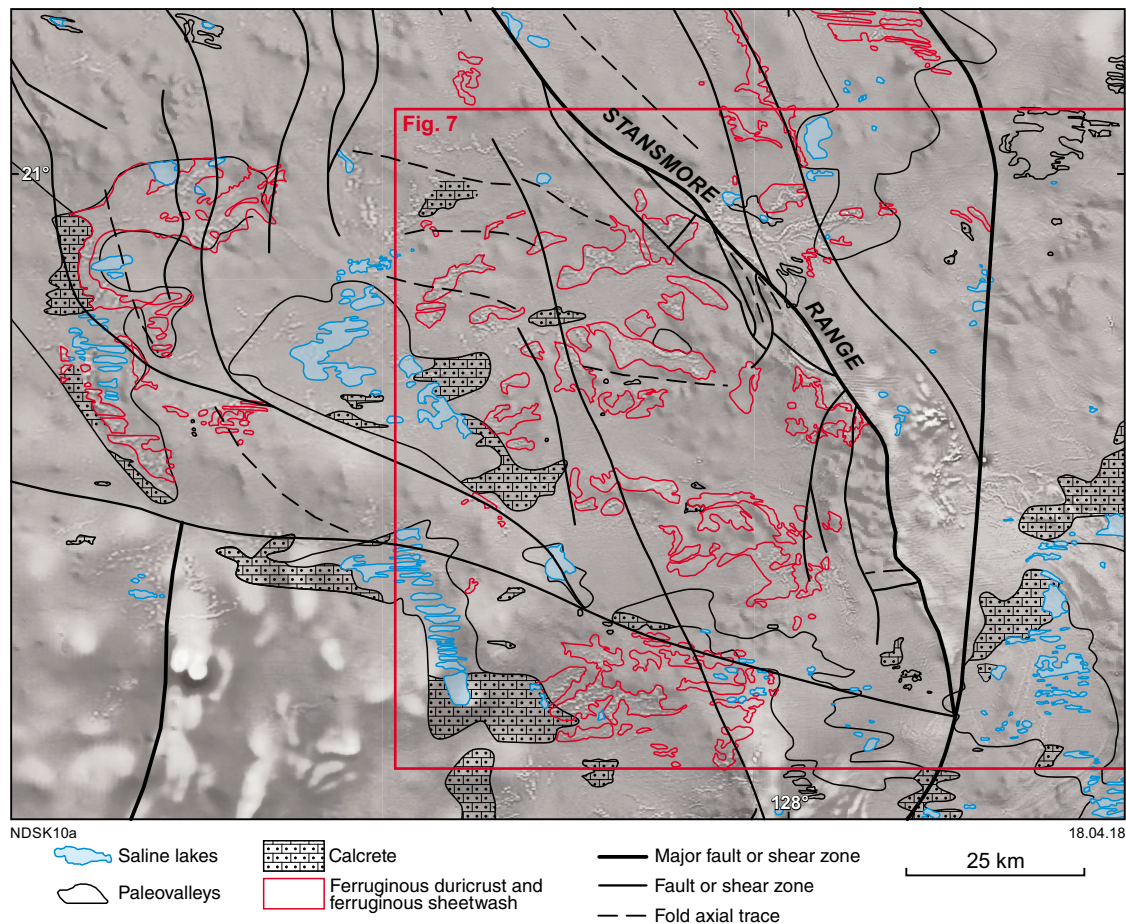


Figure 6. Detailed image of dendritic magnetic-fill paleochannels located on the margins of calcrete-filled paleovalleys, especially in the vicinity of the Stansmore Range. Background is first vertical derivative of reduced-to-pole magnetic data (RTP 1VD) and DEM. See Figure 5 for location; rectangle shows location of Figure 7

composition of surface float (Haines and Allen, 2017, fig. 20) suggests a significant time gap between the Lewis Range Sandstone and the base of the Murraba Formation. They assigned some of the carbonate-rich float in this area to the Bitter Springs Group, which outcrops to the south on WEBB. Although the Murraba Formation and Erica Sandstone consist of siliciclastic sedimentary rocks, several factors suggest that the boundary between them is time transgressive (Haines and Allen, 2016, 2017). These factors include a vertical change in depositional conditions from marine- to shallow-water to subaerial, the relative mineralogical maturity of sandstones, and a younger age of late Proterozoic to early Paleozoic for the upper part of the succession on the basis of trace fossils and similarities to parts of basin successions in the Northern Territory.

Blake et al. (1979) argued that the Hidden Basin beds were unconformable on the Redcliff Pound Group, but gravity data for the Ngurrupa program area show that the Hidden Basin beds correspond to a gravity high, meaning that these rocks are unlikely to be underlain by any significant thickness of sedimentary rocks. Furthermore, the Hidden Basin beds are more deformed than the Redcliff Pound Group, and lithologically similar to older successions to the north and south of the program area (e.g. parts of the Birrindudu Basin, Lake McKay Quartzite). Thus, the Hidden Basin beds are likely to be older than the Redcliff

Pound Group. Haines and Allen (2016, 2017) have argued that, based on suggested stratigraphic revisions, the Redcliff Pound Group should be abandoned, and replaced by an undivided Murraba Basin succession.

Canning Basin

Ordovician to Devonian rocks of the Canning Basin are not exposed in the program area, but are inferred at depth west of the Stansmore Fault based on gravity, seismic and magnetic data, and drillcore. Sandstone, siltstone and shale at 2000–2500 m in the Point Moody No 1 well (Fig. 2) are possibly part of the ?lower Carboniferous Andrews Formation, although this unit is not exposed. Thin-bedded calcareous sandstone of the Paleozoic Lucas Formation is located on the extreme northeastern edge of the program area, although most Paleozoic rocks occur in the western part of the program area, where they are generally in fault contact with either the Redcliff Pound Group or the Hidden Basin beds (Fig. 2).

Permian sedimentary rocks are well exposed in the Stansmore Range, where fossils indicate both terrestrial and marine conditions of deposition. Approximately 1300 m of conglomerate, sandstone, siltstone and lignite of the upper Carboniferous – Permian Grant

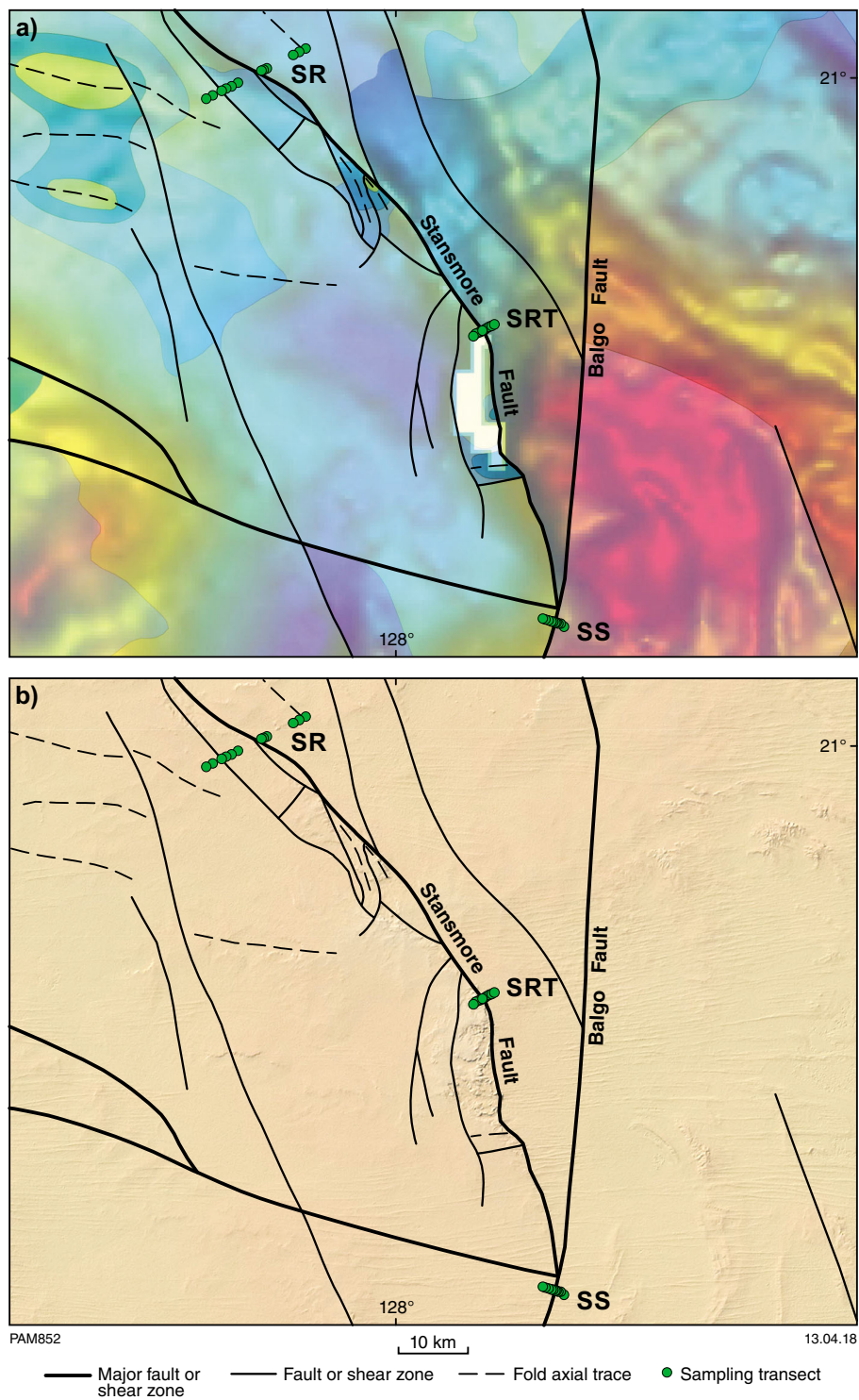


Figure 7. a) Gravity data shown in relation to 1:500 000-scale interpreted bedrock geology, faults (solid lines), and folds (dashed lines) (from GSWA, 2016); b) DEM and interpreted fault traces (solid lines) and folds (dashed lines). Green circles delineate three sampling transects (SR, SRT and SS) across regional faults

Group overlies the Andrews Formation in the Point Moody No 1 drillhole (Fig. 2). Detailed descriptions of lithostratigraphy have been made by Mory (2010). An outcrop of the Grant Group, comprising polymictic glaciogene conglomerate, is adjacent to the Stansmore Fault approximately 23 km northeast of the Point Moody No 1 drillhole. The Grant Group is unconformably overlain by thin-bedded to laminated, well-sorted, fine-grained sandstone and interbedded siltstone of the lower Permian Poole Sandstone, which was deposited in a deltaic to marine environment. The unit is locally cross-bedded, and has a carbonate-rich member at the base. Siltstone, shale and less common limestone of the Noonkanbah Formation overlie the Poole Sandstone. Compared to other Permian units, it has a high proportion of mudstone relative to sandstone (Mory, 2010). Large parts of the program area are made up of the overlying Liveringa Group. Areas of undivided Mesozoic siliciclastic rocks on either side of the Stansmore Fault consist of conglomerate, sandstone, siltstone and claystone.

Sandstone and conglomerate of the Triassic Millyit Sandstone occupies a small area north of the program boundary. The unit is disconformable on the Liveringa Group, and has a transitional contact with the overlying Blina Shale. This latter unit consists mainly of siltstone, claystone and fine-grained sandstone. The overlying Erskine Sandstone is massive and cross-bedded, consisting of silty sandstone with localized conglomerate beds. The youngest unit in the program area is the Callawa Formation (Playford et al., 1975), composed of sandstone and conglomerate, which unconformably overlies the Noonkanbah Formation in the southwest (Fig. 2).

Faults

An array of regional faults in the Ngururra area, including the Stansmore and Balgo Faults, trends north to northwest. The Stansmore Fault in particular is well constrained in part by regional gravity (Fig. 7a) and digital elevation data (Fig. 7b). The results of stratigraphic drilling show the Stansmore Fault has been periodically reactivated, with unconformities in the Carboniferous linked to fault movement. Evidence for the amount of offset is inconsistent. Blake and Yeates (1976) reported work of Garrett (1956) and Casey and Wells (1964), who suggested a downthrow of approximately 2400 m to the west, but this is inconsistent with stratigraphy in other areas.

Bedrock lithology and chemistry

Murraba and Canning Basin lithologies are dominated by silica-rich siliciclastic sedimentary rocks that show a limited range in texture and mineralogy. They are mainly moderately sorted to well-sorted, granoblastic quartz-rich sandstones, with minor amounts of interstitial mica (after clay), and accessory zircon, opaque oxides, tourmaline, and quartz-rich rock fragments. Secondary iron staining is variably developed in some outcrops.

Whole-rock geochemical data for 18 samples from the Murraba and Canning Basins (Table 2) include five samples from the Erica Sandstone, three samples from the Hidden Basin beds, four samples of the Lewis Range Sandstone, and one sample from each of the Heavitree Quartzite,

Munyu Sandstone, Noonkanbah Formation, Liveringa Group, and Millyit Sandstone. Also tabulated is an analysis of a manganiferous crust from the Redcliff Pound Group. Apart from the Millyit Sandstone and Liveringa Group, samples have between 92 and 99 wt% SiO₂, with correspondingly low concentrations of other elements. This is consistent with the high proportion of quartz.

Regolith mapping

The Ngururra 1:250 000-scale interpreted regolith–landform map (Plate 1) shows the distribution of different regolith–landform units according to GSWA’s regolith classification scheme and approach to regolith mapping (GSWA, 2013). The scheme is based on the residual–erosional–depositional (RED) approach of Anand et al. (1993). The GSWA tripartite classification uses a primary code to identify the landform, a secondary code for regolith composition, and a tertiary code for the parent rock, or cement composition. Each code can be further subdivided using a series of subscripts. A simplified version of Plate 1 is shown as Figure 8.

Separating regolith–landform units utilizes a combination of datasets:

- remotely sensed data (Google Earth, geophysics, satellite imagery, digital elevation modelling or DEM)
- published 1:250 000-scale geological map sheets (STANSMORE: Blake and Yeates, 1976; LUCAS: Crowe and Muhling, 1977; BILLILUNA: Blake et al., 1977; HELENA: Yeates, 1977; CORNISH: Crowe, 1978; WILSON: Towner, 1978)
- ground observations from the GSWA WAROX database
- site observations made during the Ngururra regolith sampling program.

Some indications of regolith thickness are included in the results of stratigraphic drilling reported from the Granites–Tanami Orogen area by Blake (1974). Estimates of regolith thickness using single-station passive seismic are discussed below.

Remotely sensed data can be used to map the extent of different regolith types when used in conjunction with DEM, which means that different types of regolith can be viewed in a geomorphological context (Wilford et al., 1997). Single-element images for potassium (K), thorium (Th) and uranium (U) represent the radiometric response of minerals in the top layer of the Earth’s surface (Wilford et al., 1997). The K response reflects the concentration of minerals such as feldspars and micas, as well as secondary clay minerals. The responses for U and Th are commonly related to resistant minerals such as zircon and monazite, but small amounts of U and Th in quartz and feldspars, and weathering products such as oxides and clays, are also present in U and Th images (Dentith and Mudge, 2014). K–T–U images can be used to separate transported regolith (GSWA, 2013) from more intensely weathered in situ (i.e. residual) regolith in areas of outcrop (Morris et al., 2016), and to separate older landforms that have undergone deep weathering from younger landforms undergoing active erosion (Wilford et al., 1992).

Table 2. Whole-rock chemistry of 18 bedrock samples from the Ngururupa region. Analysis by a combination of X-ray fluorescence (XRF) spectrometry and inductively coupled plasma (ICP) spectrometry at Intertek-Genalysis (Maddington, Perth). Data are available at <www.dmp.wa.gov.au/geochem>

GSWA sample number	184339	222161	222158	222162	184342	222156	222155	178851	178852	222153	222159	222154	222160	222163	222165	222164	222157	222166
Lithology	Quartz-rich sandstone	Quartz-rich sandstone	Quartz-rich sandstone	Quartz-rich sandstone	Sandstone	Fine-grained sandstone	Quartz-rich sandstone	Sandstone	Sandstone	Fine-grained sandstone	Quartz-rich sandstone	Quartz-rich sandstone	Quartz-rich sandstone	Quartz-rich sandstone	Quartz-rich sandstone	Quartz-rich sandstone	Sandstone	Manganese lithology
Easting	347508	426981	439711	425028	468222	430547	430553	467033	452715	454493	490046	495336	475245	469632	345096	393691	400169	482892
Northing	7476842	7595812	7570405	7590530	7563309	7726368	7726355	7841700	7843418	7724372	7649963	7645093	7645212	7639987	7604615	7628423	7724767	7612334
Zone	52	52	52	52	52	52	52	52	52	52	52	52	52	52	52	52	52	52
1:500 000 geological unit	Heavitree Quartzite	Hidden Basin beds	Hidden Basin beds	Hidden Basin beds	Munyu Sandstone	Lewis Range Sandstone	Lewis Range Sandstone	Lewis Range Sandstone	Lewis Range Sandstone	Erica Sandstone	Erica Sandstone	Erica Sandstone	Erica Sandstone	Erica Sandstone	Noonkanbah Formation	Liveringa Group	Millyit Sandstone	
1:250 000 map sheet	WEBB	STANSMORE	STANSMORE	STANSMORE	WEBB	LUCAS	LUCAS	BILLILUNA	BILLILUNA	LUCAS	STANSMORE	STANSMORE	STANSMORE	STANSMORE	LUCAS	STANSMORE	LUCAS	
SiO ₂ (wt%)	94.92	96.69	98.13	99.28	98.322	94.63	93.34	97.805	97.465	93.93	92.48	94.03	93.9	93.54	96.58	72.51	72.33	14.11
TiO ₂ (wt%)	0.042	0.07	0.03	0.1	0.04	0.12	0.1	0.03	0.047	0.16	0.18	0.16	0.18	0.12	1.9	0.55	0.03	0.15
Al ₂ O ₃ (wt%)	0.699	0.84	0.58	0.08	0.699	2.28	3.62	0.7	0.093	2.9	3.92	3.23	3.15	2.14	0.19	7.18	0.62	1.32
Fe ₂ O ₃ (wt%)	0.12	1.34	0.86	0.63	0.089	1.62	1.22	0.106	0.095	1.11	0.52	0.93	0.85	1.85	0.69	16.06	23.76	1.29
MnO (wt%)	<0.005	<0.01	<0.01	<0.01	<0.005	<0.01	<0.01	<0.005	<0.005	<0.01	<0.01	<0.01	<0.01	0.01	<0.01	0.02	0.01	59.13
MgO (wt%)	0.017	0.06	0.03	0.01	0.017	0.11	0.17	0.013	<0.01	0.21	0.08	0.1	0.12	0.15	0.01	0.07	<0.01	0.36
CaO (wt%)	0.022	<0.01	0.01	<0.01	0.023	<0.01	<0.01	<0.002	<0.002	0.01	0.23	0.04	0.02	0.26	0.01	0.03	<0.01	0.38
Na ₂ O (wt%)	<0.01	0.03	0.02	0.02	<0.01	0.02	0.02	0.084	0.082	0.04	0.03	0.03	0.03	0.04	0.04	0.03	0.02	0.26
K ₂ O (wt%)	0.409	0.27	0.08	0.02	0.128	0.72	1.1	0.142	0.017	0.61	0.26	0.32	0.4	0.79	0.03	0.26	0.02	3.41
P ₂ O ₅ (wt%)	0.016	0.024	0.016	0.007	0.025	0.031	0.069	0.026	0.024	0.033	0.025	0.021	0.019	0.017	0.013	0.07	0.493	0.134
SO ₃ (wt%)	0.035	0.2	0.03	0.04	0.023	0.01	0.02	0.043	0.031	0.02	0.37	0.15	0.14	0.27	0.04	0.03	0.04	0.099
LOI (wt%)	2.917	0.19	0.07	<0.01	0.675	0.2	0.36	1.085	2.194	0.65	1.58	0.93	0.91	0.49	0.17	3.07	2.8	9.42
Au (ppb)		<1	<1	<1		<1	<1			<1	<1	<1	<1	<1	<1	<1	<1	
Ag (ppm)		0.02	0.01	<0.01	<0.6	0.02	<0.01	<0.6	<0.6	0.03	0.02	0.02	0.05	0.04	0.07	<0.01	0.16	
As (ppm)	1.1	1.8	0.9	1.4	0.8	0.9	1.4	<0.5	<0.5	3.1	2.9	3.6	3.5	3.7	<0.5	24.8	10.6	
Ba (ppm)	448	3215	217	113	48	132	147	100	55	139	824	979	2143	807	195	89	37	
Be (ppm)	<0.3	0.13	0.11	<0.05	0.4	0.28	0.39	0.3	1.5	0.36	0.3	0.32	0.26	0.73	0.09	1.03	1.51	
Bi (ppm)	0.24	0.02	0.05	0.01	0.27	0.03	0.03	<0.02	<0.02	0.08	0.1	0.14	0.1	0.11	0.22	0.53	0.07	
Cd (ppm)	0.04	<0.02	<0.02	<0.02	<0.02	<0.02	<0.02	0.05	<0.02	<0.02	<0.02	<0.02	<0.02	<0.02	<0.02	<0.02	<0.02	
Co (ppm)		0.3	0.4	0.4		0.4	0.4			0.8	0.7	0.7	0.6	1.8	0.4	2.7	6.4	
Cr (ppm)	5	21	45	23	2	34	28	5	3	23	32	<20	27	25	76	109	<20	
Cs (ppm)	0.12	0.3	0.2	0.2	0.21	0.8	0.8	0.17	0.06	1.3	0.7	0.7	0.7	1.7	0.3	0.9	0.2	
Cu (ppm)	<1	1	1.3	1.4	<1	0.5	2	<1	<1	6.8	7.6	5.9	6	14.2	9.9	1.1	7.2	380
Ga (ppm)	1.7	1.4	0.9	<0.1	0.8	2.4	4.1	0.7	0.2	3.3	3.6	3.5	2.4	2.5	1.1	10	1.7	
Ge (ppm)	0.7	0.9	0.89	0.97	0.8	0.83	0.89	1.1	1.3	0.21	1.28	1.37	1.37	1.39	0.31	0.65	0.32	
Hf (ppm)	1.27	1.6	1.3	2.1	1.2	4.7	1.9	1.1	2.71	2.8	3.6	2.2	4.1	2.1	9.5	21	1	
In (ppm)		<0.01	<0.01	<0.01		<0.01	0.01			0.02	0.02	<0.01	0.02	0.01	0.02	0.07	0.01	
Li (ppm)		1.7	2.2	1.5		2.1	4.4			5.8	10.5	5.5	7.6	17.3	3.3	4.5	2.8	
Mo (ppm)		0.1	0.3	0.2	<0.3	0.1	0.2	<0.3	<0.3	0.1	0.1	<0.1	0.2	0.2	0.3	2.8	0.6	
Nb (ppm)	1	0.9	0.2	1.2	0.9	1.7	2	0.6	0.9	2.8	3.4	2.5	2.5	1.8	40.5	22.3	0.8	
Ni (ppm)	5	0.6	1	1.7	6	2.3	2.6	10	10	1.4	<0.5	1.5	1.1	6.5	<0.5	5.4	60.8	
Pb (ppm)	2.16	50.9	1	5.8	2.26	0.8	0.8	2.81	4.53	2.1	5.6	5.8	4.4	3	8.9	24.9	8.9	<50
Pd (ppb)		<0.5	<0.5	<0.5		<0.5	<0.5			1.4	<0.5	<0.5	<0.5	<0.5	<0.5	<0.5	<0.5	
Pt (ppb)		<0.5	<0.5	<0.5		<0.5	<0.5			<0.5	<0.5	<0.5	<0.5	<0.5	<0.5	<0.5	<0.5	
Rb (ppm)	10.8	10.7	3.4	0.6	4.3	21.5	35.3	2.9	<0.2	31.5	14.5	16.1	20.7	39.3	2	15.2	0.9	

Table 2. continued

GSWA sample number	184339	222161	222158	222162	184342	222156	222155	178851	178852	222153	222159	222154	222160	222163	222165	222164	222157	222166
Lithology	Quartz-rich sandstone	Quartz-rich sandstone	Quartz-rich sandstone	Quartz-rich sandstone	Sandstone	Fine-grained sandstone	Quartz-rich sandstone	Sandstone	Sandstone	Fine-grained sandstone	Quartz-rich sandstone	Quartz-rich sandstone	Quartz-rich sandstone	Quartz-rich sandstone	Quartz-rich sandstone	Quartz-rich sandstone	Sandstone	Manganese lithology
Easting	347508	426981	439711	425028	468222	430547	430553	467033	452715	454493	490046	495336	475245	469632	345096	393691	400169	482892
Northing	7476842	7595812	7570405	7590530	7563309	7726368	7726355	7841700	7843418	7724372	7649963	7645093	7645212	7639987	7604615	7628423	7724767	7612334
Zone	52	52	52	52	52	52	52	52	52	52	52	52	52	52	52	52	52	52
1:500 000 geological unit	Heavitree Quartzite	Hidden Basin beds	Hidden Basin beds	Hidden Basin beds	Munyu Sandstone	Lewis Range Sandstone	Lewis Range Sandstone	Lewis Range Sandstone	Lewis Range Sandstone	Erica Sandstone	Erica Sandstone	Erica Sandstone	Erica Sandstone	Erica Sandstone	Noonkanbah Formation	Liveringa Group	Millyit Sandstone	
1:250 000 map sheet	WEBB	STANSMORE	STANSMORE	STANSMORE	WEBB	LUCAS	LUCAS	BILLILUNA	BILLILUNA	LUCAS	STANSMORE	STANSMORE	STANSMORE	STANSMORE	LUCAS	STANSMORE	LUCAS	
Re (ppm)		<0.002	<0.002	<0.002		<0.002	<0.002			<0.002	<0.002	<0.002	<0.002	<0.002	<0.002	<0.002	0.002	
S (wt%)		0.09	0.01	0.02		<0.01	<0.01			<0.01	0.16	0.06	0.06	0.12	0.02	0.01	0.01	
Sb (ppm)	<0.8	0.22	<0.05	0.08	<0.8	0.24	0.3	2.5	2	0.32	0.34	0.31	0.43	0.22	0.16	0.58	0.08	
Sc (ppm)	<1	<10	<10	<10	0.9	<10	<10	2.5	2.9	<10	<10	<10	<10	<10	<10	<10	<10	
Se (ppm)		<0.5	<0.5	<0.5		<0.5	<0.5			<0.5	<0.5	<0.5	<0.5	<0.5	<0.5	<0.5	<0.5	
Sn (ppm)	0.3	1	<1	<1	0.3	1	<1	0.2	0.2	2	<1	3	2	1	7	3	1	
Sr (ppm)	11	38.6	8	10	19.7	27.8	34.6	60.8	25.9	8.2	32.7	28.1	41	24.5	10	21	13.5	
Ta (ppm)	0.33	<0.1	<0.1	0.2	0.33	0.1	0.3	<0.05	<0.05	0.3	0.3	0.2	0.2	0.2	3.2	1.1	<0.1	
Te (ppm)		0.2	<0.1	<0.1		<0.1	<0.1			<0.1	<0.1	<0.1	<0.1	<0.1	<0.1	0.2	<0.1	
Th (ppm)	3.56	3.7	2.6	1.3	3.9	7.2	5.6	1.88	2.01	4.3	5.8	3.9	5.2	3.6	8.9	28.3	2.3	
Tl (ppm)		0.02	0.02	0.02		0.07	0.12			0.18	0.08	0.1	0.14	0.21	0.03	0.16	<0.02	
U (ppm)	0.28	0.5	0.4	0.4	0.44	1.1	1.6	0.33	0.37	0.8	0.7	0.6	0.8	0.6	2.1	2.3	1.3	
V (ppm)	3	14	<10	11	4	10	10	4	2	28	19	16	20	14	39	317	30	90
W (ppm)		1	<1	<1		4	2			<1	1	1	1	1	7	4	<1	
Y (ppm)	2.2	3.1	3.1	2.7	8.3	20.8	30.1	3	3.2	8.2	10.4	6.2	8.2	8	10.5	21.8	4.7	
Zn (ppm)	<1	2	2	<1	<1	2	2	<1	<1	7	4	3	5	15	2	15	157	
Zr (ppm)	47	53	44	74	42.8	165	79	43.3	111.9	106	126	90	159	73	363	783	31	
La (ppm)	10.66	22.3	10.6	1.8	25.86	19.2	24.9	10.09	11.12	13.3	18.7	13.1	15.2	9.4	3.9	14.5	12.8	
Ce (ppm)	20.21	35.3	20	3.6	45.63	34.3	47.9	23.2	21.03	23.2	34.1	22.4	26.1	19.2	7.4	20.7	24.4	
Pr (ppm)	2	3.6	2	0.5	4	3.6	5	2.31	2.63	2.5	4.1	2.6	2.9	2.3	0.8	1.8	3.1	
Nd (ppm)	6.82	12.8	7.2	1.9	11.99	10.6	16.5	8.38	8.85	8	13.8	8.8	9.7	8.6	2.7	4.8	11.1	
Sm (ppm)	1.07	2.5	1.3	0.3	1.52	1.8	2.5	1.48	1.45	1.2	2.5	1.4	1.6	1.6	0.7	1.2	1.4	
Eu (ppm)	0.149	0.6	0.2	<0.1	0.155	0.4	0.6	0.291	0.16	0.2	0.5	0.3	0.3	0.4	0.2	0.3	0.2	
Gd (ppm)	0.61	2.1	0.9	0.3	1.3	2.8	3.6	1.1	0.88	1.1	2.2	0.9	1.4	1.7	0.9	1.7	1.2	
Tb (ppm)	0.07	0.2	<0.1	<0.1	0.25	0.6	0.8	0.11	0.09	0.2	0.3	0.2	0.2	0.3	0.1	0.4	0.2	
Dy (ppm)	0.36	0.7	0.5	0.5	1.53	3.6	5.5	0.59	0.6	1.3	2.1	1.3	1.5	1.4	1.5	3.5	1	
Ho (ppm)	0.07	0.1	0.1	0.1	0.28	0.7	1.1	0.1	0.08	0.2	0.4	0.2	0.3	0.3	0.4	0.8	0.2	
Er (ppm)	0.2	0.3	0.4	0.4	0.72	2.2	3	0.27	0.35	0.9	1.2	0.7	0.9	0.7	1.6	2.6	0.6	
Tm (ppm)		<0.1	<0.1	<0.1		0.3	0.3			0.1	0.2	0.1	<0.1	0.1	0.3	0.4	<0.1	
Yb (ppm)	0.28	0.4	0.3	0.3	0.53	1.6	2	0.32	0.36	0.8	1.1	0.7	1	0.7	1.6	3.3	0.6	
Lu (ppm)	0.03	<0.1	<0.1	<0.1	0.06	0.3	0.3	0.02	0.03	0.2	0.2	0.1	0.1	0.1	0.4	0.6	0.1	
(La/Yb) _{CN}	27.3	40.0	25.3	4.3	35.0	8.6	8.9	22.6	22.2	11.9	12.2	13.4	10.9	9.6	1.7	3.2	15.3	
(La) _{CN}	45.0	94.1	44.7	7.6	109.1	81.0	105.1	42.6	46.9	56.1	78.9	55.3	64.1	39.7	16.5	61.2	54.0	
(La/Sm) _{CN}	6.4	5.8	5.3	3.9	11.0	6.9	6.4	4.4	5.0	7.2	4.8	6.0	6.1	3.8	3.6	7.8	5.9	
(Gd/Yb) _{CN}	1.8	4.3	2.5	0.8	2.0	1.4	1.5	2.8	2.0	1.1	1.7	1.1	1.2	2.0	0.5	0.4	1.7	
Y/Ho	31.43	31	31	27	30	30	27	30	40	41	26	31	27	27	26	27	24	
Eu/Eu*	0.56	0.80	0.57		0.34	0.54	0.61	0.70	0.43	0.53	0.65	0.82	0.61	0.74	0.77	0.64	0.47	

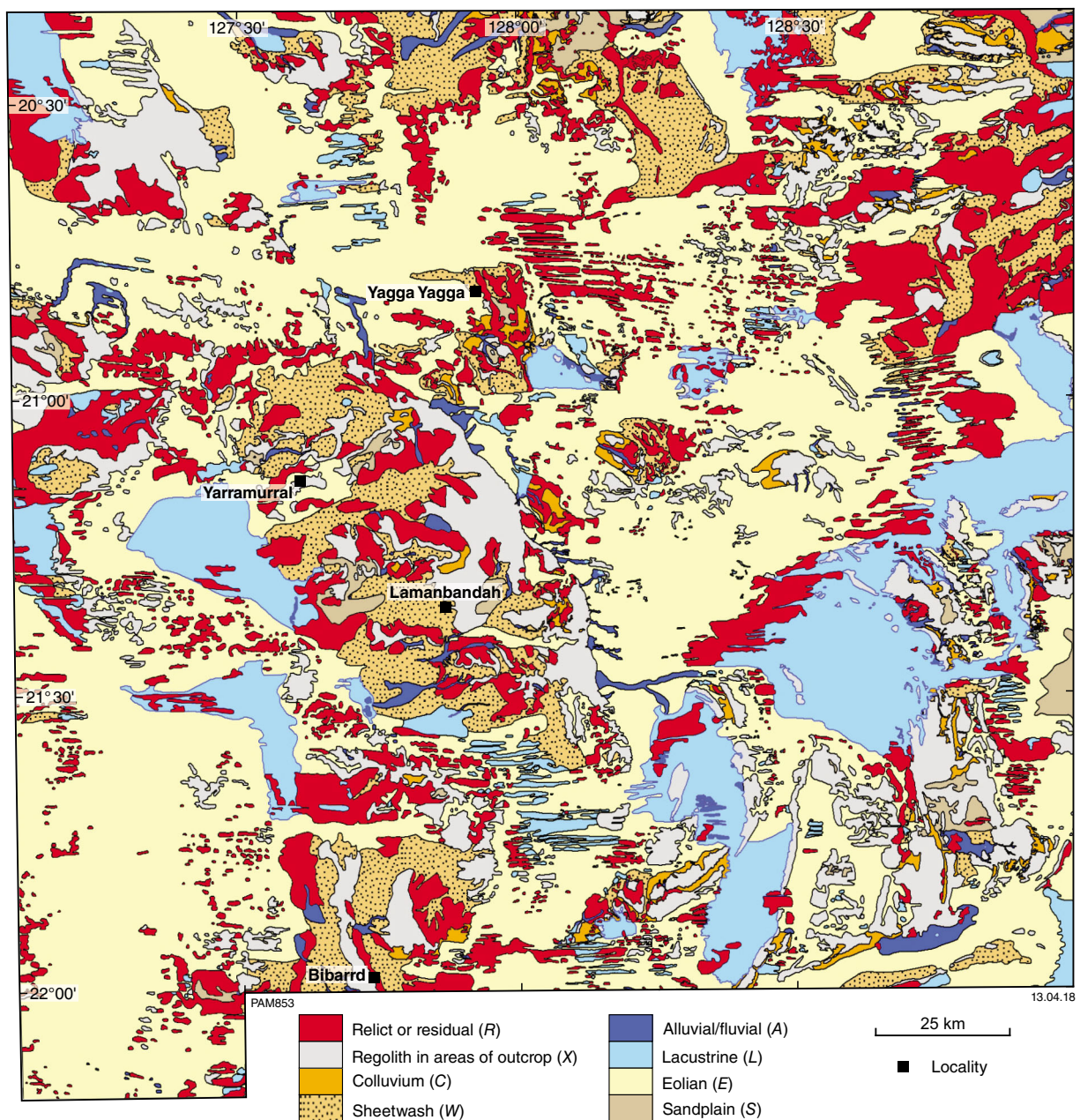


Figure 8. Simplified regolith–landform map of the Ngururupa area, showing regolith–landform units according to the primary code only (GSWA, 2013). See Plate 1 for detailed regolith–landform coverage, and Table 3 for extent of each unit and number of samples per unit

In the Ngururupa area, felsic igneous rocks, siltstones and fine-grained metasedimentary rocks display a high response for K (feldspar and clay-rich lithologies), Th and U (monazite, zircon). Mafic igneous rocks have a high response to K and moderate to low responses for Th and U, indicating abundance of K-bearing minerals relative to minerals containing Th and U. Quartz-rich sedimentary and metasedimentary rocks have a low response for K and moderate response for Th and U, consistent with chemical maturity.

In addition to radiometric data, Landsat images can be used to examine regolith composition, in particular the AGSO ratio image. This is the principle component 2 of

band ratios 4/3 and 5/7 (red: depicting clay), the ratio of bands 5/4 (green, depicting iron), and a composite of bands 1 and 7 (blue, depicting silica; Wilford and Creasey, 2002). In the Ngururupa area, exposed bedrock comprises predominantly siliciclastic sedimentary rock, which is commonly ferruginized. These rocks appear as green hues in the Landsat AGSO ratio. Associated ferruginous duricrust appears as yellow, indicating a combination of iron (green) and silica (blue). Sheetwash fans and clay in duricrust are more reddish, indicating higher amounts of clay relative to eroded ferruginous duricrust. Sand dunes appear in shades of blue and purple (silica and clay), indicative of the abundance of quartz sand and minor clay.

In most cases, calcrete appears as white patches, indicating the absence of clay, iron and silica, but patches of green within or adjacent to calcrete in some areas indicate the presence of iron minerals. Evaporitic minerals associated with lakes also appear as white patches, contrasting with regolith in lakes which has a pink hue consistent with a higher clay content (Plate 1).

The ASTER satellite system collects information in 14 spectral bands in the visible and near-infrared (VNIR), short wavelength infrared (SWIR), and thermal infrared (TIR) spectral regions. ASTER maps depict the content or composition of minerals and minerals groups (Cudahy et al., 2012), with 14 commonly used images. The ASTER ferric oxide content image shows areas of high Fe-oxide abundance in red and low abundances in blue. In the Ngururrpa area, exposed ferruginous duricrust and paleochannels containing ferruginous minerals show a high response for this image. Paleochannels are also delineated on a RTP 1VD image. The ASTER gypsum index provides

a good definition of gypsum around saline lakes and in playa terrains.

Distribution of regolith–landform units

More than 87% of the Ngururrpa program area is covered by regolith (Plate 1, Fig. 8; Table 3). Of this, transported regolith accounts for >70% by area, made up of 20 regolith–landform units. Residual or relict regolith (*R*), which covers approximately 16% by area, has been subdivided into 10 regolith–landform units. Regolith in areas of exposed bedrock (*X*), which occupies a similar area, has been divided into nine regolith–landform units.

Observations recorded at each sample site are compiled in Appendix 1A and 1B. These observations are taken from a standard site observation form completed at each sample site (Appendix 3B and 3C).

Table 3. Summary of regolith–landform units for the Ngururrpa area (Plate 1) in terms of area and number of regolith samples; % is percentage of the total area

Code	Description	Area (km ²)	% area	Number of samples	% samples
Relict or residual					
_Ri-g-pm	In situ weathered monzogranite or monzonite	<1			
_Ri-q-s	Quartz-rich weathered sedimentary rock	10	0.03	1	0.2
_Rr-f-m	Residual ferruginous duricrust on metamorphic rock	3	0.01		
_Rr-f-pm	Residual ferruginous duricrust on monzogranite or monzonite	6	0.02	1	0.2
_Rr-f-s	Residual ferruginous duricrust on sedimentary rock	1830	4.92	30	4.7
_Rr-hm	Duricrust (residual or relict) containing magnetite/maghemite	1616	4.35	28	4.4
_Rr-k-k	Calcrete; undifferentiated	419	1.13	1	0.2
_Rr-k-kg	Groundwater calcrete in paleovalleys	1933	5.20	41	6.4
_Rr-z-z	Silcrete	14	0.04	1	0.2
_Rs	Residual sand	34	0.09		
	Total R	5865	15.79	103	16.2
Regolith in areas of outcrop					
_X-g-pg	Granitic rock; undifferentiated	3	0.01		
_X-g-pm	Monzogranite or monzonite	<1			
_X-k-c	Calcareous sedimentary rock	2	0.01		
_X-l-m	Metamorphic rock; undifferentiated	10	0.03		
_X-l-s	Sedimentary rock; undifferentiated	2513	6.76	40	6.3
_X-l-v	Volcanic rock; undifferentiated	<1			
_X-m-vb	Basalt	<1			
_X-q-m	Quartzite	9	0.02		
_X-q-s	Siliciclastic sedimentary rock; quartz rich	2227	5.99	60	9.4
	Total X	4765	12.8	100	15.7
Depositional					
Colluvial					
_C	Colluvium; undifferentiated	502	1.35	16	2.5
_C-f	Fe-rich colluvium	67	0.18	1	0.2
_C-g-pg	Quartzofeldspathic colluvium from granitic rocks	16	0.04	0	0

Table 3. continued

Code	Description	Area (km ²)	% area	Number of samples	% samples
Total C		585	1.57	17	2.7
Sheetwash					
_W	Sheetwash; undifferentiated	1734	4.67	17	2.7
_W-f	Fe-rich sheetwash	1792	4.82	43	6.8
Total W		3526	9.48	60	9.4
Alluvial/fluvial					
_Ad	Drainage depression	45	0.12		
_Ai	Claypan	141	0.38	8	1.3
_Au	Superficial channel	303	0.82	3	0.5
_Av	Alluvial fan	68	0.18	2	0.3
_Ay	Depression in eolian sandplain	22	0.06		
Total A		579	1.56	13	2.1
Lacustrine					
_L	Lake and lacustrine deposits; undifferentiated	11	0.03		
_Ld	Fringing dunes	31	0.08	1	0.2
_Lg	Fringing bedded deposits	40	0.11	3	0.5
_Li	Freshwater lake	3	0.01		
_Lm	Dune and playa terrain	2066	5.56	46	7.2
_Lp	Playa	795	2.14	23	3.6
_Ls	Saline lake	1240	3.34	7	1.1
Total L		4187	11.26	80	12.6
Sandplain					
_S	Sandplain	464	1.25	9	1.41
Total S		464	1.25	9	1.41
Eolian					
_El	Longitudinal dunefield	17195	46.25	255	40.0
_En	Net-like dunefield	12	0.03		
Total E		17207	46.28	255	40.0
Total depositional		26547	71.41	434	68.2
Total		37177	100.01	637	100

Residual and relict regolith (R)

In the GSWA regolith classification scheme, the primary code *R* corresponds either to regolith that has developed by weathering of the underlying bedrock (residual regolith, *R_i*), or to the eroded remnants of a previous regolith–landform unit (relict regolith, *R_r*). Although relict regolith may have developed in situ, it is more likely that it represents regolith that has been transported, and is therefore genetically unrelated to the underlying bedrock. Thus, there is a gradation from residual to relict regolith with increasing amount of transport. Of the relict or residual regolith–landform units in the Ngururupa area, saprolite is represented by small areas of weathered monzonite and monzogranite (*R_igp_m*) or siliciclastic sedimentary rocks (*R_iqs*; one sample).

Duricrust, representing indurated, cemented or variably consolidated material, is the most abundant type of residual–relict regolith, totalling approximately 16% by

area. Duricrust comprises 102 samples collected from seven regolith–landform units. Although they have all been coded as relict rather than residual, some may have only undergone short-distance transport, such as ferruginous duricrust on metamorphic rocks (*R_ifm*), monzogranite (*R_ifp_m*; one sample), and sedimentary rocks (*R_ifs*; 30 samples).

Other relict or residual regolith types consist of undivided calcrete (*R_ikk*; one sample) or silcrete (*R_izz*; one sample). Undivided calcrete (<1% by area) includes both groundwater calcrete or, less commonly, that produced by in situ weathering of the underlying rock. Silcrete or siliceous duricrust is usually a veneer on bedrock of the Murraba Basin. Most silcrete exposures are too small to be represented at the mapped scale of 1:250 000, but large silcrete exposures were mapped in the vicinity of granitic rocks in the northeast of the program area. Unconsolidated sand developed on or near to areas of outcrop (*Rs*) covers <1% by area. It is most common in areas of granitic rocks.

Duricrust developed in paleochannels represents cementation of alluvium and adjacent weathered bedrock, and is therefore of relict origin. This regolith–landform unit includes material with a strong Fe response in the Landsat images, indicative of magnetite or maghemite ($R_r h_m$; 4.3% by area, 28 samples). Groundwater calcrete ($R_k k_g$; 41 samples) is of similar extent, and is generally located in the central part of paleovalleys.

Regolith in areas of outcrop (X)

Regolith in areas of outcrop is coded X in the GSWA regolith classification scheme. It commonly has a relatively high proportion of variably altered lithic fragments, and is poorly sorted. Of the nine regolith–landform divisions (Table 3), areas of heterogeneous sedimentary rock (Xls ; 7% by area, 40 samples) and quartz-rich siliciclastic sedimentary rocks (Xqs ; 6% by area, 60 samples) are the most common. The remaining units are spread across a range of igneous, metamorphic and sedimentary rocks of limited outcrop area, with no samples collected.

Transported regolith

Transported regolith is made up of varying proportions of gravel, sand, silt, clay and evaporate minerals such as gypsum and halite. The most common regolith type in the Ngururra area is sandplain with elongate sand dunes (coded as longitudinal dunefields, E_l) accounting for over 46% of the Ngururra area and 255 samples. A small part of this eolian cover consists of net-like dunefields (E_n ; Table 3). The sandplain substrate that supports dunes varies from less than one metre thick to more than 20 m thick in paleovalleys. Where the sandplain is thin, ferruginous lag, weathered bedrock fragments and, in some cases, outcrop is observed.

Regolith related to lakes or dune and playa terrain (L) occupies over 11% of the area (80 samples) and is spatially associated with paleovalleys. Most of this regolith type is dune (L_m ; 46 samples) and/or playa terrain (L_p ; 23 samples), totalling 7.6% by area, with less common saline lakes (L_s ; 3.3% by area, 7 samples). Most lake systems are located over the Murraba Basin in the eastern part of the Ngururra area.

Sheetwash deposits occupy 9.5% of the total area and account for 60 samples. Undifferentiated sheetwash (W ; 17 samples) covers about 5% by area, and a similar area is accounted for by Fe-rich sheetwash fan deposits (W_f ; 43 samples), which are common adjacent to the Stansmore Range. Colluvial deposits occupy a notably smaller area (1.6%), consistent with the subdued topography of the program area. They are proximal and low-angle slope deposits represented by three regolith–landform units. The most common type is undivided colluvium (C ; 16 samples), with smaller amounts of colluvium derived from granitic rocks (Cgp_g). Iron-rich colluvium is designated Cf (one sample). The aridity and subdued topography of the Ngururra area is reflected in the paucity of alluvial or fluvial material (1.6% by area). Five subdivisions include claypans (A_c ; eight samples), drainage depressions (A_d), depressions in eolian sandplain (A_v), superficial channels (A_u ; three samples), and alluvial fans (A_f ; two samples).

Regolith thickness

Drilling

Limited exploration in the Ngururra area means there has been little drilling, resulting in minimal data on regolith thickness. Stratigraphic drilling discussed by Blake (1974) included data from 152 holes, mainly to the north of the Ngururra area, but 26 of the holes are on LUCAS. In the majority of drillholes, the uppermost unit consists of unconsolidated sand, usually about 5 m thick and occasionally Fe stained. In some holes, this overlies lateritized ‘ironstone’. The underlying weathered rock extends down to 70 m in paleovalleys.

A rotary air blast (RAB) drilling program for diamonds east of the Stansmore Ranges (Gunn, 1983) noted <1 to 16.5 m of red sand overlying 1–2 m of silcrete or calcrete, which in turn overlies 2–7 m of weathered rock.

Passive seismic

To investigate the thickness of regolith and sedimentary rocks in the Ngururra area, a single-station passive seismic data acquisition program was carried out along a 15 km transect (SR1–16) southwest of Yagga Yagga, across a faulted succession of Canning Basin lithologies (Fig. 9). Passive seismic data were acquired at 12 sites using a Tromino single-station passive seismic system (Scheib, 2014b; Scheib et al., 2016b). Two control sites were located close to the Point Moody No 1 petroleum well (Point Moody, Point Moody A; Fig. 9; Table 4). Sites 1–3 and 8–10 are located over the Liveringa Group to the northeast of the Stansmore Fault, sites 11–13 are on the Noonkanbah Formation, and sites 15 and 16 are on the Liveringa Group at the western end of the traverse. Site 14 is located close to an unnamed fault between the Noonkanbah Formation and the Liveringa Group. The uneven spacing of the sites along the transect reflects the need to avoid registered heritage sites.

Data acquisition

Scheib (2014b) has presented a detailed account of passive seismic data acquisition and analysis using the Tromino system, and only a summary is given here. The location of acquisition sites and the length of data acquisition are summarized in Table 4. Acquisitions at sites SR3 and SR9 were repeated (SR3A and SR9A), because initial results appeared to have been affected by strong winds. For SR3, a stability plot shows intermittent noise patterns (Fig. 10). This disturbance is also evident in the plot of horizontal vs vertical (H/V) amplitude against frequency (red line for SR3 and SR9 in Fig. 11a,b). Measurements were repeated at the same locations six days later under less windy conditions, with the Tromino shielded by a bucket. The resulting H/V vs frequency plot (green lines for SR3A and SR9A in Fig. 11a,b) has the same featureless characteristics as most other sites along the transect (e.g. Figs 11c, 12). Therefore, data for SR3 and SR9 were discarded.

Table 4. Tromino passive seismic site locations, acquisition times, and site notes

SiteID	Easting	Northing	Date	Time	Comment	Site observations
Point Moody	376136	7648518	31/08/2015	9:26	Four acquisitions of 1 x 20 min and 3 x 10 min (Point Moody 2–4) at the same location	Evidence of drilling
Point Moody A	376358	7648579	31/08/2015	10:55	Four acquisitions of 1 x 20 min and 3 x 10 min (Point Moody A2–4) at the same location. Light vehicle drove past at 5–6 minutes before the end of recording Point Moody A3	Point Moody collar location, next to track
SR1	383940	7681639	01/09/2015	9:22	Acquisition of 1 x 20 min reading	Sandplain, more clay rich and compacted at depth
SR2	383070	7681170	01/09/2015	9:48	Acquisition of 1 x 20 min reading	Sandplain with lithic fragments
SR3	382233	7680717	01/09/2015	10:13	Acquisition of 1 x 20 min reading	Sandplain with lithic fragments
SR8	378730	7678808	01/09/2015	12:32	Acquisition of 1 x 20 min reading	Sandplain, more clay rich and compacted at depth
SR9	378299	7678569	01/09/2015	13:01	Acquisition of 1 x 20 min reading	Sandplain; well-sorted sand with some clay
SR10	378004	7678440	14/09/2015	8:45	Acquisition of 1 x 20 min reading	Sandplain; well-sorted sand with some clay
SR11	374874	7676710	14/09/2015	9:25	Acquisition of 1 x 20 min reading	Sheetwash/sandplain; sand with lithic fragments
SR12	373997	7676188	14/09/2015	10:03	Acquisition of 1 x 20 min reading	Sheetwash/sandplain; sand with lithic fragments
SR13	373252	7675828	14/09/2015	10:48	Acquisition of 1 x 20 min reading	Sheetwash/sandplain; sand with lithic fragments
SR14	372678	7675537	14/09/2015	11:26	Acquisition of 1 x 20 min reading	Sandplain/sheetwash
SR15	371506	7674872	14/09/2015	12:02	Acquisition of 1 x 20 min reading	Sandplain with some lithic fragments
SR16	370625	7674389	14/09/2015	12:37	Acquisition of 1 x 20 min reading	Sandplain with some lithic fragments

Data analysis

Passive seismic data were processed with Tromino's proprietary Grilla software using the averaged horizontal to vertical spectral ratio (HVSr) method. This method produces an HVSr trace for each acquisition showing the amplitude of the ambient noise ratio on the y-axis and the frequency range in Hz on the x-axis (Fig. 12). A peak in the trace with an amplitude >2 marks the resonance frequency of the subsurface, which is directly related to an impedance contrast at a certain depth (h). This impedance relates to a change in the rheological (elastic) properties of two subsurface layers, which causes an amplification of the ambient noise signal. A critical property is the shear-wave velocity (V_s). A peak in the trace is particularly strong where the contrast between shear-wave velocities is large; for example, where unconsolidated regolith with V_s of 200–400 m/s overlies crystalline bedrock with V_s values >1500 m/s.

The relationship between the resonance frequency (f_z), shear-wave velocity (V_s) and depth (h) is shown by the equation:

$$f_z = V_s / (4 \times h)$$

Lower resonance frequency corresponds to greater depth of a boundary between units with contrasting shear-wave velocities. Where the depth to the impedance contrast (h) is known (such as from drillhole data), V_s can be estimated for a particular frequency. Alternatively, the V_s of the upper layer can be estimated from shear-wave measurements or using documented values.

Results and data interpretation

Control sites — Point Moody well

Passive seismic traces at each of the two sites at or close to the Point Moody No 1 well are shown in Figure 11c,d. To examine reproducibility and the effects of acquisition time, four measurements were taken at each site, one of 20 minutes duration and three each of 10 minutes duration. Traces from approximately 150 m south of the Point Moody No 1 collar location (site labelled Point Moody, Fig. 11c; Table 4) are broadly similar, regardless of acquisition time. Three of the four traces measured approximately 240 m southeast of the Point Moody No 1 collar location (Point Moody A, Fig. 11d) are similar, and resemble traces from Point Moody at frequencies lower than about 30 Hz (Fig. 11c). The fourth trace (blue line, Fig. 11d) is distinctive, with peaks at 40 Hz and smaller features at 4.55 and 9.5 Hz. These peaks are similar to less prominent features in the other three traces. The elevated peaks in the blue trace can be attributed to a vehicle driving past five to six minutes before the end of the 10-minute acquisition period.

The limited variation in H/V amplitude over a wide frequency interval from 150 m south of the Point Moody collar location (Fig. 11c) provides little information on the thickness of either regolith or sedimentary units. Data from 240 m southeast of the collar location (Fig. 11d) indicate some weak impedance at high frequency. The peak at 40 Hz relates to a shallow impedance within the upper metre, whereas features between 40 and 4 Hz

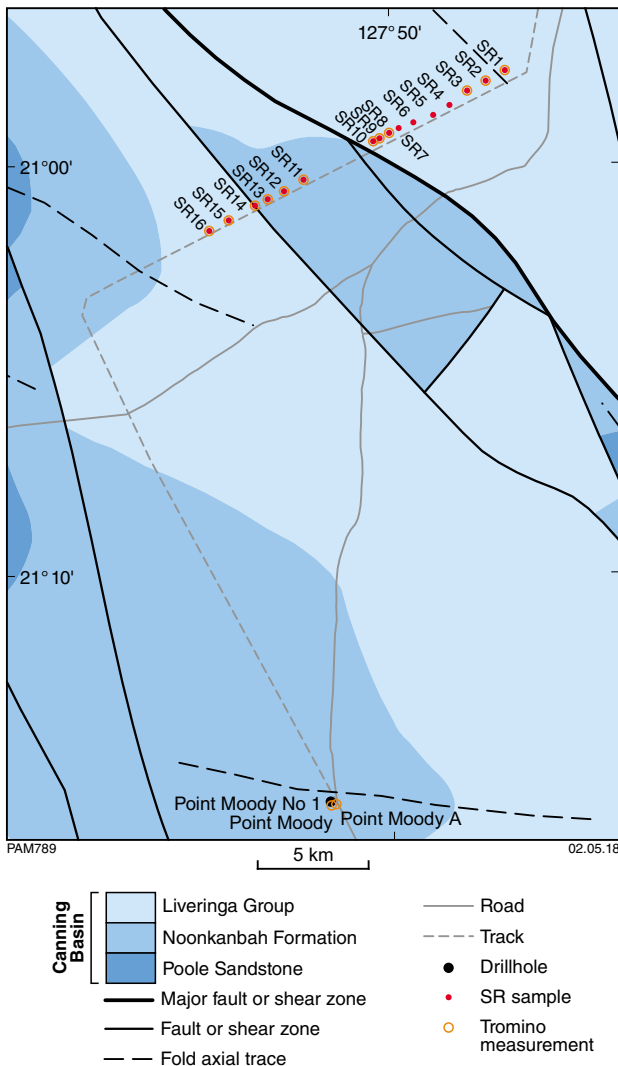


Figure 9. Single-station passive seismic site locations along the SR traverse across the Stansmore Fault. See Figure 2 for location of this figure

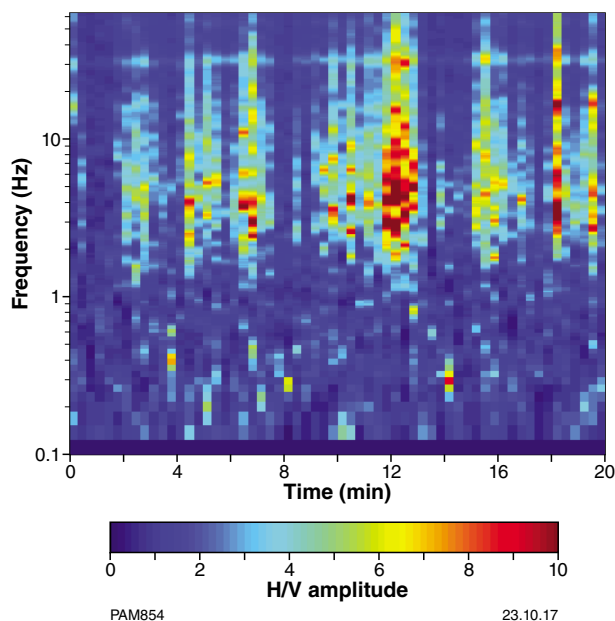


Figure 10. Stability plot for passive seismic data acquired at site SR3A

are possibly related to subtle impedance contrasts in the upper few tens of metres. The lack of resolution of subsurface regolith and stratigraphy using passive seismic is consistent with the Point Moody drill log, which shows about 8 m of alluvium overlying a succession of Permian to Carboniferous sedimentary rocks. Such lithologies would provide little rheological contrast, which may explain the lack of response in the HVSR at lower resonance frequencies. If the peak at 4.55 Hz (Fig. 11c,b) corresponds to regolith cover, the estimated shear-wave velocity would be approximately 150 m/s, which is lower than values of 300 m/s for unconsolidated sand-dominated cover. If the higher value of 300 m/s is used, a thickness of eight metres would correspond to a resonance frequency of about 10 Hz, which may be indicated by a subtle feature in the Point Moody A3 trace in Figure 11d.

Transect sites

HVSR plots for the transect sites (Fig. 12; Table 4) show that at all sites, peaks with amplitudes >2 only occur at resonance frequencies above 20–30 Hz, indicating shallow impedance contrasts. These high-frequency peaks indicate a thin regolith cover of about 1–2 m. The lack of peaks at lower frequencies is consistent with bedrock units having similar elastic properties (i.e. they are rheologically similar), complicated by the low level of ambient or natural noise due to the distance of the Ngururpa area from the coast. There is no discernible difference in passive seismic traces either side of the Stansmore Fault.

Although passive seismic traces lack prominent peaks at frequencies less than 30 Hz, subtle features within the HVSR can be imaged by contouring and interpolating the HVSR intensity of the 12 sites along the transect (Fig. 13). This depth profile indicates some strong contrasts between low (blue) and high (red or pink) H/V intensities, although the actual range of $\log(H/V)$ only corresponds to HVSR amplitudes up to 1.6. Despite this, the profile indicates lower intensities in the upper part of the subsurface, particularly for sites SR1, SR2 and SR3 northeast of the Stansmore Fault. At these locations, the lower intensity horizons extend to about 100 m below the surface. At site SR9, there is a break in the continuity of the elevated $\log(H/V)$, which could correspond to a bedrock structure, such as a fault. Site SR14 corresponds to a thin elevated H/V layer overlying a lower H/V response, which may indicate a more resistant layer at shallow depth, and a fault trace at depth.

Discussion

The limited amount of exploration in the Ngururpa area means there is little direct evidence of regolith thickness that is afforded by drilling. Available data indicate a thin, sand-dominated regolith cover typically <10 m thick, which is consistent with passive seismic data for most sites along a 15 km transect. Subtle peaks at resonance frequencies >20 Hz indicate a regolith cover of 1–3 m. The lack of low-frequency peaks reflects largely homogenous sedimentary bedrock with little variation in rheological properties.

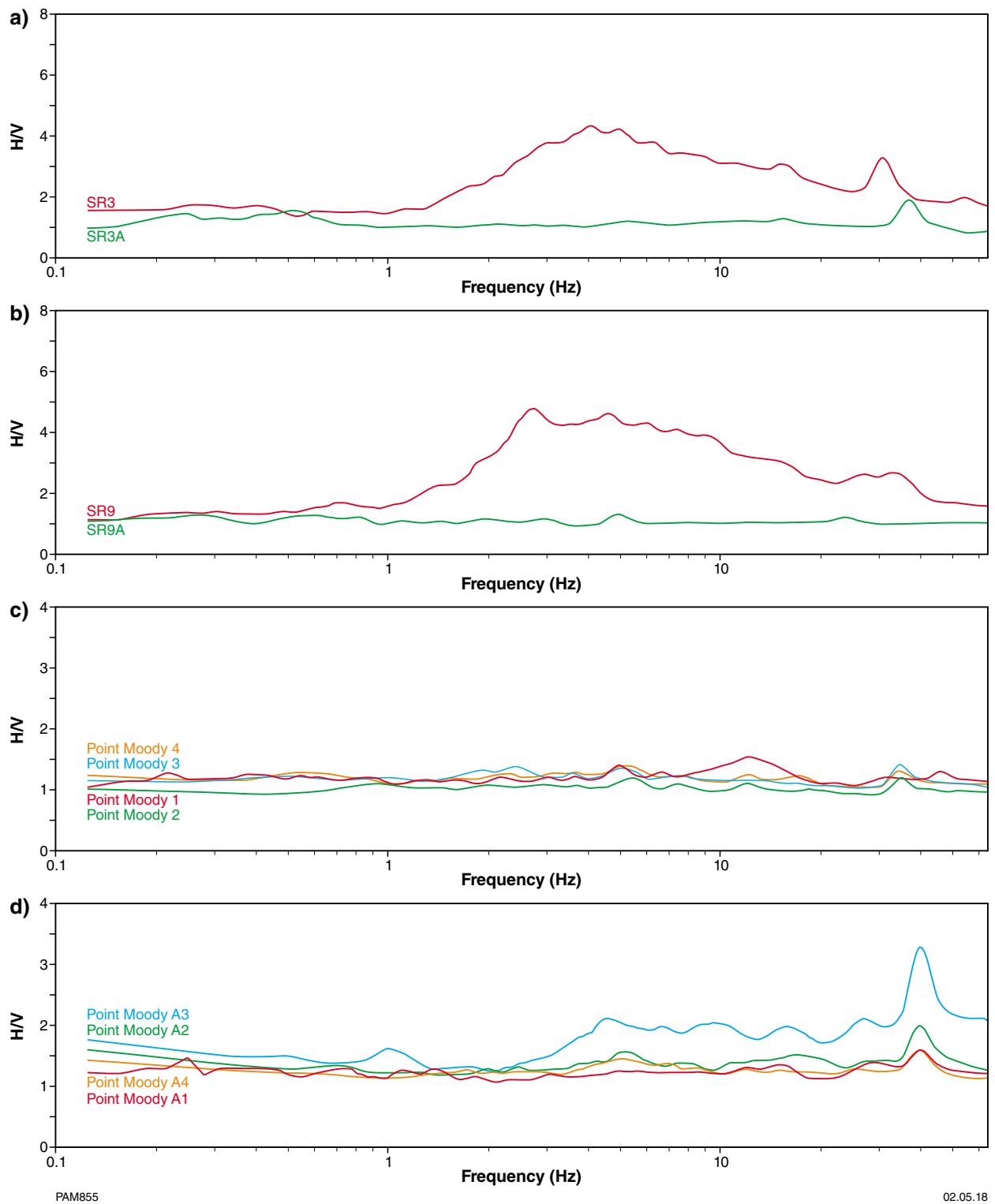


Figure 11. Passive seismic data at control sites: a), b) comparison of data at sites SR3 and SR9 in terms of H/V vs frequency (Hz). Initial data for SR3 and SR9, which show signs of being affected by wind during data acquisition, have not been used; interpretations are instead based on data for SR3A and SR9A; c) passive seismic trace at site approximately 150 m south of Point Moody drillhole; d) passive seismic trace at site approximately 240 m southeast of Point Moody drillhole

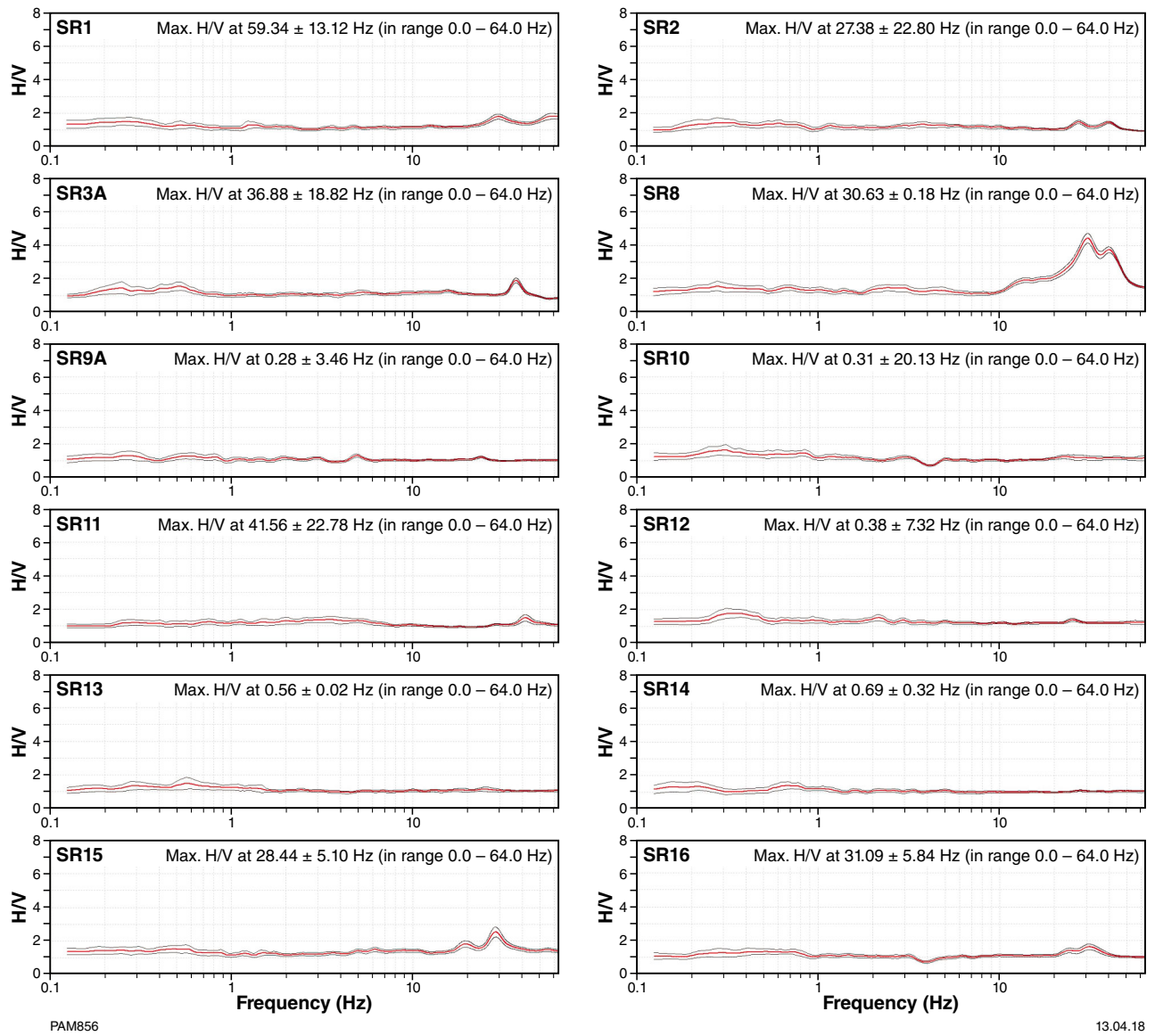


Figure 12. H/V vs frequency (Hz) for passive seismic data along a transect across the Stansmore Fault. See Figure 9 for seismic sampling site locations

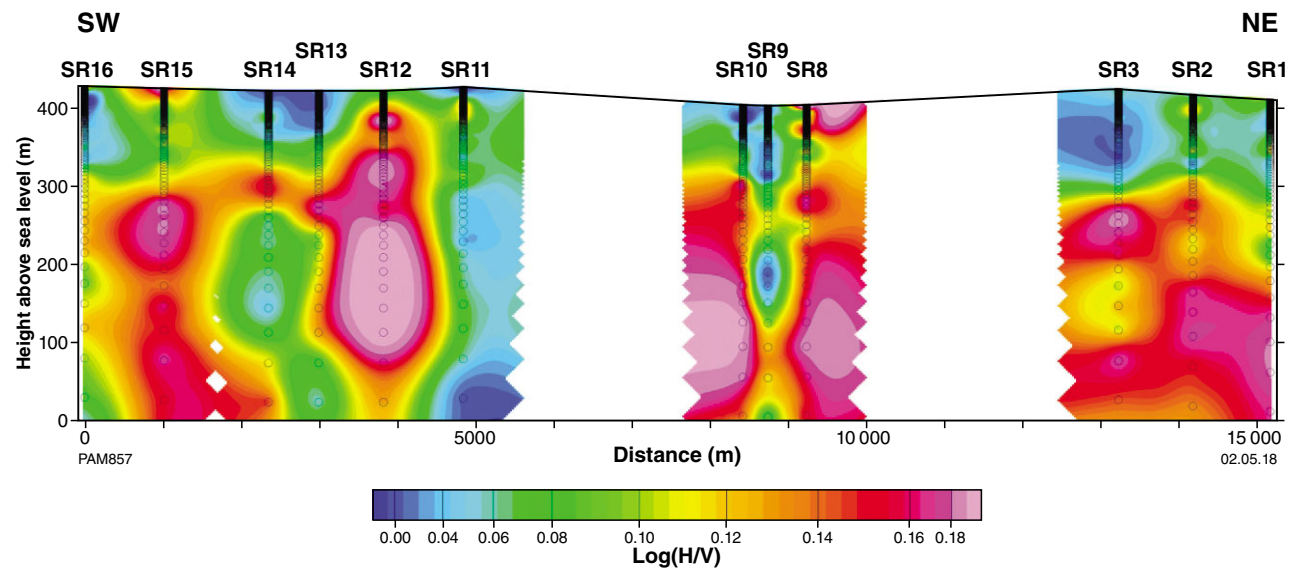


Figure 13. Contoured passive seismic data (HVSr) acquired along the transect shown in Figure 9

Regolith chemistry

Reconnaissance

Prior to the regional regolith sampling program carried out in September 2015, a reconnaissance program was undertaken in October 2014 (Fig. 14) to determine if regolith composition varied noticeably according to either grain size or depth in the regolith profile. Samples were collected at 17 sites, and 12 of these samples were analysed. Seven samples are from the Liveringa Group, two from the Hidden Basin beds, and one each from the Redcliff Pound Group, Poole Sandstone and Noonkanbah Formation. At each site, a surface sample was collected from 2–4 cm depth using a spade, along with samples from the regolith profile using a power auger. Surface lag was collected from four sites. Site information is summarized in Appendix 1A, with analytical data contained in Appendix 2.

At all sample sites, surface and downhole regolith is dominated by moderately sorted to well-sorted quartz-rich sand. At some sites (e.g. YY2, Liveringa Group), there is a higher proportion of silt and clay, whereas at sites such as YY3 (Liveringa Group), regolith is variably iron cemented, resulting in patches of ferricrete at the surface (Fig. 15a). At some sites, subangular and locally ferruginized lithic fragments up to 1.5 cm long are usually accompanied by iron-rich granules or nodules up to 5 mm diameter. Patches of calcrete at the surface and calcrete fragments throughout the regolith profile occur at some sites located in dune swales (M604, Hidden Basin beds; Fig. 15b).

The nature of surface regolith is generally a reliable indicator of regolith at depth. For example, where ferruginous lag, ferruginized lithic fragments or calcrete clasts occur at the surface, they are usually present downhole, although at lower concentrations. If ferruginous lag is present on the surface and downhole, lithic fragments or calcrete are usually not present.

Chemistry of reconnaissance samples

The coarse (<2 mm) and fine (<50 µm) fractions of regolith sample were screened, milled (<2 mm fraction only), digested with aqua regia, and analysed for 63 analytes. The <4 mm fraction of lag has been analysed for 70 analytes following combined fusion and acid digestion, and X-ray fluorescence (XRF) and ICP finish (Appendix 3).

Normalized multi-element plots (spider diagrams) have been used to compare the chemistry of different grain-size fractions of individual samples, assess any changes in regolith chemistry with depth, and compare the chemistry of regolith and lag (Fig. 16). Data have been normalized to average upper continental crust (UCC; Rudnick and Gao, 2003). The 30 analytes shown in these diagrams illustrate the behaviour of different element groups, including lithophile elements (Rb, Ba, K, Ca, Mg, Al, Fe, Th, P), high field strength elements (HFSE: Hf, Zr, Ti, Nb), light rare earth elements (LREE: La, Ce, Nd, Sm, Eu), heavy rare earth elements (HREE: Gd, Er, Y), transition elements (Fe, Ni, Cr, V), base metals (Pb, Cu, Zn), and chalcophile elements (As, Sb, Bi).

Variations with grain size

Analyte concentrations are generally higher in the <50 µm fraction of regolith compared to the <2 mm fraction (Fig. 16a–i), apart from regolith over the Liveringa Group at sites YY2 and YY3 (Fig. 16a,b). At these two sites, only the REE are at higher concentrations in the fine fraction, and Al, Fe, HFSE, Cr, V and the chalcophile elements, in particular, are at higher concentrations in the <2 mm fraction. The higher concentration of transition elements and HFSE reflects the inclusion of fine-grained lag in the <2 mm fraction, which is common at both sites.

Apart from concentration differences, the normalized patterns of the <2 mm and <50 µm fractions at most sample sites are similar. The chemical maturity of the Ngururupa regolith is shown by the depletion in lithophile element concentrations compared to UCC, although the relatively high concentration of Al indicates the conservation of this element (Scott and Pain, 2008). Low HFSE, Cr, Th and V concentrations indicate only small amounts of resistate minerals, and the ineffectiveness of aqua regia to dissolve them. The concentration of base metals (Cu, Pb, Zn) and chalcophile elements (e.g. As, Bi, Sb) can be controlled by bedrock composition, but more likely in this case by precipitation of secondary Fe minerals resulting from weathering (Smith et al., 1989; Smith and Singh, 2007; Anand and Butt, 2010). This is consistent with the behaviour of Cu in relation to Fe in the <2 mm and <50 µm fractions of regolith (Fig. 17), which shows a positive relationship for both grain-size fractions, and a higher Cu concentration in the <50 µm fraction for a given Fe concentration. The higher content of REE in the <50 µm fraction of regolith compared to the <2 mm fraction is contributed to by both resistate minerals such as monazite ((Ce, La)PO₄), xenotime (YPO₄), and zircon (ZrSiO₄), and a higher proportion of clay minerals (Cullers et al., 1979; Taylor and McLennan, 1985, 1995; Bao and Zhao, 2008). Carbonate fragments are present in regolith from site M604, and this is shown in the relatively higher Ca content of regolith in both size fractions (Fig. 16f).

Variations with depth

Regolith is relatively homogeneous with depth (Fig. 16a–i), and where compositional variations do occur throughout the regolith profile, they are not consistent. For example, the REE concentrations are higher in the <50 µm fraction of the surface sample at site M604 (Hidden Basin beds; Fig. 16f), but slightly lower in the surface sample at both M677 (Liveringa Group; Fig. 16c) and M584 (Noonkanbah Formation; Fig. 16e).

Lag chemistry

Three of the four analysed lag samples have broadly similar major element chemistry. The ranges in values are Fe₂O₃ 46–52 wt%, SiO₂ 26–33 wt%, and Al₂O₃ 12–13 wt%. Lag from site M617 has a higher proportion of lithic fragments, shown by higher SiO₂ (61.1 wt%), and lower Fe₂O₃ (24.81 wt%) and Al₂O₃ (8.97 wt%). Relative to the <2 mm and <50 µm fraction of regolith, lag has consistently higher HFSE, Al, Th, Fe, Cr, V, Pb and chalcophile elements (Fig. 16a,b,h,i). In three of the four samples, REE in lag are in similar concentrations to regolith, but at site M644 (Fig. 16i), lag has elevated REE concentrations.

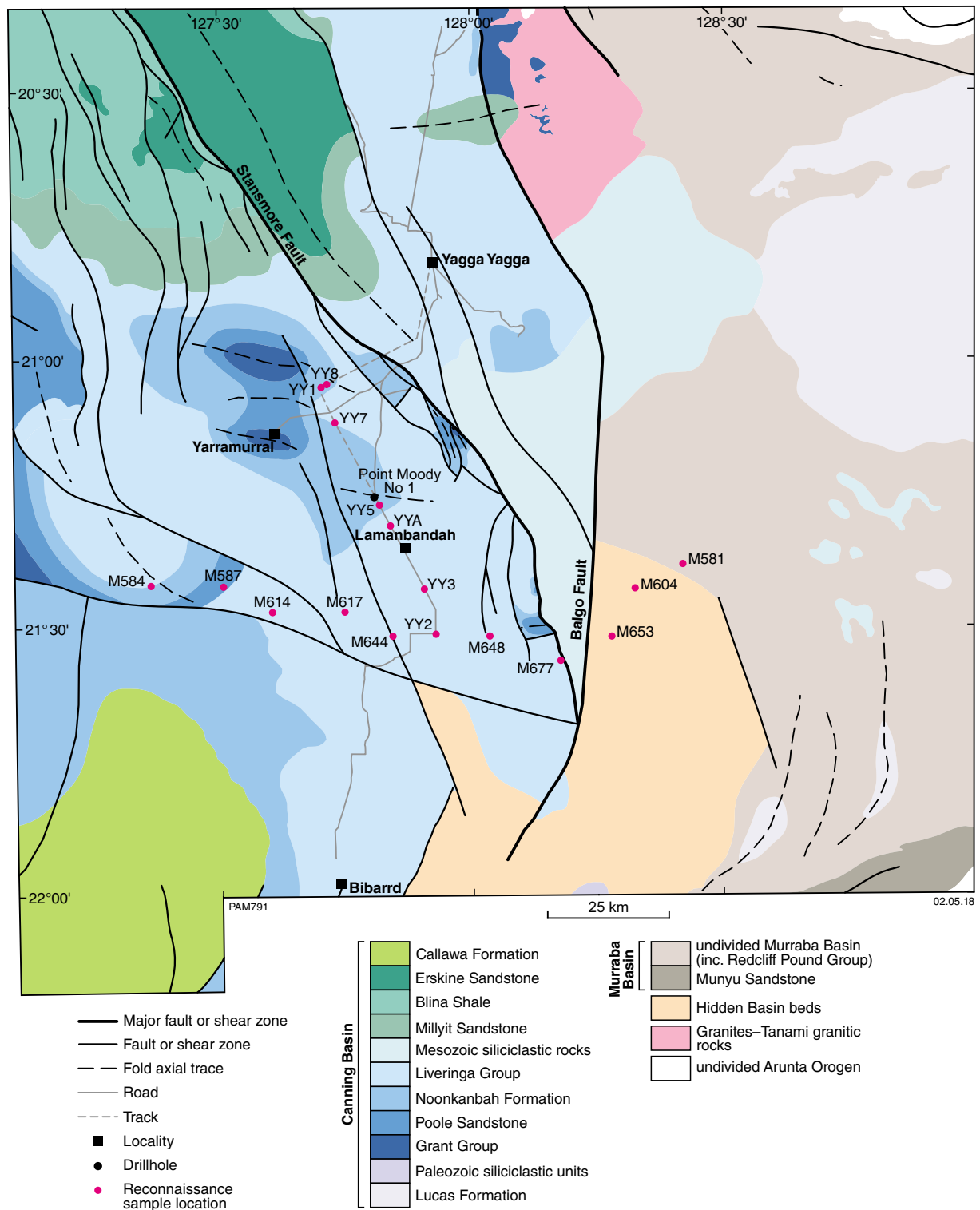


Figure 14. Reconnaissance regolith sample sites displayed over 1:500 000 interpreted bedrock geology and structures (GSWA, 2016)

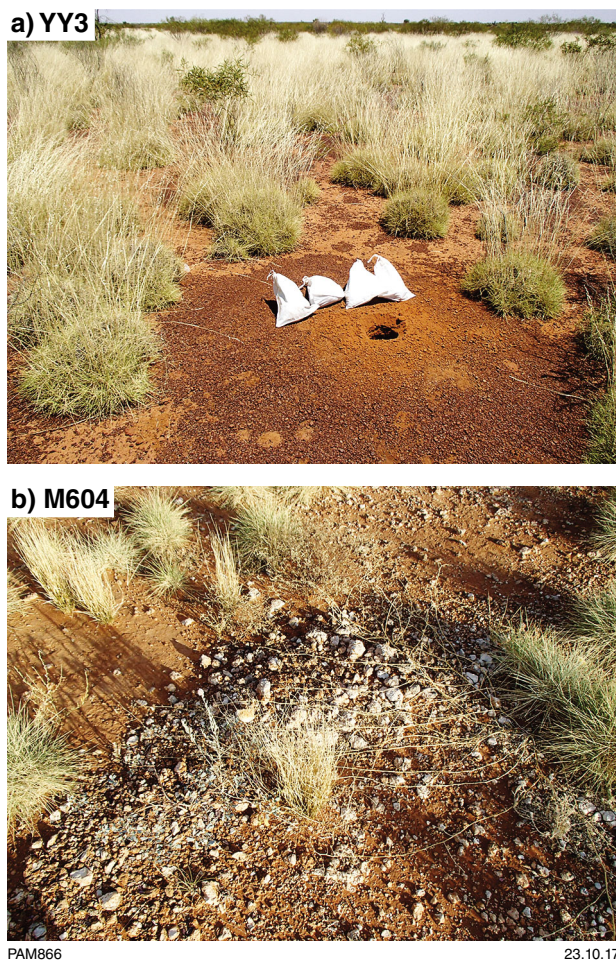


Figure 15. Reconnaissance site photographs: a) site YY3 (Liveringa Group) showing development of isolated ferricrete patches at the surface and abundant ferruginous lag; b) site M604 (Hidden Basin beds) where calcrete clasts are common in quartz sand-rich regolith

Rare earth element patterns for lag are weakly convex, compared to weakly concave patterns for regolith. The intense chemical weathering to produce lag (Carver et al., 1987; Anand and Paine, 2002; Anand and Butt, 2010) results in the concentration of resistate minerals. Ferruginization results in an increase in transition element concentrations and leads to the crystallization of Fe oxyhydroxides which can take up chalcophile elements and base metals.

Discussion

The chemistry of reconnaissance samples shows consistent differences in element concentrations in terms of grain size, but little variation in depth for regolith samples of the same grain-size fraction. The only exceptions are when fine-grained ferruginous lag is incorporated in the <2 mm fraction.

Fine-fraction regolith chemistry

As in most desert areas, the Ngururrpa program area is dominated by transported regolith, composed of quartz-rich sand with a small amount of silt and clay. The high cation exchange capacity (CEC) of the fine fraction (particularly the clay component; Hall, 1998) of regolith means it can weakly bond or bind ions, and microparticulate or colloidal material that may have migrated vertically from bedrock and any bedrock-hosted mineralization. This is the exogenic component discussed by Cameron et al. (2010), whereas the same component that makes up the regolith itself is referred to as the endogenic component. As the endogenic component is an integral part of the transported regolith, it is an unreliable indicator of either the underlying bedrock composition or bedrock-hosted mineralization. Dilution effects of quartz sand on the fine-fraction exogenic component can be minimized by screening. Partial digestion of the fine fraction liberates the exogenic component into solution while at the same time dissolving little of the (exogenic) fine-fraction component itself. Lixivants such as aqua regia are particularly effective in this regard, in that they are relatively ineffective in terms of dissolving silicates (Chao and Sanzolone, 1992; Mann, 2010; Leybourne and Rice, 2013). This approach of combined screening and partial digest of the fine fraction was used for the east Wongatha regional regolith geochemistry program, carried out by GSWA (Morris, 2011, 2013) on the margin of the Archean Yilgarn Craton, an area of approximately 70% sandplain cover (McGuinness, 2010). The program successfully identified hidden bedrock lithologies and bedrock-hosted mineralization through subtle changes in regolith fine-fraction chemistry.

The <50 μm fraction of samples from 637 sites (as well as 51 site duplicates) was dry screened in two batches at Intertek Genalysis Laboratory Services (Maddington, Perth). Each regolith sample weighed between 2.3 and 5.7 kg (Fig. 18a), with an average weight of approximately 3.9 kg. The majority of samples have little coarse-grained material (<15% of samples have >2 mm material; Fig. 18b), and most samples have a high proportion of sand (grain size 50 μm to <2 mm; Fig. 18c). The <50 μm fraction ranges between 17 and 405 g, or 0.6 to 16.9% of the total sample weight (Fig. 18d), with an average of 2.8%. The amount of the <50 μm fraction is broadly similar for sites where a duplicate sample was taken (Fig. 19), but the scatter indicates some metre-scale heterogeneity. There is generally good agreement between parent and duplicate, especially when both are screened in the same batch.

Appendix 3 includes information related to sample preparation, sample analysis and related quality-control data generated during the analysis of the regolith fine fraction. The chemistry of the regolith fine fraction, which was analysed in six batches, is compiled in Appendix 4A.

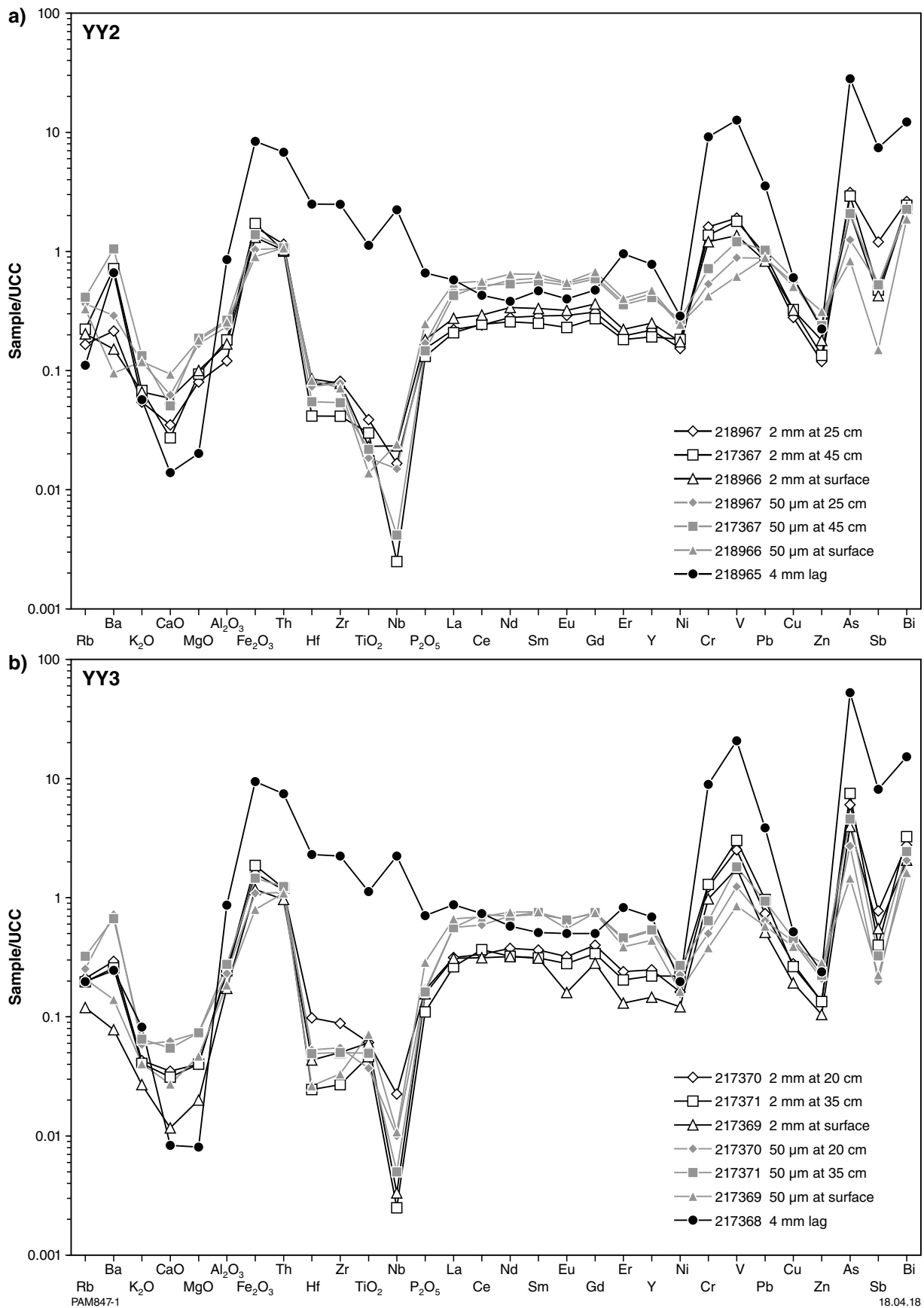


Figure 16. Multi-element spider diagrams for a range of lithophile elements, HFSE, REE, transition elements, base metals, and chalcophile elements normalized to concentrations in average upper continental crust (UCC; Rudnick and Gao, 2003): a) site YY2 (Liveringa Group); b) site YY3 (Liveringa Group)

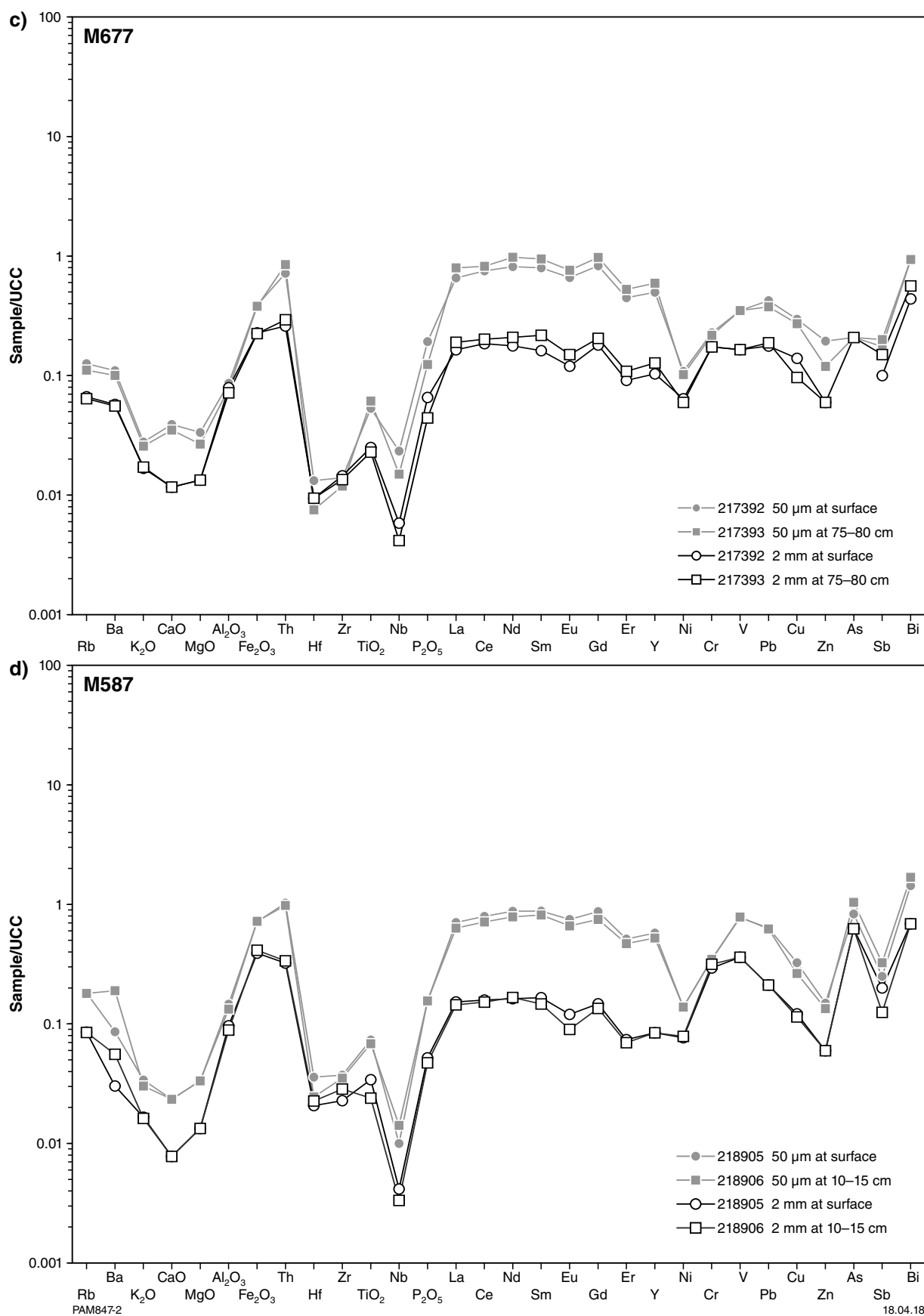


Figure 16. c) Site M677 (Liveringa Group); d) site M587 (Poole Sandstone)

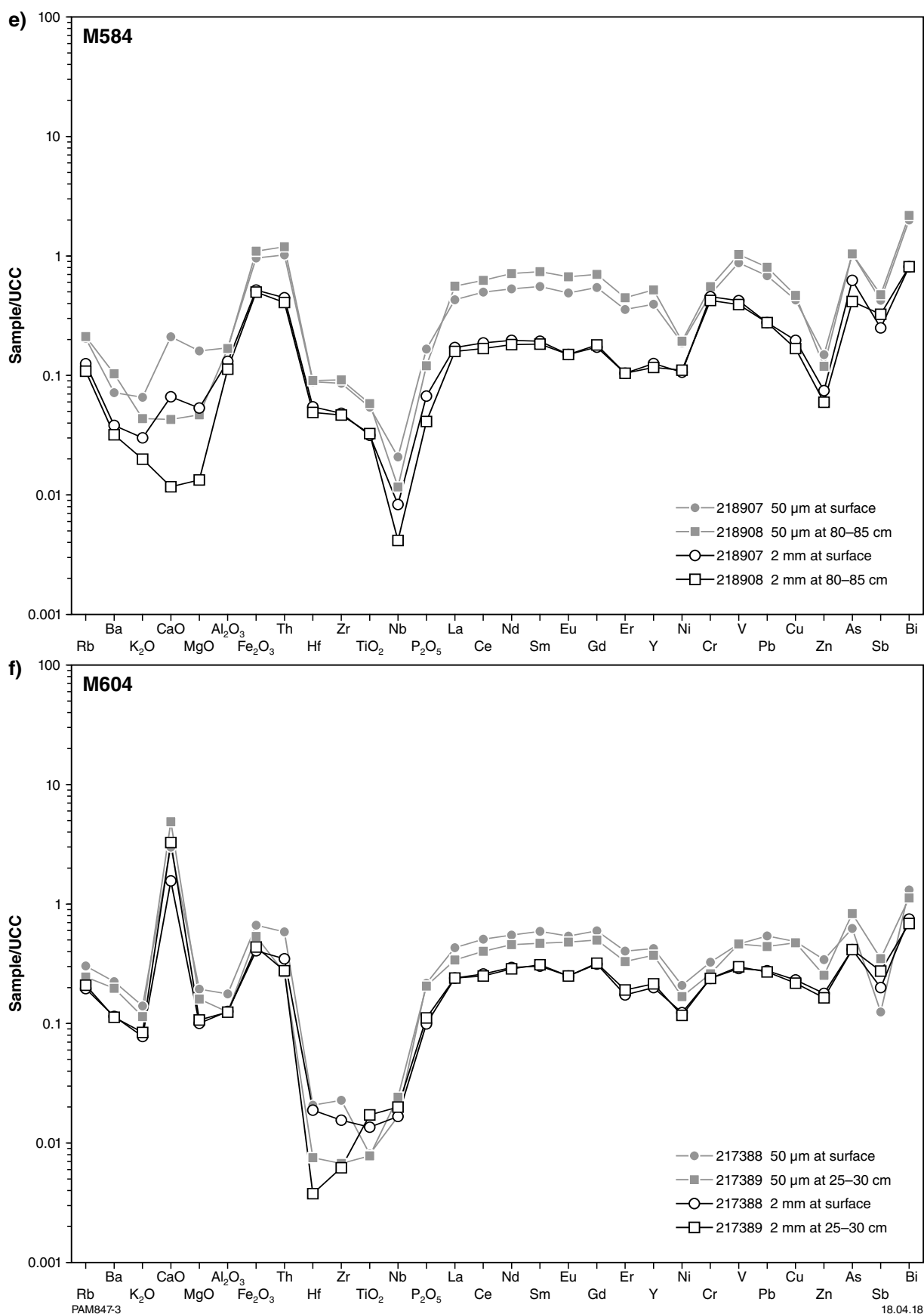


Figure 16. e) Site M584 (Noonkanbah Formation); f) site M604 (Hidden Basin beds)

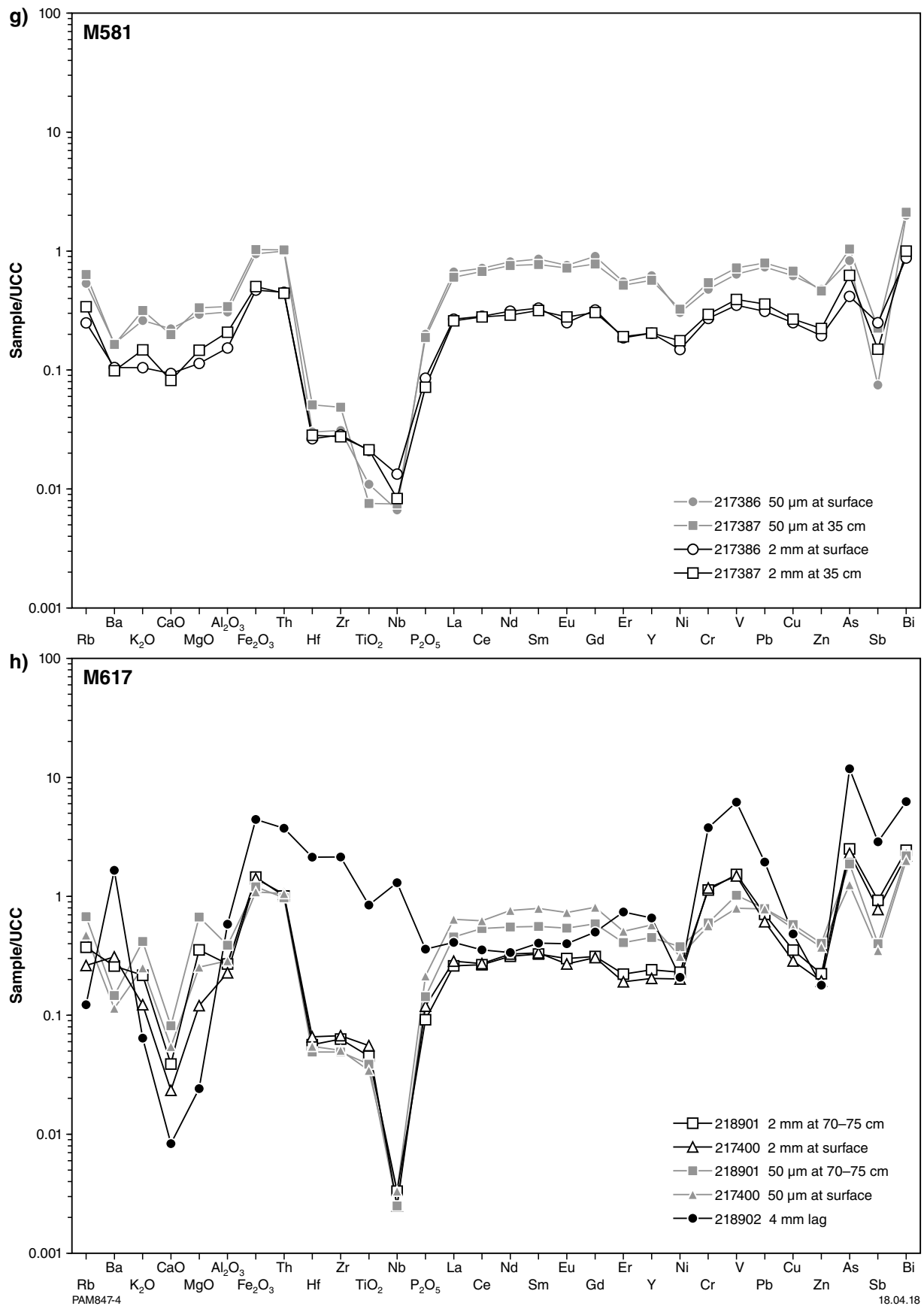


Figure 16. g) Site M581 (Redcliff Pound Group); h) site M617 (Liveringa Group)

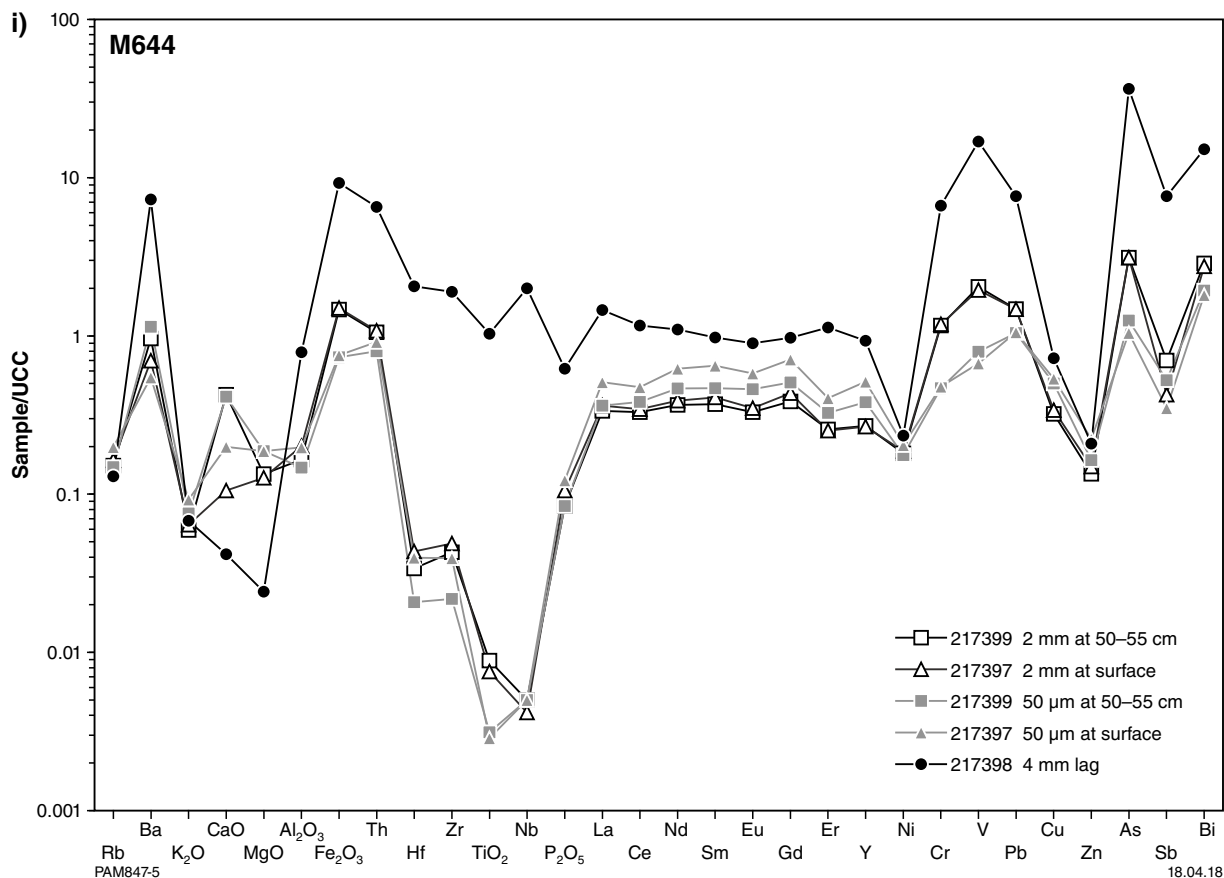


Figure 16. i) Site M644 (Liveringa Group)

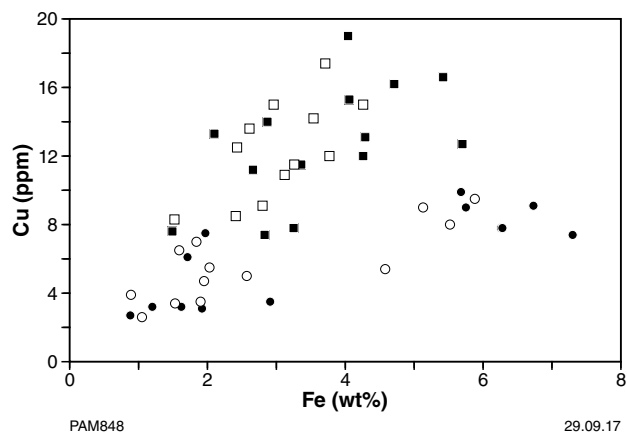


Figure 17. Variation in Cu (ppm) and Fe (wt%) in the <50 µm (squares) and <2 mm (circles) fractions of regolith from reconnaissance samples. Open symbols – surface samples; closed symbols – profile (subsurface) samples

Statistical treatment of regolith geochemical data

Most geochemical data have been statistically treated to generate class breaks for bubble plots of individual elements (Figs B20–B27), identify samples with anomalous concentrations, and compare sample populations on the basis of underlying bedrock lithology or regolith–landform unit. Similar to other regional regolith geochemical datasets (e.g., Morris and Verren, 2001; Morris, 2013), the Ngururrpa regolith geochemical data consist of a high proportion of samples with low concentrations for a number of analytes, resulting in a positively skewed distribution (Table 5). For some elements, there is a high proportion of samples that returned concentrations less than the lower level of detection (LLD) for a number of elements (Table 5); that is, the data are censored. In particular, for Ag, Au, Pd, Pt, Re, Se, Ta, Te, W and Cd, more than >30% of samples returned censored values, and data for these elements have not been treated statistically. For plotting and (where appropriate) statistical purposes, censored values have been replaced by a value equal to half the LLD (Reimann et al., 2008; Grunsky, 2010). As skewed sample populations do not show a normal distribution, a nonparametric approach for the comparison of medians has been used to compare different sample populations (Reimann et al., 2008).

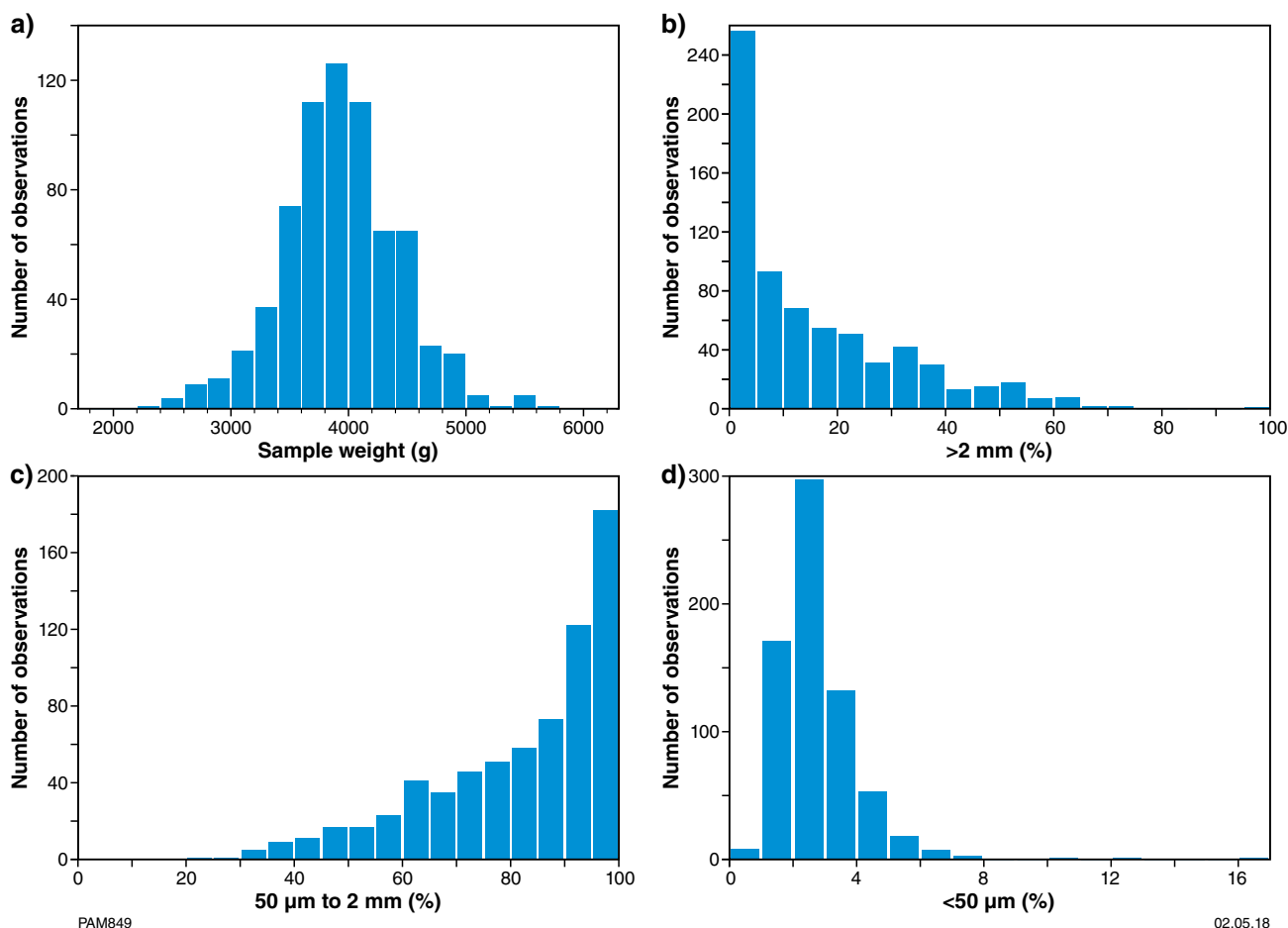


Figure 18. Screening results for Ngururupa regolith samples: a) weight of bulk sample (g); b) percentage of >2 mm fraction; c) percentage of >50 μm to <2 mm fraction; d) percentage of <50 μm fraction

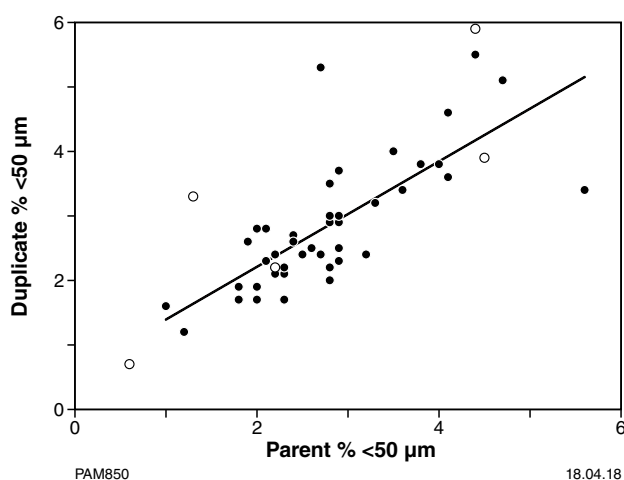


Figure 19. Comparison of percentage <50 μm in parent and site duplicate samples. Closed circles – parent and site duplicate from same screening batch (n = 46); open circles – parent and site duplicate from different screening batch (n = 6). For parent and duplicate samples screened in the same batch, $R^2 = 0.56$, slope of line = 0.82

In the bubble plots (Figs B20–B27), the diameter of the bubble is proportional to the analyte concentration, apart from anomalous concentrations, which are shown as stars. For data that have been treated statistically, class boundaries correspond to the 10th, 25th, 50th (i.e. median), and 75th percentiles. Anomalous concentrations have been identified using box and whisker plots (Reimann et al., 2008), and are divided into either outlier (purple stars) or extreme (red stars) values. Outlier values are those that exceed a value equal to 75th percentile + $(1.5 \times [\text{interquartile range}])$, but are less than the extreme boundary, which is defined as 75th percentile + $(3 \times [\text{interquartile range}])$. For data that have not been treated statistically, class boundaries correspond to natural breaks in the data. Samples with statistically anomalous analyte concentrations, detectable Pt and Ag, and Au ≥ 4 ppb are listed in Appendix 6.

Selected statistics for regolith geochemical data are shown in Table 5. Median values and a limited number of statistical parameters for regolith according to lithological unit are shown in Table 6, and median, maximum and minimum values for regolith according to primary code subdivision are shown in Table 7.

Table 5. Regolith chemistry statistics, and class intervals for bubble plots and identifying samples with anomalous element concentrations. Abbreviations: LLD, lower level of detection; SD, standard deviation; Min, minimum; Max, maximum; QR, quartile range; SK, skewness

Analyte	Unit	LLD	Method	No. < LLD	% < LLD	Mean	SD	Min	10th percentile	25th percentile	Median	75th percentile	Outlier	Extreme	Max	Range	QR	SK
Au	ppb	1	ARU10/MS	195	30.6	1.58		<1			1.00				63	63		
Ag	ppm	0.05	ARU10/MS	617	96.9	0.03		<0.05			0.03				0.19	0.19		
Al	ppm	20	ARU10/OE	0	0.0	12257	5726	785	6504	7997	10536	15186	25970	36753	33544	32759	7189	0.99
Al ₂ O ₃	wt%		Calculated	0	0.0	2.32	1.08	0.15	1.23	1.51	1.99	2.87	4.91	6.94	6.34	6.19	1.36	0.99
As	ppm	1	ARU10/MS	19	3.0	4	3.2	<1	1	2	3	5	10	14	33	33	3	3.64
Ba	ppm	1	ARU10/MS	0	0.0	99	130.9	3	22	33	59	109	223	337	1181	1178	76	4.38
Be	ppm	0.05	ARU10/MS	1	0.2	0.71	0.36	<0.05	0.34	0.45	0.64	0.90	1.58	2.25	3.38	3.38	0.45	1.84
Bi	ppm	0.01	ARU10/MS	0	0.0	0.25	0.08	0.02	0.17	0.20	0.24	0.31	0.48	0.64	0.73	0.71	0.11	0.72
Ca	%	0.01	ARU10/OE	0	0.0	0.47	1.59	0.02	0.040	0.050	0.09	0.20	0.43	0.65	15.12	15.10	0.150	6.07
CaO	wt%		Calculated	0	0.0	0.65	2.23	0.03	0.06	0.07	0.13	0.28	0.59	0.91	21.16	21.13	0.21	6.07
Cd	ppm	0.01	ARU10/MS	203	31.9			<0.01							0.08	0.08		
Ce	ppm	0.01	ARU10/MS	0	0.0	39.92	15.54	0.76	26.53	31.21	38.51	45.31	66	88	247.82	247.06	14.10	4.45
Co	ppm	0.1	ARU10/MS	0	0.0	6.9	3.17	0.5	3.2	4.4	6.5	8.7	15	22	22.5	22.0	4.3	0.99
Cr	ppm	1	ARU10/OE	0	0.0	33	9.47	2	23	26	30	38	56	74	77	75	12	0.81
Cs	ppm	0.01	ARU10/MS	0	0.0	1.16	0.58	0.11	0.66	0.79	0.99	1.37	2.24	3.11	4.79	4.68	0.58	2.13
Cu	ppm	0.5	ARU10/OE	0	0.0	9.1	4.15	1.4	4.5	6.0	8.1	11.7	20.25	28.80	26.4	25.0	5.7	0.99
Dy	ppm	0.01	ARU10/MS	0	0.0	2.21	0.74	0.05	1.46	1.73	2.11	2.60	3.91	5.21	7.46	7.41	0.87	1.23
Er	ppm	0.01	ARU10/MS	0	0.0	1.07	0.37	0.02	0.69	0.82	1.03	1.28	1.97	2.66	3.53	3.51	0.46	1.08
Eu	ppm	0.01	ARU10/MS	0	0.0	0.64	0.23	0.01	0.41	0.49	0.61	0.76	1.17	1.57	2.25	2.24	0.27	1.29
Fe	%	0.01	ARU10/OE	0	0.0	2.75	0.96	0.13	1.73	2.03	2.54	3.43	5.53	7.63	6.66	6.53	1.40	0.59
Fe ₂ O ₃	wt%		Calculated	0	0.0	3.94	1.37	0.19	2.47	2.90	3.63	4.90	7.91	10.91	9.52	9.34	2.00	0.59
Ga	ppm	0.05	ARU10/MS	0	0.0	6.04	2.32	0.32	3.49	4.31	5.61	7.68	12.74	17.79	20.90	20.58	3.37	0.85
Gd	ppm	0.05	ARU10/MS	0	0.0	3.02	1.03	0.07	2.01	2.37	2.87	3.51	5.22	6.93	10.56	10.49	1.14	1.41
Hf	ppm	0.01	ARU10/MS	0	0.0	0.18	0.08	0.01	0.09	0.13	0.17	0.21	0.33	0.45	0.60	0.59	0.08	1.32
Hg	ppm	0.01	ARU10/MS	42	6.6	0.03	0.03	0.01	0.01	0.02	0.03	0.03	0.05	0.06	0.22	0.22	0.01	3.57
Ho	ppm	0.01	ARU10/MS	0	0.0	0.40	0.14	0.01	0.25	0.31	0.38	0.48	0.74	0.99	1.35	1.34	0.17	1.17
In	ppm	0.01	ARU10/MS	13	2.0	0.03	0.01	0.01	0.02	0.02	0.03	0.04	0.07	0.10	0.09	0.09	0.02	0.55
K	ppm	20	ARU10/OE	0	0.0	1510	1632.42	216	416	570	902	1696	3385	5074	11884	11668	1126	2.90
K ₂ O	wt%		Calculated	0	0.0	0.18	0.20	0.03	0.05	0.07	0.11	0.20	0.41	0.61	1.43	1.41	0.14	2.90
La	ppm	0.01	ARU10/MS	0	0.0	1760	5.55	0.30	11.99	14.14	17.12	20.23	29.37	38.50	56.40	56.10	6.09	1.28
Li	ppm	0.1	ARU10/MS	0	0.0	8.0	5.47	0.5	3.0	4.1	6.4	10.2	19.4	28.5	33.4	32.9	6.1	1.70
Lu	ppm	0.01	ARU10/MS	4	0.6	0.12	0.04	0.01	0.08	0.09	0.12	0.15	0.24	0.33	0.39	0.39	0.06	1.04
Mg	%	0.01	ARU10/OE	0	0.0	0.13	0.21	0.01	0.02	0.04	0.06	0.14	0.29	0.44	3.45	3.44	0.10	7.55
MgO	wt%		Calculated	0	0.0	0.21	0.35	0.02	0.03	0.07	0.10	0.23	0.48	0.73	5.72	5.70	0.17	7.55
Mn	ppm	1	ARU10/OE	0	0.0	266	176.58	21	110	147	226	335	617	899	2564	2543	188	4.35
MnO	wt%		Calculated	0	0.0	0.03	0.02	0.00	0.01	0.02	0.03	0.04	0.08	0.12	0.33	0.33	0.02	4.35
Mo	ppm	0.1	ARU10/MS	3	0.5	0.4	0.17	0.1	0.3	0.3	0.4	0.5	0.8	1.1	1.4	1.4	0.2	0.98

Table 5. continued

Analyte	Unit	LLD	Method	No. < LLD	% < LLD	Mean	SD	Min	10th percentile	25th percentile	Median	75th percentile	Outlier	Extreme	Max	Range	QR	SK
Na	%	0.01	ARU10/OE	18	2.8	0.05	0.14	0.01	0.01	0.02	0.02	0.03	0.05	0.06	2.13	2.13	0.01	8.42
Na ₂ O	wt%		Calculated	18	2.8	0.07	0.19	0.01	0.01	0.03	0.03	0.04	0.06	0.08	2.87	2.87	0.01	8.42
Nb	ppm	0.02	ARU10/MS	11	1.7	0.16	0.09	0.01	0.05	0.09	0.16	0.21	0.39	0.57	0.68	0.67	0.12	1.04
Nd	ppm	0.01	ARU10/MS	0	0.0	18.77	6.25	0.32	12.66	14.87	18.01	21.51	31.47	41.43	55.89	55.57	6.64	1.34
Ni	ppm	0.5	ARU10/OE	0	0.0	8.8	5.33	1.4	4.1	5.2	7.5	11.0	19.7	28.4	54.2	52.8	5.8	2.57
P	ppm	20	ARU10/OE	0	0.0	109	36.89	37	69	83	104	127	193	259	344	307	44	1.45
P ₂ O ₅	wt%		Calculated	0	0.0	0.03	0.01	0.01	0.02	0.02	0.02	0.03	0.04	0.06	0.08	0.07	0.01	1.45
Pb	ppm	0.5	ARU10/MS	0	0.0	9.7	3.61	0.7	5.8	7.2	9.1	11.8	18.7	25.6	31.8	31.1	4.6	1.28
Pd	ppb	10	ARU10/MS	637	100.0			<10							<10	0		
Pr	ppm	0.01	ARU10/MS	0	0.0	4.81	1.56	0.08	3.31	3.80	4.69	5.52	8.10	10.68	13.66	13.58	1.72	1.25
Pt	ppb	5	ARU10/MS	632	99.2			<5							7	7		
Rb	ppm	0.02	ARU10/MS	0	0.0	18.67	11.21	1.33	8.85	11.05	14.92	23.12	41.23	59.33	88.44	87.11	12.07	2.00
Re	ppm	0.001	ARU10/MS	621	97.5			<0.001							0.01	0.001		
S	ppm	50	ARU10/OE	2	0.3	737	3476.27	25	106	121	143	204	329	453	31351	31326	83	7.28
Sb	ppm	0.02	ARU10/MS	3	0.5	0.20	0.52	0.01	0.08	0.10	0.14	0.19	0.33	0.46	9.11	9.10	0.09	14.75
Sc	ppm	0.1	ARU10/MS	0	0.0	5.7	2.06	0.2	3.4	4.3	5.6	7.0	11.1	15.1	18.8	18.6	2.7	0.66
Se	ppm	1	ARU10/MS	636	99.8			<1							1	1		
Sm	ppm	0.01	ARU10/MS	0	0.0	3.71	1.3	0.08	2.46	2.90	3.55	4.26	6.30	8.34	11.98	11.90	1.36	1.4
Sn	ppm	0.05	ARU10/MS	0	0.0	1.68	0.56	0.08	1.06	1.25	1.57	2.10	3.38	4.65	4.59	4.51	0.85	0.59
Sr	ppm	0.02	ARU10/MS	0	0.0	24.00	69.05	2.26	4.22	5.76	9.27	20.49	42.59	64.68	1264.15	1261.89	14.73	11.62
Ta	ppm	0.01	ARU10/MS	637	100.0			<0.01							<0.01			
Tb	ppm	0.01	ARU10/MS	1	0.2	0.42	0.14	0.01	0.28	0.33	0.41	0.49	0.73	0.97	1.40	1.40	0.16	1.22
Te	ppm	0.05	ARU10/MS	537	84.3			<0.05							0.15	0.15		
Th	ppm	0.01	ARU10/MS	0	0.0	9.93	2.61	0.23	7.09	8.38	9.97	11.38	15.88	20.38	22.50	22.27	3.00	0.07
Ti	ppm	5	ARU10/OE	5	0.8	176	8770	3	44	111	184	240	434	627	422	420	129	-0.06
TiO ₂	wt%		Calculated	5	0.8	0.03	0.01	0.00	0.01	0.02	0.03	0.04	0.07	0.10	0.07	0.07	0.02	-0.06
Tl	ppm	0.01	ARU10/MS	1	0.2	0.15	0.08	0.01	0.08	0.09	0.13	0.20	0.37	0.53	0.69	0.69	0.11	1.67
Tm	ppm	0.01	ARU10/MS	3	0.5	0.14	0.05	0.01	0.09	0.11	0.13	0.17	0.26	0.35	0.46	0.46	0.06	1.11
U	ppm	0.01	ARU10/MS	0	0.0	1.25	0.60	0.15	0.78	0.93	1.16	1.39	2.08	2.77	8.05	7.90	0.46	4.56
V	ppm	2	ARU10/OE	0	0.0	64	24.47	3	40	47	58	77	122	167	197	194	30	1.12
W	ppm	0.05	ARU10/MS	567	89.0			<0.05				0.17			0.17	0.15		
Y	ppm	0.02	ARU10/MS	0	0.0	10.16	3.64	0.25	6.34	7.65	9.69	12.14	18.88	25.61	33.69	33.44	4.49	1.13
Yb	ppm	0.01	ARU10/MS	0	0.0	0.87	0.29	0.02	0.55	0.68	0.84	1.03	1.56	2.08	2.78	2.76	0.35	1.09
Zn	ppm	1	ARU10/OE	0	0.0	13	7.59	2	7	8	11	15	26	36	70	68	7	2.36
Zr	ppm	0.1	ARU10/MS	0	0.0	7.2	2.83	0.2	4.0	5.5	7.0	8.5	13.0	17.5	19.9	19.7	3.0	0.78

NOTE: Rows shaded grey are analytes for which data are censored

Precious metals (Ag, Au, Pd and Pt)

Only 20 samples returned detectable Ag (LLD = 0.05 ppm), of which only four have concentrations >0.1 ppm (Fig. B20a). Six of the samples with detectable Ag are from the Redcliff Pound Group, six from the Hidden Basin beds, and five samples are from the Liveringa Group. Sample 221027* (M839†, regolith over quartz-rich siliciclastic sedimentary rocks, *Xqs*) from the Redcliff Pound Group has the highest Ag concentration of 0.19 ppm.

Thirty-one percent of samples returned censored data for Au (LLD = 1 ppb; Table 5), and of the samples with detectable Au, only 76 returned concentrations of >2 ppb (Fig. B20b). The maximum Au concentration of 63 ppb is in 221058 (M91, colluvium, *C*) from the Redcliff Pound Group in the northern part of the program area. An adjacent sample over the same lithological unit (220759; M63, regolith from longitudinal dunefield, *E_l*) has 7 ppb Au. Other samples in this area with elevated Au concentrations include 220709 (16 ppb; M109, Liveringa Group, *E_l*), 220848 (5 ppb; M53, Millyit Sandstone, *E_l*), and 220663 (6 ppb; M56, Granites–Tanami Orogen, sheetwash, *W*). To the southwest, 221169 from the Liveringa Group (M558, *E_l*) has 10 ppb Au. Of the 76 regolith samples with >2 ppb Au, 24 are from the Redcliff Pound Group, 19 are from the Liveringa Group, and 13 are from the Hidden Basin beds.

Platinum group element (PGE) concentrations are low. Only five regolith samples have detectable concentrations of Pt (>5 ppb), and no samples returned detectable concentrations of Pd (Table 5; Appendix 6). The two samples with the highest Pt concentration of 7 ppb (Fig. B20c) are both from areas of longitudinal dunefield (*E_l*) over the Granites–Tanami Orogen (220621; M169) and a nearby sample from the Liveringa Group (221232; M195).

Chalcophile elements

Chalcophile elements in low concentrations in regolith from the Ngururrpa program area (Fig. B21a–h; Tables 6, 7) include Bi, Mo and Sb, which have median values <1 ppm. A high proportion of samples returned censored values for Cd, Re, Se, Te and W.

Arsenic concentrations range from <1 to 33 ppm. All samples with statistically anomalous concentrations of As (>10 ppm) are from the Canning Basin (Fig. B21a), in particular the Liveringa Group (12 samples) and the Noonkanbah Formation (six samples). Despite this, the median content of As according to lithological unit shows a limited range of 2–4 ppm. The maximum As concentration of 33 ppm is in Fe-rich sheetwash (221364; M620, *W_f*) from the Liveringa Group. In terms of regolith type, the highest median value and widest range in As concentration is shown by sheetwash (*W*). Of the 20 samples with anomalous As concentrations, nine are from areas of iron-rich regolith (*W_f*, *R_{fs}*, or *R_{h_m}*).

Median values for Bi according to lithological unit also show a limited range (Table 6). Concentrations are low, with a maximum value of only 0.73 ppm, in 220833 (E8767, dune and playa terrain, *L_m*) from the Redcliff Pound Group (Fig. B21b). The other sample with anomalous Bi is 220955 (0.52 ppm; M592, Fe-rich sheetwash from the Liveringa Group, *W_f*), which also has anomalous As (22 ppm).

Almost 32% of Cd data are censored (LLD = 0.01 ppm), and the maximum concentration of Cd is only 0.08 ppm. A high proportion of samples with detectable Cd are found in regolith from the Redcliff Pound and Liveringa Groups (Fig. B21c).

Of the 13 samples with anomalous concentrations of Mo (>0.8 ppm), all but one are from the Canning Basin, including eight from the Liveringa Group (Fig. B21d). A sample from this unit with the highest Mo concentration of 1.4 ppm (221364; M620, Fe-rich sheetwash, *W_f*) also has the highest concentration of As (33 ppm) and Cd (0.08 ppm). Another sample of Fe-rich sheetwash from the same unit has 1.2 ppm Mo.

Eighty-three samples have anomalous sulfur concentrations (Fig. B21e), of which 61 have extreme concentrations >453 ppm. Thirty-nine samples have concentrations >1000 ppm. Median S values according to lithological unit show a limited range of 122–250 ppm (Table 6), with most values <150 ppm. A high number of samples with anomalous concentrations are from the Redcliff Pound Group in areas of salt lakes. Approximately equal numbers of samples with anomalous concentrations occur over the Hidden Basin beds and Liveringa Group. In terms of regolith type, there is a wide range in S concentration for samples from areas of bedrock. Samples from lacustrine regolith (*L*) and residual or relict regolith (*R*) also have high S contents.

Median values for Sb show a limited range from 0.12 – 0.17 ppm for regolith according to lithological unit (Table 6). Thirty-four regolith samples have anomalous Sb concentrations of (>0.33 ppm), with most samples from either the Liveringa Group or Noonkanbah Formation (Fig. B21f), but the maximum Sb concentration of 9.11 ppm is in sample 221296 (M907, *E_l*) from the Redcliff Pound Group in the southeast of the program area. A nearby sample from the same unit (220659; M942, *E_l*) has 3.74 ppm Sb.

A high proportion of samples returned censored data for both Te and W (Table 5), and the maximum concentration of both elements is low (Te = 0.15 ppm and W = 0.17 ppm). Thirty-six of the 76 regolith samples with detectable Te are from the Liveringa Group (Fig. B21g), including the sample with the highest Te content of 0.15 ppm (220790; SRT10, regolith over quartz-rich siliciclastic sedimentary rocks, *Xqs*), which also has anomalous As (30 ppm). Thirty of the 64 samples with detectable W (i.e. >0.05 ppm) are from the Redcliff Pound Group, but the sample with the highest W content of 0.17 ppm (221048; M83, *E_l*) is from the Granites–Tanami Orogen in the north of the program area (Fig. B21h). This sample also has anomalous Sb (0.36 ppm).

* Six-digit numbers in the remainder of the document refer to GSWA sample numbers

† Three- or four-digit numbers prefixed by 'M' or 'E' are regolith sampling site numbers

Table 6. Median, minimum, and maximum values for regolith chemistry according to lithological unit

Analyte	LLD	Unit	Granites-Tanami (n = 26)			Hidden Basin beds (n = 127)			Munyu Sandstone (n = 11)			Redcliff Pound Group (n = 150)			Lucas Formation (n = 6)			Undivided Mesozoic (n = 37)		
			Median	Min	Max	Median	Min	Max	Median	Min	Max	Median	Min	Max	Median	Min	Max	Median	Min	Max
TiO ₂		wt%	0.03	0.02	0.06	0.03	0.00	0.06	0.04	0.01	0.07	0.03	0.00	0.07	0.02	0.00	0.04	0.03	0.00	0.07
Al ₂ O ₃		wt%	1.53	0.70	3.67	2.07	0.30	6.34	2.52	1.20	4.70	1.90	0.15	5.84	3.05	2.00	5.56	1.89	1.01	3.88
Fe ₂ O ₃		wt%	3.02	1.92	5.75	3.46	0.40	6.25	3.93	2.19	5.89	3.52	0.19	6.89	4.74	3.12	7.55	3.57	2.32	9.01
MnO		wt%	0.024	0.008	0.045	0.028	0.006	0.148	0.041	0.018	0.097	0.031	0.003	0.093	0.041	0.016	0.080	0.024	0.009	0.073
MgO		wt%	0.05	0.02	0.30	0.10	0.03	1.77	0.12	0.08	5.72	0.13	0.03	1.67	0.32	0.12	0.90	0.08	0.03	0.93
CaO		wt%	0.07	0.04	0.27	0.13	0.04	21.16	0.14	0.10	6.39	0.15	0.04	10.98	0.26	0.08	0.50	0.08	0.06	0.92
K ₂ O		wt%	0.06	0.03	0.24	0.12	0.03	1.43	0.16	0.08	0.53	0.14	0.03	1.34	0.21	0.13	0.54	0.09	0.04	0.75
Na ₂ O		wt%	0.02	<0.01	0.05	0.03	<0.01	0.93	0.04	0.03	1.73	0.03	<0.01	2.87	0.03	0.01	0.38	0.03	0.01	0.92
P ₂ O ₅		wt%	0.018	0.010	0.029	0.025	0.012	0.049	0.027	0.022	0.036	0.025	0.008	0.068	0.032	0.022	0.048	0.022	0.013	0.065
Ag	0.05	ppm	<0.05	<0.05	0.06	<0.05	<0.05	0.11	<0.05	<0.05	<0.05	<0.05	<0.05	0.19	<0.05	<0.05	<0.05	<0.05	<0.05	0.06
Al	20	ppm	8081	3690	19442	10970	1562	33544	13353	6366	24869	10034	785	30935	16122	10569	29440	9978	5368	20542
As	1	ppm	2	1	6	2	1	10	2	<1	5	2	<1	7	4	2	5	3	1	30
Au	1	ppb	<1	<1	6	<1	<1	6	<1	<1	3	<1	<1	63	<1	<1	3	<1	<1	4
Ba	1	ppm	58	12	216	61	16	869	87	25	526	71	3	661	216	45	949	53	16	1015
Be	0.05	ppm	0.58	0.23	0.96	0.62	0.08	1.37	0.91	0.30	1.44	0.64	<0.05	2.92	1.09	0.63	3.38	0.68	0.30	1.47
Bi	0.01	ppm	0.22	0.14	0.37	0.23	0.04	0.42	0.30	0.14	0.40	0.23	0.02	0.73	0.28	0.20	0.41	0.22	0.15	0.41
Ca	0.01	ppm	0.05	0.03	0.19	0.09	0.03	15.12	0.10	0.07	4.57	0.11	0.03	7.85	0.19	0.06	0.36	0.06	0.04	0.66
Cd	0.01	ppm	<0.01	<0.01	0.03	<0.01	<0.01	0.07	<0.01	<0.01	0.07	<0.01	<0.01	0.08	<0.01	<0.01	0.05	<0.01	<0.01	0.04
Ce	0.01	ppm	30.87	20.75	5705	39.27	1.33	102.16	45.30	13.95	59.74	40.21	0.76	89.75	79.19	45.28	98.91	40.27	23.91	109.09
Co	0.1	ppm	5.3	2.1	10.2	6.4	0.8	17.8	7.9	2.7	12.9	6.7	0.5	21.9	9.7	3.6	20.1	6.1	2.4	14.2
Cr	1	ppm	25	19	62	29	4	45	31	23	41	28	2	50	35	28	47	30	22	59
Cs	0.01	ppm	0.89	0.46	2.14	0.98	0.20	4.52	1.48	0.61	2.80	1.01	0.11	4.79	1.25	0.72	2.22	1.09	0.56	2.53
Cu	0.5	ppm	6.3	2.7	13.2	8.4	2.6	20.6	11.8	5.8	22.5	9.2	1.4	26.4	12.7	7.9	18.6	7.7	3.7	18.7
Dy	0.01	ppm	2.20	1.23	3.45	2.02	0.15	4.03	2.92	0.88	3.75	2.25	0.05	5.55	3.38	2.76	7.46	2.22	1.29	4.88
Er	0.01	ppm	1.10	0.54	1.75	0.98	0.08	1.86	1.47	0.55	1.90	1.09	0.02	2.80	1.59	1.40	3.53	1.07	0.63	1.85
Eu	0.01	ppm	0.64	0.31	1.06	0.58	0.03	1.34	0.84	0.27	1.13	0.64	0.01	1.55	1.21	0.81	2.25	0.65	0.35	1.50
Fe	0.01	ppm	2.11	1.34	4.02	2.42	0.28	4.37	2.75	1.53	4.12	2.46	0.13	4.82	3.32	2.18	5.28	2.50	1.62	6.30
Ga	0.05	ppm	4.62	2.76	9.33	5.33	0.59	11.88	6.04	2.85	10.14	4.92	0.32	20.90	7.62	4.06	10.51	5.41	3.31	11.64
Gd	0.05	ppm	2.88	1.58	4.87	2.79	0.18	5.46	4.00	1.14	5.45	3.09	0.07	7.67	5.22	3.69	10.56	3.05	1.92	7.90
Hf	0.01	ppm	0.17	0.10	0.37	0.16	0.01	0.37	0.15	0.09	0.23	0.16	0.01	0.60	0.18	0.08	0.29	0.17	0.05	0.47
Hg	0.01	ppm	0.02	<0.01	0.05	0.03	<0.01	0.15	0.03	<0.01	0.21	0.03	<0.01	0.22	0.03	0.03	0.16	0.02	<0.01	0.12
Ho	0.01	ppm	0.40	0.20	0.65	0.36	0.03	0.74	0.55	0.19	0.71	0.41	0.01	1.07	0.59	0.52	1.35	0.41	0.23	0.77
In	0.01	ppm	0.03	0.02	0.06	0.03	<0.01	0.07	0.03	<0.01	0.05	0.03	<0.01	0.09	0.05	0.02	0.06	0.03	0.01	0.08
K	20	ppm	523	238	1968	1015	222	11884	1321	689	4431	1165	224	11115	1780	1052	4518	754	305	6191
La	0.01	ppm	16.95	10.42	2758	1758	0.70	36.79	20.54	6.40	27.21	18.16	0.30	35.39	33.76	21.45	49.16	18.04	11.96	56.40
Li	0.1	ppm	4.5	1.3	24.7	6.7	1.1	22.2	8.3	3.4	17.0	6.3	0.5	33.4	10.4	3.5	15.2	5.2	2.0	26.3
Lu	0.01	ppm	0.12	0.06	0.20	0.11	<0.01	0.22	0.17	0.07	0.22	0.12	<0.01	0.34	0.17	0.16	0.39	0.12	0.07	0.18
Mg	0.01	ppm	0.03	0.01	0.18	0.06	0.02	1.07	0.07	0.05	3.45	0.08	0.02	1.01	0.19	0.07	0.54	0.05	0.02	0.56
Mn	1	ppm	189	65	351	214	47	1143	314	137	750	239	21	720	320	124	616	187	71	569
Mo	0.1	ppm	0.4	0.2	0.7	0.4	<0.1	1.0	0.5	0.1	0.7	0.4	<0.1	0.8	0.4	0.2	0.5	0.5	0.2	0.9
Na	0.01	ppm	0.02	<0.01	0.04	0.02	<0.01	0.69	0.03	0.02	1.28	0.02	<0.01	2.13	0.03	0.01	0.28	0.02	0.01	0.68
Nb	0.02	ppm	0.18	0.05	0.44	0.15	<0.02	0.41	0.13	<0.02	0.21	0.17	<0.02	0.67	0.05	0.				

Table 6. continued

Analyte	LLD	Unit	Poole Sandstone (n = 4)			Noonkanbah Formation (n = 48)			Livingina Group (n = 168)			Mililyt Sandstone (n = 5)			Callawa Formation (n = 51)		
			Median	Min	Max	Median	Min	Max	Median	Min	Max	Median	Min	Max	Median	Min	Max
TiO ₂		wt%	0.04	0.04	0.05	0.03	0.00	0.06	0.03	0.00	0.06	0.04	0.03	0.05	0.04	0.01	0.07
Al ₂ O ₃		wt%	1.67	1.52	2.68	2.31	1.19	6.04	2.43	0.74	5.43	1.45	1.12	2.23	1.52	0.88	3.71
Fe ₂ O ₃		wt%	3.57	3.26	5.76	3.85	2.20	7.41	4.45	1.54	9.52	2.73	2.44	5.59	3.05	2.09	6.18
MnO		wt%	0.025	0.014	0.048	0.025	0.012	0.096	0.035	0.008	0.331	0.022	0.015	0.062	0.019	0.011	0.087
MgO		wt%	0.05	0.03	0.07	0.11	0.03	2.06	0.12	0.03	1.64	0.03	0.03	0.08	0.05	0.02	0.27
CaO		wt%	0.06	0.04	0.08	0.13	0.03	15.75	0.15	0.03	15.52	0.07	0.06	0.21	0.06	0.03	0.66
K ₂ O		wt%	0.07	0.05	0.09	0.12	0.04	0.99	0.12	0.04	0.92	0.05	0.04	0.09	0.05	0.03	0.20
Na ₂ O		wt%	0.04	0.04	0.05	0.04	<0.01	0.07	0.04	0.01	0.90	0.01	0.01	0.03	0.03	<0.01	0.08
P ₂ O ₅		wt%	0.019	0.018	0.024	0.024	0.016	0.079	0.025	0.010	0.049	0.016	0.015	0.027	0.019	0.011	0.043
Ag	0.05	ppm		<0.05	0.07		<0.05	<0.05		<0.05	0.16		<0.05	<0.05		<0.05	0.05
Al	20	ppm	8814	8053	14160	12240	6309	31965	12862	3934	28730	7649	5931	11791	8037	4640	19618
As	1	ppm	4	2	6	4	1	19	5	1	33	2	2	10	2	1	9
Au	1	ppb		1	2		<1	3		<1	16		<1	5		<1	3
Ba	1	ppm	30	24	52	51	16	412	74	15	1181	43	23	106	27	11	427
Be	0.05	ppm	0.45	0.42	0.99	0.63	0.25	1.53	0.74	0.20	2.36	0.45	0.31	0.78	0.38	0.19	1.11
Bi	0.01	ppm	0.24	0.20	0.36	0.24	0.16	0.47	0.27	0.08	0.52	0.20	0.16	0.34	0.200	0.130	0.40
Ca	0.01	ppm	0.04	0.03	0.06	0.09	0.02	11.26	0.11	0.02	11.09	0.05	0.04	0.15	0.04	0.02	0.47
Cd	0.01	ppm		<0.01	0.01		<0.01	0.05		<0.01	0.08		<0.01	0.02	0.010	<0.01	0.04
Ce	0.01	ppm	36.83	33.35	53.61	35.30	23.58	74.55	39.80	12.04	247.82	31.77	26.84	44.28	31.63	19.68	49.88
Co	0.1	ppm	5.2	3.7	9.9	5.9	2.7	18.5	7.7	1.9	22.5	4.1	2.5	12.4	4.6	2.3	12.0
Cr	1	ppm	31	29	52	34	21	57	37	17	77	25	23	42	28	18	52
Cs	0.01	ppm	0.93	0.73	1.13	1.01	0.62	3.12	1.06	0.37	4.18	0.74	0.62	1.19	0.79	0.43	1.66
Cu	0.5	ppm	5.8	5.1	7.0	7.5	3.8	21.6	8.7	2.4	25.7	5.4	4.2	7.5	5.1	1.8	13.4
Dy	0.01	ppm	1.97	1.89	2.27	2.11	1.33	4.10	2.18	0.64	5.42	2.04	1.68	2.06	1.67	1.14	2.87
Er	0.01	ppm	0.92	0.87	1.13	1.02	0.63	1.98	1.08	0.31	2.35	0.97	0.81	1.00	0.79	0.50	1.45
Eu	0.01	ppm	0.57	0.52	0.68	0.60	0.37	1.36	0.63	0.18	1.59	0.59	0.48	0.61	0.47	0.32	0.83
Fe	0.01	ppm	2.50	2.28	4.03	2.70	1.54	5.18	3.11	1.08	6.66	1.91	1.71	3.91	2.13	1.46	4.32
Ga	0.05	ppm	5.36	4.28	9.74	6.08	3.65	13.83	6.70	2.05	11.49	4.23	3.37	8.05	4.80	3.06	10.16
Gd	0.05	ppm	2.77	2.46	3.25	2.87	1.81	5.82	2.94	0.89	7.63	2.60	2.21	2.80	2.28	1.51	3.66
Hf	0.01	ppm	0.22	0.20	0.38	0.16	0.05	0.33	0.18	0.03	0.60	0.14	0.12	0.27	0.17	0.09	0.40
Hg	0.01	ppm	0.01	<0.01	0.04	0.03	<0.01	0.05	0.02	<0.01	0.18	0.02	0.02	0.03	0.02	<0.01	0.17
Ho	0.01	ppm	0.34	0.30	0.38	0.38	0.22	0.75	0.39	0.11	0.95	0.34	0.29	0.37	0.31	0.20	0.53
In	0.01	ppm	0.04	0.02	0.06	0.04	0.02	0.07	0.04	<0.01	0.09	0.02	0.02	0.05	0.03	<0.01	0.07
K	20	ppm	582	435	733	994	298	8253	972	296	7623	401	310	715	422	216	1619
La	0.01	ppm	15.94	14.15	19.83	16.64	10.08	33.96	17.14	5.72	29.31	15.23	14.24	17.55	13.97	9.05	22.07
Li	0.1	ppm	4.7	4.5	14.3	8.1	2.6	30.7	7.6	1.8	28.0	3.8	2.1	7.9	3.4	1.6	12.7
Lu	0.01	ppm	0.10	0.08	0.12	0.12	0.07	0.23	0.12	0.03	0.25	0.11	0.09	0.11	0.09	0.06	0.19
Mg	0.01	ppm	0.03	0.02	0.04	0.07	0.02	1.24	0.07	0.02	0.99	0.02	0.02	0.05	0.03	0.01	0.16
Mn	1	ppm	194	111	372	193	92	746	270	65	2564	167	119	483	147	84	676
Mo	0.1	ppm	0.5	0.3	0.6	0.4	0.2	1.0	0.5	<0.1	1.4	0.4	0.3	0.6	0.4	0.2	0.7
Na	0.01	ppm	0.03	0.03	0.04	0.03	<0.01	0.05	0.03	0.01	0.67	0.01	0.01	0.02	0.02	<0.01	0.06
Nb	0.02	ppm	0.17	0.14	0.22	0.18	0.02	0.43	0.13	<0.02	0.68	0.20	0.15	0.29	0.17	<0.02	0.46
Nd	0.01	ppm	17.05	15.24	20.01	17.77	11.03	37.41	17.86	6.04	37.94	16.61	14.83	18.03	14.68	10.08	23.17
Ni	0.5	ppm	5.0	4.6	6.7	7.2	3.7	20.9	8.2	3.1	30.5	4.5	3.0	9.3	4.6	2.6	25.8
P	20	ppm	85	78	105	103	68	344	109	44	212	68	65	118	81	47	189
Pb	0.5	ppm	7.9	6.8	14.1	8.9	5.2	17.8	11.0	3.8	26.7	6.2	5.6	11.7	7.4	4.9	17.6
Pd	10	ppb		<10	<10		<10	<10		<10	<10		<10	<10		<10	<10
Pr	0.01	ppm	4.56	4.06	5.60	4.64	2.94	8.80	4.70	1.59	9.26	4.18	3.73	4.43	3.71	2.61	6.11
Pt	5	ppb		<5	5		<5	<5		<5	7		<5	<5		<5	<5
Rb	0.02	ppm	12.01	9.87	16.04	18.48	7.88	72.28	16.27	6.19	73.34	9.54	7.57	17.01	9.92	5.96	24.93
Re	0.001	ppm		<0.001	<0.001		<0.001	0.001		<0.001	0.011		<0.001	<0.001		0.001	<0.001
S	50	ppm	135	109	170	146	62	267	137	25	5620	125	116	143	132	57	1750
Sb	0.02	ppm	0.17	0.11	0.44	0.16	0.06	0.52	0.15	0.03	1.92	0.12	0.10	0.15	0.13	0.03	0.25
Sc	0.1	ppm	5.7	5.0	7.5	5.6	3.1	11.8	6.5	1.9	12.6	4.5	3.8	6.8	4.9	2.8	9.6
Se	1	ppm		<1	<1		<1	<1		<1	<1		<1	<1		<1	<1
Sm	0.01	ppm	3.41	3.06	3.96	3.48	2.11	7.56	3.56	1.16	9.05	3.27	2.81	3.38	2.85	1.93	4.54
Sn	0.05	ppm	1.51	1.35	2.41	1.67	1.12	3.28	1.92	0.68	3.37	1.19	1.01	1.89	1.38	0.93	2.69
Sr	0.02	ppm	4.17	3.11	8.49	8.79	2.65	127.47	11.46	2.57	239.57	5.65	4.22	14.82	4.26	2.26	35.54
Ta	0.01	ppm		<0.01	<0.01		<0.01	<0.01		<0.01	<0.01		<0.01	<0.01		<0.01	<0.01
Tb	0.01	ppm	0.39	0.36	0.45	0.41	0.24	0.78	0.41	0.12	1.06	0.37	0.31	0.38	0.32	0.22	0.53
Te	0.05	ppm		<0.05	0.08		<0.05	0.06		<0.05	0.12		<0.05	0.12		<0.05	0.07
Th	0.01	ppm	10.29	8.55	15.65	9.98	4.70	18.70	10.98	2.89	16.80	7.95	7.29	12.17	9.62	5.82	17.09
Ti	5	ppm	247	229	292	164	24	362	179	3	372	252	191	272	231	53	422
Tl	0.01	ppm	0.10	0.08	0.16	0.13	0.07	0.43	0.15	0.04	0.51	0.11	0.07	0.18	0.08	0.05	0.25
Tm	0.01	ppm	0.13	0.11	0.14	0.14	0.08	0.26	0.14	0.04	0.31	0.12	0.11	0.13	0.11	0.07	0.20
U	0.01	ppm	1.05	0.87	1.36	0.96	0.43	1.74	1.13	0.33	2.73	1.03	0.95	1.30	0.92	0.52	1.77
V	2	ppm	65	54	98	62	38	133	78	23	166	47	40	106	55	37	197
W	0.05	ppm		<0.05	<0.05		<0.05	0.05		<0.05	0.09		<0.05	<0.05		<0.05	0.06
Y	0.02	ppm	7.94	7.52	10.28	9.78	5.17	19.79	9.95	3.05	23.15	9.01	7.37	9.52	7.41	4.59	13.81
Yb	0.01	ppm	0.78	0.64	0.92	0.86	0.52	1.57	0.88	0.26	1.86	0.74	0.64	0.86	0.68	0.42	1.25
Zn	1	ppm	9	8	10	12	7	41	11	5	59	7	6	11	7	4	30
Zr	0.1	ppm	8.8	7.6	17.6	6.9	1.9	15.8	7.6	1.1	19.6	5.8	5.4	10.7	7.4	4.4	15.1

NOTE: Rows shaded grey indicate analytes for which data are censored

Rare earth elements

Light rare earth elements (LREE; La–Eu)

Median LREE values for 10 of the 11 lithological units in Table 6 show a limited range (e.g. La: 15.23 – 20.54 ppm; Nd: 14.68 – 25.35; Eu: 0.47 – 0.84). The exception is the Lucas Formation, which has higher median values for all LREE. Several samples with anomalous LREE concentrations are from two areas in the southeast of the program area (Fig. B22a–e; Appendix 6), along with a number of samples from transects across the Stansmore Fault, including 220790 (SRT10, *Xqs*), which has the highest La content of 56.4 ppm. In terms of regolith type, there is little difference in the spread or median values for La, apart from lacustrine regolith (*L*) which has a lower median value and anomalously low La concentrations, and regolith from eolian sandplain (*E*) which has a high proportion of samples with anomalous La concentrations (Table 7). The highest Ce content of 247.82 ppm is in 222125 (M649, *Xqs*) from the Liveringa Group. Samples with anomalously high LREE concentrations in the southeast of the program area are close to the Lucas Formation, including 221188 (M902, *El*), which has the highest concentrations of Sm (11.98 ppm; Fig. B22d) and Nd (55.89 ppm; Fig. B22c). Europium shows similar behaviour to La and Ce.

Heavy rare earth elements (HREE; Gd–Yb, Y)

Many of the samples with anomalously high concentrations of LREE also have anomalous concentrations of HREE (Fig. B22f–j). Sample 221188 (M902, *El*) from the Lucas Formation close to the contact with the Redcliff Pound Group in the southeast of the program area has the highest concentrations of all HREE (Appendix 6), and nearby sample (221284; M866, *El*) also has extreme concentrations of all HREE. Median values of HREE are similar for different lithological units, apart from a higher median value for the Lucas Formation. In terms of regolith type, HREE show a similar behaviour to LREE. For example, HREE are generally lower in lacustrine regolith (*L*), and include some samples with anomalously low concentrations. A number of samples from areas of sandplain (*E*) have statistically high anomalous HREE concentrations (e.g. Fig. 22f,j).

Transition elements

Median values for Co in regolith according to lithological unit (Table 6) show a limited concentration range from 4.1 to 7.5 ppm, apart from a value of 9.7 ppm over the Lucas Formation (221188; Fig. B23a). Three samples with anomalous Co concentrations are from the Redcliff Pound Group. A sample of Fe-rich sheetwash from the Liveringa Group (221364; M620, *Wf*) has the highest Co concentration of 22.5 ppm.

Regolith samples with anomalous Cr concentrations are confined to regolith on or close to the Liveringa Group, including two samples from the SR transect, one of which (221257; SR16, *Wf*) has the highest Cr content of 77 ppm (Fig. B23b). As well as having the highest median value for Cr, regolith from this unit also has the widest range in Cr content of 17–77 ppm (Table 6). A box and whisker

plot for Cr according to regolith type shows that lacustrine regolith has a lower median value and a higher proportion of regolith samples with low Cr contents (Fig. B23b), as well as samples with anomalously low concentrations. There is a wide range in Cr content for residual or relict regolith, with a relatively high median value and a number of samples with high Cr concentrations from samples of sheetwash (*W*). Of the 12 samples with anomalous Cr concentrations, six are ferruginous.

Samples with anomalously high Ni concentrations show a different spatial distribution to samples with high Co and Cr (Fig. B23c). A cluster of eight samples with anomalous Ni concentrations ranging from 20 to 39 ppm are from part of the Redcliff Pound Group, where salt lakes are well developed, but the sample with the highest Ni content of 54.2 ppm (221188; M902, *El*) is from the Lucas Formation (Appendix 6). A group of four regolith samples in the southwest of the project area over the Callawa Formation, including relict regolith and sandplain, also have anomalous Ni concentrations from 20.0 to 25.8 ppm. Unlike Cr, the Ni content of lacustrine regolith (*L*) has a similar median value to other regolith types, but a high proportion of samples with elevated concentrations (Fig. 23c; Table 7). Nickel is notably lower in concentration in samples from areas of sheetwash (*W*).

The range in Sc concentration in regolith is 0.2 – 18.8 ppm (Fig. B23d), with a limited range in median values according to lithology of 4.5 – 7.6 ppm (Table 6). The Liveringa Group and the Noonkanbah Formation have a relatively high proportion of samples with anomalous Sc concentrations >11.1 ppm, but the sample with the highest Sc content of 18.8 ppm is 220833 (E8767, *L_m*) from the Redcliff Pound Group. In terms of regolith type, Sc shows similar behaviour to Cr, with lower concentrations in lacustrine regolith and higher concentrations in sheetwash.

Samples with high concentrations of V are similar to those with elevated Cr contents (Fig. 23e), and most samples with anomalous V concentrations are from the Liveringa Group. This is consistent with the higher median value for V from this lithological unit (75 ppm) compared to other units (Table 6). The sample with the highest V content is residual or relict Fe-rich duricrust developed over sedimentary rocks (*Rfs*; 221270, site M985) from the Callawa Formation, which also has anomalous concentrations of Ni. In areas of salt lakes on the Redcliff Pound Group, regolith samples have anomalously low concentrations of V. Considered by regolith type, the highest median value for V and the greatest number of samples with high V concentrations are from areas of sheetwash (Fig. B23e; Table 7).

Lithophile elements

Barium (Fig. B24a) shows a wide range in concentration from <0.05 to 1181 ppm. Nine of the 27 samples with extreme Ba concentrations (>337 ppm) are in regolith from the Liveringa Group, including 220741 (M612), from a bedded deposit adjacent to saline lakes (*L_g*) which has the highest Ba concentration of 1181 ppm (Appendix 6). Baryte was recorded at a number of sites with elevated Ba concentrations, and a number of samples

with high Ba concentrations from the Redcliff Pound Group are in lacustrine areas. Samples with anomalous Ba concentrations come from a variety of regolith–landform units, including regolith from areas of outcrop, (*X*), sheetwash (*W*), eolian sand (*E*), relict or residual (*R*), and lacustrine (*L*) units.

Samples with particularly high concentrations of Be (range <0.05 – 3.38 ppm) are on or close to the Lucas Formation and parts of the Liveringa Group (Fig. B24b). Median values for all lithological units are <1 ppm (Table 6), with a limited range in concentration.

Samples with anomalous concentrations of Cs (>2.24 ppm) are not confined to any particular lithological unit, but a number of high-Cs samples come from the Redcliff Pound Group and Hidden Basin beds, including six of the seven samples with extreme Cs concentrations (>3.11 ppm; Fig. B24c). Several other samples are from the Liveringa Group and Noonkanbah Formation. Median values (Table 6) are typically low (near 1 ppm). The range in Cs concentration of 0.11 – 4.79 ppm is wider for regolith from the Redcliff Pound Group than regolith from other lithological units.

Most samples with elevated Ga concentrations are in regolith from the Canning Basin (Fig. B24d), especially the Liveringa Group, which has a slightly higher median value of 6.55 ppm (Table 6), although the widest range in Ga concentration is in regolith from the Noonkanbah Formation (3.65 – 13.83 ppm). The maximum Ga concentration is in 220833 (E8767, L_m), from the Redcliff Pound Group.

Mercury shows a limited range in concentration (<0.01 to 0.22 ppm), with only 19 samples returning >0.1 ppm Hg. Three samples with relatively high Hg contents are on or close to the Redcliff Pound Group, including 221106 (M743, Xls) with the maximum concentration of 0.22 ppm. A number of samples with anomalous Hg concentrations of >0.05 ppm are from batch 3, and the bubble plot for Hg (Fig. B24e) should be viewed with caution.

The median concentrations of indium (In) in regolith according to lithological unit are all <0.1 ppm (Table 6), and the maximum In concentration is only 0.09 ppm (Fig. B24f). Some of the highest values and one of the widest ranges of In concentration are in regolith from the Liveringa Group (<0.01 – 0.9 ppm). Indium concentrations are generally higher in sheetwash (cf. Sc, Cr, V), with lower concentrations in lacustrine and eolian regolith (Table 7). There is a wider range in In concentrations in regolith from areas of outcrop, and in residual–relict regolith.

Lithium ranges from 0.5 – 33.4 ppm (Fig. B24g). The two samples with the highest Li content are from the Redcliff Pound Group, 220833 (M8767, L_m) with 33.4 ppm, which also has the highest concentration of Sc (18.8 ppm), and sample 221241 (M9243, Xqs) with 32.1 ppm Li. The remaining four samples with extreme concentrations of Li (29.4 – 30.7 ppm) are from the Noonkanbah Formation, all of which are relict or residual (Appendix 6). The linear distribution of anomalous samples over parts of the Noonkanbah Formation (north–south) and Liveringa Group (east–west; Fig. B24g) is unlikely to be analytical, as samples are from a number of batches. Box and whisker

plots show the wide range in Li contents of regolith from the Redcliff Pound Group, Noonkanbah Formation, and Liveringa Group (Fig. B24g; Table 6). Considered by regolith type, samples from areas of eolian (*E*) and relict–residual regolith (*R*), and regolith in areas of outcrop (*X*), show a relatively wide range in Li content. Three of the four samples with extreme concentrations of Li are from areas of groundwater calcrete (R_{kg}).

Some of the highest Rb concentrations in regolith are seen in samples from the Redcliff Pound Group (Fig. B24h), in which Rb ranges from 1.3 to 88.4 ppm (Table 6). However, among the 33 samples with anomalous Rb concentrations (>41.2 ppm), there are roughly equal numbers of samples from the Redcliff Pound Group, Hidden Basin beds, and Noonkanbah Formation. Samples with high Rb concentrations throughout the project area also have elevated Li contents, including 220833 (M9243, Redcliff Pound Group), which has 88.4 ppm Rb and the highest measured Li concentration. The distribution of Rb according to regolith type is similar to that for Li.

Tin reaches a maximum concentration of 4.59 ppm in 220833 (E8767, L_m) from the Redcliff Pound Group (Fig. B24i), which is the only sample with an anomalous Sn concentration. This sample also has the highest concentration of Li and Sc. Median values and concentration ranges are generally similar regardless of lithological unit (Table 6), but there is a wider range for regolith from the Liveringa Group (0.68 – 3.37 ppm) and Redcliff Pound Group (0.08 – 4.59 ppm).

Strontium has a wide range in concentration from 2.3 to 1264.2 ppm (Table 6). Of the 56 samples with anomalous Sr contents (>42.6 ppm), 20 are from the Redcliff Pound Group, and there are roughly equal numbers from the Hidden Basin beds and Liveringa Group (Fig. B24j). Within the Redcliff Pound Group anomalous samples are found in or close to salt lakes. However, the maximum concentration of 1264.2 ppm Sr is in 221133 from site M926 (groundwater calcrete, R_{kg}), and a high proportion of regolith samples with elevated Sr concentrations are from areas where carbonate is developed. The range in Sr content in residual–relict regolith is probably due to high concentrations in carbonate-bearing regolith, and low concentrations in ferruginous regolith.

Median values for thorium (Th) are similar across lithological units, with slightly higher values for regolith from the Munyu Sandstone and Lucas Formation (Table 6). Sample 220790 (SRT10, Xqs , undivided Mesozoic rocks, Canning Basin) has the highest Th content of 22.5 ppm. There are only a few samples with anomalously high Th concentrations (>15.9 ppm; Fig. B24k). Lacustrine regolith has a lower median value for Th compared to other regolith types, and includes a number of samples with anomalously low Th concentrations. There is a wide range in Th concentrations from residual–relict regolith, possibly related to the concentration of Th-bearing resistate minerals.

Thallium (Tl) is present in low concentrations in regolith throughout the program area, with comparably low median values across different lithological units (Fig. B24l; Table 6). Samples with anomalous Tl concentrations are not confined to any particular lithological unit. There are 14 samples with anomalously high Tl concentrations of

Table 7. Median, minimum, and maximum values for analytes according to primary regolith–landform code

Analyte	Unit	LLD	R (n = 102)			X (n = 101)			C (n = 17)			W (n = 60)			L (n = 80)			E (n = 255)			S (n = 4)			A (n = 13)		
			Median	Min	Max	Median	Min	Max	Median	Min	Max	Median	Min	Max	Median	Min	Max	Median	Min	Max	Median	Min	Max	Median	Min	Max
TiO ₂	wt%		0.03	<0.01	0.06	0.03	<0.01	0.07	0.03	0.01	0.05	0.03	0.00	0.06	0.01	<0.01	0.07	0.03	<0.01	0.06	0.04	0.02	0.04	0.02	0.00	0.05
Al ₂ O ₃	wt%		2.33	0.36	6.04	2.12	0.74	4.97	2.00	1.18	4.29	2.67	1.23	5.24	2.31	0.15	6.34	1.69	1.23	5.24	1.65	0.88	1.88	2.71	0.59	4.91
Fe ₂ O ₃	wt%		4.05	0.41	9.01	3.95	1.54	7.19	3.93	2.56	6.45	5.30	2.42	9.52	3.20	0.19	6.78	3.30	2.42	9.52	3.01	1.50	3.70	4.96	2.14	7.19
CaO	wt%		0.20	0.04	21.16	0.13	0.04	6.38	0.13	0.06	0.43	0.15	0.04	2.50	0.40	0.07	15.52	0.08	0.04	2.50	0.08	0.04	0.10	0.28	0.11	14.89
MnO	wt%		0.035	0.005	0.098	0.040	0.008	0.096	0.029	0.013	0.085	0.041	0.011	0.331	0.024	0.003	0.148	0.023	0.011	0.331	0.023	0.005	0.039	0.040	0.020	0.052
MgO	wt%		0.13	0.03	2.06	0.12	0.03	1.21	0.13	0.07	0.41	0.13	0.05	1.64	0.22	0.03	5.72	0.07	0.05	1.64	0.07	0.03	0.08	0.35	0.07	1.08
Na ₂ O	wt%		0.03	0.01	0.82	0.04	0.01	2.87	0.03	0.01	0.15	0.03	0.01	0.90	0.04	0.01	1.60	0.03	0.01	0.90	0.03	0.03	0.03	0.05	0.03	0.58
K ₂ O	wt%		0.13	0.05	1.29	0.13	0.04	0.84	0.14	0.06	0.34	0.16	0.05	0.92	0.20	0.03	1.43	0.08	0.05	0.92	0.08	0.06	0.10	0.38	0.05	1.25
P ₂ O ₅	wt%		0.026	0.008	0.046	0.027	0.010	0.079	0.027	0.018	0.038	0.027	0.016	0.049	0.025	0.009	0.062	0.020	0.016	0.049	0.019	0.008	0.022	0.035	0.024	0.049
Ag	ppm	0.05		<0.05	0.07		<0.05	0.19		<0.05	0.11		<0.05	0.16		<0.05	0.06		<0.05	0.16		<0.05	<0.05		<0.05	0.05
As	ppm	1	4	<1	16	3	<1	30	3	1	8	6	1	33	2	<1	8	2	1	33	2	<1	4	5.00	2.000	15.00
Au	ppb	1	1.00	<1	4.00	1.00	<1	5.00	<1	<1	63	2	<1	6	1	<1	5	1	<1	6	2	<1	4	2	<1	4
Ba	ppm	1	75	3	926	68	16	661	66	25	1015	91	16	1151	63	3	1181	42	16	1151	34	14	47	80	21	328
Be	ppm	0.05	0.66	0.10	1.53	0.68	0.20	2.12	0.72	0.44	1.36	0.89	0.39	2.36	0.63	<0.05	2.92	0.54	0.39	2.36	0.55	0.21	0.69	0.78	0.42	1.66
Bi	ppm	0.01	0.26	0.03	0.46	0.24	0.08	0.47	0.26	0.17	0.33	0.32	0.17	0.52	0.23	0.02	0.73	0.21	0.17	0.52	0.20	0.11	0.25	0.27	0.12	0.41
Cd	ppm	0.01		<0.01	0.07		<0.01	0.08		<0.01	0.07		<0.01	0.08		<0.01	0.08		<0.01	0.08		<0.01	0.010		0.005	0.05
Ce	ppm	0.01	35.80	1.14	62.69	42.86	12.04	247.82	42.73	25.82	70.28	39.11	26.37	75.14	32.81	0.76	102.16	38.20	26.37	75.14	39.92	17.27	42.23	42.88	27.83	96.52
Co	ppm	0.1	7.0	0.9	14.2	7.4	1.9	17.8	7.4	3.1	13.1	8.8	2.9	22.5	4.9	0.5	21.9	5.5	2.9	22.5	5.4	1.4	8.2	8.4	3.5	12.2
Cr	ppm	1	34	5	62	30	17	67	31	24	51	42	23	77	28	2	51	29	23	77	28	17	31	39	18	65
Cs	ppm	0.01	1.05	0.20	3.73	1.02	0.37	3.18	1.08	0.68	4.52	1.27	0.70	2.27	0.95	0.11	4.79	0.89	0.70	2.27	0.92	0.46	1.13	1.19	0.39	3.71
Cu	ppm	0.5	8.7	2.3	21.6	8.6	2.4	22.5	10.6	5.8	19.4	10.0	4.0	26.4	9.9	1.4	24.2	6.7	4.0	26.4	6.2	2.3	6.6	13.3	5.0	20.6
Dy	ppm	0.01	2.00	0.09	3.60	2.25	0.64	4.88	2.33	1.42	3.17	2.41	1.44	5.42	1.76	0.05	5.55	2.08	1.44	5.42	2.07	0.77	2.60	2.55	1.30	3.74
Er	ppm	0.01	0.99	0.06	1.91	1.09	0.31	2.12	1.14	0.69	1.53	1.22	0.67	2.35	0.85	0.02	2.68	0.99	0.67	2.35	0.94	0.34	1.23	1.25	0.55	1.73
Eu	ppm	0.01	0.57	0.02	1.24	0.65	0.18	1.50	0.72	0.43	1.07	0.71	0.40	1.59	0.51	0.01	1.53	0.59	0.40	1.59	0.63	0.19	0.77	0.79	0.36	1.48
Ga	ppm	0.05	6.11	0.76	13.83	5.84	2.05	10.58	6.02	3.47	10.39	7.61	4.07	11.49	5.15	0.32	20.90	4.92	4.07	11.49	4.29	2.14	5.67	6.63	1.95	11.41
Gd	ppm	0.05	2.75	0.11	5.38	3.14	0.89	7.90	3.24	1.93	5.21	3.30	2.11	7.63	2.47	0.07	6.62	2.83	2.11	7.63	2.94	1.10	3.59	3.68	2.03	6.03
Hf	ppm	0.01	0.18	0.01	0.55	0.18	0.05	0.46	0.21	0.05	0.45	0.21	0.07	0.37	0.13	0.01	0.60	0.16	0.07	0.37	0.16	0.10	0.20	0.17	0.01	0.42
Hg	ppm	0.01	0.03	<0.01	0.18	0.03	<0.01	0.22	0.03	0.01	0.14	0.02	<0.01	0.18	0.03	<0.01	0.21	0.02	<0.01	0.18	0.02	<0.01	0.02	0.03	0.01	0.16
Ho	ppm	0.01	0.37	0.02	0.72	0.40	0.11	0.81	0.44	0.27	0.61	0.45	0.26	0.95	0.31	0.01	1.03	0.37	0.26	0.95	0.37	0.13	0.48	0.47	0.22	0.63
In	ppm	0.01	0.04	<0.01	0.07	0.03	<0.01	0.08	0.03	0.02	0.06	0.05	0.02	0.09	0.03	<0.01	0.09	0.03	0.02	0.09	0.03	0.01	0.04	0.04	0.02	0.06
La	ppm	0.01	16.11	0.56	27.31	19.07	5.72	56.40	18.88	12.95	29.60	17.42	11.60	24.72	14.57	0.30	36.79	17.13	11.60	24.72	18.28	8.01	19.28	18.99	12.95	40.49
Li	ppm	0.1	7.3	0.8	30.7	6.3	2.1	32.1	6.4	2.8	18.6	9.3	3.2	28.0	7.6	0.5	33.4	5.0	3.2	28.0	6.6	1.9	8.5	8.9	2.8	22.2
Lu	ppm	0.01	0.11	<0.01	0.22	0.12	0.03	0.25	0.13	0.08	0.19	0.14	0.08	0.25	0.09	<0.01	0.33	0.11	0.08	0.25	0.12	0.04	0.16	0.14	0.05	0.19
Mn	ppm	1	272	38	760	308	65	746	221	104	659	319	86	2564	186	21	1143	178	86	2564	179	39	303	308	154	405
Mo	ppm	0.1	0.4	<0.1	0.8	0.5	0.2	1.0	0.5	0.2	0.7	0.5	0.2	1.4	0.3	<0.1	0.8	0.4	0.2	1.4	0.4	0.2	0.5	0.4	0.1	1.0
Nb	ppm	0.02	0.16	<0.02	0.68	0.17	<0.02	0.49	0.19	<0.02	0.36	0.11	<0.02	0.44	0.15	<0.02	0.42	0.17	<0.02	0.44	0.12	0.08	0.16	0.07	0.02	0.43
Nd	ppm	0.01	17.18	0.45	33.85	19.33	6.04	53.57	20.10	12.53	34.27	19.87	12.48	37.94	15.22	0.32	39.26	17.94	12.48	37.94	19.28	7.75	20.39	21.83	13.43	51.74
Ni	ppm	0.5	7.6	1.5	23.3	8.1	3.1	22.0	9.0	4.8	16.1	9.9	4.2	30.5	8.9	1.4	39.0	6.0	4.2	30.5	5.7	3.3	6.1	11.7	5.5	16.4
P	ppm	20	116	37	199	117	44	344	119	79	165	117	68	212	109	39	271	86	68	212	84	37	95	152	104	213
Pb	ppm	0.5	10.1	0.8	17.5	10.4	3.8	18.9	10.3	5.9	14.7	11.6	6.1	21.5	9.2	0.7	31.8	8.1	6.1	21.5	7.0	2.8	10.8	11.7	4.5	17.0
Pd	ppb	10		<10	<10		<10	<10		<10	<10		<10	<10		<10	<10		<10	<10		<10	<10	5.00	5.000	5.00
Pr	ppm	0.01	4.47	0.11	8.86	5.09	1.59	13.40	5.16	3.31	8.67	4.93	3.20	9.26	3.94	0.08	10.65	4.62	3.20	9.26	4.56	2.09	5.26	5.78	3.38	13.66
Pt	ppb	5		<5	5		<5	<5		<5	<5		<5	5		<5	<5		<5	5		<5	<5		<5	<5
Rb	ppm	0.02	17.14	3.49	72.28	15.85	6.19	46.19	14.83	9.85	46.51	21.55	9.46	43.15	15.60	1.33	88.44	12.54	9.46	43.15	12.13	5.94	14.92	24.60	6.71	56.57
Re	ppm	0.001		<0.001	<0.001		<0.001	0.011		<0.001	0.002		<0.001	0.002		<0.001	0.001		<0.001	0.002		<0.001	<0.001	0.00	0.001	0.00
S	ppm	50	146	59	28437	156	25	3220	173	106	403	136	71	5620	244	106	31351	128	71	5620	103	102	103	177	76	944
Sb	ppm	0.02	0.14	0.03	8.23	0.15	0.01	0.62	0.15	0.06	0.40	0.16	0.04	1.92	0.15	0.01	1.15	0.13	0.04	1.92	0.13	0.07	0.21	0.13	0.08	0.23

Table 7. continued

Analyte	Unit	LLD	R (n = 102)			X (n = 101)			C (n = 17)			W (n = 60)			L (n = 80)			E (n = 255)			S (n = 4)			A (n = 13)		
			Median	Min	Max	Median	Min	Max	Median	Min	Max	Median	Min	Max	Median	Min	Max	Median	Min	Max	Median	Min	Max	Median	Min	Max
Sc	ppm	0.1	5.9	0.4	11.8	5.7	2.0	10.2	5.3	3.6	9.8	7.2	4.2	12.6	4.5	0.2	18.8	5.3	4.2	12.6	4.5	1.6	7.6	6.3	1.7	10.0
Se	ppm	1		<1	<1		<1	<1		<1	<1		<1	<1		<1	<1		<1	<1		<1		0.50	0.500	1.00
Sm	ppm	0.01	3.38	0.09	6.85	3.83	1.16	10.57	3.92	2.42	6.80	3.86	2.50	9.05	3.01	0.08	7.98	3.51	2.50	9.05	3.67	1.37	4.55	4.43	2.40	9.26
Sn	ppm	0.05	1.67	0.21	3.28	1.65	0.68	2.68	1.59	1.09	2.69	2.11	1.13	3.13	1.49	0.08	4.59	1.43	1.13	3.13	1.28	0.66	1.67	1.92	0.75	3.15
Sr	ppm	0.02	12.48	2.51	1264.15	11.38	3.15	77.54	12.06	5.44	46.88	11.23	3.53	239.57	20.98	4.12	509.05	6.38	3.53	239.57	5.28	2.51	5.94	21.62	5.71	54.91
Ta	ppm	0.01		<0.01	<0.01		<0.01	<0.01		<0.01	<0.01		<0.01	<0.01		<0.01	<0.01		<0.01	<0.01		<0.01	<0.01	0.01	0.005	0.01
Tb	ppm	0.01	0.38	0.01	0.71	0.43	0.12	1.02	0.44	0.29	0.64	0.46	0.30	1.06	0.34	<0.01	0.98	0.40	0.30	1.06	0.40	0.14	0.48	0.53	0.26	0.81
Te	ppm	0.05		<0.05	0.12		<0.05	0.15		<0.05	0.06		<0.05	0.10		<0.05	0.08		<0.05	0.10		<0.05	<0.05		0.025	0.07
Th	ppm	0.01	10.20	0.28	15.65	10.57	5.30	22.50	10.99	6.65	12.88	11.26	7.42	15.39	8.57	0.23	21.05	9.74	7.42	15.39	9.16	4.86	11.74	10.69	4.81	18.36
Tl	ppm	0.01	0.15	0.02	0.43	0.13	0.04	0.50	0.14	0.09	0.29	0.21	0.06	0.53	0.13	<0.01	0.69	0.11	0.06	0.53	0.12	0.05	0.14	0.20	0.04	0.36
Tm	ppm	0.01	0.13	<0.01	0.26	0.14	0.04	0.29	0.15	0.09	0.21	0.16	0.09	0.31	0.11	<0.01	0.36	0.13	0.09	0.31	0.13	0.04	0.17	0.16	0.06	0.23
U	ppm	0.01	1.12	0.43	2.48	1.25	0.33	5.12	1.29	0.96	1.65	1.25	0.48	2.19	1.08	0.15	5.52	1.10	0.48	2.19	1.23	0.56	1.49	1.18	0.68	1.60
V	ppm	2	68	6	197	58	33	158	59	40	96	82	40	166	51	3	100	55	40	166	45	24	73	77	33	124
W	ppm	0.05		<0.05	0.13		<0.05	0.11		<0.05	0.12		<0.05	0.08		<0.05	0.10		<0.05	0.08		<0.05	<0.05	0.03	0.025	0.06
Y	ppm	0.02	8.92	0.47	18.18	10.36	3.05	20.61	10.66	6.55	15.29	11.66	6.26	23.15	7.94	0.25	24.99	9.36	6.26	23.15	9.60	3.07	11.83	12.25	5.35	16.07
Yb	ppm	0.01	0.83	0.05	1.57	0.88	0.26	1.77	0.93	0.61	1.32	0.97	0.54	1.86	0.69	0.02	2.35	0.81	0.54	1.86	0.78	0.27	1.07	0.95	0.37	1.36
Zn	ppm	1	11	3	38	12	5	70	14	6	20	14	5	59	15	2	50	9	5	59	9	5	10	23	13	29
Zr	ppm	0.1	7.0	0.3	19.6	7.4	2.0	15.8	8.1	2.2	15.6	8.4	3.5	12.9	5.2	0.2	19.9	3.5	2.1	15.8	5.6	4.3	7.6	7.5	1.0	16.0

>0.2 ppm, nine of which are from Canning Basin regolith. The highest concentration of 0.69 ppm is in 220790 (SRT10, *Xqs*), which also has the highest concentration of Th.

Most samples with elevated U concentrations are from the Murraba Basin, with a high proportion of these samples coming from the Munyu Sandstone. Regolith from this lithological unit also has a higher median value of 2.36 ppm (Fig. B24m; Table 6), and six of the 12 samples from the Munyu Sandstone have anomalous U concentrations >2.1 ppm. Uranium concentrations appear lower in regolith from the Callawa Formation, as shown by a relatively low median value and a range of 0.52 – 1.77 ppm. Regolith from lacustrine areas (*L*) has a relatively high median value for U and this type of regolith also has a number of samples with anomalous U contents (Fig. B24m). Regolith from eolian dunefields (*E*) also has a wide range in U content. Of the 14 samples with anomalous U contents, all but two are from either *L_m* or *E_l*.

Major element oxides

The Al_2O_3 concentrations in regolith samples are mostly <2 wt%, with median values ranging by lithological unit from 1.45 to 2.52 wt%, apart from the Lucas Formation (3.05 wt%; Table 6). Several samples with anomalous Al_2O_3 concentrations form an arcuate array in the Noonkanbah Formation in the southwest of the project area (cf. the distribution of Li [Fig. B24g] and Rb [Fig. B24h]), whereas other high values occur in regolith from the Redcliff Pound Group and Hidden Basin beds in the southeast (Fig. B25a). Regolith with high Al_2O_3 concentrations is spatially associated with salt lakes over the Redcliff Pound Group. A number of samples with anomalous Al_2O_3 also come from areas of eolian regolith (*E*).

There are only three samples with anomalous Fe_2O_3 concentrations (Fig. B25b), two of which are Fe-rich sheetwash from the Liveringa Group (220955, M592; 9.52 wt% and 221257, SR16; 8.62 wt%). Regolith from the Liveringa Group and Lucas Formation show a wider range in Fe_2O_3 concentration (1.54 – 9.52 and 3.12 – 7.55 wt%) and higher median values of 4.45 and 4.74 wt%, respectively (Fig. B25b; Table 6). In terms of regolith type, sheetwash has a higher median Fe_2O_3 value and a wider range in Fe_2O_3 content than other regolith materials, whereas eolian and lacustrine regolith have lower median values.

The range in MgO is 0.02 – 5.72 wt%, but there are few samples with >1 wt% MgO (Fig. B25c). Most MgO-rich samples are located in areas of salt lakes overlying the Hidden Basin beds and Redcliff Pound Group. Sample 221334 (M910; *L_g*) from the Munyu Sandstone has the highest MgO content of 5.72 wt%. There are a number of eolian regolith samples with high MgO concentrations up to 1.64 wt% (Table 7).

Manganese concentrations in regolith reach 2564 ppm (0.33 wt%; Fig. B25d). Median values across all lithological units are between 150 and 350 ppm, but some units have wider ranges in Mn concentrations, including regolith from the Liveringa Group (65–2564 ppm), Noonkanbah Formation (92–746 ppm) and Hidden Basin beds (47–1143 ppm; Table 6). Lower Mn concentrations

are in regolith samples from lacustrine areas (*L*). A slightly higher median value is recorded for Mn from areas of sheetwash (*W*).

Samples with elevated concentrations of CaO (>0.59 wt%) are mostly from salt lake areas (Fig. B25e). There is a wide range in CaO concentration (0.03 – 21.16 wt%), but most samples have <1 wt% CaO. Of the 54 samples with extreme concentrations of CaO (>0.91 wt%), 18 are from areas of relict, carbonate-rich regolith and 24 are from lacustrine areas (Appendix 6). A number of samples from eolian areas have elevated CaO contents which probably reflects patches of carbonate developed close to the surface.

Similarly to CaO, higher concentrations of Na_2O in regolith are from areas of salt lakes (Fig. B25f). Most regolith samples have extremely low concentrations of Na_2O (<0.1 wt%), but samples from saline areas have up to 2.87 wt% (Table 6). There are 100 samples with anomalous Na_2O contents, spread over a variety of regolith types. Of the four samples with the highest Na_2O content, two are from areas of quartz-rich sedimentary rock (221241, E9243; 221208, M977; *Xqs*) and two are from deposits marginal to salt lakes (220785, E9979; 220644, E8769; *L_m*).

Potassium also shows some correlation between regolith concentration and the distribution of lacustrine deposits (Fig. B25g), but there are a number of samples with anomalously high K_2O concentrations from areas of eolian dunefields (*E*) and relict-residual regolith (*R*). The maximum concentration of K_2O (1.43 wt%) is in sample 220690 (M969, *L_m*) from the Hidden Basin beds. The arcuate distribution of samples with anomalous K_2O contents over parts of the Noonkanbah Formation corresponds to the distribution of samples with anomalous Li (Fig. B24g) and Rb (Fig. B24h).

Eighteen samples have anomalous concentrations of P (>193 ppm; 0.08 wt% P_2O_5), seven of which are from the Redcliff Pound Group, and four from the Noonkanbah Formation (Fig. B25h; Table 6). The majority of samples with elevated P contents are from areas of saline regolith. Of the 18 samples with anomalous concentrations of P, six are from regolith in areas of outcrop (*X*), and several samples are from eolian areas (*E*).

Base metals

Median Cu values range from 5.1 ppm in regolith from the Callawa Formation, to 12.7 ppm in the Liveringa Formation (Table 6). The maximum Cu concentration of 26.4 ppm is in sheetwash over the Redcliff Pound Group (221211; M773, *W*) (Fig. B26a). Regolith from this lithological unit accounts for six of the 10 samples that have anomalously high Cu concentrations (>20.3 ppm). The median value for eolian regolith (*E*) is lower than other regolith types, but this type of regolith contains a few samples with anomalous Cu concentrations. Regolith from lacustrine areas (*L*) has a relatively wide range in Cu concentrations (Fig. B26a; Table 7).

Lead concentrations range from 0.7 to 31.8 ppm, with the maximum concentration of 31.8 ppm in 220833 (E8767; *L_m*), from an area of saline regolith over the Redcliff Pound Group (Fig. B26b). Sample 221216 (M449; *E_l*) has a similar Pb concentration of 31.5 ppm. There are a

few samples with anomalous Pb concentrations in regolith from the Liveringa Group, including 26.7 ppm in 221189 (M670; playa terrain regolith, L_p). Of the eight samples with anomalous Pb concentrations, five are from regolith over the Liveringa Group. The median values for different types of regolith are similar, with a relatively wide range in Pb concentrations in lacustrine regolith (L).

Median Zn values according to lithological unit vary from 7 to 14 ppm (Table 6). Thirty-five samples have anomalous Zn concentrations >15 ppm, most of which are from regolith over the Redcliff Pound Group (Fig. B26c). The maximum Zn concentration of 70 ppm is from 220790 (SRT10; Xqs), and seven samples with anomalous Zn concentrations are from two transects over the Stansmore Fault. Similar to Pb, the median Zn values are similar for different regolith types, but eolian regolith (E), lacustrine regolith (L), regolith in areas of outcrop (X) and sheetwash (W) have wider ranges in Zn content (Table 7).

High field strength elements

The high field strength elements (HFSE) Ti, Nb, Hf, Zr and Ta are all in low concentrations in regolith from the Ngururrpa area, especially Ta, which returned censored data for all samples (i.e. concentrations <0.01 ppm). Titanium concentrations are low for all regolith materials, and the maximum Ti value is only 422 ppm (0.07 wt% TiO_2) in 220827 (M775, Callawa Formation, regolith from dunefields, E_d). No samples have statistically anomalous concentrations (Fig. B27a), and median values range from 93 ppm (0.02 wt% TiO_2) for regolith over the Lucas Formation to 252 ppm (0.04 wt% TiO_2) in regolith over the Millyit Sandstone (Table 6). In terms of regolith–landform unit, fluvial/alluvial regolith and lacustrine regolith have lower median values (Table 7).

The maximum Nb concentration of 0.68 ppm is in 220920 (M666, Liveringa Group, ferruginous duricrust, R_{fs}) whereas 220837 (E9721, Redcliff Pound Group, sandplain, S) has 0.67 ppm Nb. The 13 samples with anomalous Nb concentrations (>0.39 ppm) are from a variety of lithological units, particularly eolian regolith and regolith in areas of outcrop, including four samples over the Liveringa Group (Fig. B27b; Table 6). Fluvial/alluvial regolith has lower Nb concentrations than other types of regolith.

Twenty-nine samples have anomalous concentrations of Hf (>0.33 ppm), although the maximum concentration is only 0.6 ppm in 220833 (E8767, dune and playa terrain, L_m) over the Redcliff Pound Group; Fig. B27c). Nineteen of these anomalous samples are from the Liveringa Group, including 220920 (M666, ferruginous duricrust, R_{fs}), which also has the maximum concentration of Nb (0.68 ppm; Appendix 6). In terms of regolith–landform type, median values are broadly similar, apart from lacustrine regolith, which has a lower median value and lower concentrations. Residual–relict regolith, regolith in areas of outcrop, and eolian regolith have a high number of samples with anomalous Hf concentrations.

The maximum concentration of Zr is 19.9 ppm in sample 220833 (E8767, Redcliff Pound Group, dune and playa terrain, L_m ; Fig. B27d), which also has the highest concentration of Hf (0.6 ppm). Sample 220920

(M666, ferruginous duricrust, R_{fs}) has a similarly high Zr concentration of 19.6 ppm, as well as the highest concentration of Nb (0.68 ppm) and elevated Hf (0.55 ppm). Median Zr values for regolith according to lithological unit show a limited range from 5.8 ppm in the Millyit Sandstone to 8.8 ppm in the Poole Sandstone (Table 6). Of the 25 samples with anomalous Zr concentrations, 14 are from the Liveringa Group. Regolith from areas of outcrop (X), eolian regolith (E) and residual–relict regolith (R) have high proportions of samples with anomalously high Zr concentrations, and a few samples of eolian and lacustrine regolith have anomalously low concentrations (Table 7; Appendix 6).

Discussion

Bedrock control on regolith composition

The dominance of quartz-rich siliciclastic sedimentary rocks throughout the stratigraphy of the Ngururrpa area means that evidence of bedrock control in regolith chemistry may be difficult to determine. One example of bedrock control is afforded by regolith overlying the Lucas Formation. Although there are only six regolith samples from this unit, they have high concentrations of REE (particularly LREE), and some lithophile elements (e.g. Be, Th, Rb, Ba) compared to regolith overlying other bedrock units. A compilation of samples with high concentrations for a number of analytes (Appendix 6) shows that of the 16 samples with the high concentrations of 10 or more analytes, three are from the Lucas Formation, including 220833 (M902, E_d), which has elevated concentrations of transition elements and REE. Elevated REE is a characteristic of regolith samples from this unit (Fig. 28), although concentrations of LREE overlap with values for the North American Shale Composite (NASC) and Post-Archaeon Australian Shale (PAAS; McLennan, 1989).

Statistical testing can be carried out to determine if regolith composition is influenced by the underlying bedrock. Regolith that can be spatially linked to the underlying or nearby bedrock includes residual regolith (R ; developed by in situ weathering), or thin and lithic-rich regolith located on or near areas of outcrop (X). As residual regolith is of limited extent, forming small isolated exposures, and accounting for <10% of regolith by area and only one sample, statistical testing has focused on regolith in areas of outcrop, which is of wider extent (13% by area). This regolith–landform type includes 19 samples of regolith from heterogeneous sedimentary rocks (Xls) and 20 samples of regolith from quartz-rich sedimentary rocks (Xqs) over the Redcliff Pound Group. To test whether the two populations are compositionally different, they have been statistically compared using the Mann–Whitney U test, a nonparametric approach for comparison of median values (Reimann et al., 2008). The results of this comparison (Table 8) show that there is no statistical difference between the median values at the 95% confidence level for any elements. This reflects the compositional homogeneity of the Redcliff Pound Group.

Despite the evidence for an eolian influence on the origin of sandplain deposits (presence of dunes, dominance of well-sorted quartz sand comprising frosted and polished grains), Blake et al. (1974) and Veevers and Wells (1961) have suggested a genetic relationship with the underlying

bedrock in the Ngururupa region. This is consistent with the results of regolith mapping and geochemistry carried out in the Fraser Range area of southern Western Australia (Morris et al., 2000) where it was shown that regional-scale changes in sandplain chemistry could be linked to the composition of the underlying bedrock. This relationship was tested for sandplain regolith in the Ngururupa area by comparing the median values of eolian sandplain (*E*) from different bedrock units. Median values for sandplain overlying the Redcliff Pound Group (*n* = 45) and Hidden Basin beds (*n* = 52) show few statistical differences in median values (in particular, for Cu, S or U; Table 8). This reflects the limited range in composition and chemical maturity of both bedrock and regolith. Discernible differences in S and U indicate an influence from lacustrine regolith in the Redcliff Pound Group.

A comparison of median values for eolian regolith from the Liveringa Group (*n* = 44) and the Noonkanbah Formation (*n* = 22) also shows limited variability. The Liveringa Group has statistically higher median values for Be, CaO, and Sr, and a lower median value for Ti (Table 8). The association of Ca and Sr indicates that sandplain from the Liveringa Group has a higher carbonate content (i.e. regolith vs bedrock influence).

A more marked difference is seen in median values for eolian regolith from the Callawa Formation (*n* = 38) and the Noonkanbah Formation (*n* = 22). The results of statistical analysis (Table 8) show higher median values for a variety of lithophile elements, REE, base metals, transition elements, and Al, Ba, REE, transition elements, but not HFSE, in regolith overlying the Noonkanbah Formation.

The broad range and number of elements with statistically different median values is interpreted as evidence for some bedrock influence on regolith composition.

A statistical comparison of median values of eolian regolith from the Liveringa Group (*n* = 44) and Hidden Basin beds (*n* = 52) shows that there are few median values that are statistically different (Table 8). This is surprising, as regolith overlying the Liveringa Group has a relatively high proportion of fine-grained ferruginous lag, which was shown during the reconnaissance chemistry program to influence the chemistry of the fine fraction of regolith. This only shows up in terms of higher median values for As and V.

Regolith–landform unit chemistry

Subjectively, there are clear examples where the chemistry of regolith is a direct result of the regolith-forming process with no bedrock influence. For example, regolith associated with lake deposits (*L*) has elevated concentrations of Ba, Sr, Ca, U, Na, Rb, K and Ni, due to the relative abundance of carbonates, evaporate minerals (gypsum, halite), and clay. In other cases, although regolith chemistry reflects the dominance of regolith-forming processes, they cannot be completely separated from the influence of bedrock. Regolith over the Liveringa Group and parts of the Noonkanbah Formation has a higher lag content, and if lithic fragments are present, they are variably ferruginized. The single analysis obtained for the Liveringa Group (222164; Table 2) has lower SiO₂ (72.51 wt%) and higher bedrock Fe₂O₃ (16.06 wt%), transition elements (e.g. Cr, V), HFSE (Zr, Hf, but not Nb), As and Th than most other lithologies.

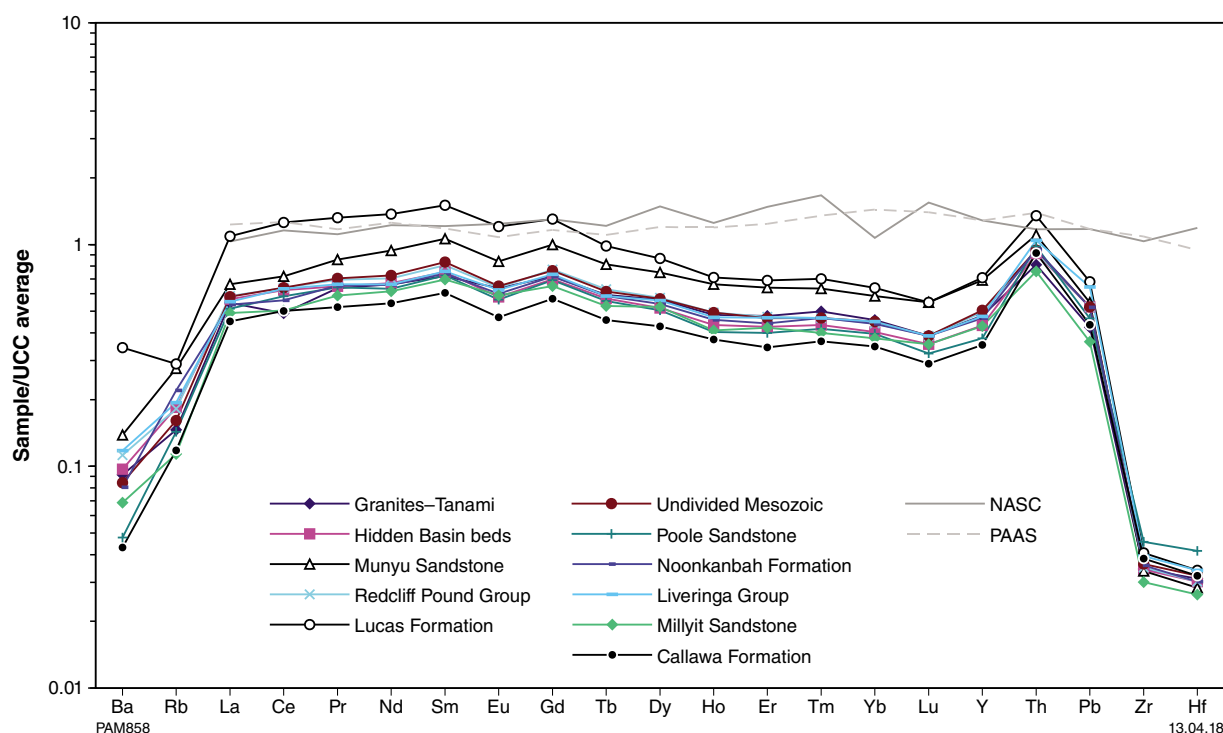


Figure 28. Spider diagram of median values of <50 µm fraction of regolith according to lithological unit. Data normalized to upper crust average (UCC; Rudnick and Gao, 2003). Abbreviations: NASC, North American Shale Composite; PAAS, Post-Archaean Australian Shale

Table 8. Results of statistical comparison of median values using the Mann–Whitney U test (Reimann et al., 2008): Xls vs Xqs from the Redcliff Pound Group; E over Redcliff Pound Group vs E over Hidden Basin beds; E over Liveringa Group vs E over Noonkanbah Formation; E over Callawa Formation vs E over Noonkanbah Formation; E over Noonkanbah Formation; E over Hidden Basin beds vs E over Liveringa Group. Elements with significant censored data not treated statistically. Values shaded grey indicate a statistical difference in median value

Analyte	Unit	LLD	Bedrock unit Regolith type	Redcliff Pound Group Xls (n = 19)	Redcliff Pound Group Xqs (n = 20)	Redcliff Pound Group E (n = 45)	Hidden Basin beds E (n = 52)	Liveringa Group E (n = 44)	Noonkanbah Formation E (n = 22)	Callawa Formation E (n = 38)	Noonkanbah Formation E (n = 22)	Hidden Basin beds E (n = 52)	Liveringa Group E (n = 44)
Al ₂ O ₃	wt%			1.692	2.13	2.01	1.805	1.680	1.553	1.367	1.553	1.805	1.680
As	ppm	1		2	2	2	2	4	2	2	2	2	4
Ba	ppm	1		56	84	71	49	45	33	24	33	49	45
Be	ppm	0.05		0.71	0.72	0.67	0.60	0.66	0.46	0.33	0.46	0.60	0.66
Bi	ppm	0.01		0.22	0.23	0.25	0.21	0.24	0.20	0.19	0.20	0.21	0.24
CaO	wt%			0.14	0.11	0.13	0.10	0.10	0.06	0.06	0.06	0.10	0.10
Ce	ppm	0.01		42.65	44.09	41.62	40.77	38.29	35.78	29.20	35.78	40.77	38.29
Co	ppm	0.1		7.4	7.8	7.0	5.9	5.9	5.1	4.3	5.1	5.9	5.9
Cr	ppm	1		26	29	31	29	31	28	28	28	29	31
Cs	ppm	0.01		1.00	1.22	1.13	0.93	0.91	0.87	0.73	0.87	0.93	0.91
Cu	ppm	0.5		7.9	10.5	8.80	7.4	7.6	5.6	4.6	5.6	7.4	7.6
Dy	ppm	0.01		2.31	2.24	2.32	2.16	2.07	2.22	1.63	2.22	2.16	2.07
Er	ppm	0.01		1.06	1.13	1.13	1.03	0.98	1.10	0.77	1.10	1.03	0.98
Eu	ppm	0.01		0.65	0.65	0.67	0.60	0.61	0.62	0.46	0.62	0.60	0.61
Fe ₂ O ₃	wt%			3.63	3.91	4.05	3.27	3.54	3.14	2.87	3.14	3.27	3.54
Ga	ppm	0.05		4.77	5.43	5.83	5.04	5.68	4.83	4.45	4.83	5.04	5.68
Gd	ppm	0.05		3.27	3.15	3.20	2.97	2.73	2.93	2.17	2.93	2.97	2.73
Ho	ppm	0.01		0.43	0.42	0.42	0.39	0.37	0.40	0.30	0.40	0.39	0.37
K ₂ O	wt%			0.12	0.14	0.11	0.09	0.08	0.05	0.05	0.05	0.09	0.08
La	ppm	0.01		19.36	19.25	19.14	18.37	16.81	16.96	13.31	16.96	18.37	16.81
Li	ppm	0.1		5.1	7.2	7.3	6.4	5.6	4.2	3.1	4.2	6.4	5.6
Lu	ppm	0.01		0.12	0.13	0.13	0.12	0.11	0.12	0.09	0.12	0.12	0.11
MgO	wt%			0.12	0.12	0.10	0.08	0.08	0.05	0.03	0.05	0.08	0.08
Mn	ppm	1		326	299	239	214	183	149	134	149	214	183
Na ₂ O	wt%			0.03	0.04	0.03	0.03	0.04	0.04	0.03	0.04	0.03	0.04
Nb	ppm	0.02		0.18	0.12	0.16	0.16	0.17	0.19	0.18	0.19	0.16	0.17

Table 8. continued

Analyte	Unit	LLD	Bedrock unit Regolith type	Redcliff Pound Group Xls (n = 19)	Redcliff Pound Group Xqs (n = 20)	Redcliff Pound Group	Hidden Basin beds	Liveringa Group	Noonkanbah Formation	Callawa Formation E (n = 38)	Noonkanbah Formation E (n = 22)	Hidden Basin beds E (n = 52)	Liveringa Group E (n = 44)
Nd	ppm	0.01		19.85	20.01	20.11	18.56	17.57	17.92	13.95	17.92	18.56	17.57
Ni	ppm	0.5		6.6	9.6	7.9	6.4	5.9	4.6	4.3	4.6	6.4	5.9
P	ppm	20		118	115	99	94	92	80	70	80	94	92
Pb	ppm	0.5		9.7	10.3	8.8	8.3	9.2	7.7	6.2	7.7	8.3	9.2
Pr	ppm	0.01		5.30	5.00	5.24	4.97	4.58	4.77	3.64	4.77	4.97	4.58
Rb	ppm	0.02		13.33	18.27	17.90	14.14	12.17	10.48	9.02	10.48	14.14	12.17
S	ppm	50		169	183	156	128	127	132	130	132	128	127
Sb	ppm	0.02		0.15	0.15	0.14	0.13	0.14	0.13	0.13	0.13	0.13	0.14
Sc	ppm	0.1		4.8	5.4	5.6	5.3	5.7	5.3	4.7	5.25	5.3	5.7
Sm	ppm	0.01		3.92	3.91	4.02	3.66	3.43	3.63	2.79	3.63	3.66	3.43
Sn	ppm	0.05		1.41	1.57	1.53	1.39	1.65	1.36	1.22	1.36	1.39	1.65
Sr	ppm	0.02		9.82	9.74	8.21	6.62	7.47	4.66	3.96	4.66	6.62	7.47
Tb	ppm	0.01		0.46	0.44	0.45	0.41	0.40	0.42	0.31	0.42	0.41	0.40
Th	ppm	0.01		9.71	10.02	10.27	9.63	9.98	9.89	8.68	9.89	9.63	9.98
Ti	ppm	5		171	204	180	187	188	266.50	231	267	187	188
U	ppm	0.01		1.31	1.27	1.32	1.22	1.07	0.96	0.88	0.96	1.22	1.07
V	ppm	2		47	56	56	54	61	55	51	55.00	54	61
Y	ppm	0.02		10.50	10.53	10.66	9.54	9.24	10.08	7.19	10.08	9.54	9.24
Yb	ppm	0.01		0.84	0.92	0.90	0.82	0.82	0.89	0.64	0.89	0.82	0.82
Zn	ppm	1		11	12	11	9	9	8	7	8	9	9
Zr	ppm	0.1		6.8	7.3	7.8	7.0	6.9	7.5	7.1	7.5	7.0	6.9

Regolith samples with anomalous concentrations of K_2O , Li and Rb over parts of the Noonkanbah Formation southwest of Yagga Yagga (Figs B25g, B24g,h) are oriented subparallel to the contacts with the overlying Callawa Formation and underlying Liveringa Group. These regolith samples could outline a more clay-rich unit within the Noonkanbah Formation. Alternatively, as eight of these samples are either dune and playa terrain regolith (L_m) or groundwater calcrete assigned to paleochannels (R_{pk_g}), they could represent clay-rich sediments (cf. paleovalley 2, Fig. 6).

A statistical comparison of median values for lacustrine (L ; $n = 30$) and eolian (E ; $n = 45$) regolith from the Redcliff Pound Group (Table 9) shows that lacustrine regolith has higher median values for CaO, K_2O , MgO, Ni, Sr, and Zn, and lower median values for REE, transition elements, Fe, and HFSE. The higher carbonate and evaporate mineral content of saline lake deposits is highlighted in this comparison, with a correspondingly lower content of silicate-related elements. A similar statistical comparison for lacustrine and eolian regolith from the Hidden Basin beds (Table 9) produced comparable results.

The majority of sheetwash samples (W) are located over the Liveringa Group in the vicinity of the Stansmore Range. A statistical comparison of the median values of regolith from areas of outcrop (X ; $n = 32$) and sheetwash (W ; $n = 42$) from the Liveringa Group shows that median values for some lithophile elements (Al_2O_3 , Be, Cs, Ga, Li, Rb, Tl), chalcophile elements (As, Bi), transition elements (Co, Cr, Fe, Ni, Sc, and V), and Pb are higher in sheetwash (Table 9). Lithophile element variations indicate a higher clay content in sheetwash, whereas elevated transition elements and chalcophile elements are indicative of ferruginization (39 of the 42 sheetwash samples from the Liveringa Group are classified as Fe rich; W_p). The control of ferruginization on the concentration of some transition elements is shown by the positive correlation of Cr and V in regolith, and the higher concentrations of both elements in samples with elevated Fe (wt%) contents (Fig. 30a).

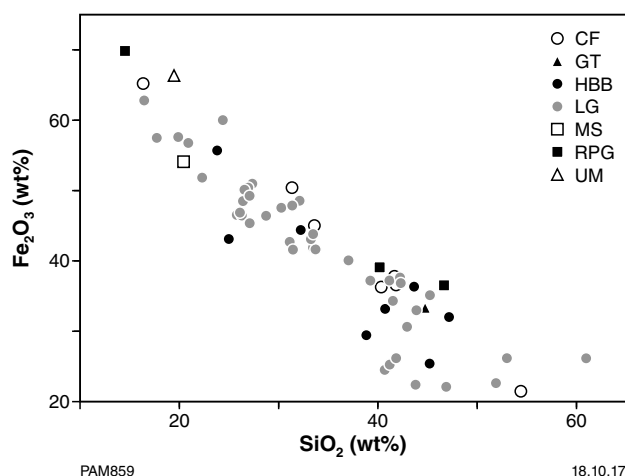


Figure 29. Bivariate plot of Fe_2O_3 (wt%) vs SiO_2 (wt%) for analyses of lag. Abbreviations: CF, Callawa Formation; GT, Granites-Tanami Orogen; HBB, Hidden Basin beds; LG, Liveringa Group; MS, Munyu Sandstone; RPG, Redcliff Pound Group; UM, Mesozoic siliciclastic rocks, Canning Basin

Lag chemistry

Ferruginous lag is conspicuous at some sample sites as a veneer of dark-brown to black, commonly shiny, subrounded to rounded granules or more irregular nodules. In some locations, lag is adjacent to areas of ferruginous duricrust, ferricrete, or ferruginized lithic fragments. Lag is most common over the Liveringa Group, which indicates some bedrock control on its formation.

Lag from 63 sites has been analysed (Appendix 4B), the majority of which are from the Liveringa Group (42 samples), the Hidden Basin beds (eight samples), and the Callawa Formation (seven samples). Statistics for all lag data (Table 10) show a wide range in SiO_2 (15.52 – 60.97 wt%) and Fe_2O_3 (21.47 – 69.84 wt%), with the complete range in both SiO_2 and Fe_2O_3 represented by lag from the Liveringa Group. The strong negative correlation between SiO_2 and Fe_2O_3 (Fig. 29) shows that the process of lag formation involves the progressive ferruginization of siliciclastic bedrock. The range in concentration of some elements for lag is narrow regardless of Fe content (e.g. CaO, MgO, Rb, K_2O , Ni), but other elements show a wide concentration range. For example, Ba ranges from 33 to 6546 ppm (Table 10). Lag samples with the highest Ba contents tend to have low Si/Fe (molar ratio), and most of these samples are from the Liveringa Group (Fig. 30a). At ratios greater than Si/Fe = 4, most Ba concentrations are <200 ppm. Arsenic shows a similar broad decrease in concentration with increasing Si/Fe (Fig. 30b), and most samples high in As are from either the Liveringa Group or Callawa Formation. For most lag samples, REE concentrations (e.g. La; range 5.8 – 51.6 ppm; Fig. 30c) show little variation with Si/Fe. The Au content of lag samples is low, with a maximum concentration of 2 ppb in 223430 (M55, Granites-Tanami, R_{zz}). The <50 μm fraction from the same site also has 2 ppb Au. The maximum Pd content of lag is 3 ppb in 222169 from site M716 (XIs) over the Callawa Formation, whereas the <50 μm sample from this site returned <10 ppb Pd. Compared to the <50 μm fraction of regolith, lag generally has a wider range and higher Pt concentrations, reaching 9 ppb in 223411 (E9499, undivided Mesozoic rocks, W_p). The equivalent <50 μm fraction sample has <5 ppb Pt.

Regolith chemistry along fault transects

In exploring for mineralization, faults can provide both a pathway for mineralizing fluids, and a means for focusing these fluids (Wyborn et al., 1994; McCuaig et al., 2010; McCuaig and Hronsky, 2014; Lindsay et al., 2015). Whether a particular fault is a fluid conduit related to buried mineralization depends on the fault morphology and its movement history. For example, Johnson et al. (2013) showed that gold and base metal mineralization in the Gascoyne region of Western Australia was spatially related to deep-penetrating, periodically reactivated faults, whereas shallower, largely inactive structures were not mineralized.

In areas of outcrop, fault traces can be precisely located, and the sense of movement can be determined by bedrock offset. Furthermore, minerals that have crystallized from fault-controlled fluids can provide textural and

Table 9. Results of statistical comparison of median values using the Mann–Whitney U test (Reimann et al., 2008): L vs E over Redcliff Pound Group and Hidden Basin beds; X vs W over Liveringa Group. Elements with significant censored data not treated statistically. Values shaded grey indicate a statistical difference in median value

Analyte	Unit	LLD	Redcliff Pound Group		Hidden Basin beds		Liveringa Group	
			L (n = 30)	E (n = 45)	L (n = 26)	E (n = 52)	X (n = 32)	W (n = 42)
Al ₂ O ₃	wt%		1.69	2.01	2.23	1.80	2.22	2.78
As	ppm	1	2	2	2	2	5	7
Ba	ppm	1	76	71	56	49	76	96
Be	ppm	0.05	0.52	0.67	0.59	0.60	0.66	0.91
Bi	ppm	0.01	0.20	0.25	0.23	0.21	0.25	0.33
CaO	wt%		0.45	0.13	0.22	0.10	0.14	0.15
Ce	ppm	0.01	31.99	41.62	31.64	40.77	43.05	40.01
Co	ppm	0.1	4.25	7.00	4.90	5.90	7.85	9.15
Cr	ppm	1	27	31	28	29	34	44
Cs	ppm	0.01	0.90	1.13	0.88	0.93	0.98	1.25
Cu	ppm	0.5	9.1	8.8	9.6	7.4	8.8	10.0
Dy	ppm	0.01	1.89	2.32	1.62	2.16	2.24	2.32
Er	ppm	0.01	0.90	1.13	0.79	1.03	1.07	1.17
Eu	ppm	0.01	0.52	0.67	0.48	0.60	0.64	0.69
Fe ₂ O ₃	wt%		2.87	4.05	3.22	3.27	4.21	5.65
Ga	ppm	0.05	3.91	5.83	5.15	5.04	6.00	8.28
Gd	ppm	0.05	2.58	3.20	2.30	2.97	3.19	3.11
Ho	ppm	0.01	0.35	0.42	0.30	0.39	0.40	0.43
K ₂ O	wt%		0.17	0.11	0.21	0.09	0.10	0.156
La	ppm	0.01	14.55	19.14	14.33	18.37	19.01	16.780
Li	ppm	0.1	6.1	7.3	7.5	6.4	6.4	10.0
Lu	ppm	0.01	0.10	0.13	0.09	0.12	0.12	0.130
MgO	wt%		0.17	0.10	0.19	0.08	0.11	0.133
Mn	ppm	1	199	239	164	214	322	350
Na ₂ O	wt%		0.04	0.03	0.04	0.03	0.04	0.027
Nb	ppm	0.02	0.19	0.16	0.16	0.16	0.17	0.085
Nd	ppm	0.01	15.22	20.11	14.12	18.56	19.28	18.880
Ni	ppm	0.5	13.9	7.9	7.4	6.4	6.9	10.0
P	ppm	20	115	99	106	94	121	117
Pb	ppm	0.5	7.8	8.8	8.6	8.3	10.8	12.1
Pr	ppm	0.01	4.11	5.24	3.56	4.97	5.04	4.830
Rb	ppm	0.02	13.97	17.90	15.43	14.14	15.18	22.240
S	ppm	50	525	156	190	128	142	136
Sb	ppm	0.02	0.16	0.14	0.14	0.13	0.14	0.155
Sc	ppm	0.1	3.8	5.6	4.3	5.3	6.1	7.6
Sm	ppm	0.01	3.09	4.02	2.83	3.66	3.86	3.710
Sn	ppm	0.05	1.12	1.53	1.49	1.39	1.69	2.200
Sr	ppm	0.02	15.91	8.21	20.12	6.62	11.79	12.4750
Tb	ppm	0.01	0.37	0.45	0.31	0.41	0.44	0.4400
Th	ppm	0.01	8.25	10.27	8.48	9.63	11.80	11.9500
Ti	ppm	5	127	180	133	187	191	175
Tl	ppm	0.01	0.11	0.15	0.14	0.12	0.14	0.22
Tm	ppm	0.01	0.12	0.15	0.11	0.13	0.14	0.1600
U	ppm	0.01	1.14	1.32	1.28	1.22	1.23	1.2150
V	ppm	2	44	56	47	54	77	94
Y	ppm	0.02	8.23	10.66	7.59	9.54	9.94	10.9550
Yb	ppm	0.01	0.73	0.90	0.63	0.82	0.88	0.9500
Zn	ppm	1	16	11	13	9	12	14
Zr	ppm	0.1	5.4	7.8	4.8	7.0	8.0	8.8

Table 10. Statistics for analysis of lag

<i>Analyte</i>	<i>Unit</i>	<i>LLD</i>	<i>Mean</i>	<i>Median</i>	<i>Minimum</i>	<i>Maximum</i>	<i>Range</i>	<i>Skewness</i>
Au	ppb	1			<1	2	2	7.0
Ag	ppm	0.01	0.18	0.18	0.02	0.53	0.51	0.9
Al ₂ O ₃	wt%	0.01	15.16	14.93	7.98	24.28	16.30	0.4
As	ppm	0.5	120.0	101.0	48.4	273.7	225.3	0.7
Ba	ppm	1	867	235	33	6546	6513	2.6
BaO	wt%	0.01	0.09	0.03	0.01	0.71	0.71	2.5
Be	ppm	0.05	1.48	1.33	0.67	3.44	2.77	1.6
Bi	ppm	0.01	1.64	1.63	0.57	3.18	2.61	0.4
C	wt%	0.01	0.12	0.12	0.04	0.30	0.26	1.5
CaO	wt%	0.01	0.08	0.03	0.01	1.35	1.34	5.4
Cd	ppm	0.02	0.04	0.03	0.01	0.14	0.13	1.6
Ce	ppm	0.5	31.6	27.8	10.2	84.4	74.2	1.1
Co	ppm	0.1	5.9	4.9	2.2	18.7	16.5	2.3
Cr	ppm	20	565	597	172	789	617	-0.9
Cr ₂ O ₃	wt%	0.01	0.08	0.09	0.02	0.12	0.10	-0.7
Cs	ppm	0.1	0.8	0.8	0.2	2.2	2.0	0.9
Cu	ppm	0.5	18.5	17.6	7.6	57.4	49.8	3.0
Dy	ppm	0.1	2.8	2.8	1.4	5.0	3.6	0.6
Er	ppm	0.1	2.1	2.0	0.9	3.8	2.9	0.6
Eu	ppm	0.1	0.4	0.4	0.1	0.9	0.8	1.1
Fe ₂ O ₃	wt%	0.01	41.83	41.90	21.47	69.84	48.37	0.2
Ga	ppm	0.1	42.3	42.6	22.8	63.4	40.6	0.1
Gd	ppm	0.1	2.1	1.9	0.8	4.7	3.9	1.3
Ge	ppm	0.05	0.90	0.92	0.14	1.71	1.57	0.1
Hf	ppm	0.1	13.8	12.8	6.6	32.0	25.4	1.6
Ho	ppm	0.1	0.7	0.6	0.3	1.2	0.9	0.6
In	ppm	0.01	0.30	0.30	0.15	0.46	0.31	-0.1
K ₂ O	wt%	0.01	0.15	0.15	0.03	0.36	0.33	0.6
LOI	wt%	0.01	6.66	6.55	2.95	10.67	7.72	-0.1
La	ppm	0.2	18.7	16.4	5.8	51.6	45.8	1.2
Li	ppm	0.1	10.8	9.7	4.0	25.9	21.9	1.2
Lu	ppm	0.1	0.4	0.4	0.2	0.8	0.6	1.7
MgO	wt%	0.01	0.09	0.08	0.03	0.18	0.15	0.8
MnO	wt%	0.01	0.03	0.02	0.01	0.17	0.17	3.7
Mo	ppm	0.1	3.6	3.5	1.8	6.1	4.3	0.2
Na ₂ O	wt%	0.01	0.02	0.02	0.01	0.04	0.04	0.3
Nb	ppm	0.1	21.4	22.5	8.3	44.1	35.8	0.3
Nd	ppm	0.1	11.2	10.0	3.8	32.0	28.2	1.3
Ni	ppm	0.5	15.8	15.1	4.8	34.8	30.0	1.1
P ₂ O ₅	wt%	0.002	0.091	0.092	0.0420	0.211	0.169	1.1
Pb	ppm	0.5	56.8	52.7	25.6	121.8	96.2	1.2
Pd	ppb	1			<1	3	3	1.4
Pr	ppm	0.1	3.4	3.1	0.9	9.5	8.6	1.1
Pt	ppb	1			<1	9	8	4.8
Rb	ppm	0.1	10.2	9.4	2.2	23.5	21.3	0.7
Re	ppm	0.002			<0.001	<0.001		
S	wt%	0.01	0.03	0.02	0.01	0.17	0.17	2.6
SO ₃	wt%	0.01	0.09	0.05	0.02	0.44	0.42	2.3

Table 10. continued

Analyte	Unit	LLD	Mean	Median	Minimum	Maximum	Range	Skewness
Sb	ppm	0.05	2.52	2.22	1.20	8.10	6.90	2.9
Sc	ppm	10			<10	26	26	-0.3
Se	ppm	0.5	3.1	3.1	1.6	6.4	4.8	0.7
SiO ₂	wt%	0.01	34.57	33.47	14.52	60.97	46.45	0.1
Sm	ppm	0.1	2.3	2.0	0.6	5.5	4.9	1.1
Sn	ppm	1	6	6	2	9	7	0.0
Sr	ppm	0.2	35.5	22.8	6.9	190.9	184.0	2.3
Ta	ppm	0.1	1.4	1.5	0.6	2.7	2.1	0.2
Tb	ppm	0.1	0.4	0.4	0.2	0.8	0.6	1.0
Te	ppm	0.1	0.7	0.7	0.3	1.3	1.0	0.5
Th	ppm	0.1	66.9	64.0	22.4	127.2	104.8	0.7
TiO ₂	wt%	0.01	0.73	0.77	0.39	1.10	0.71	-0.3
Tl	ppm	0.02	0.12	0.10	0.03	0.51	0.48	3.1
Tm	ppm	0.1	0.3	0.3	0.1	0.6	0.5	0.2
U	ppm	0.1	3.2	2.7	1.3	15.9	14.6	4.9
V	ppm	10	1061	1011	534	1722	1188	0.3
W	ppm	1	3	3	2	4	2	-0.3
Y	ppm	0.5	16.5	15.8	7.7	30.9	23.2	0.7
Yb	ppm	0.1	2.6	2.6	1.1	4.9	3.8	0.5
Zn	ppm	1	18	16	7	50	43	1.8
Zr	ppm	1	448	416	224	1043	819	1.7

geochronological information on the history of fault movement (Boullier et al., 2004; Wibberley et al., 2008; Frery et al., 2015). In areas of thick and contiguous cover where topography is subdued and there is little outcrop, it is difficult to determine both the location of the fault trace, its subsurface morphology, and the history of fault movement. In this case, the location of fault traces is usually interpreted from geophysical data, such as gravity or magnetics, yet these datasets have low spatial resolution because the scale of data acquisition ranges from 10⁰ to 10¹ km (Dentith and Mudge, 2014). Fault morphology and movement history commonly relies on seismic profiles and drillhole information, and information from scattered outcrops.

To address this issue of more precisely locating faults, determining whether they are or have been fluid conduits, and investigating the composition of any fault-controlled fluid, a pilot study was undertaken using samples of the fine fraction of regolith, and of spinifex, collected on three transects, labelled SR, SRT and SS, across the mapped traces of the Stansmore and Balgo Faults (GSWA, 2016; Figs 2, 7). The rationale behind this study is that, closer to the fault, there is a higher probability of an increased fluid flux, and the fine fraction of regolith has the capacity to weakly bond or adsorb fluid-mobile elements through cation exchange (Hall, 1998; Ma and Eggleton, 1999). Thus, higher concentrations of fluid-mobile elements in the fine fraction of regolith can be used

to infer enhanced fluid flux, and the existence of a fluid conduit such as a fault, in the vicinity of those samples. Similarly, plants, such as spinifex, can take up fluid-mobile elements through their roots by either cation exchange or diffusion from soil water (Hawkes and Webb, 1962; Brooks, 1972; Dunn, 2007). The approach to sampling of spinifex, spinifex analysis, and QA/QC are discussed in Appendix 3A. The chemistry the fine fraction of regolith along the fault transects is compiled in Appendix 4A, and the chemistry of spinifex across the faults is compiled in Appendix 5.

Structural coverage at 1:500 000 scale (GSWA, 2016; Fig. 2) shows two regional-scale faults, the Stansmore and Balgo Faults (Yeates et al., 1975; Mory, 2010) across which samples have been collected (Fig. 7a,b). In some areas, such as the Stansmore Range, the position of the Stansmore Fault is well constrained through a combination of gravity (Fig. 7a) and digital elevation data (Fig. 7b), but elsewhere there is less convincing evidence for its position. Stratigraphic drilling carried out near the Stansmore Fault provides evidence of periodic reactivation. Blake and Yeates (1976) have attributed unconformities in Carboniferous rocks to movement on the Stansmore Fault, and they have argued that fault activity probably affected crystalline basement. In general, geophysical and DEM data provide little information on the position of the Balgo Fault (Fig. 7a,b), and the movement history of the Balgo Fault is poorly understood.

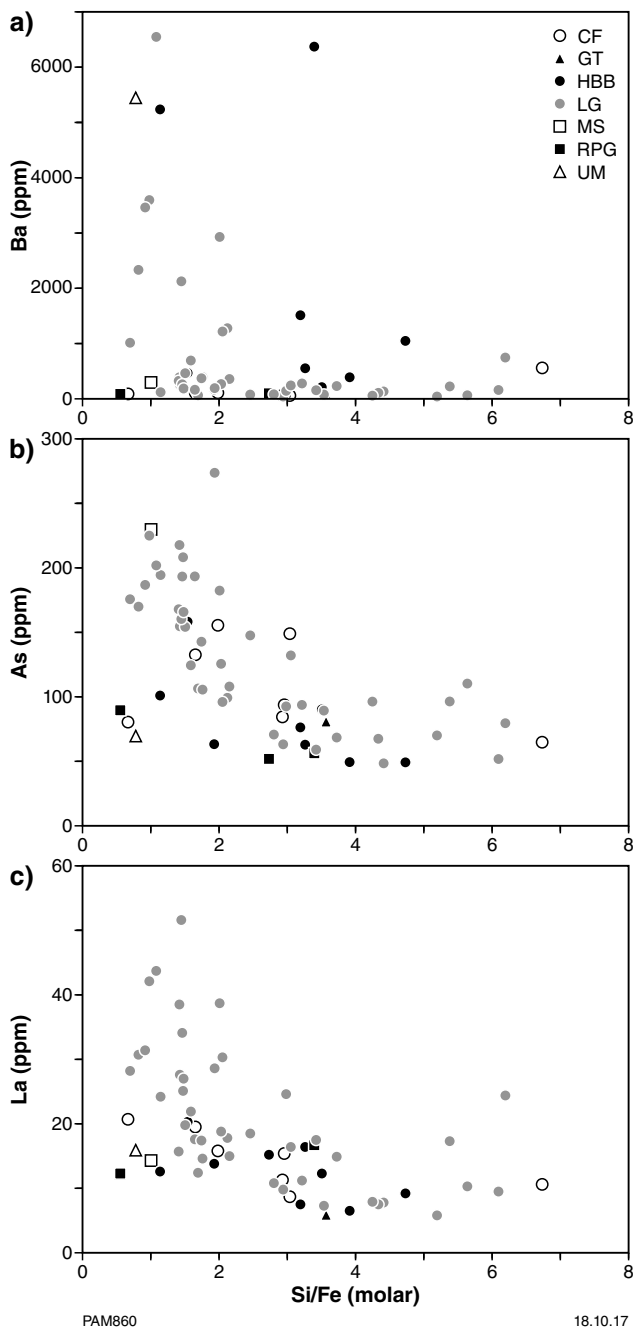


Figure 30. Bivariate plots of selected elements vs Si/Fe: a) Ba (ppm) vs molar Si/Fe; b) As (ppm) vs molar Si/Fe; c) La (ppm) vs molar Si/Fe for lag. Bedrock unit abbreviations as for Figure 29

Stansmore Fault traverses

SRT transect

The 3.5 km long SRT transect is located approximately 100 km southeast of Yagga Yagga (Figs 2, 7, 31a). Here, the Stansmore Fault separates undivided Mesozoic Canning Basin rocks to the east from Permian Liveringa Group rocks to the west (see Plate 1). The Stansmore Fault trace is marked by a well-defined scarp, which coincides with a strong gravity gradient (Fig. 7a) and DEM features (Fig. 7b). Regolith over undivided Canning Basin rocks consists of quartz-rich sandplain, with scattered lithic fragments downhole. Regolith over the Liveringa Group is thin, comprising patches of quartz sand among areas of outcrop, with a relatively higher content of lithic fragments, some of which are ferruginized. Spinifex is dominant at all sites, but shrubs are more common over sandplain on the Canning Basin, compared to trees on the Liveringa Group.

Ten regolith samples were collected along the SRT transect (Fig. 31a). The concentrations of most lithophile elements (Fig. 32a), REE (Fig. 32b), base metals, and chalcophile elements (Fig. 32c) show little variation according to bedrock lithology. The highest concentration of a number of lithophile elements (including Rb, Li, Cs, Be, Tl, and K) and REE are in 220790 (site SRT10), which coincides with the Stansmore Fault. High field strength elements (e.g. Ti, Zr, Nb, Hf) show a spike in concentration in this sample relative to adjacent samples, but HFSE concentrations similar to those in 220790 are seen in other samples along the transect (Fig. 32b). Base metals Cu and Pb show little variation in concentration along the traverse (Fig. 32d), but Zn shows a strong positive anomaly in 220790, with a concentration of 70 ppm, the highest value measured in the 837 samples from the Ngururrpa program (Appendix 6). Other samples along the transect have between 11 and 29 ppm Zn. Chalcophile elements show some lithological control, with As generally in higher concentration over undivided Mesozoic rocks northeast of the fault, but the highest As concentration of 30 ppm is in sample 220790, which also shows a positive Bi anomaly (0.41 ppm). Transition elements (Fe, Cr and V) also show some lithological control, with higher concentrations in regolith overlying undivided Mesozoic sedimentary rocks. Some elements at low concentrations show an erratic behaviour (e.g. Te), but others, such as Tl, show a positive anomaly in 220790.

SR transect

The SR transect, approximately 20 km north of Yagga Yagga, includes an upfaulted block of the Noonkanbah Formation between two blocks of the Liveringa Group, bounded by the Stansmore Fault to the east and an unnamed fault to the west (Figs 2, 7, 31b). A more complex fault architecture compared to the SRT transect is suggested by the presence of a minor splay fault approximately 320 m west of the Stansmore Fault in the Noonkanbah Formation (Fig. 31b). DEM data (Fig. 7b) are equivocal in locating the Stansmore Fault.

Twelve samples of regolith and spinifex were collected along a 15.2 km transect. Due to limitations imposed by heritage, the sample spacing is uneven, and no samples

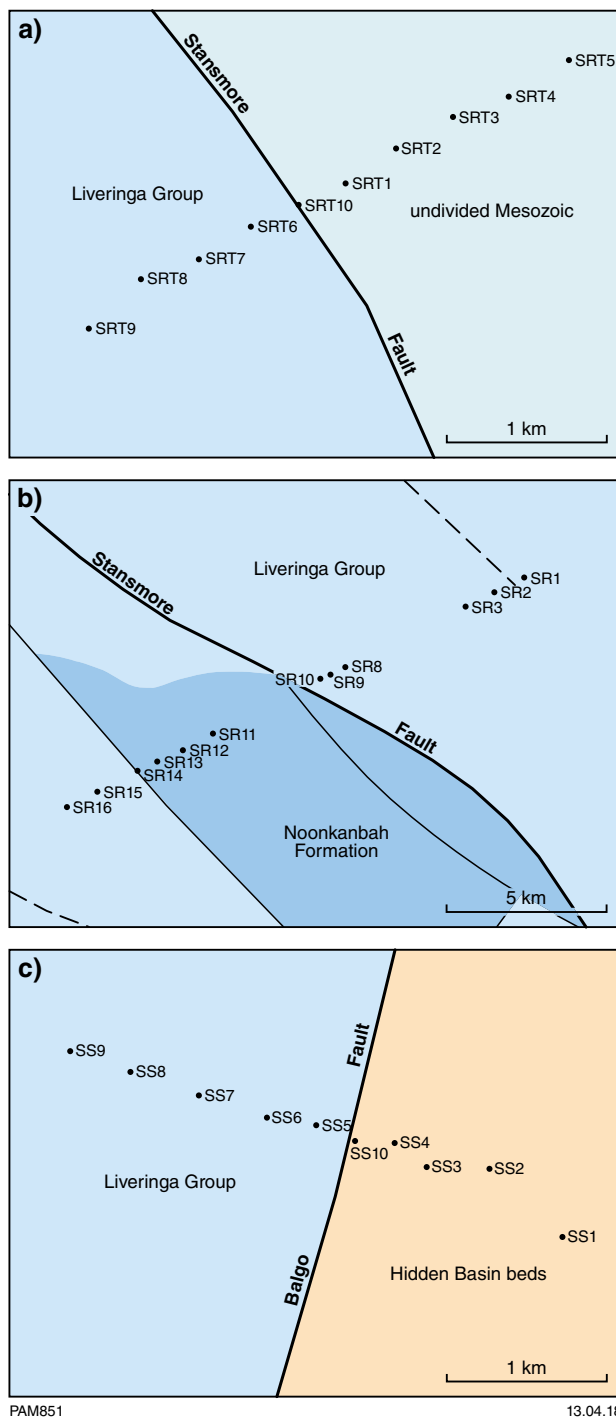


Figure 31. Simplified maps and sample locations for transects across faults: a) SRT; b) SR; c) SS. See Figures 2 and 7 for regional context

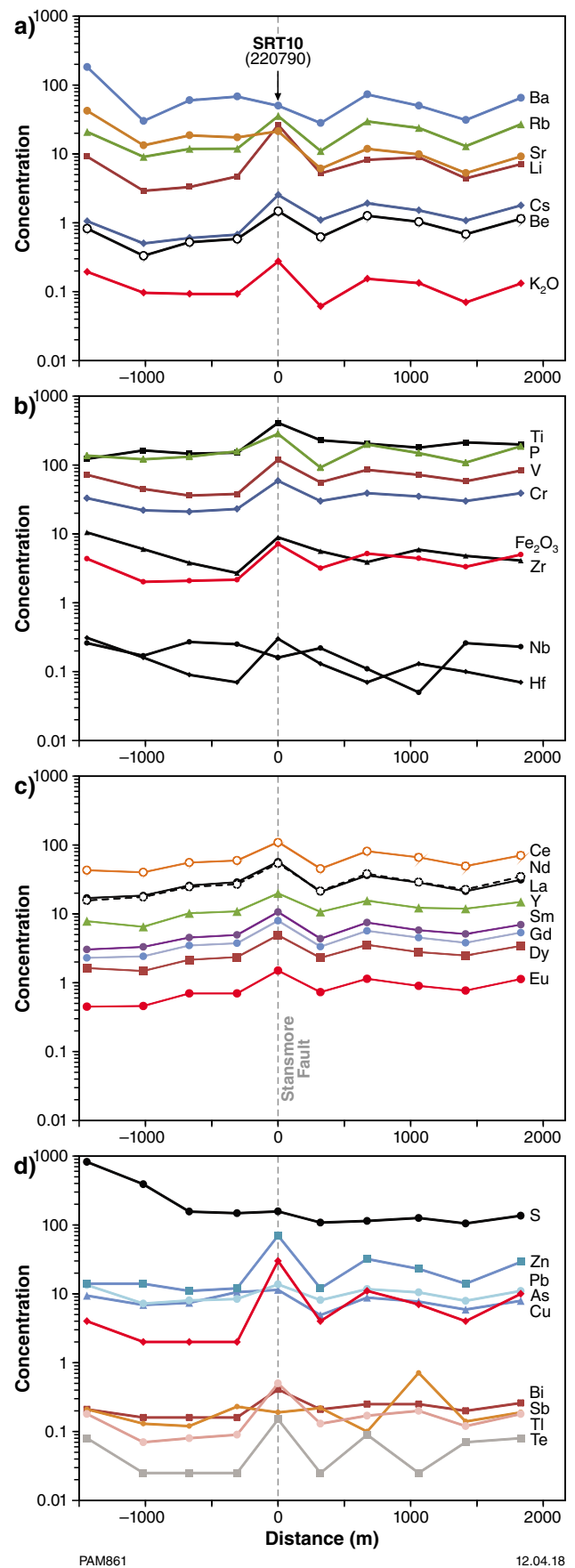


Figure 32. Concentration of analytes in the <50 µm micron fraction of regolith from sites on the SRT transect across the Stansmore Fault. Values on x-axis are sample distance (metres) from the fault, calculated perpendicular to the fault trace: a) lithophile elements; b) HFSE, transition elements, and P; c) rare earth elements; d) base metals, chalcophile elements and Tl (ppm)

could be collected directly on the main trace of the Stansmore Fault. Site SR14 is directly on the unnamed fault towards the western end of the transect. The closest site to the Stansmore Fault is SR10, approximately 660 m east of the fault trace. Along the whole transect, regolith is dominantly well-sorted, quartz-rich sand. Ferruginous nodules and granules are common at sites on the Noonkanbah Formation, and at sites SR8 and SR9 over the Liveringa Group. Sedimentary rock fragments downhole, lag, and the range in maximum augered depth from 30 to 90 cm indicates that regolith forms a thin veneer over bedrock, consistent with passive seismic data discussed previously. Spinifex is common at all sites, with subordinate shrubs and trees.

Regolith chemistry

Some lithological control on regolith composition is shown by slightly higher concentrations of Cs, Rb, Sr, and K, and lower concentrations of Hf and Nb in regolith over the Noonkanbah Formation (SR11–14; Fig. 33a,b). There is little change in the concentrations of lithophile elements on or close to fault traces. The REE (Fig. 33c) show similar patterns to lithophile elements, and in terms of lithological control, REE concentrations tend to be higher in regolith samples from the Noonkanbah Formation. Some of the highest REE concentrations are in 220626 (SR14, coincident with the western fault trace) and REE show a sharp positive spike in 220899 (SR9) relative to adjacent samples, approximately 900 m east of the mapped position of the Stansmore Fault. Base metals, transition elements and chalcophile elements (Fig. 33b,d) show little variation according to lithology. Copper and Pb show no variation in samples close to fault traces, but Zn is notably higher in concentration in 220626 (SR14) over the western unnamed fault.

Spinifex chemistry

Compared to regolith, some elements in spinifex are close to or less than the level of detection, or show limited variation at low concentrations (e.g. Hf, Nb, Ti), whereas others are at measurable concentrations (e.g. B and Re). Spinifex chemistry provides little information on bedrock lithology, with a range of lithophile elements, HFSE, base metals and transition elements, concentrations varying only slightly over the Liveringa Group and Noonkanbah Formations. However, REE concentrations are lower in samples from the Noonkanbah Formation compared to the Liveringa Group (Fig. 34). Lithium and boron (878 ppm) are elevated in spinifex from site SR14, and these and other elements show a positive spike in spinifex from SR9, approximately 900 m east of the Stansmore Fault trace. The REE patterns for spinifex are all subparallel (Fig. 34c) and spinifex from SR9 forms a strong positive REE anomaly relative to other samples.

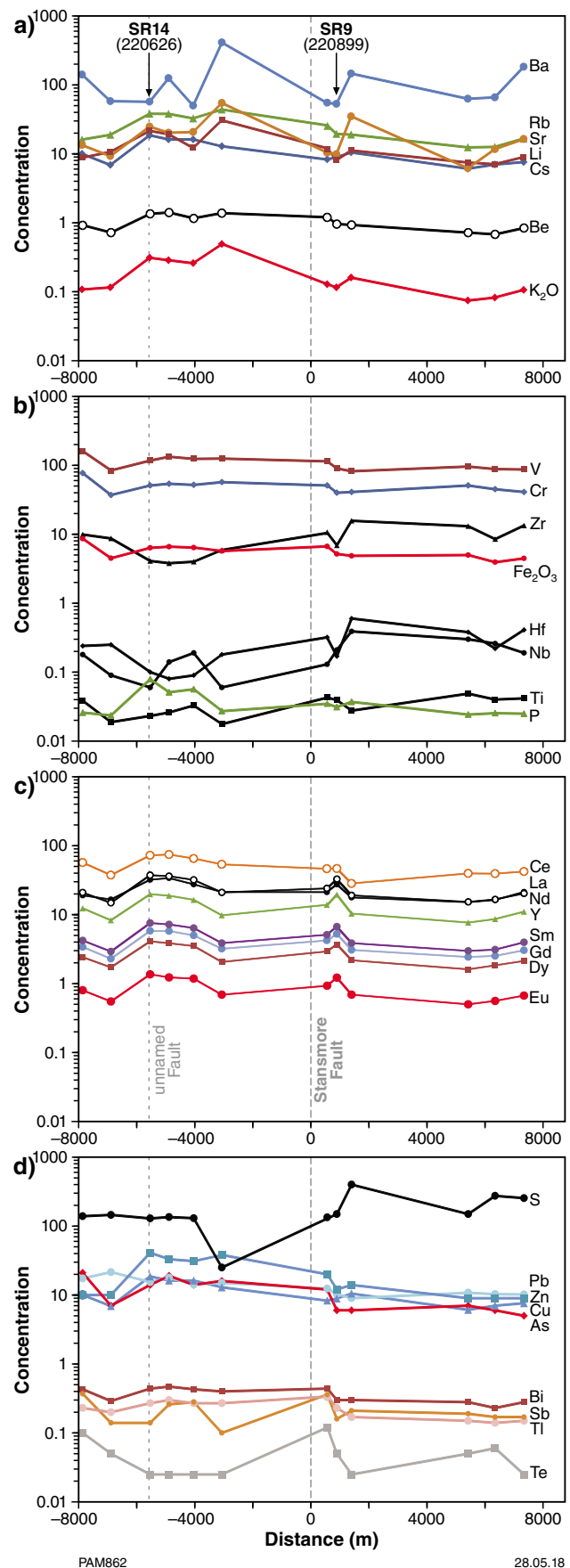


Figure 33. Concentration of analytes in the <50 µm micron fraction of regolith from sites on the SR transect across the Stansmore Fault. Values on the x-axis are sample distance (metres) from the fault, calculated perpendicular to the fault trace: a) lithophile elements; b) HFSE, transition elements, and P; c) rare earth elements; d) base metals, chalcophile elements and Ti (ppm)

Copper and lead show a limited concentration range along the transect (4.8 – 8.4 ppm and 6.5 – 12.6 ppm, respectively), but Zn is enriched in spinifex from SR14 (205.5 ppm) and SR12 (324.7 ppm), and forms a small positive anomaly in SR9 (79.9 ppm) relative to adjacent samples. Both Re and Cd are in generally low concentrations in spinifex along the transect, but in sample SR14 Re reaches 22 ppb and the Cd content is 1.35 ppm. The concentration of Te is either close to or at the LLD (0.02 ppm) apart from sample SR9 (0.05 ppm).

Balgo Fault transect

SS transect

Regolith samples were collected at 10 sites along a 3.5 km traverse at the southern extent of the Balgo Fault (Figs 2, 7, 31c). Here, the fault juxtaposes the Hidden Basin beds and the Livinginga Group. Along the transect, regolith comprises sandplain with occasional sand dunes. Regolith is well-sorted, quartz-rich sand with ferruginous nodules and granules at most sites. Nodules and granules are particularly common at site SS1 (estimated at 80% of surface cover) over the Hidden Basin beds, where ferruginous lag granules are between 0.1 and 1 mm diameter. Nodules and granules are only present at depth if they are abundant at the surface. In most cases, downhole regolith is homogeneous and dominated by quartz sand, with a higher clay content at depth at some sites resulting in regolith compaction. Carbonate at site SS5 over the Livinginga Group forms patches at the surface and fragments downhole.

Lithophile and HFSE in the fine fraction of regolith show little variation according to underlying bedrock along the transect (Fig. 35a,b). The REE have parallel patterns (Fig. 35c), with the lowest concentrations in the sample closest to the inferred trace of the Balgo Fault (221109, SS10) and the highest concentration in the sample approximately 300 m to the east of the fault (220669, SS4). There is little variation in terms of lithology or proximity to the Balgo Fault trace for base metals, chalcophile elements or transition elements (Fig. 35d), although there is a relative spike in As concentration in 220669 (SS4). Unlike samples from the SRT transect, Cu, Pb and Zn have similar concentrations and vary only a little along the transect (Fig. 35d).

Controls on transect chemistry

There are few examples of bedrock control on either regolith or spinifex composition along the transects, compared to the influence of fault proximity. The clearest example of fault control on the chemistry of the regolith fine fraction is from the SRT transect, where there are relatively high concentrations of several lithophile elements, REE, transition elements, some base metals (Zn), and chalcophile elements (As) in sample 220790 (SRT10;

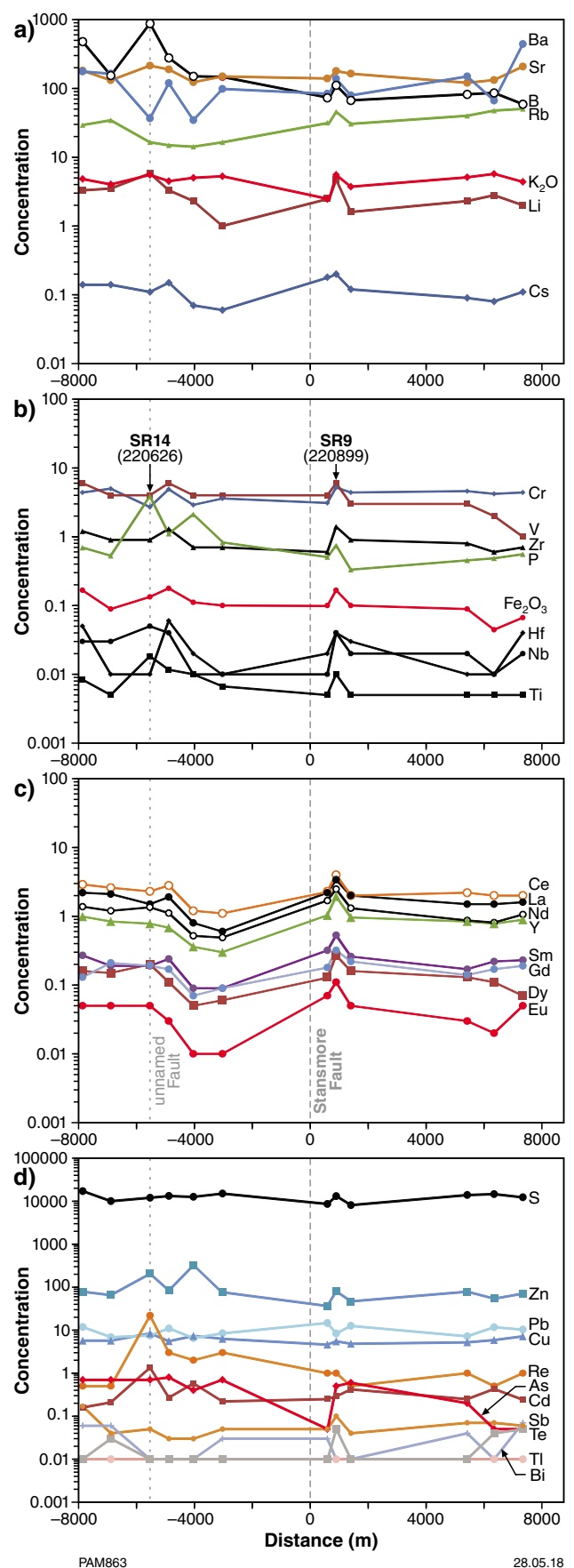


Figure 34. Concentration of analytes in spinifex from sites on the SR transect across the Stansmore Fault. Values on x-axis are sample distance (metres) from the fault, calculated perpendicular to the fault trace: a) lithophile elements; b) HFSE, transition elements, and P; c) rare earth elements; d) base metals, chalcophile elements (Re in ppb), and Ti (ppm)

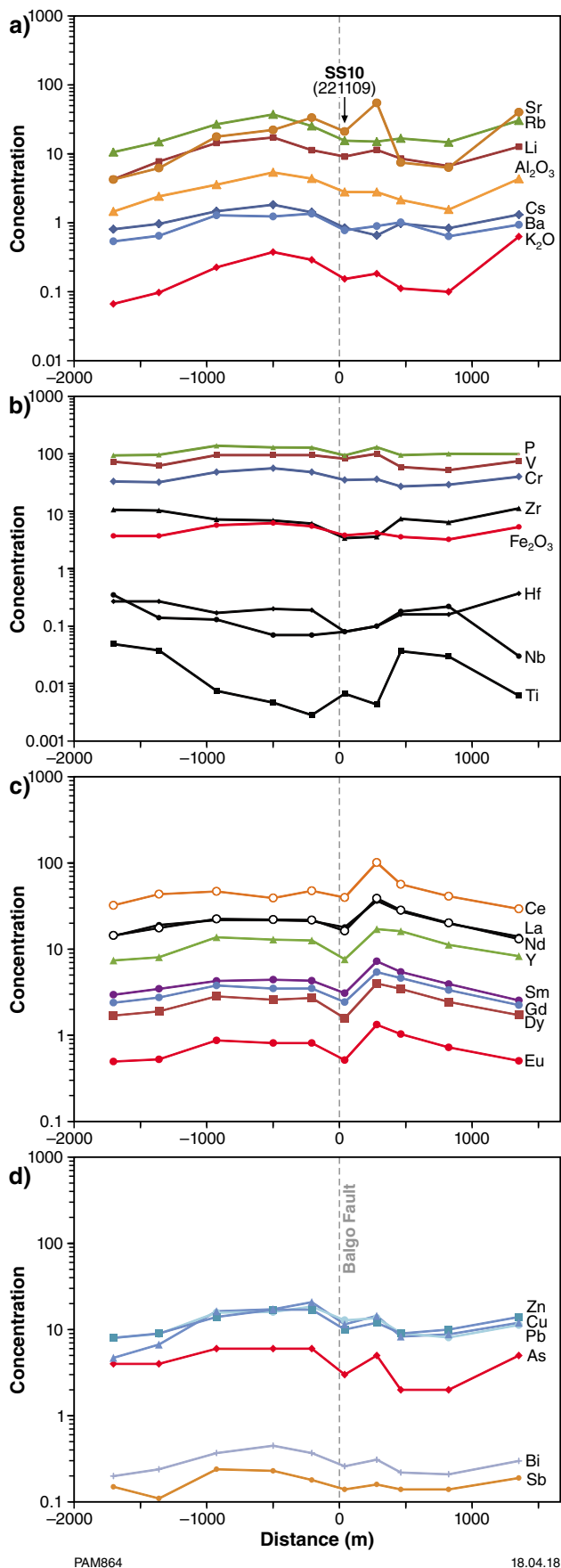


Figure 35. Concentration of analytes in the <50 µm micron fraction of regolith from sites on the SS transect across the Balgo Fault. Values on x-axis are sample distance (metres) from the fault, calculated perpendicular to the fault trace: a) lithophile elements; b) HFSE, transition elements, and P; c) rare earth elements; d) base metals and chalcophile elements

Fig. 32) coincident with the Stansmore Fault. In contrast, most HFSE and the remaining base metals (Cu, Pb), and other chalcophile elements (Bi, Sb, S) show no anomalism in this sample.

Fault control on the composition of regolith is less clear in the SR transect. Only REE and Zn in regolith sample 220626 (SR14 over the western unnamed fault) show any control by faulting (Fig. 33). Spinifex from this site has unusually high concentrations of B, Re, and Cd, but not REE (Fig. 34). However, high concentrations of REE are recorded in 220899 (SR9) from about 900 m east of the Stansmore Fault (Fig. 33), and this sample also has elevated concentrations of several lithophile elements, Zn (but not Cu or Pb), and Sb (but not As or Bi).

On the SS transect over the Balgo Fault, the highest concentrations of REE, Sr and V are in 220679 (SS4) from about 300 m east of the fault rather than on the fault trace itself (i.e. 221109; SS10), so either regolith chemistry is not spatially related to faulting, or the position of the subsurface trace of the Balgo Fault might have been misinterpreted from geophysical data, and could lie farther east than mapped. However, unlike data from the SRT transect, fluid-mobile elements and Zn are not elevated in 220679.

Fault-controlled fluid flux and composition

The mobility of elements in fluids, and the ability of either the fine fraction of regolith or plants to take up elements, is related to the element's ionic potential (Hawkes and Webb, 1962; Brooks, 1972; Dunn, 2007), which is the ratio of the charge (Z) to the ionic radius (r). Lithophile elements, such as Cs, Rb, Li and K, have $Z/r < 2$ (Table 11) and these are more likely to be fluid mobile than HFSE, such as Nb, Zr, Hf and Ta which have $Z/r > 5$.

On the SRT transect across the Stansmore Fault (Figs 31a, 32), the higher concentrations of low Z/r elements (especially Li and Cs) in GSWA 220790 (SRT10; Fig. 32a,b) are consistent with higher fluid flux close to the fault. A higher fluid flux may also explain the elevated concentrations of the REE, Be, Ti and Te, even though they have higher Z/r values (Table 11). The variation in concentration of elements with similar Z/r can provide information on fluid composition. Copper and Zn have similar Z/r values (2.78 and 2.70 respectively), but only Zn is enriched in 220790 (Fig. 32d). Similarly, As and Bi have similar Z/r values (Table 11), but only As is enriched in 220790.

Interpreting the influence of faulting on the chemistry of regolith and spinifex on the SR transect is more problematic, as only one site (SR14) coincides with a fault trace. Elevated concentrations of REE in regolith sample 220626 from this site (SR14) are broadly coincident with the western unnamed fault, and there is a spike in REE concentrations in GSWA 220899 (SR9) from approximately 900 m east of the Stansmore Fault.

Table 11. Ionic charge (Z), ionic radius (r) and ionic potential (Z/r) for selected elements. Data from Shannon (1976) and Krauskopf (1967). Shading highlights different element groupings: unshaded, lithophile elements; brown, base metals; yellow, chalcophile elements; blue, transition elements; green, rare earth elements and Y; grey, high field strength elements

Element	Coord	Charge	Ionic radius	Z/r
Ba		2	1.61	1.24
Be		2	0.27	7.41
Al		3	0.54	5.56
Cs		1	1.88	0.53
Tl		1	1.7	0.59
Rb		1	1.72	0.58
K		1	1.64	0.61
Sr		2	1.26	1.59
Na		1	1.18	0.85
Li		1	0.76	1.32
Ca		2	1.12	1.79
Ag		1	1.26	0.79
B		3	0.27	11.11
P		5	0.17	29.41
Cu		2	0.73	2.74
Pb		2	1.29	1.55
Zn		2	0.74	2.70
As		3	0.58	5.17
Sb		5	0.62	8.06
Te		6	0.56	10.71
Bi		3	0.96	3.13
Fe		3	0.65	4.62
Cr		3	0.62	4.84
Sc		3	0.75	4.00
V		3	0.64	4.69
Ni		2	0.69	2.90
La	6	3	1.16	2.59
Ce	6	3	1.14	2.63
Nd	6	3	1.11	2.70
Sm	6	3	1.08	2.78
Eu	6	2	1.25	1.60
Gd	6	3	1.05	2.86
Dy	6	3	1.03	2.91
Yb	6	3	0.99	3.03
Y		3	1.02	2.94
Zr		4	0.84	4.76
Nb		5	0.64	7.81
Hf		4	0.83	4.82
Ti		4	0.61	6.56

High concentrations of low Z/r elements such as B, Na and Li in spinifex from SR14 provide support for some fluid flux along the western unnamed fault. All of the REE in spinifex are strongly enriched in SR9, with a more subdued response at site SR14. The behaviour of base metals in spinifex is analogous to their behaviour in regolith samples from the SRT transect, in that Zn, but not Cu or Pb, are in higher concentrations in SR9 and SR14. However, chalcophile elements show contrary enrichments and depletions relative to regolith on the SRT transect. Spinifex is enriched in Sb and Re at SR9, but depleted in As and Bi. Cadmium shows a broad anomaly in relation to the western fault, with a pattern similar to that for Re. These data indicate fluid flux along the western unnamed fault, as well as some flux coincident with site SR9, which suggests either a previously unmapped fault nearby, or a more easterly position for the Stansmore Fault. More precise interpretation of regolith and spinifex chemistry is hampered by the complex structural situation along this transect.

Despite one sample located within 40 m of the Balgo Fault, there is no clear relationship of fine-fraction regolith chemistry and fault location on the SS transect (Fig. 35a–d). The highest REE concentrations are in 220679 approximately 300 m east of the fault, but other elements show no significant change in concentration in this sample, and unlike the SRT transect, there is no contrasting behaviour of Zn in relation to Cu and Pb. Thus, either the Balgo Fault is not a fluid conduit, or the fluid flux is too weak to be registered in the fine fraction of regolith.

Spinifex chemistry and plant metabolism

Apart from an element's ionic radius, plant metabolism can also affect element uptake (Dunn, 2007). For example, Zn is an essential nutrient for plants, so it could be argued that elevated Zn in spinifex at site SR14 (Fig. 35d) is due to preferential uptake, rather than a characteristic of the fluid. However, on the SR transect, Zn is elevated in regolith sample 220790 over the Stansmore Fault but not at other sites (Fig. 32d), indicating that it is a compositional characteristic of a fault-controlled fluid. Thus, elevated Zn in spinifex at site SR14 probably reflects both a heightened fluid flux controlled by the fault and a compositional characteristic of the fluid.

Relationship to mineralization

The elevated concentrations of various element groups with a range of Z/r values in regolith are interpreted as evidence of a heightened fluid flux on the Stansmore Fault along the SRT transect. This is also evident in the structurally more complex part of the fault trace in the vicinity of the SR transect. The behaviour of Zn compared with Cu and Pb, and the elevated content of Tl (despite its low concentration), is analogous to geochemical vectors to sediment-hosted exhalative (SEDEX)-style mineralization discussed by Large and McGoldrick (1998) and Large et al. (2000). They noted that Zn shows moderate dispersion (<100 m) and Tl shows broad dispersion (<200 m) around the Proterozoic Lady Loretta deposit in Queensland, and Zn, Pb and Tl haloes extended up to 250 m in the hangingwall and 50–100 m in the footwall of the HYC deposit in the Northern Territory. However, they provided

no discussion on the behaviour of REE, which is the group of elements that shows the most convincing evidence for fault-controlled fluid flux on the Ngururrpa transects.

The behaviour of REE in SEDEX deposits is variable. Data from the Late Devonian Tom and Nidd deposits from the Yukon (Magnall et al., 2014), show a progressive depletion in both LREE and HREE, an increasingly positive Eu anomaly with increasing Zn content (Fig. 36a), and negative Ce anomalies. Magnall et al. (2014) attributed the strong positive Eu anomaly to the presence of Ba-rich feldspar. Unmineralized or weakly mineralized shales have REE patterns typical of shales such as NASC and PAAS (cf. Fig. 28), with sloping LREE patterns, negative Eu anomalies and flatter HREE patterns. Broadly similar but more variable REE patterns from the middle Devonian Dengjiashan Zn–Pb SEDEX deposits (Fig. 36b; Qinling Belt, China) were attributed to oxidized seawater that leached Eu from feldspars in the underlying bedrock (Ma et al., 2007). In contrast, there is little difference in the REE patterns of host rocks and bedded and massive sulfides in the Devonian Changba Pb–Zn SEDEX deposit (Fig. 36c; Qinling Belt). This deposit is hosted by biotite-quartz schist, with mineralization as either a bedded facies or breccia lenses (Ma et al., 2004). Sulfur isotope data indicate that reduced sulfur was derived from the mixing of seawater sulfate and heavier hydrothermal sulfur. The similarity of host-rock, bedded and massive sulfide REE patterns indicate that hydrothermal fluids leached REE from the underlying bedrock (Ma et al., 2004).

The REE patterns of regolith and spinifex from the Ngururrpa transects are parallel, with no change in concentrations of elements such as Eu or Ce that can be attributed to the effects of hydrothermal alteration or seawater that may be related to SEDEX-style mineralization. Instead, the elevated REE concentrations in spinifex or regolith samples on or near the Stansmore Fault are interpreted in terms of elevated fluid flux, rather than a compositional characteristic indicative of a specific style of mineralization.

Independent evidence in support of SEDEX-style mineralization in the Ngururrpa area is provided by the results of mineral exploration to the south of the Ngururrpa area on WEBB, and revisions made to Murraba Basin stratigraphy by Haines and Allen (2016, 2017). On the northern part of WEBB, Cassini Resources Limited has identified SEDEX-style base metal mineralization at the Enceladus and Iapetus prospects (Cassini Resources Limited, 2015, 2016a,b,c; Fig. 37) in the Bitter Springs Group, part of the Neoproterozoic Amadeus Basin. They have argued that these deposits are analogous to the Century Zn–Pb deposit in the Mt Isa area of Queensland. Rock chip samples with up to 4700 ppm Zn, and elevated concentrations of Pb, Cd, Ni, Cu and Tl have been reported. Near-surface Zn enrichment has been attributed to hydromorphic dispersion from nearby primary zinc mineralization (Cassini Resources Limited, 2016c), whereas elevated Cd has been equated to the presence of sphalerite (Cassini Resources Limited, 2015).

In their revision of Murraba Basin stratigraphy, Haines and Allen (2016, 2017) discussed the distribution of float approximately 200 km northeast of the Enceladus and Iapetus prospects (Fig. 37; note location of figure 7 of Haines and Allen, 2017). They noted that part of the

stratigraphy they interpreted from this float comprised calcrete, and clasts of chert and carbonate (micrites and grainstones, with possible stromatolites) that they assigned to the Bitter Springs Group. Regolith samples from the Ngururrpa program do not extend to the location discussed by Haines and Allen (2017), but the area immediately to the west, north and south has 16 of the 35 regolith samples with anomalous Zn concentrations (i.e. >26 ppm). These 16 samples (purple and red stars in Fig. 37) represent a variety of regolith–landform types, including relict carbonate-rich regolith, lacustrine regolith, regolith in areas of outcrop, and sandplain, so the high Zn content of these samples cannot be accounted for by a particular regolith-forming process.

Ngururrpa project area — mineralization potential

Due to its remoteness, extensive cover of largely transported regolith, and chemically mature siliciclastic-dominated bedrock, the Ngururrpa area has attracted little mineral exploration activity, and can be classed as a greenfields area. Results of GSWA's regolith geochemistry program presented and discussed in this Record indicate three areas of potential mineralization:

1. In the north of the Ngururrpa project area are several samples with elevated and anomalous concentrations of Au, including a sample of colluvium from M733 (221058) over the Hidden Basin beds, which contains 63 ppb Au. Revisions to the Murraba Basin geology discussed by Haines and Allen (2016, 2017) have resulted in an increase in the area assigned to the Granites–Tanami Orogen, a terrane with demonstrated gold mineralization (Bagas et al., 2009, 2010). Only a few samples with >4 ppb Au have anomalous concentrations of other elements, and in terms of regolith type, they include colluvium, sandplain, lacustrine regolith and sheetwash. This implies that gold is probably present as small discrete particles. This may also explain the poor reproducibility of Au in 221058 from umpire laboratory analysis (63 ppb vs 10.7 ppb).

Of the 20 samples with ≥4 ppb Au, six are from the Redcliff Pound Group, six are from the Hidden Basin beds, and four are from the Liveringa Group (Fig. B20b). Some samples from the Liveringa Group have anomalous concentrations of chalcophile and transition elements, indicating that elevated Au could be associated with development of secondary sulfides and Fe compounds through weathering. Ferruginous lag is not present at all sampling sites, and the Au concentration of lag is similar to that in the <50 µm fraction of regolith, so lag sampling is not considered preferable to the fine fraction of regolith.

2. Regolith–landform mapping, aeromagnetism, ASTER, and drillhole data have been combined to identify three paleodrainage systems, with channels up to 90 m deep. The largest system drains southwest from the Granites–Tanami Orogen. Anand and Paine (2002) and Anand and Butt (2010) have discussed the importance of paleochannels for gold mineralization in the Yilgarn Craton, and paleochannels identified in the Ngururrpa area — particularly those related to the

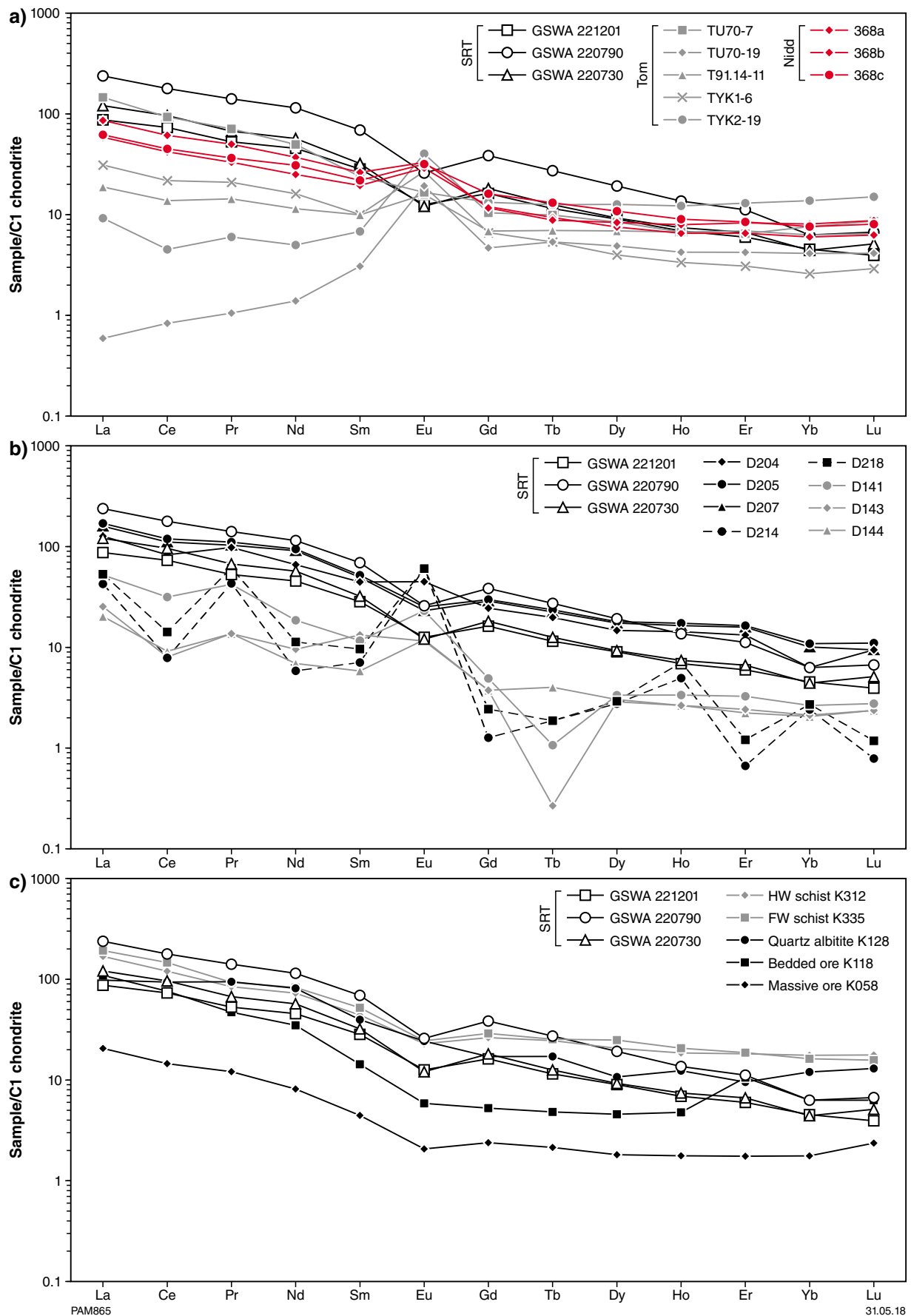


Figure 36. Chondrite-normalized REE chemistry of host and mineralized rocks from various SEDEX deposits compared to Ngururupa transect data: a) Tom and Nidd deposits (Yukon, Canada; Magnall et al., 1984); b) Dengjiashan deposit (Qinling Belt, China; Ma et al., 2007); c) Changba deposit (Qinling Belt, China; Ma et al., 2004). On each plot are analyses of the fine fraction of regolith from SRT transect: sample 220790 (SRT10) on the Stansmore Fault trace, and samples 221201 (SRT1) and 220730 (SRT6) either side of 220790 (see Fig. 31a)

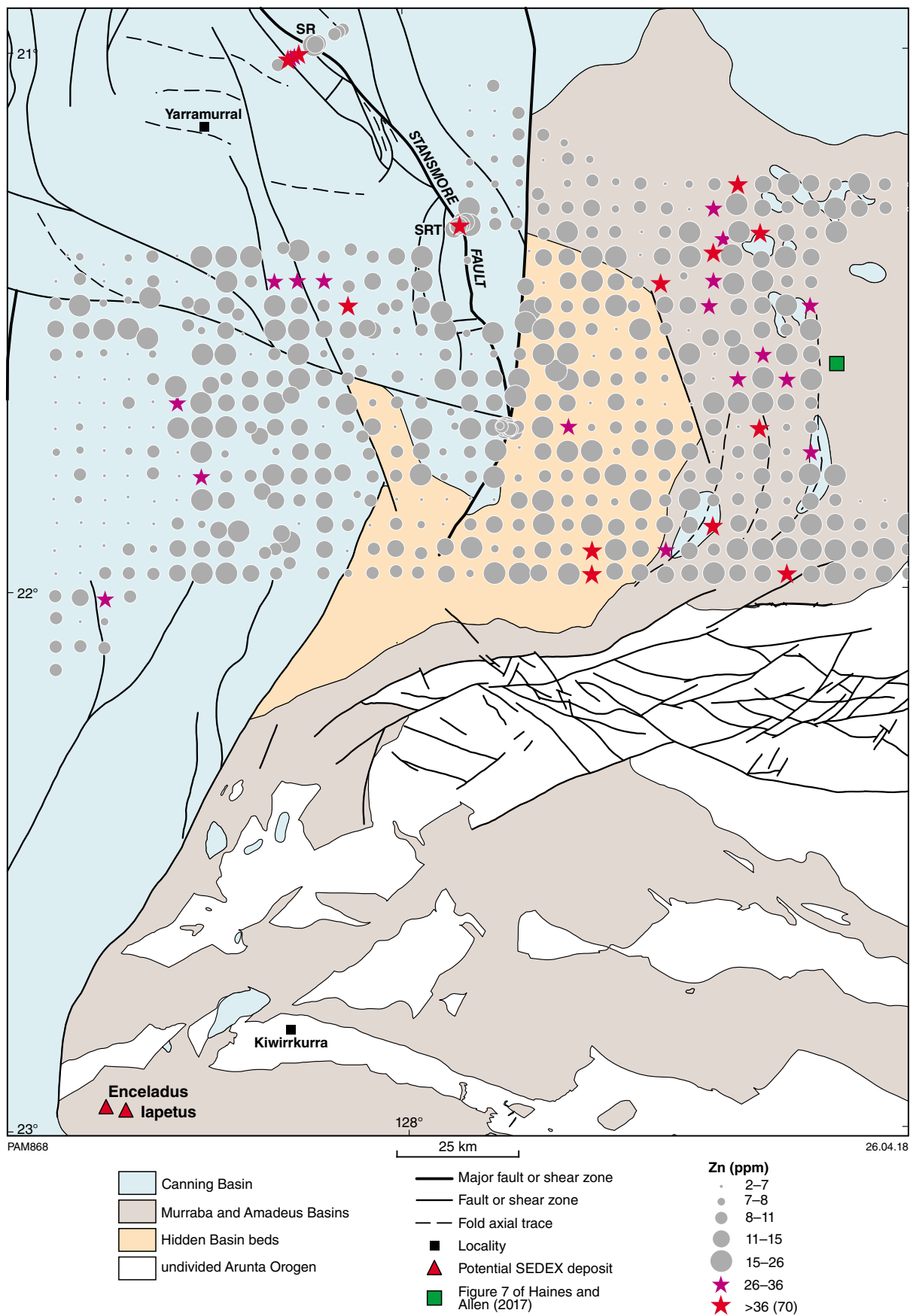


Figure 37. Zinc (ppm) in the fine fraction of regolith from the Ngurrupa program area. Also shown is the location of interpreted Bitter Springs Group stratigraphy in the Murraba Basin (Haines and Allen, 2016, 2017), and the location of Cassini Resources Pty Ltd's Enceladus and lapetus prospects on WEBB. The SRT and SR Stansmore Fault transects are indicated

Granites–Tanami Orogen area, which has proven gold mineralization — are possible exploration targets for placer gold deposits.

3. The chemistry of <50 µm fraction of regolith, and of spinifex samples, can be used to identify whether regional faults are likely fluid conduits, as well as providing some information on the type of buried mineralization. These data indicate that the Stansmore Fault could be tapping buried SEDEX-style mineralization, consistent with identification of prospective units in the southeast of the Ngururra program (Haines and Allen, 2016, 2017), and demonstrated SEDEX mineralization in the same part of the stratigraphy on WEBB.

Conclusion

Compared to other parts of the State where bedrock geology is more prospective and regolith cover of more limited extent and of local origin, the Ngururra program area in the northeastern part of Western Australia is, at first glance, an area of limited mineral prospectivity. This regional regolith geochemistry program carried out by GSWA has resulted in a multi-element dataset of chemistry from the fine fraction of 837 regolith samples collected over representative parts of the stratigraphy at a nominal density of one sample every 12.5 km². Site information collated during regolith sampling has provided valuable information for validating a regolith–landform map compiled at 1:100 000 scale using a combination of published geological mapping, digital elevation data (DEM), orthophotography, geophysics (aeromagnetism), radiometrics, ASTER and Google Earth imagery. There is limited outcrop in the Ngururra area; regolith in areas of outcrop accounts for only 13% by area, and relict or residual regolith a further 16% by area. The subdued topography means that transported regolith is dominated by eolian deposits (48% by area). This sandplain forms a thin veneer on weathered bedrock. However, the occurrence of ferruginous lag, variably ferruginized bedrock fragments, and isolated patches of ferricrete and less common calcrete suggest that bedrock is close to the surface. This is consistent with the results of exploration drilling and single-station passive seismic data, which show that quartz-rich sandplain deposits are <10 m, and more likely 1–3 m, thick.

By combining the results of regolith–landform mapping, drillhole data and aeromagnetism, four paleodrainage systems have been identified, three of which are calcrete filled and of regional extent, ultimately draining into Lake Mackay to the south of the Ngururra program area on WEBB. Drillhole data show that channel fill can attain thicknesses of up to 90 m. A more aerially restricted series of paleochannels was identified using aeromagnetic data, as the paleochannels are filled with magnetic material (most probably maghemite). They appear to be marginal to, and drain into, calcrete-filled channels.

Both the Murraba and Canning Basin successions are dominated by quartz-rich siliciclastic sedimentary rocks

(sandstones, conglomerates, and siltstones). This, combined with scattered and usually weathered outcrops, has made it difficult to establish a regional stratigraphy, especially for the Murraba Basin. The chemical maturity of bedrock and the dominance of regolith cover by quartz-rich sand means that bulk regolith chemistry is unlikely to be useful in detecting any changes in underlying bedrock composition or detecting bedrock-hosted mineralization. Use of the <50 µm fraction of regolith should in part account for the dilution effect of quartz sand, but regolith data from the Ngururra program has indicated little conclusive evidence for bedrock control on regolith composition. This result can be attributed to the chemical maturity of both bedrock and regolith. Elevated Au concentrations in samples spatially associated with the Granites–Tanami Orogen are not linked to either chalcophile element abundance, carbonation or ferruginization. Instead, it is likely that microparticulate Au has migrated vertically from bedrock as an exogenic component which is loosely bound in the fine fraction of regolith.

The chemistry of the <50 µm fraction of regolith and that of spinifex has potential to detect faults that control fluid pathways, as well as providing information on the composition of fault-controlled fluids. Data from the Ngururra area has identified the Stansmore Fault as a focusing structure, consistent with its history of periodic reactivation and likely penetration to basement. In contrast, the lack of a fluid flux across the Balgo Fault indicates either a weaker fluid flux or that the fault is not an active conduit for fluids. The elevated concentrations of Zn and elements such as Tl in regolith and/or spinifex associated with the Stansmore Fault are indicators of buried mineralization hosted in sedimentary rocks. This is consistent with SEDEX-style mineralization on WEBB, and identification of favourable stratigraphy in parts of the Murraba Basin in the Ngururra area.

The effectiveness of the fine-fraction of regolith approach is likely to be enhanced in areas where regolith is well sorted and uncemented, as this facilitates the upward migration of an exogenic component derived from bedrock and bedrock-hosted mineralization. The sequestering of this component as loosely bound or bonded component in the fine fraction of regolith has an analogy in the take-up of fluid-mobile elements by plants, and the method has potential for identifying the position and mineral potential of regional faults. The most common type of well-sorted, permeable regolith in Western Australia is quartz-rich eolian sand. Ironically, this chemically mature transported regolith has been viewed as one of the least useful sample media for regional geochemical exploration.

Acknowledgements

The traditional owners of Ngururra country (Parna Ngururra) are thanked for their guidance and hospitality during the planning and execution of the Ngururra sampling program.

References

- Ahmad, M 2013, Chapter 25: Murraba Basin, *in* Geology and mineral resources of the Northern Territory *compiled by* M Ahmad and TJ Munson: Northern Territory Geological Survey, Special Publication 5, p. 25.1–25.3.
- Anand, RR 2005, Weathering history, landscape evolution and implications for exploration, *in* Regolith landscape evolution across Australia *edited by* RR Anand and P de Broekert: CRC LEME, Perth, p. 2–40.
- Anand, RR and Butt, CRM 2010, A guide for mineral exploration through the regolith in the Yilgarn Craton, Western Australia: Australian Journal of Earth Sciences, v. 57, p. 1015–1114.
- Anand, RR, Churchward, HM, Smith, RE, Smith, K, Gozzard, JR, Craig, MA and Munday, TJ 1993, Classification and atlas of regolith–landform mapping units: Exploration perspectives for the Yilgarn Craton, Australia: CSIRO Division of Exploration and Mining Restricted Report 440R (unpublished).
- Anand, RR and de Broekert, P 2005, Regolith landscape evolution across Australia: CRC LEME, Perth, Western Australia, 345p.
- Anand, RR and Paine, MD 2002, Regolith geology of the Yilgarn Craton, Western Australia: implications for exploration: Australian Journal of Earth Sciences, v. 49, p. 3–162.
- Bagas, L, Anderson, JAC and Bierlein, FP 2009, Palaeoproterozoic evolution of the Killi Killi Formation and orogenic gold mineralization in the Granites–Tanami Orogen, Western Australia: Ore Geology Reviews, v. 35, p. 47–67.
- Bagas, L, Bierlein, FP, Anderson, JAC and Maas, R 2010, Collision-related granitic magmatism in the Granites–Tanami Orogen: Precambrian Research, v. 177, p. 212–226.
- Bao, Z and Zao, Z 2008, Geochemistry of mineralization with exchangeable REY in the weathering crusts of granitic rocks in South China: Ore Geology Reviews, v. 33, p. 519–535.
- Beard, JS and Webb, MJ 1974, Great Sandy Desert, sheet 2: The University of Western Australia, 1:100 000 Vegetation Series – Map and Explanatory Notes.
- Blake, DH 1974, Shallow stratigraphic drilling in the Granites–Tanami region, Northern Territory and Western Australia, 1971–73: Bureau of Mineral Resources, Geology and Geophysics, Record 1974/104, 93p.
- Blake, DH, Hodgson, IM and Muhling, PC 1979, Geology of the Granites–Tanami region, Northern Territory and Western Australia: Bureau of Mineral Resources, Geology and Geophysics, Bulletin 197, 91p.
- Blake, DH, Passmore, VL and Muhling, PC (compilers) 1977, Billiluna, Western Australia: Bureau of Mineral Resources and Geological Survey of Western Australia, 1:250 000 Geological Series Explanatory Notes, 28p.
- Blake, DH and Yeates, AN (compilers) 1976, Stansmore, Western Australia (2nd edition): Bureau of Mineral Resources and Geological Survey of Western Australia, 1:250 000 Geological Series Explanatory Notes, 20p.
- Boullier, A-M, Fujimoto, K, Ohtani, T, Roamn-Ross, G, Lewin, E, Ito, H, Pezard, P and Ildefonse, B 2004, Textural evidence for recent co-seismic circulation of fluids in the Nojima fault zone, Awaji Island, Japan: Tectonophysics, v. 378, p. 165–181.
- Brooks, RR 1972, Biological methods of prospecting for minerals: John Wiley and Sons, New York, 322p.
- Cameron, EM, Leybourne, MI, Reich, M and Palacios, C 2010, Geochemical anomalies in northern Chile as a surface expression of the extended supergene metallogenesis of buried copper deposits: Geochemistry: Exploration, Environment, Analysis, v. 10, p. 157–169.
- Carver, RN, Chenoweth, LM, Mazzucchelli, RH, Oates, CJ and Robbins, TW 1987, “Lag” — a geochemical sampling medium for arid regions: Journal of Geochemical Exploration, v. 23, p. 183–199.
- Casey, JN and Wells, AT 1964, The geology of the north-east Canning Basin, Western Australia: Australian Bureau of Mineral Resources, Report 49, 61p.
- Cassini Resources Limited 2015, Re-release: zinc discovery at X17 in west Arunta: Report to Australian Securities Exchange, 4 November 2015, 13p.
- Cassini Resources Limited 2016a, West Arunta zinc drilling underway: Report to Australian Securities Exchange, 9 May 2016, 4p.
- Cassini Resources Limited 2016b, EIS drilling grant for west Arunta: Report to Australian Securities Exchange, 14 June 2016, 3p.
- Cassini Resources Limited 2016c, Broad zinc zones intersected at west Arunta: Report to Australian Securities Exchange, 23 June 2016, 16p.
- Chao, TT and Sanzolone, RF 1992, Decomposition techniques: Journal of Geochemical Exploration, v. 44, p. 65–106.
- Crowe, RWA (compiler) 1978, Cornish, Western Australia (2nd edition): Geological Survey of Western Australia, 1:250 000 Geological Series Explanatory Notes, 19p.
- Crowe, RWA and Muhling, PC (compilers) 1977, Lucas, Western Australia (2nd edition): Bureau of Mineral Resources and Geological Survey of Western Australia, 1:250 000 Geological Series Explanatory Notes, 23p.
- Cudahy, T, Caccetta, M and Collings, S 2012, ASTER geoscience map of Western Australia, *in* GSWA 2012 Extended Abstracts: promoting the prospectivity of Western Australia: Geological Survey of Western Australia, Record 2012/2, p. 14–19.
- Cullers, RL, Chaudhuri, S, Kilbane, N and Koch, R 1979, Rare earths in size fractions and sedimentary rocks of Pennsylvanian–Permian age from the mid-continent of the USA: Geochimica et Cosmochimica Acta, v. 43, p. 1285–1302.
- Dentith, MC and Mudge, ST (editors) 2014, Radiometric method, *in* Geophysics for the mineral exploration geoscientist: Cambridge University Press, UK, p. 193–233.
- Dunn, CE 2007, Biogeochemistry in mineral exploration: Handbook of Exploration and Environmental Geochemistry (series editor M Hale) Volume 9, Elsevier, Amsterdam, 462p.
- English, P 2016, Ancient origins of some major Australian salt lakes: geomorphic and regolith implications, *in* Proceedings *edited by* M Thomas: Fourth Australian Regolith Geoscientists Association Conference, Thredbo, New South Wales, 7–11 February 2016, p. 10–14.
- Frery, E, Gratier, J-P, Ellouz-Zimmerman, N, Loiselet, C, Braun, J, Deschamps, P, Blamart, D, Hamelin, B and Swennen, R 2015, Evolution of fault permeability during episodic fluid circulation: Evidence for the after effects of fluid–rock interactions from travertine studies (Utah-USA): Tectonophysics, v. 651–652, p. 121–137.
- Garrett, MJ 1956, Gravity traverses by Geological Party G.C., in the eastern portion of the Fitzroy–Canning Basin: Western Australian Petroleum Pty Ltd (unpublished company report).
- Geological Survey of Western Australia 2008, West Arunta Geological Exploration Package: Geological Survey of Western Australia, Record 2008/17, digital data package.
- Geological Survey of Western Australia 2013, Revised classification system for regolith in Western Australia, and the recommended approach to regolith mapping: Geological Survey of Western Australia, Record 2013/7, 26p.
- Geological Survey of Western Australia 2016, 1:500 000 State interpreted bedrock geology of Western Australia, 2016: Geological Survey of Western Australia, digital data layer, <www.dmp.wa.gov.au/geoview>.
- Grunsky, EC 2010, The interpretation of geochemical survey data: Geochemistry: Exploration, Environment, Analysis, v. 10, p. 27–74.
- Gunn, MJ 1983, Final report exploration licence 80/3 Stansmore, Stansmore 1:250 000 sheet, Western Australia: BHP Minerals Division: Geological Survey of Western Australia Statutory mineral exploration report, A12302, 26p.

- Haines, PW and Allen, HJ 2016, The Murraba Basin: another piece of the Centralian Superbasin jigsaw puzzle falls into place, *in* GSWA 2016 extended abstracts: promoting the prospectivity of Western Australia: Geological Survey of Western Australia, Record 2016/2, p. 31–35.
- Haines, PW and Allen, HJ 2017, Geological reconnaissance of the southern Murraba Basin, Western Australia: revised stratigraphic position within the Centralian Superbasin and hydrocarbon potential: Geological Survey of Western Australia, Record 2017/4, 38p.
- Hall, GEM 1998, Analytical perspective on trace element species of interest in exploration: *Journal of Geochemical Exploration*, v. 10, p. 27–74.
- Hawkes, HE and Webb, JS 1962, *Geochemistry in mineral exploration*: Harper and Row, New York, US, 415p.
- Johnson, SP, Thorne, AM, Tyler, IM, Korsch, RJ, Kennett, BLN, Cutten, HN, Goodwin, J, Blay, OA, Blewett, RS, Joly, A, Dentith, MC, Aitken, ARA, Holzschuh, J, Salmon, M, Reading, A, Heinson, G, Boren, G, Ross, J, Costelloe, RD and Fomin, T 2013, Crustal architecture of the Capricorn Orogen, Western Australia and associated metallogeny: *Australian Journal of Earth Sciences*, v. 60, no. 6–7, p. 681–705, doi:10.1080/08120099.2013.826735.
- Joly, A, Dentith, MC, Porwal, A, Spaggiari, CV, Tyler, IM and McCuaig, TC 2013, An integrated geological and geophysical study of the west Arunta Orogen and its mineral prospectivity: Geological Survey of Western Australia, Report 113, 89p.
- Kirkland, CL, Wingate, MTD, Spaggiari, CV and Tyler, IM 2009a, 184341: quartzite, Lake Mackay; *Geochronology Record* 818: Geological Survey of Western Australia, 5p.
- Kirkland, CL, Wingate, MTD, Spaggiari, CV and Tyler, IM 2009b, 184342: sandstone, Alec Ross Range; *Geochronology Record* 819: Geological Survey of Western Australia, 5p.
- Kirkland, CL, Wingate, MTD, Tyler, IM and Spaggiari, CV 2009c, 184367: metagranodiorite, Dwarf Well; *Geochronology Record* 846: Geological Survey of Western Australia, 4p.
- Kojan, CJ and Faulkner, JA 1994, Geochemical mapping of the Menzies 1:250 000 sheet: Geological Survey of Western Australia, 1:250 000 Regolith Geochemistry Explanatory Notes, 55p.
- Krauskopf, KB 1967, *Introduction to geochemistry*: McGraw-Hill, New York, 721p.
- Large, RR, Bull, SW and McGoldrick, PJ 2000, Lithogeochemical halos and geochemical vectors to stratiform sediment-hosted Zn–Pb–Ag deposits: Part 2. HYC deposit, McArthur River, Northern Territory: *Journal of Geochemical Exploration*, v. 68, p. 105–126.
- Large, RR and McGoldrick, PJ 1998, Lithogeochemical halos and geochemical vectors to stratiform sediment-hosted Zn–Pb–Ag deposits, 1. Lady Loretta Deposit, Queensland: *Journal of Geochemical Exploration*, v. 63, p. 37–56.
- Leybourne, MI and Rice, S 2013, Determination of gold in soils and sediments by fire assay or aqua regia digestion: choosing the optimal method: *Explore*, v. 158, p. 2–10.
- Lindsay, MD, Aitken, AR, Ford, A, Dentith, MC, Hollis, JA and Tyler, IM 2015, Mineral prospectivity of the King Leopold Orogen and Lennard Shelf: analysis of potential field data in the west Kimberley region: Geological Survey of Western Australia, Report 142, 65p.
- Ma, G, Beaudoin, G, Qi, S and Li, Y 2004, Geology and geochemistry of the Changba Zn–Pb SEDEX deposit, Qinling Orogenic Belt, China: *Mineralium Deposita*, v. 39, p. 380–395.
- Ma, G, Beaudoin, G, Zhong, S, Li, Y and Zhangren, Z 2007, Geology and geochemistry of the Dengjiashan Zn–Pb SEDEX deposit, Qinling Belt, China: *Canadian Journal of Earth Sciences*, v. 44, p. 479–492.
- Ma, C and Eggleton, RA 1999, Cation exchange capacity of kaolinite: *Clays and Clay Minerals*, v. 47, p. 174–180.
- Mackey, T, Lawrie, K, Wilkes, P, Munday, T, de Souza Kovacs, N, Chan, R, Gibson, D, Chartres, C and Evans, R 2000, Paleochannels near West Wyalong, New South Wales: A case study in delineation and modelling using aeromagnetism: *Exploration Geophysics*, v. 31, p. 1–7.
- Magee, J 2009, Paleovalley groundwater resources in arid and semi-arid Australia — a literature review: *Geoscience Australia, Record* 2009/3, 224p.
- Magnall, JM, Gleeson, SA and Paradis, S 2014, SEDEX mineralisation, Macmillan Pass (Yukon): petrography, mineralogy and bulk geochemistry of the Tom and Nidd deposits: Geological Survey of Canada Open File 7457, 37p.
- Martin, DMcB, Hocking, RM, Riganti, A and Tyler, IM 2016, 1:10 000 000 tectonic units of Western Australia: Geological Survey of Western Australia, digital data layer, <www.dmp.wa.gov.au/geoview>.
- Mann, AW 2010, Strong versus weak digestions: ligand-based soil extraction geochemistry: *Geochemistry: Exploration, Environment, Analysis*, v. 10, p. 17–26.
- McCuaig, TC, Beresford, S and Hronsky, J 2010, Translating the mineral systems approach into an effective exploration targeting system: *Ore Geology Reviews*, v. 38, p. 128–138.
- McCuaig, TC and Hronsky, JMA 2014, The mineral system concept: the key to exploration targeting, *in* Building exploration capability for the 21st century *edited by* KD Kelley and HC Golden: Society of Economic Geologists, Inc., Special Publication 18, p. 153–175.
- McGuinness, SJ 2010, Regolith–landform mapping of the east Wongatha area, *in* East Albany–Fraser and southeast Yilgarn, 2011 update: Geological Survey of Western Australia, Geological Exploration Package, digital data layer.
- McLennan, SM 1989, Rare earth elements in sedimentary rocks: influence of provenance and sedimentary processes: *Reviews in Mineralogy and Geochemistry*, v. 21, no. 1, p. 169–200.
- Middleton, MF 1990, Canning Basin, *in* *Geology and mineral resources of Western Australia — Chapter 4: Basins*: Geological Survey of Western Australia, Memoir 3, p. 425–457.
- Morris, PA 2011, Fine-fraction gold chemistry of regolith from the east Wongatha area, eastern Yilgarn Craton, *in* GSWA 2011 extended abstracts: promoting the prospectivity of Western Australia: Geological Survey of Western Australia, Record 2011/2, p. 24–26.
- Morris, PA 2013, Fine-fraction geochemistry of regolith from the east Wongatha area: tracing bedrock and mineralization through cover: Geological Survey of Western Australia, Record 2012/13, 61p.
- Morris, PA, Sanders, AJ and Faulkner, JA 1997, Geochemical mapping of the Nabberu 1:250 000 sheet: Geological Survey of Western Australia, 1:250 000 Regolith Geochemistry Explanatory Notes, digital data package.
- Morris, PA, Sanders, AJ, McGuinness, SA, Coker, J and King, JD 2000, Geochemical mapping of the Fraser Range region: Geological Survey of Western Australia, 1:250 000 Regolith Geochemistry Explanatory Notes, 81p.
- Morris, PA, Scheib, AJ and de Souza Kovacs, N 2015, Regolith chemistry of the Balangarra area, north Kimberley: Geological Survey of Western Australia, Record 2015/9, 142p.
- Morris, PA, Scheib, AJ and de Souza Kovacs, N 2016, Regolith chemistry of the Dambimangari area, west Kimberley: Geological Survey of Western Australia, Record 2016/15, 126p.
- Morris, PA and Verren, AL 2001, Geochemical mapping of the Byro 1:250 000 sheet: Geological Survey of Western Australia, 1:250 000 Regolith Geochemistry Explanatory Notes, 53p.
- Mory, AJ 2010, A review of mid-Carboniferous to Triassic stratigraphy, Canning Basin, Western Australia: Geological Survey of Western Australia, Report 107, 130p.
- Playford, PE, Cope, RN, Cockbain, AE, Low, GH and Lowry, DC 1975, Chapter 2. Phanerozoic *in* *The geology of Western Australia*: Geological Survey of Western Australia, Memoir 2, p. 223–433.
- Reimann, C, Filzmoser, P, Garrett, RG and Dutter, R 2008, *Statistical data analysis explained*: John Wiley and Sons Ltd, Chichester, UK, 343p.
- Rudnick, RL and Gao, S 2003, Composition of the continental crust: *Treatise on Geochemistry*, v. 3, p. 1–64.

- Salminen, R 2011, Geochemical mapping; past, present, future, *in* Programme and Abstracts: 25th International Geochemistry Exploration Symposium, Rovaniemi, Finland, 22–26 August 2011, p. 51–52.
- Sanders, AJ and McGuinness, SA 2000, Geochemical mapping of the Ajana 1:250 000 sheet: Geological Survey of Western Australia, 1:250 000 Regolith Geochemistry Explanatory Notes, 55p.
- Scheib, AJ 2014a, Regolith geochemistry and mineral prospectivity — the southeast Yilgarn Craton and east Albany–Fraser Orogen: Geological Survey of Western Australia, Record 2014/3, 50p.
- Scheib, AJ 2014b, The application of passive seismic to estimate cover thickness in greenfields areas of Western Australia — method, data interpretation and recommendations: Geological Survey of Western Australia, Record 2014/9, 67p.
- Scheib, AJ, Morris, PA and de Souza Kovacs, N 2016a, Regolith chemistry of the Bunuba and Yuriyngem–Taam areas, south Kimberley: Geological Survey of Western Australia, Record 2015/15, 109p.
- Scheib, AJ, Morris P, Murdie RE and Delle Piane, C 2016b, A passive seismic approach to estimating the thickness of sedimentary cover on the Nullabor Plain, Western Australia: Australian Journal of Earth Sciences, v. 63, p. 583–598.
- Schoknecht, NR and Pathan, S 2013, Soil groups of Western Australia: a simple guide to the main soils of Western Australia (4th edition): Department of Agriculture and Food, Resource management Technical Report 3-2013, 175p.
- Scott, KM and Pain, CF (compilers) 2008, Regolith Science: CSIRO Publishing, Collingwood, Victoria, 461p.
- Scrimgeour, IR 2006, An overview of the North Australian Craton, *in* Evolution and metallogenesis of the North Australian Craton *edited by* P Lyons and DL Huston: Geoscience Australia, Record 2006/16, p. 1–2.
- Shannon, RD 1976, Revised effective ionic radii and systematic studies of interatomic distances in halides and chalcogenides: Acta Crystallographica, A32, p. 751–767.
- Smith, RE, Birrell, RD and Brigden, JF 1989, The implications to exploration of chalcophile corridors in the Archaean Yilgarn Block, Western Australia, as revealed by laterite geochemistry: Journal of Geochemical Exploration, v. 32, p. 169–184.
- Smith, RE and Singh, B 2007, Recognizing, in lateritic cover, detritus shed from the Archaean Gossan Hill Cu–Zn–Au volcanic-hosted massive sulphide deposit, Western Australia: Geochemistry: Exploration, Environment, Analysis, v. 7, no. 1, p. 71–86.
- Taylor, SR and McLennan, SM 1985, The continental crust: its composition and evolution: Blackwell Scientific Publications, Oxford, UK, 312p.
- Taylor, SR and McLennan, SM 1995, The geochemical evolution of the continental crust: Reviews of Geophysics, v. 33, no. 2, p. 241–265, doi:10.1029/95RG00262.
- Towner, RR (compiler) 1978, Wilson, Western Australia: Geological Survey of Western Australia, 1:250 000 Geological Series Explanatory Notes, 19p.
- Veevers, JJ and Wells, AT 1961, The geology of the Canning Basin: Bureau of Mineral Resources, Geology and Geophysics, Bulletin 60, 323p.
- Wibberley, CAJ, Yielding, G and Di Toro, G 2008, Recent advances in the understanding of fault zone internal structure: a review *in* The internal structure of fault zones: Implications for mechanical and fluid-flow properties *edited by* CAJ Wibberley, W Kurz, J Imber, RE Holdsworth and C Collettini: Geological Society of London, Special Publications, v. 299, p. 5–33.
- Wilford, JR 2005, Granites–Tanami Region, Northern Territory, *in* Regolith landscape evolution across Australia *edited by* RR Anand and P de Broekert: CRC LEME, Perth, p. 151–155.
- Wilford, JR, Bierwirth, PN and Craig, MA 1997, Application of airborne gamma-ray spectrometry in soil/regolith mapping and applied geomorphology: AGSO Journal of Australian Geology and Geophysics, v. 17, no. 2, p. 201–216.
- Wilford, JR and Creasey, J 2002, Landsat Thematic Mapper, *in* Geophysical and remote sensing methods for regolith exploration *edited by* E Papp: CRC LEME Open File Report 144, p. 6–12.
- Wilford, JR, Pain, CF and Dohrenwend, JC 1992, Enhancement and interpretation of airborne gamma-ray spectrometric and Landsat imagery for regolith mapping, Cape York Peninsula: Exploration Geophysics, v. 23, p. 441–446.
- Wyborn, LAI, Heinrich, CA and Jaques, AL 1994, Australian Proterozoic mineral systems: essential ingredients and mappable criteria, *in* Australian mining looks north — the challenges and choices *edited by* PC Hallenstein: Australasian Institute of Mining and Metallurgy; 1994 AusIMM Annual Conference, Darwin, Northern Territory, 5 August 1994, p. 109–115.
- Yeates, AN (compiler) 1977, Helena, Western Australia: Geological Survey of Western Australia, 1:250 000 Geological Series Explanatory Notes, 18p.
- Yeates, AN, Crowe, RWA, Passmore, VL, Rowner, RR and Wyborn, LAI 1975, New and revised stratigraphic nomenclature, northeast Canning Basin, *in* Annual report for the year 1974: Geological Survey of Western Australia, p. 49–51.

Figures B20–B27

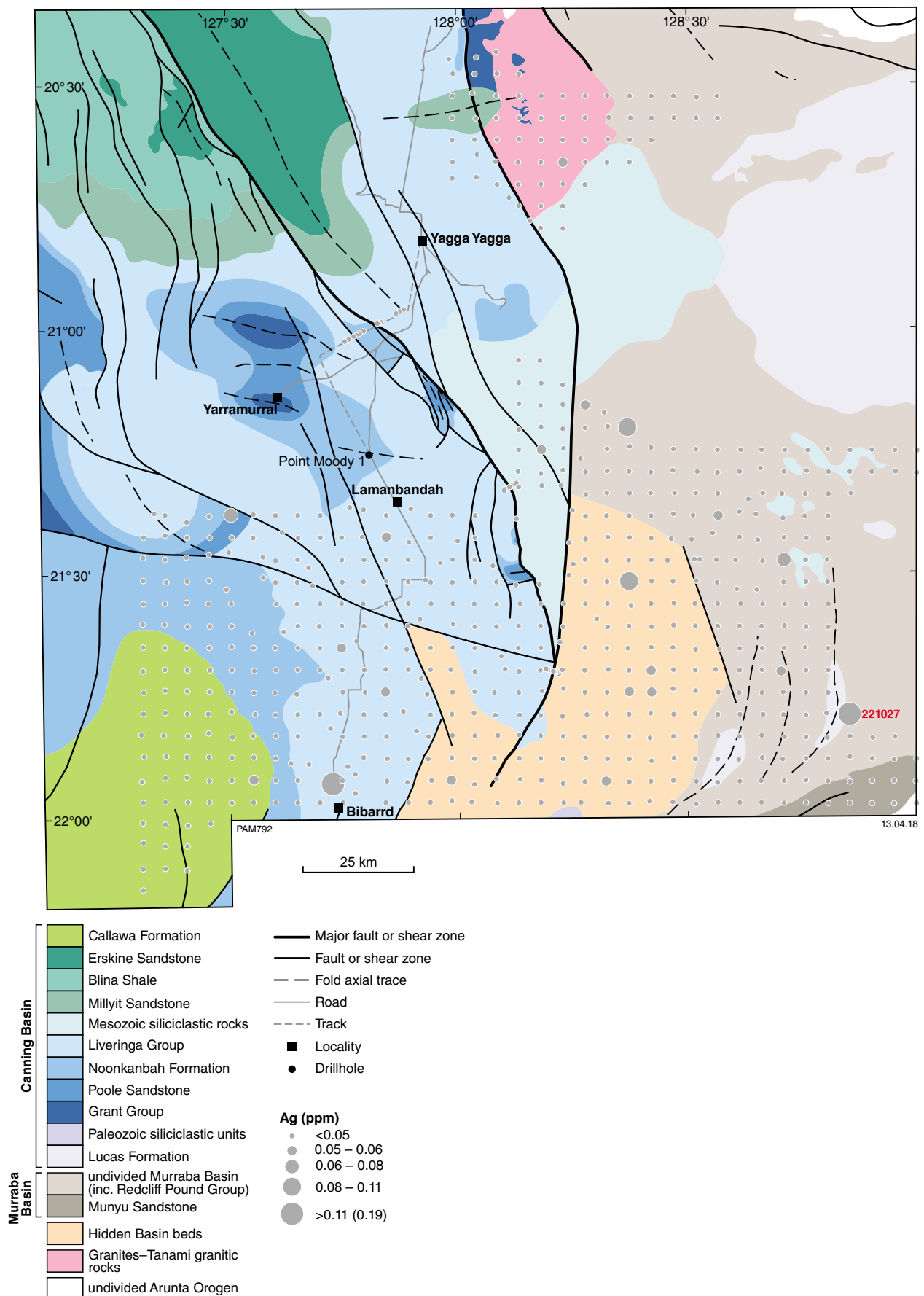


Figure B20. Bubble plot for precious metals shown against 1:500 000-scale interpreted bedrock geology and structures (GSWA, 2016) . Class boundaries based on natural breaks; data for Pd not shown as all data are censored: a) Ag (ppm)

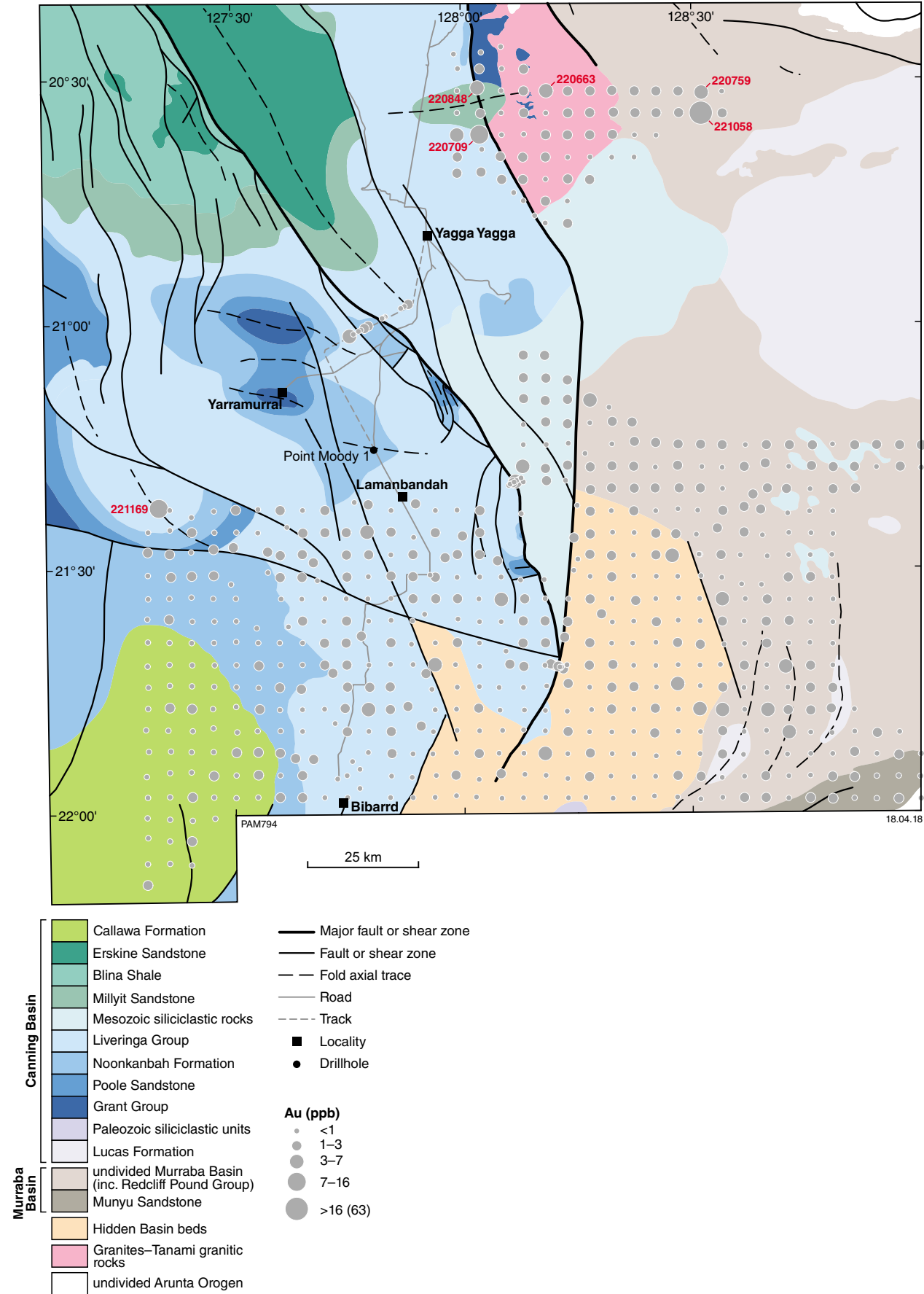


Figure B20b. Au (ppb)

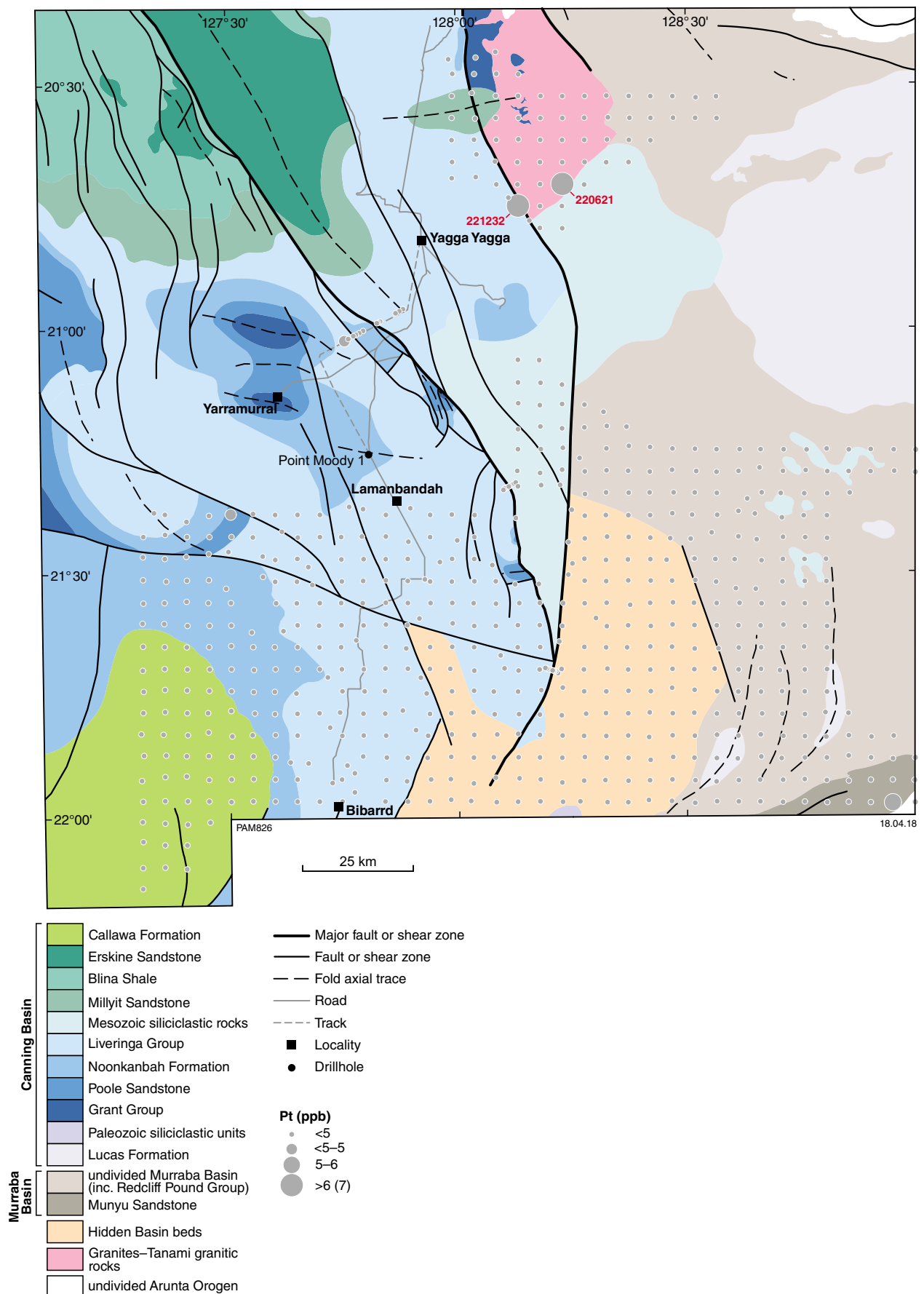


Figure B20c. Pt (ppb)

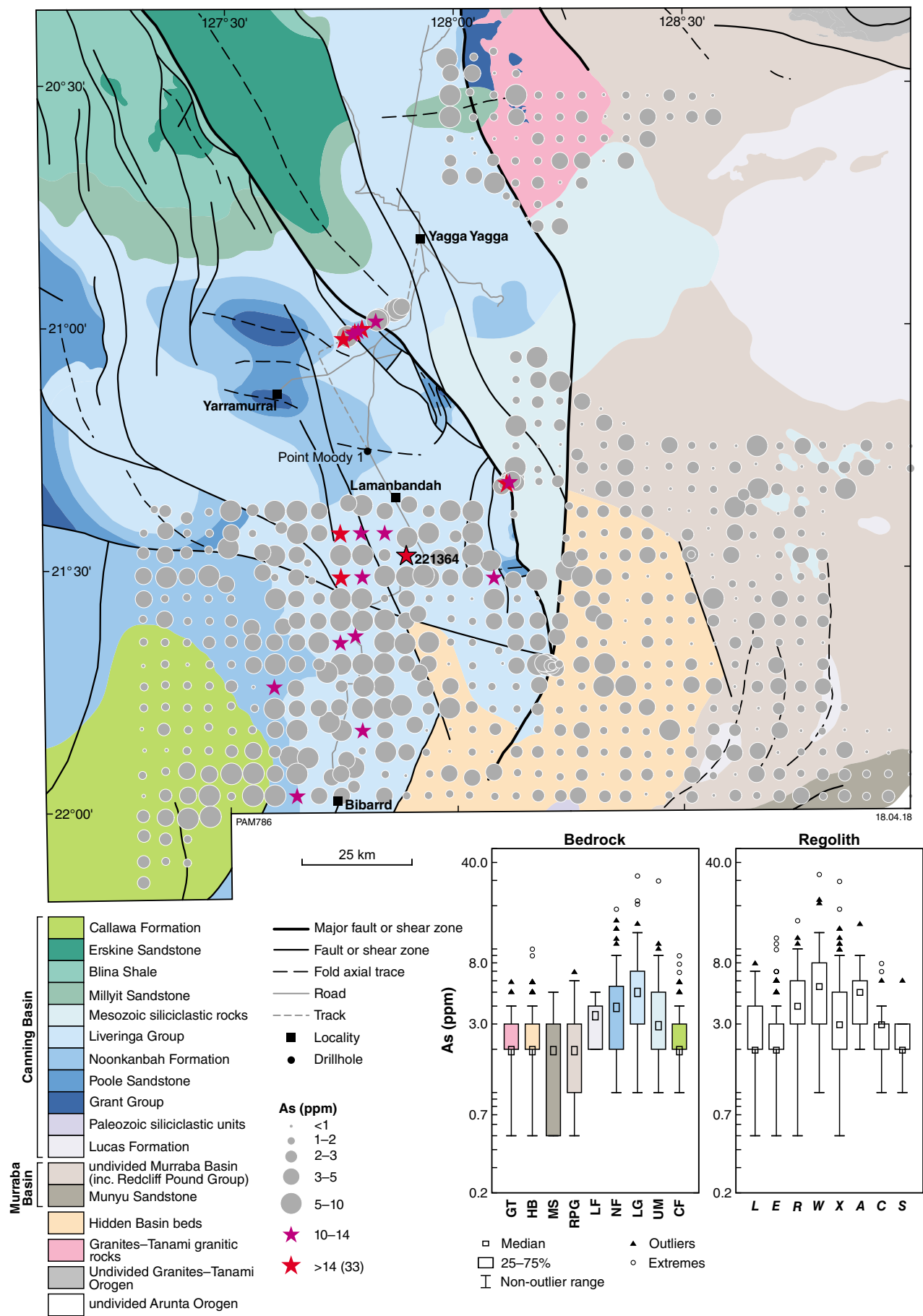


Figure B21. Bubble plot for chalcophile elements shown against 1:500 000-scale interpreted bedrock geology and structures (GSWA, 2016): a) As (ppm)

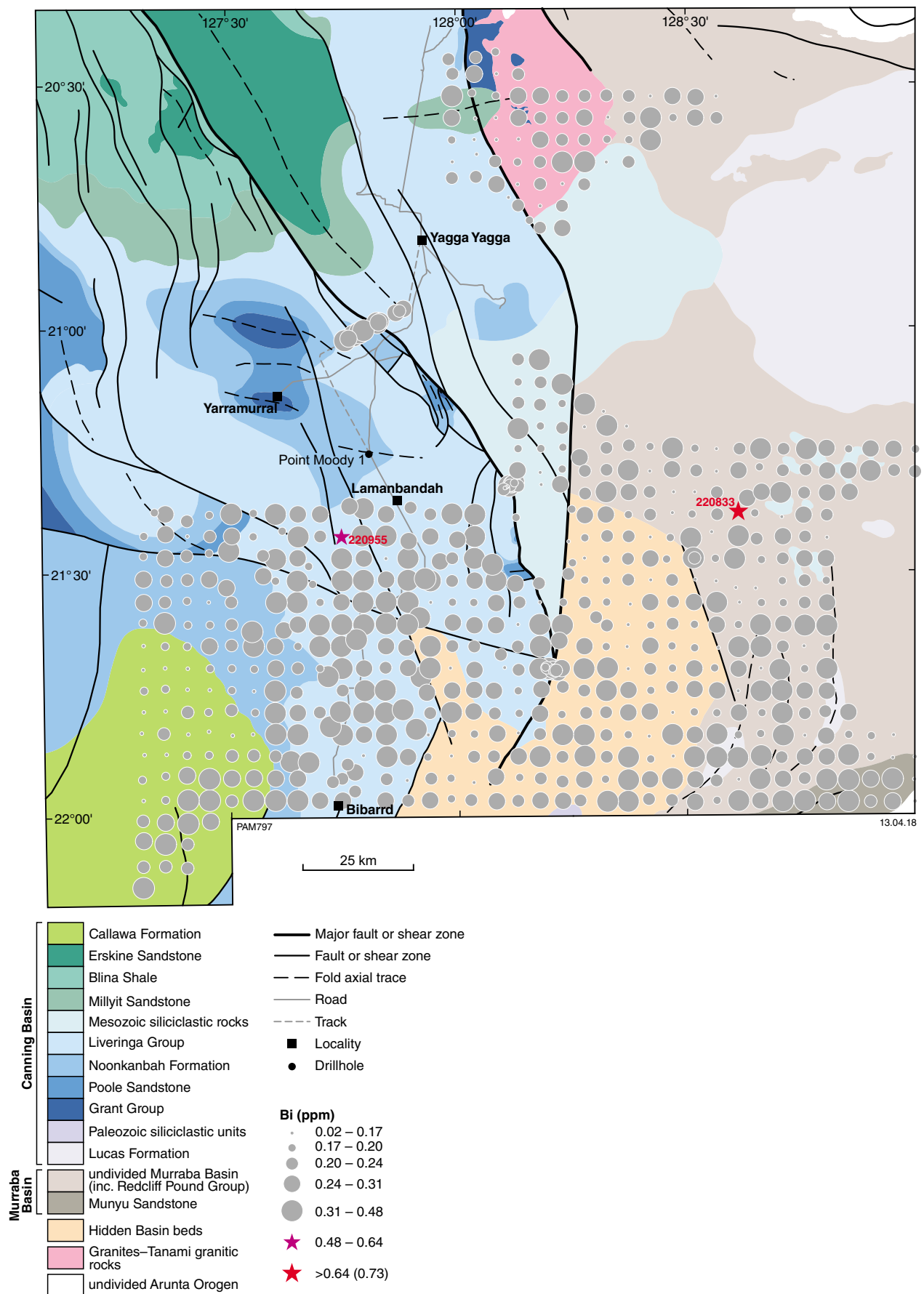


Figure B21b. Bi (ppm)

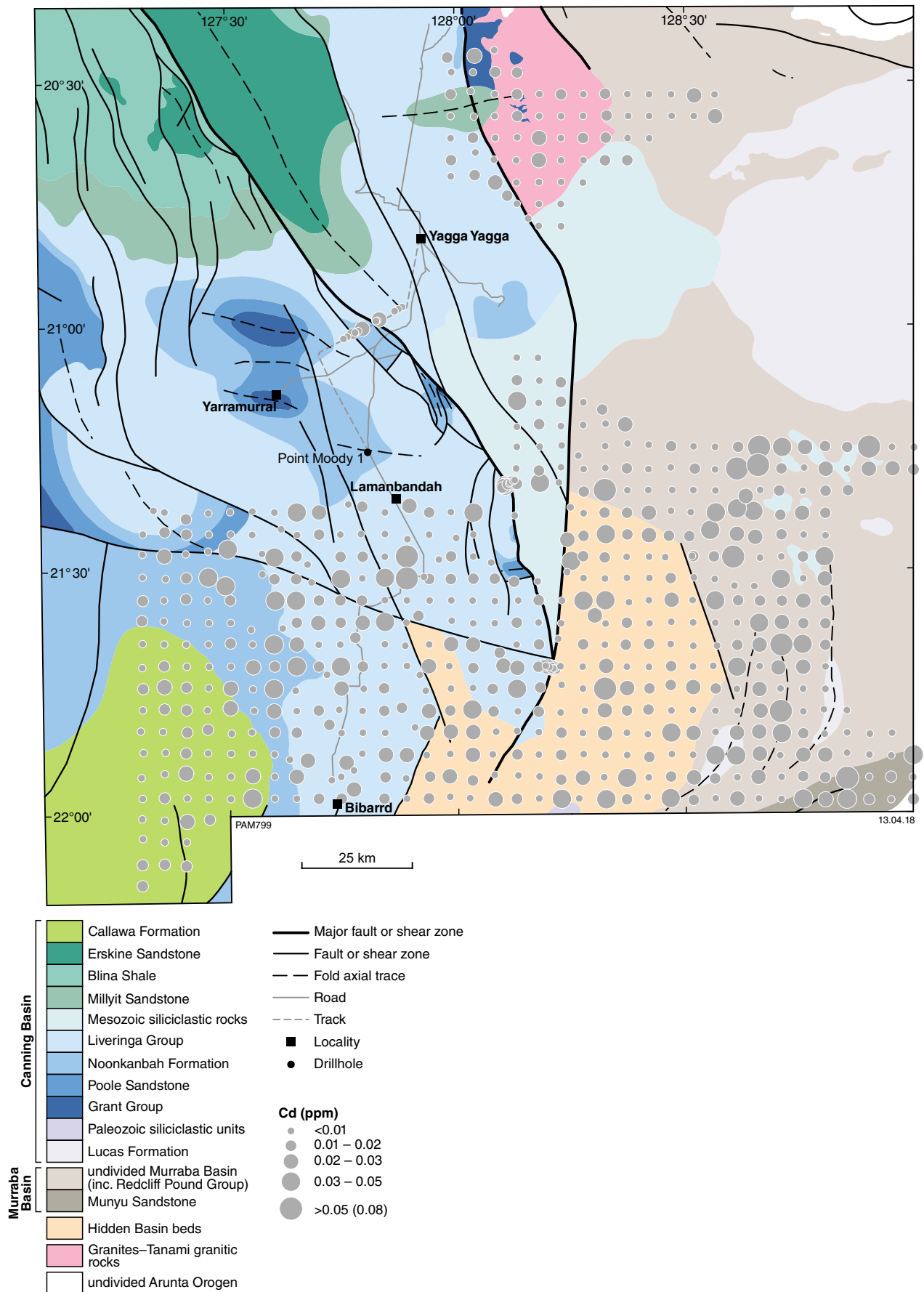


Figure B21c. Cd (ppm; class boundaries are natural breaks)

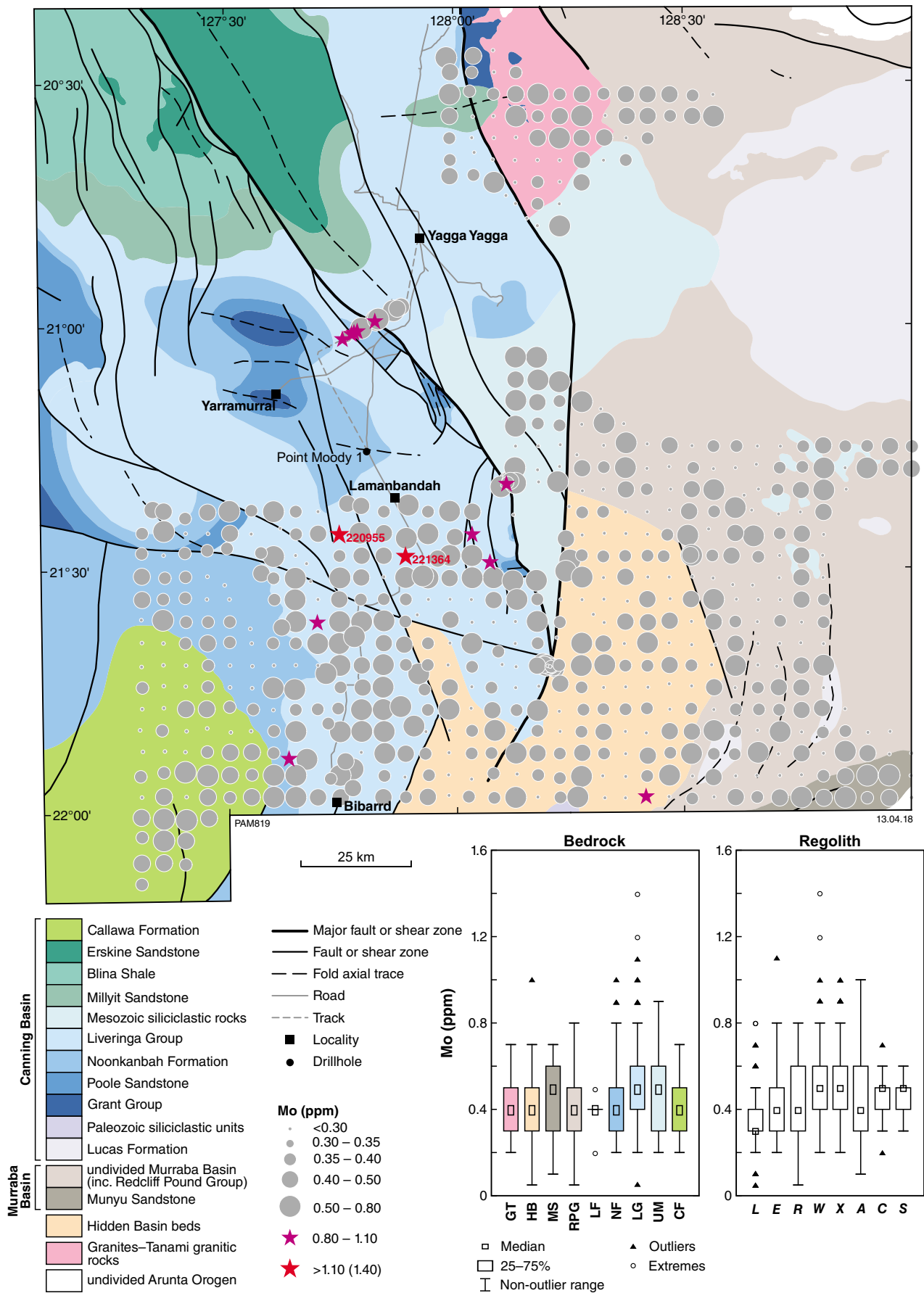


Figure B21d. Mo (ppm)

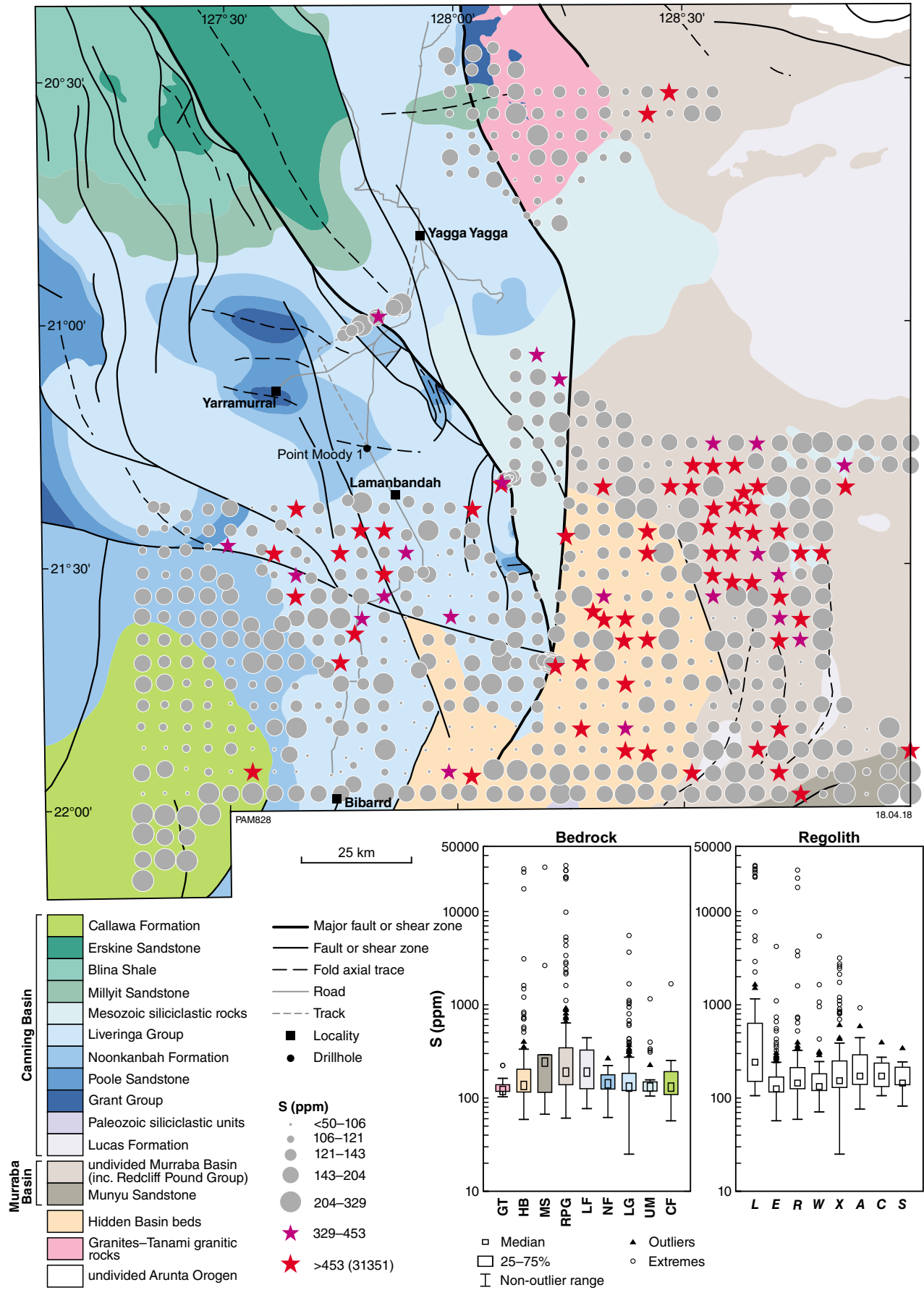


Figure B21e. S (ppm)

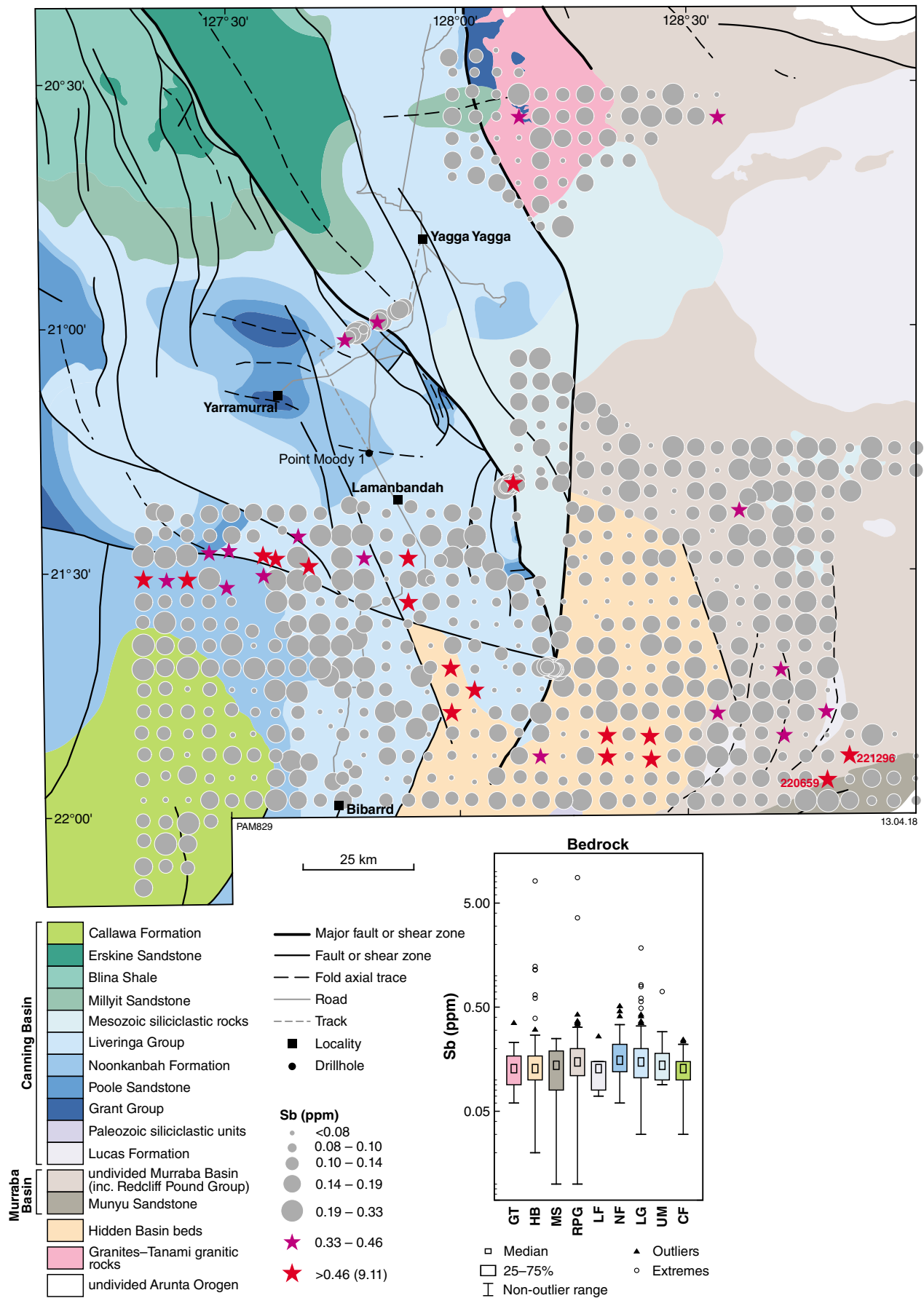
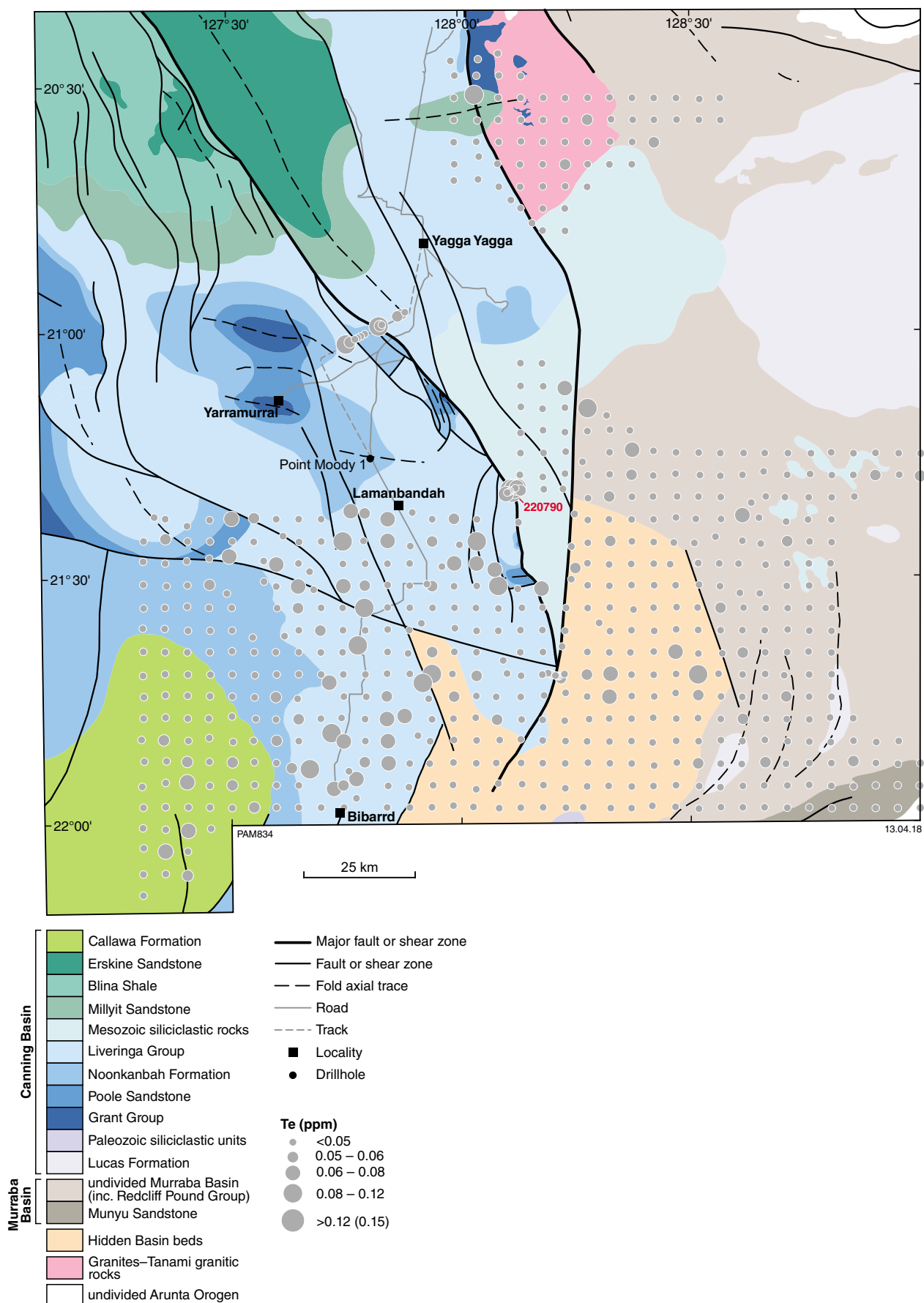


Figure B21f. Sb (ppm)



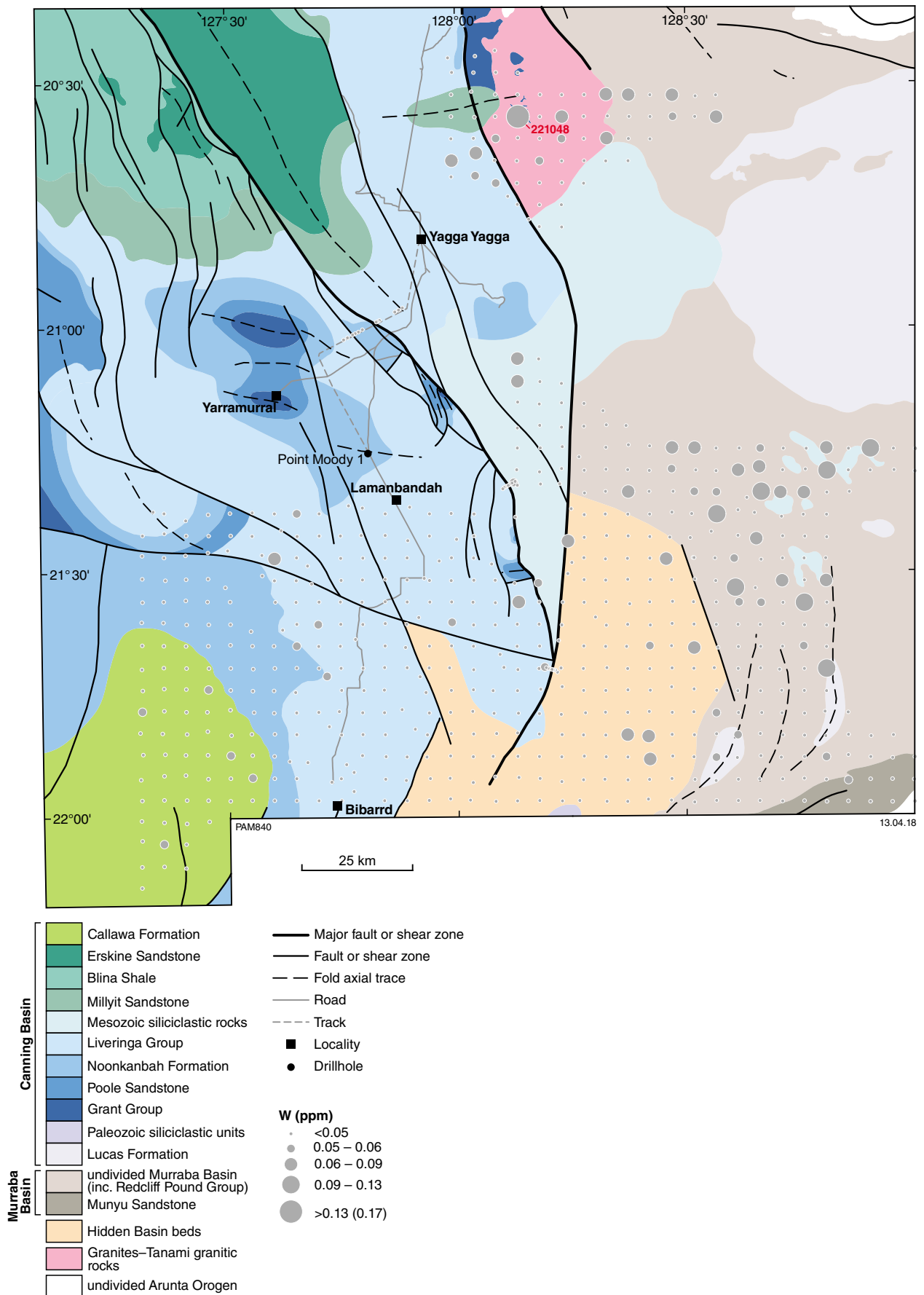


Figure B21h. W (ppm; class boundaries are natural breaks)

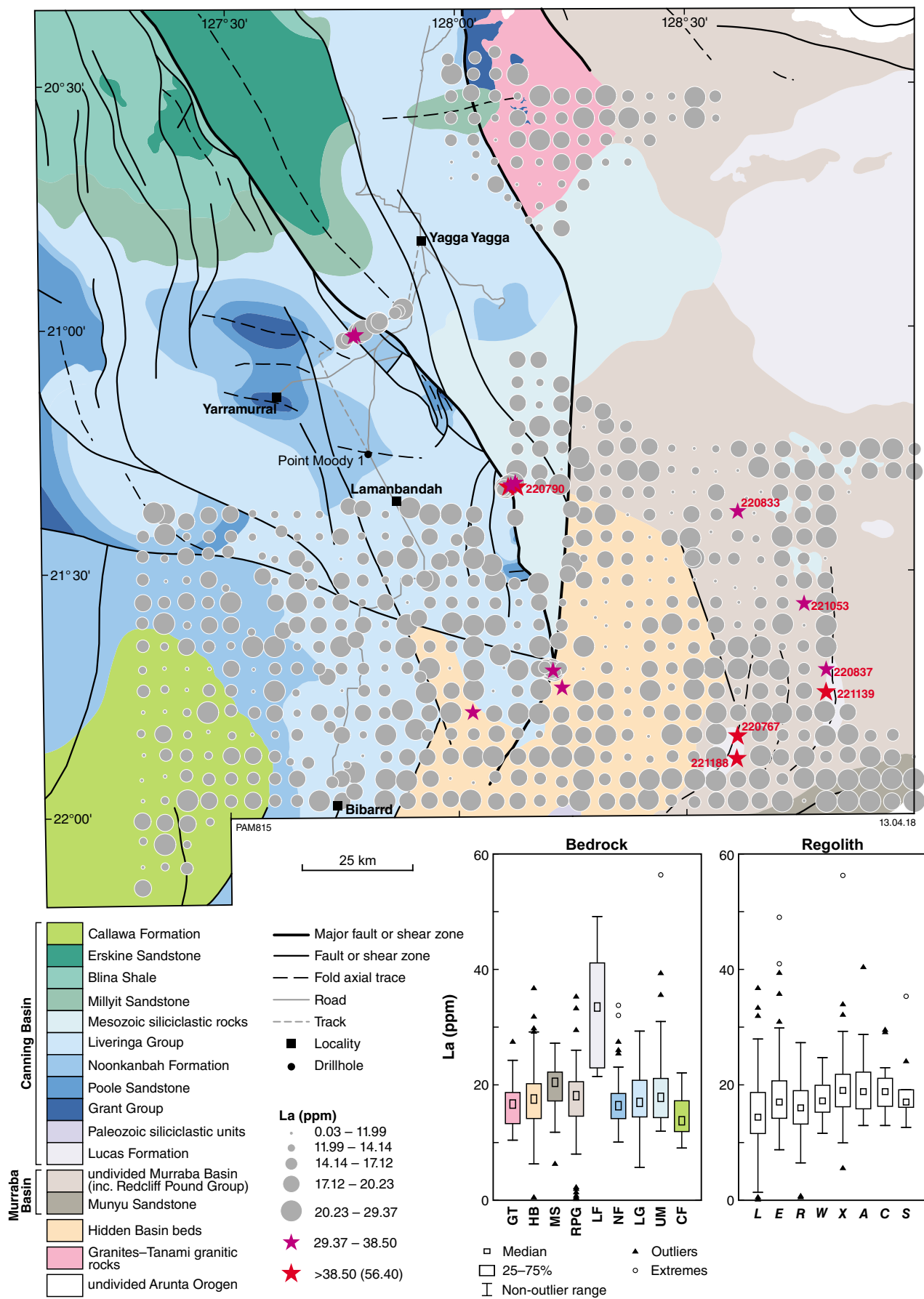


Figure B22. Bubble plot for selected REE (La–Lu, Y) shown against 1:500 000-scale interpreted bedrock geology and structures (GSWA, 2016): a) La (ppm)

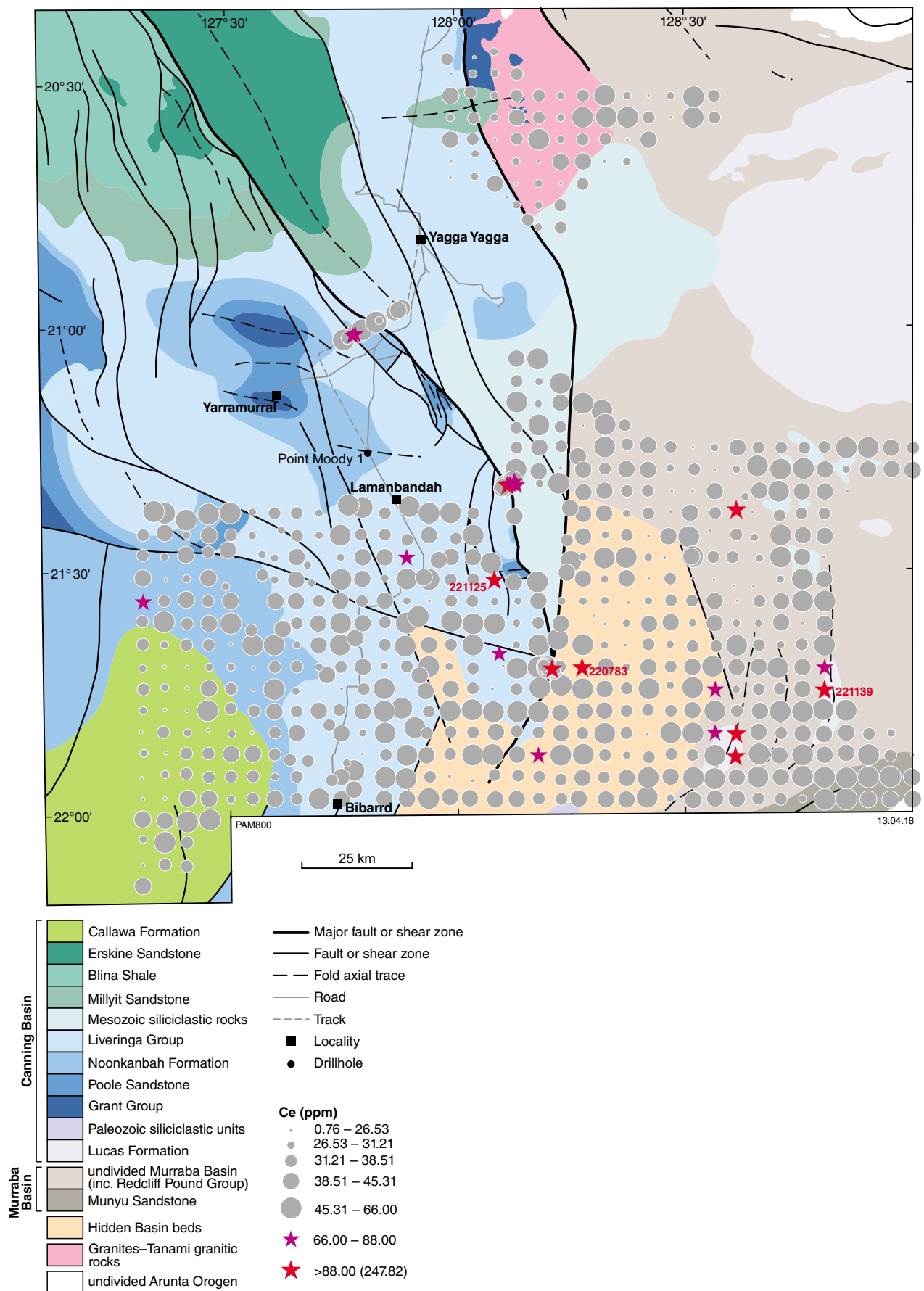


Figure B22b. Ce (ppm)

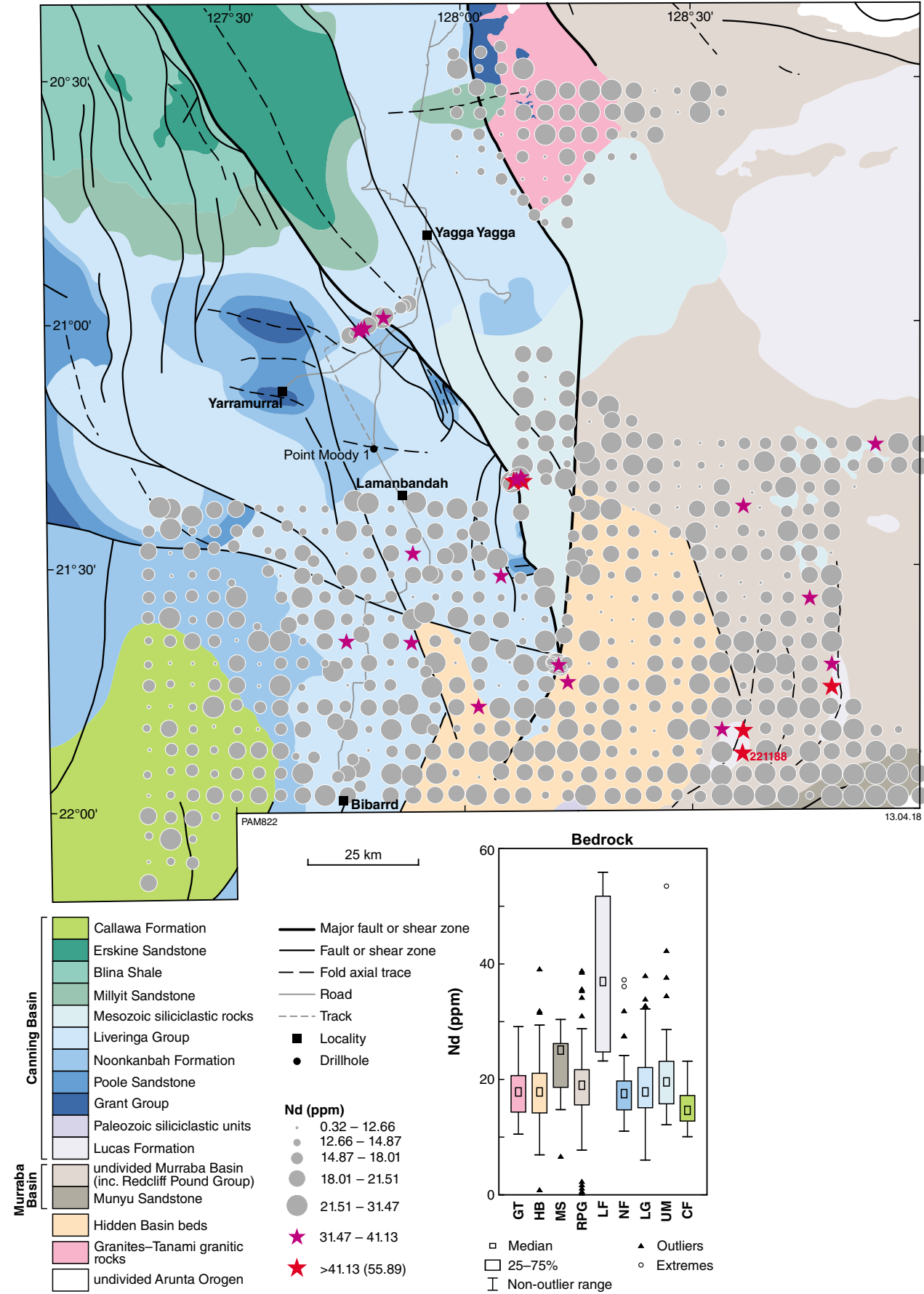


Figure B22c. Nd (ppm)

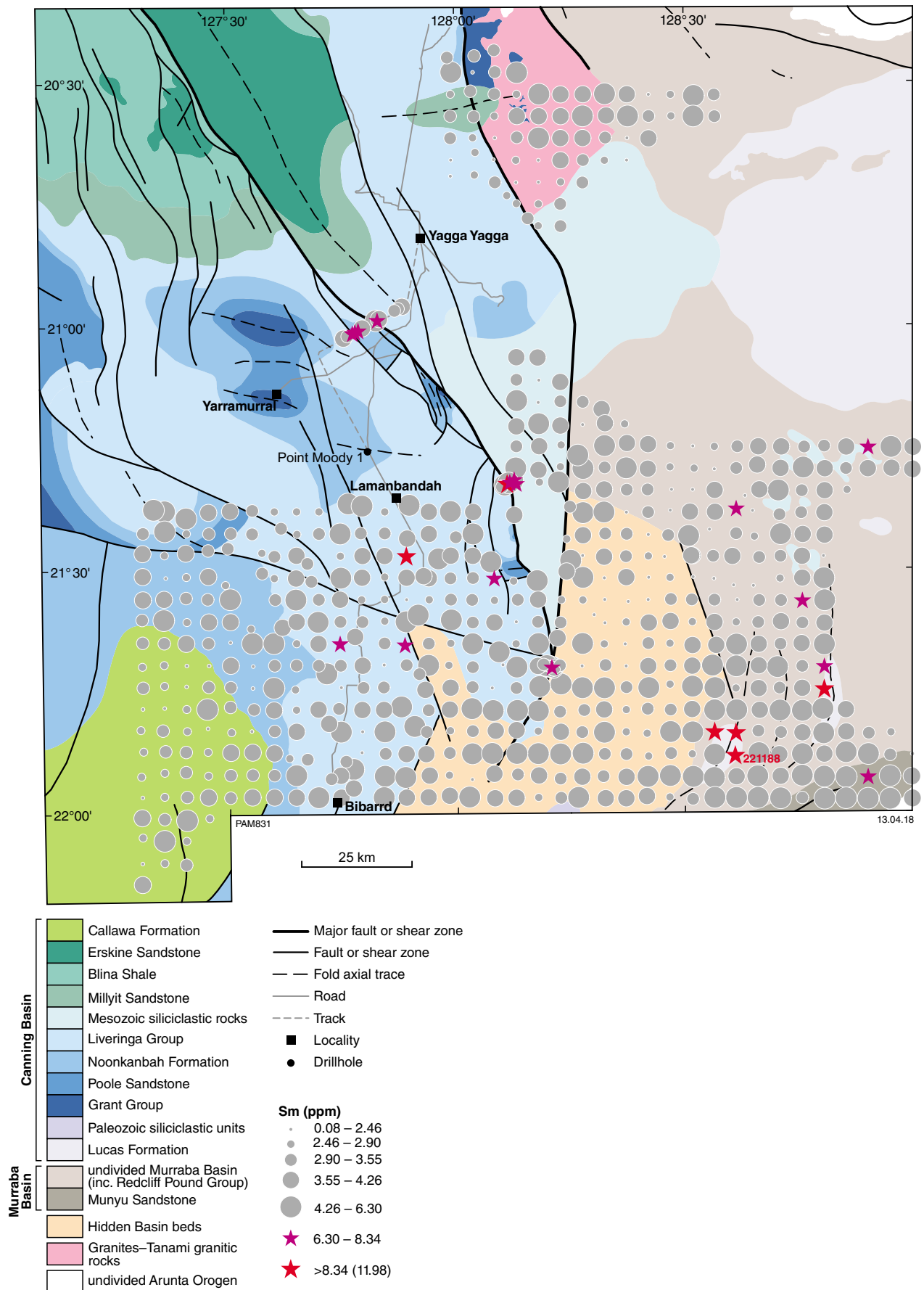


Figure B22d. Sm (ppm)

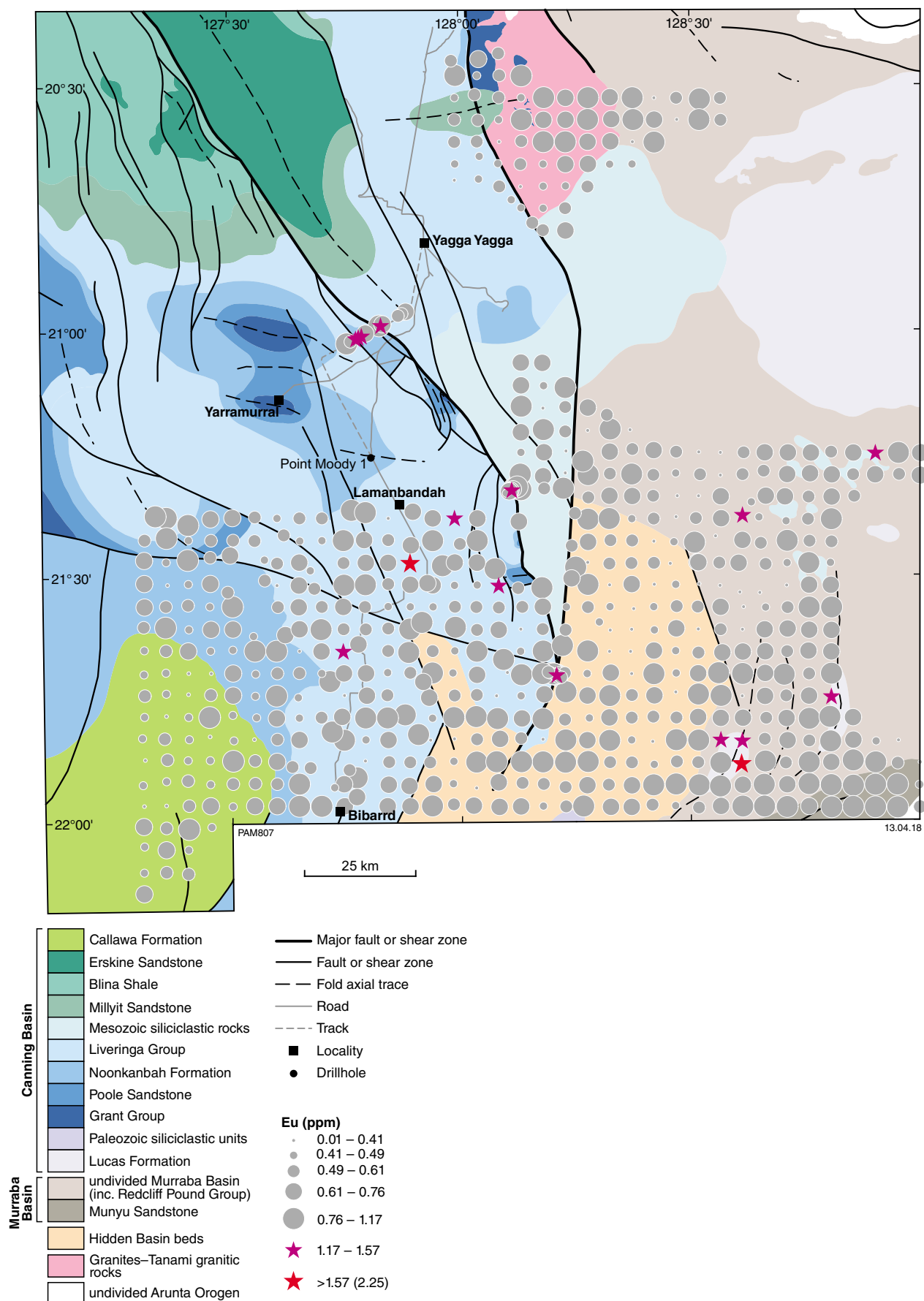
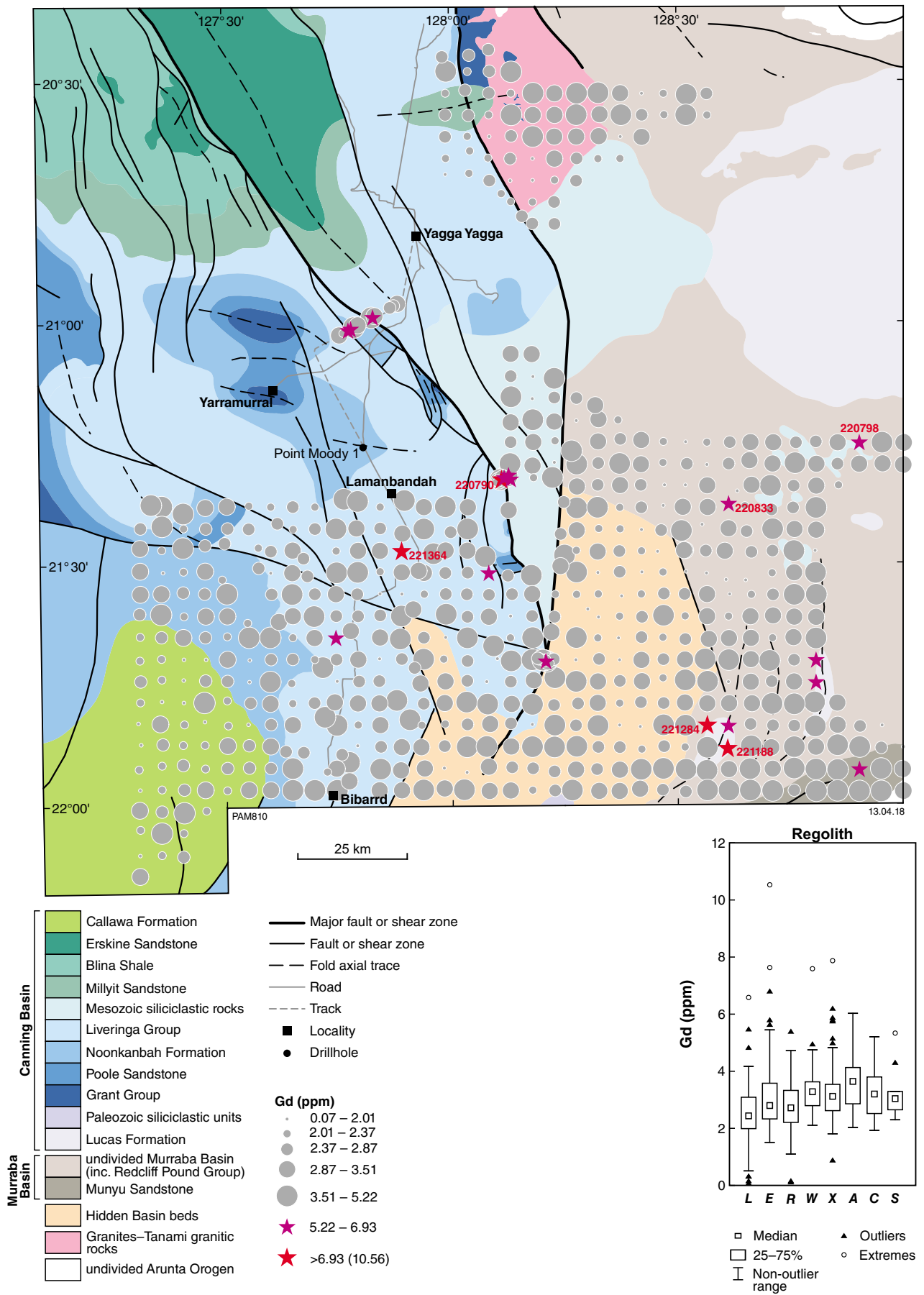


Figure B22e. Eu (ppm)



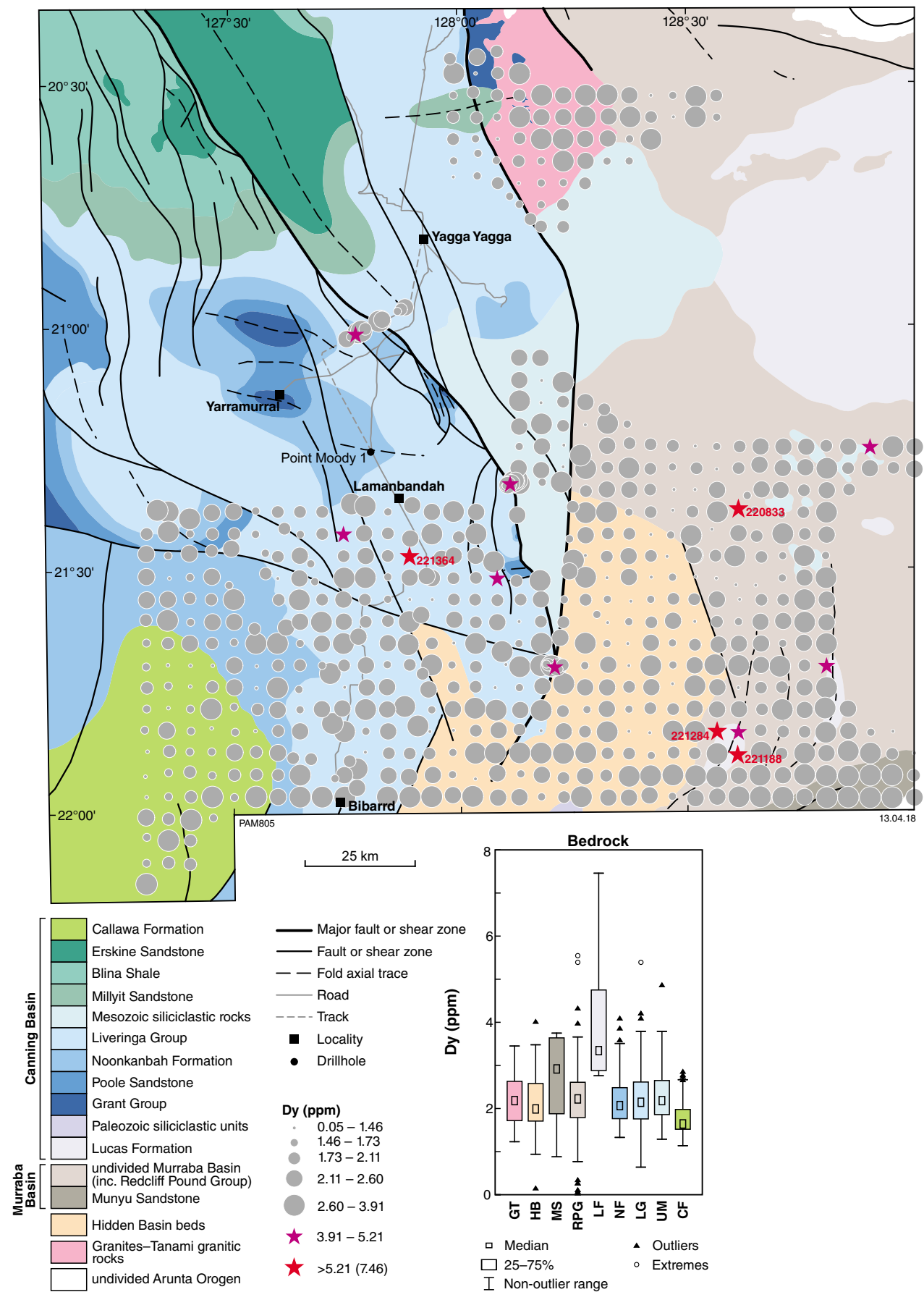


Figure B22g. Dy (ppm)

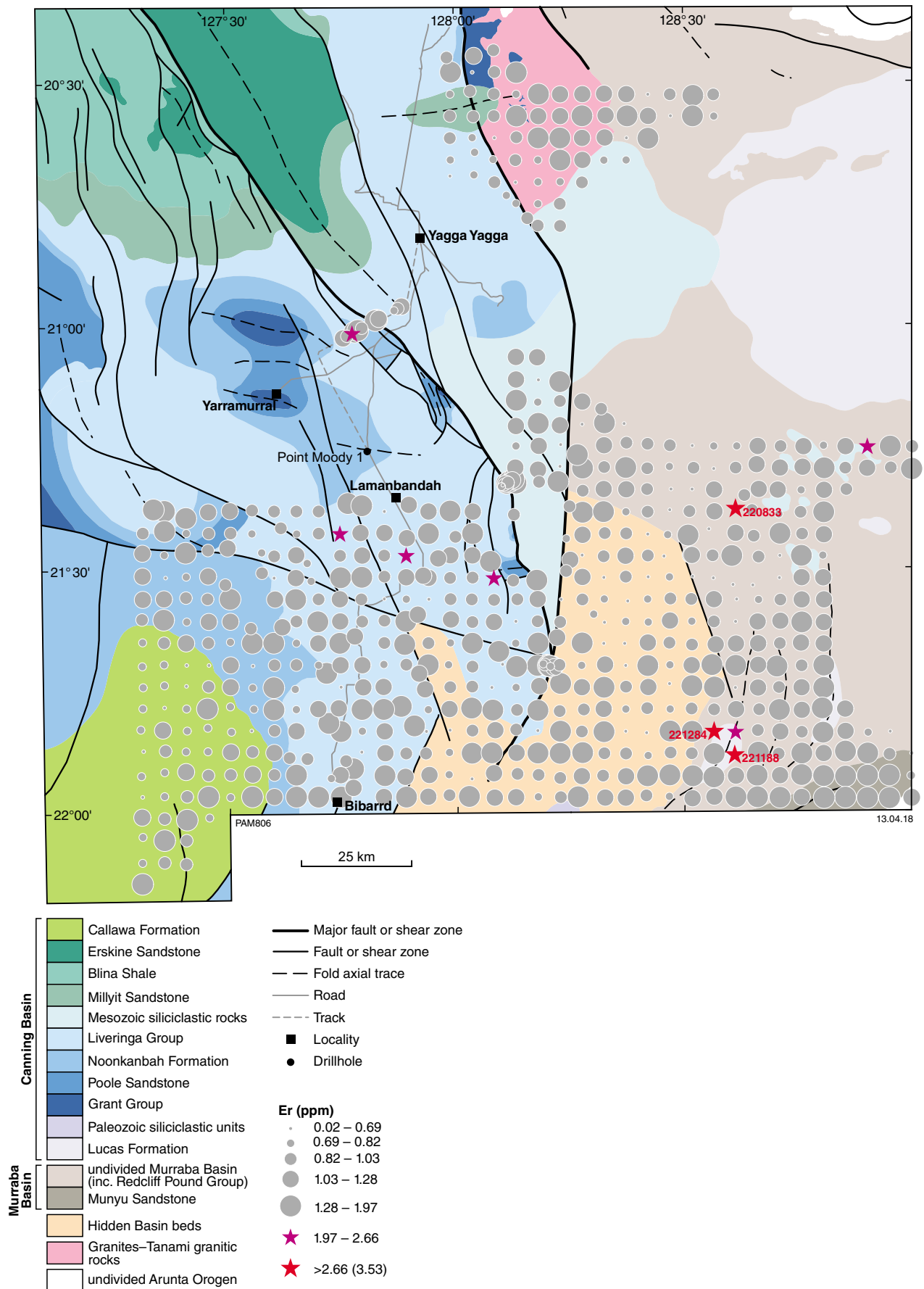
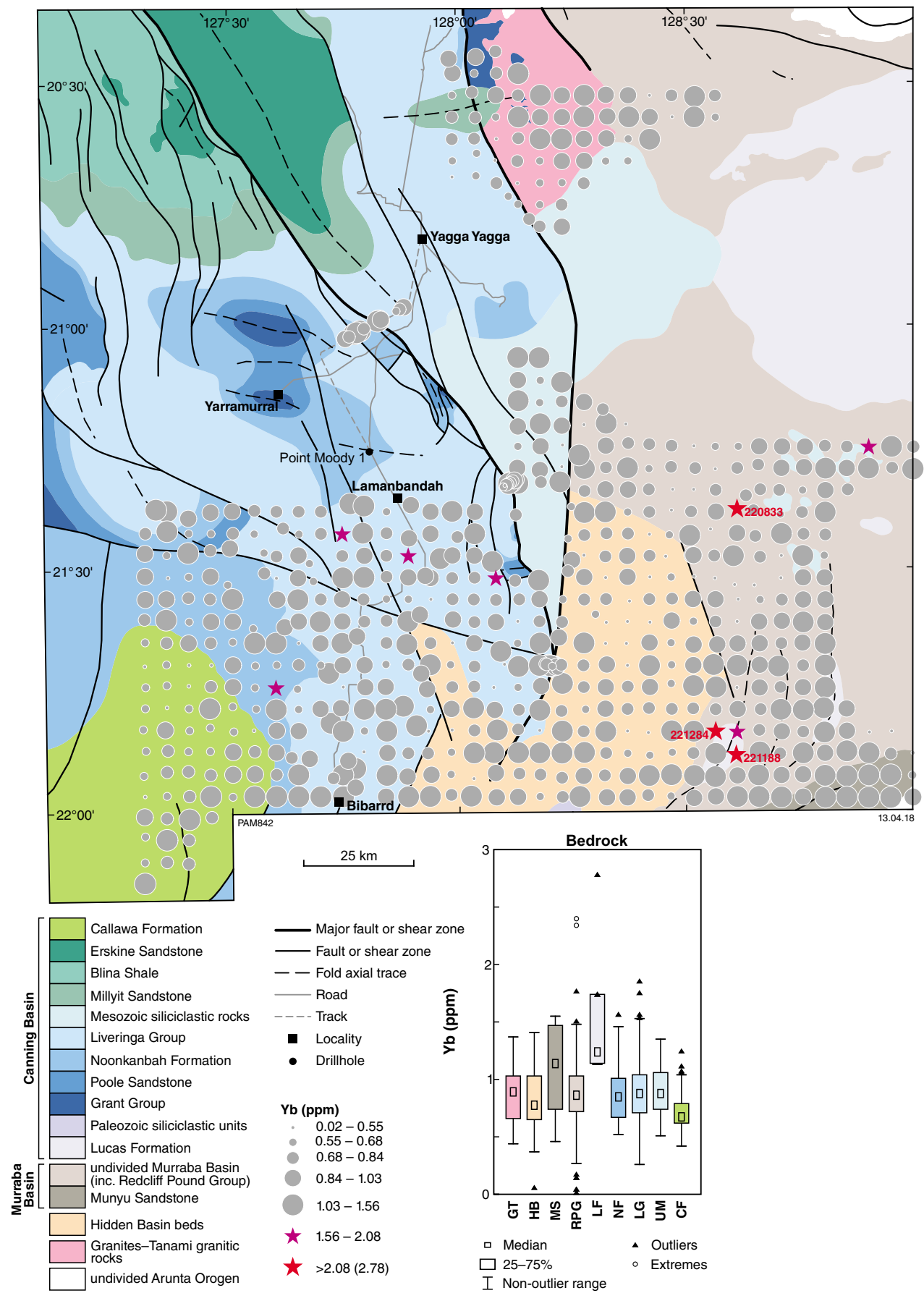


Figure B22h. Er (ppm)



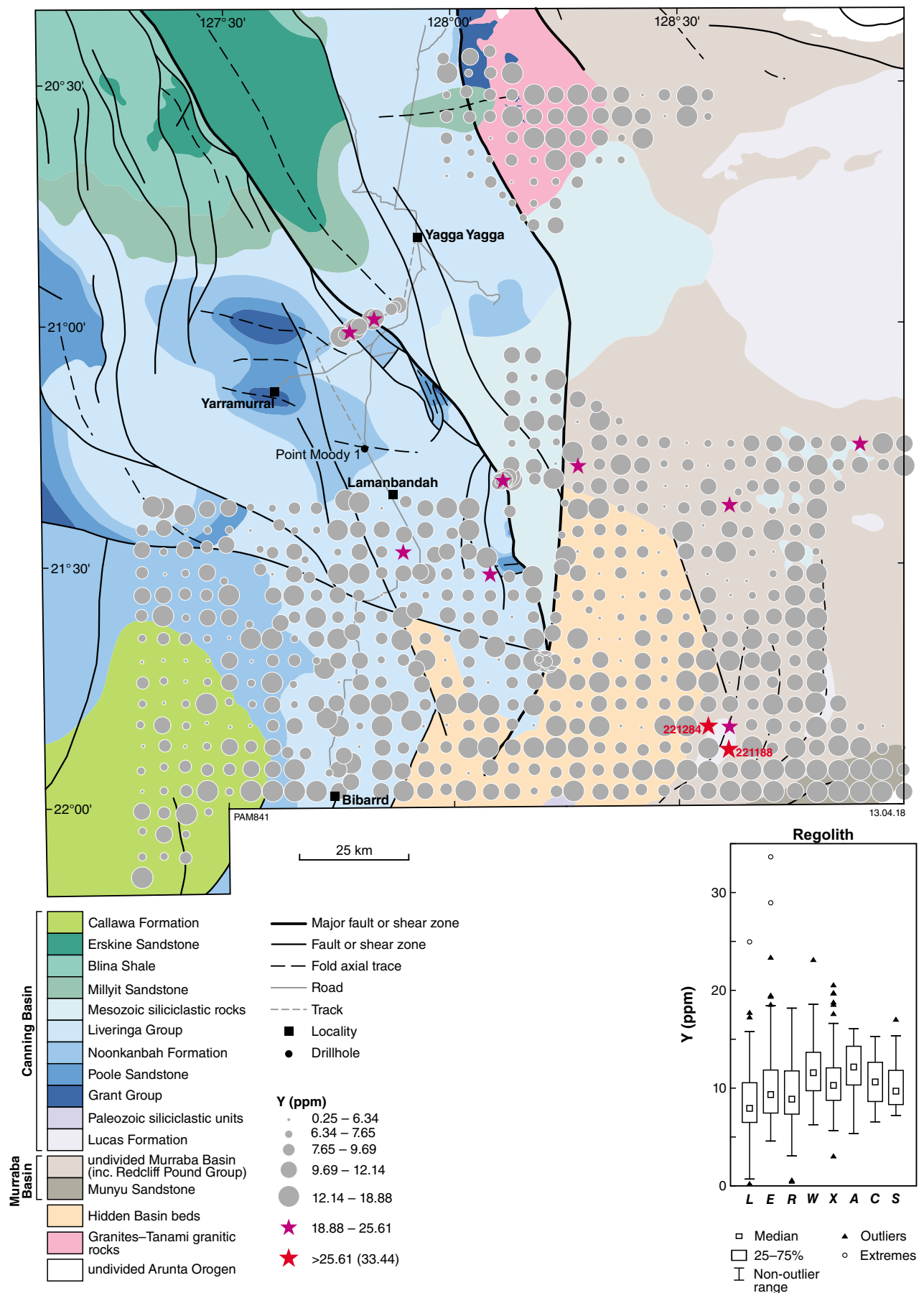


Figure B22j. Y (ppm)

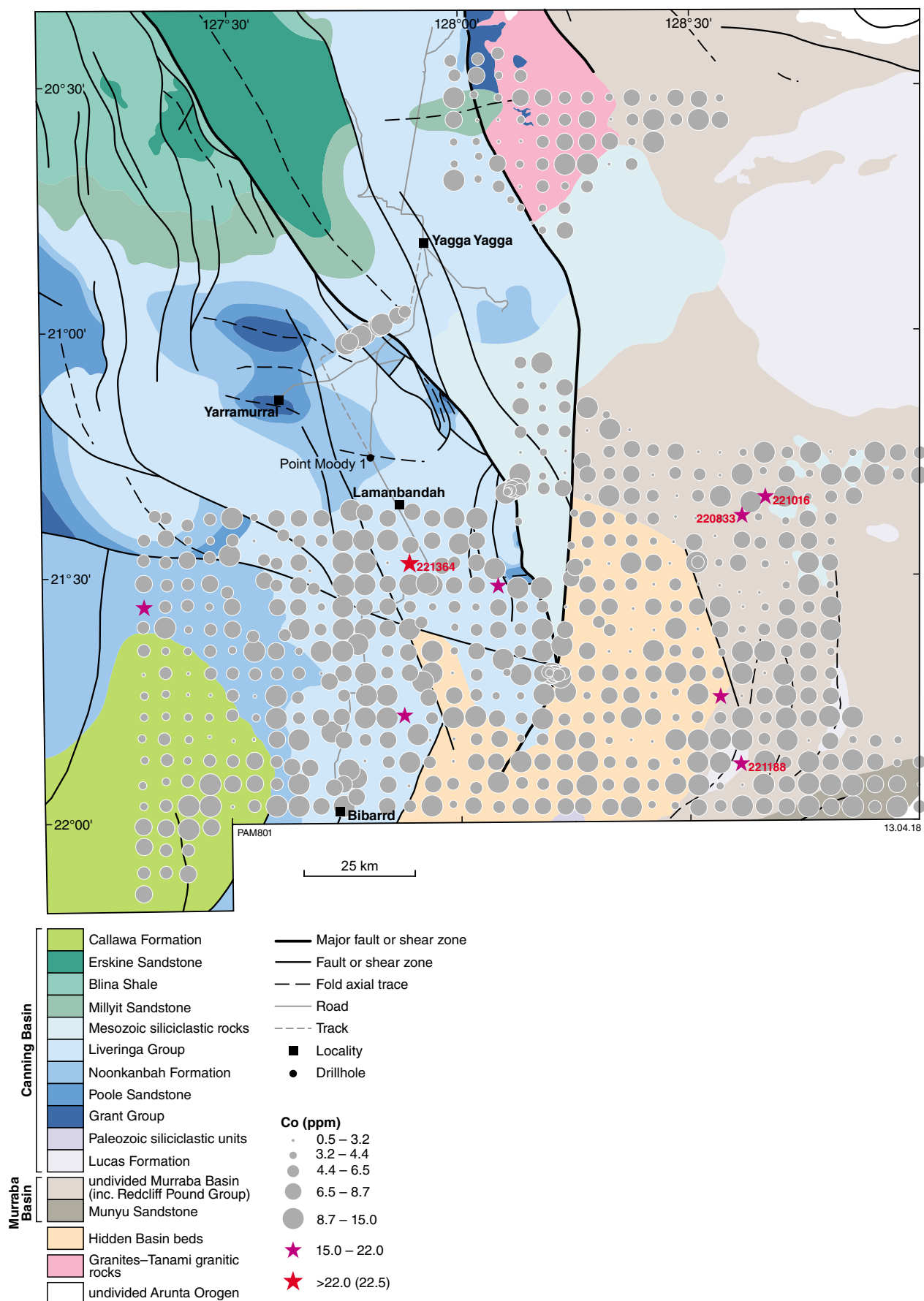


Figure B23. Bubble plots for transition elements shown against 1:500 000-scale interpreted bedrock geology and structures (GSWA, 2016): a) Co (ppm)

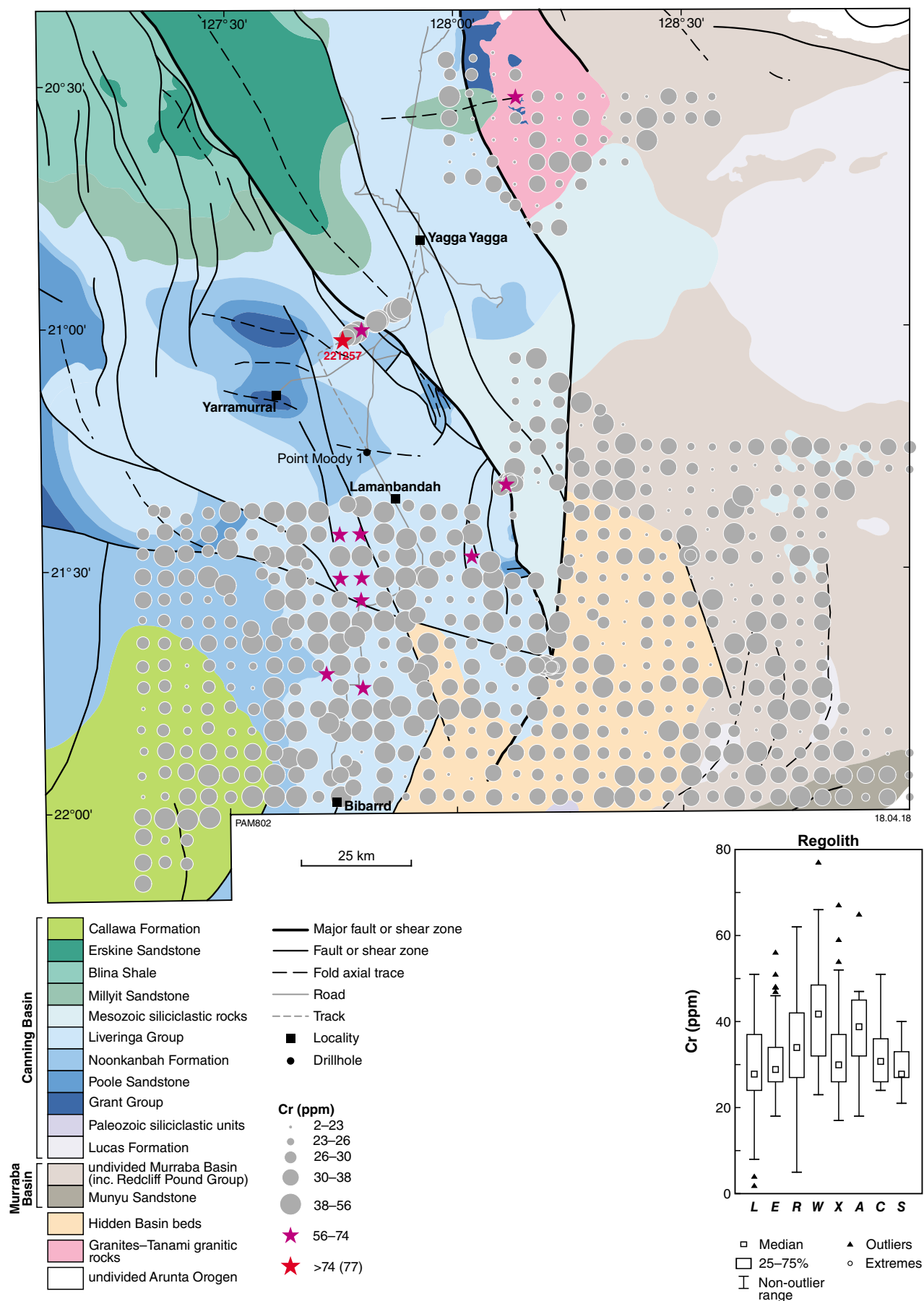
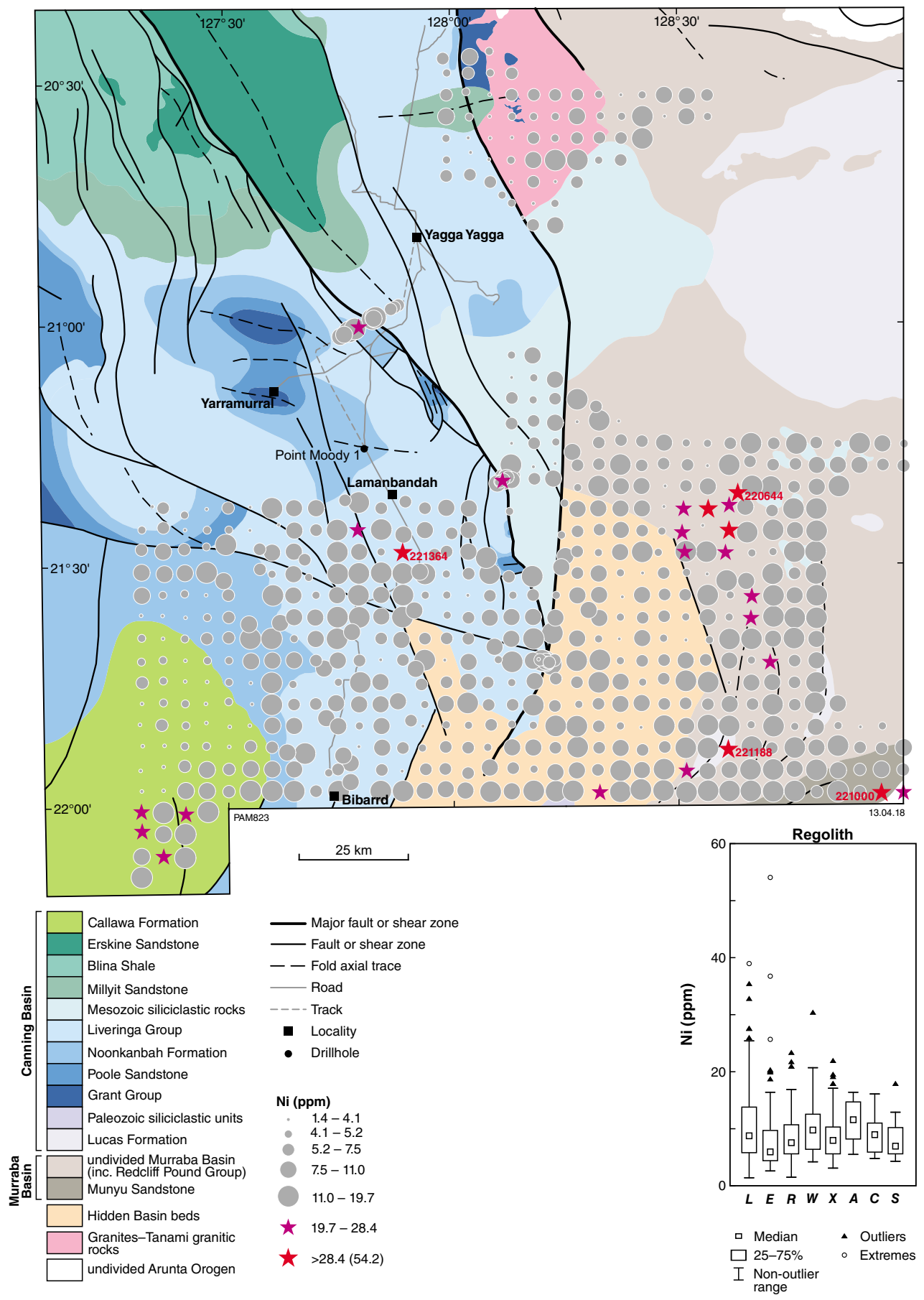


Figure B23b. Cr (ppm)



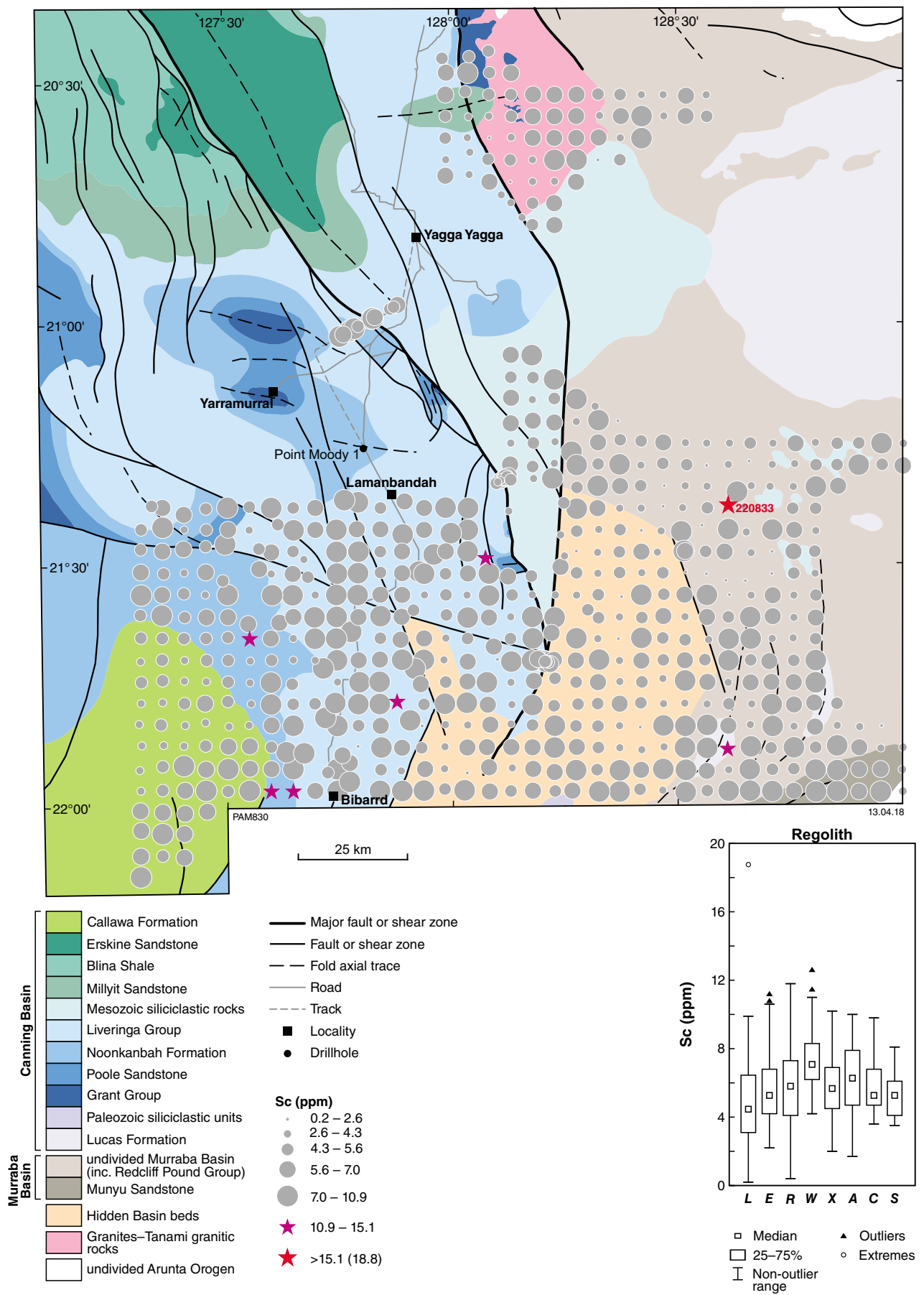
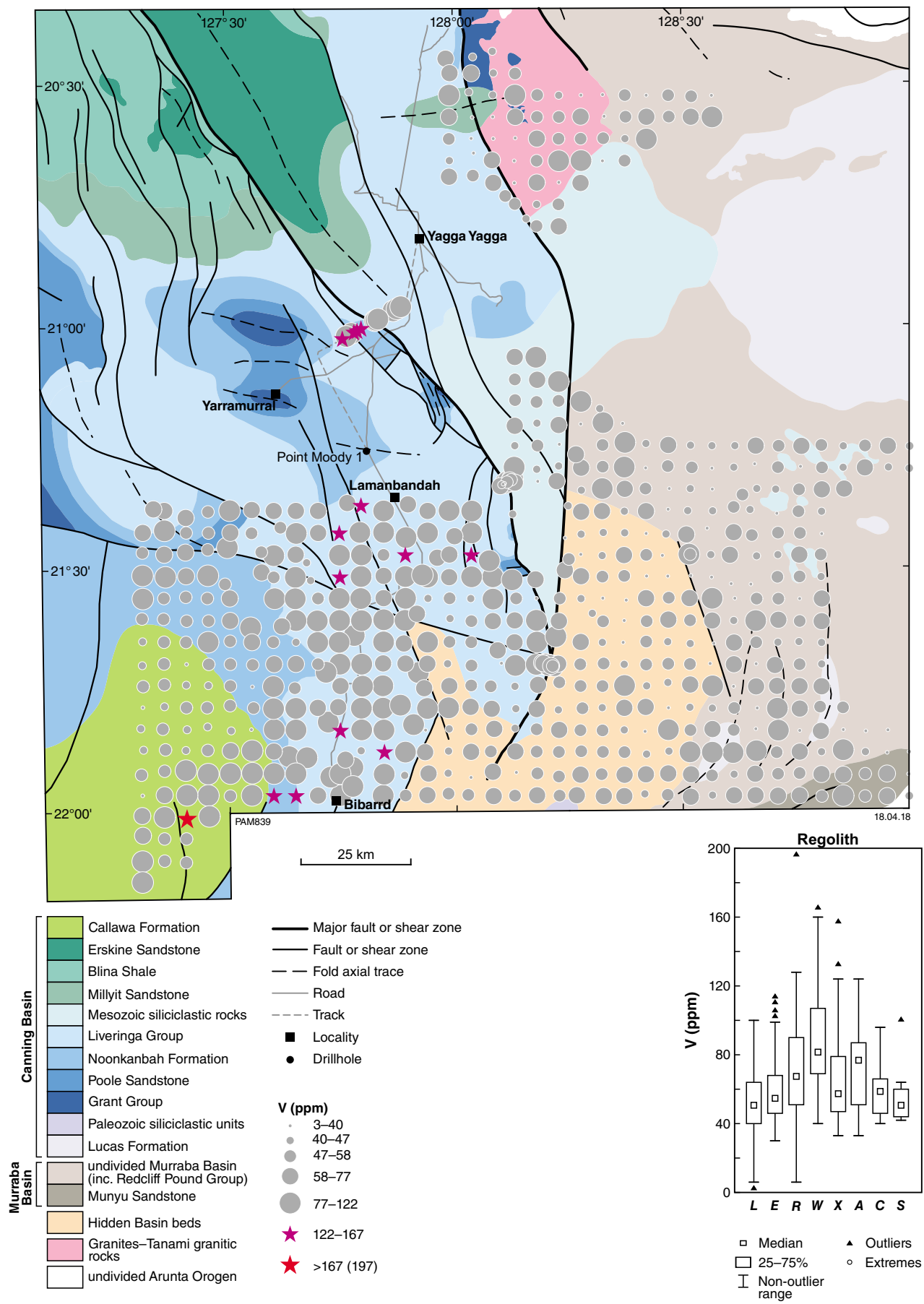


Figure B23d. Sc (ppm)



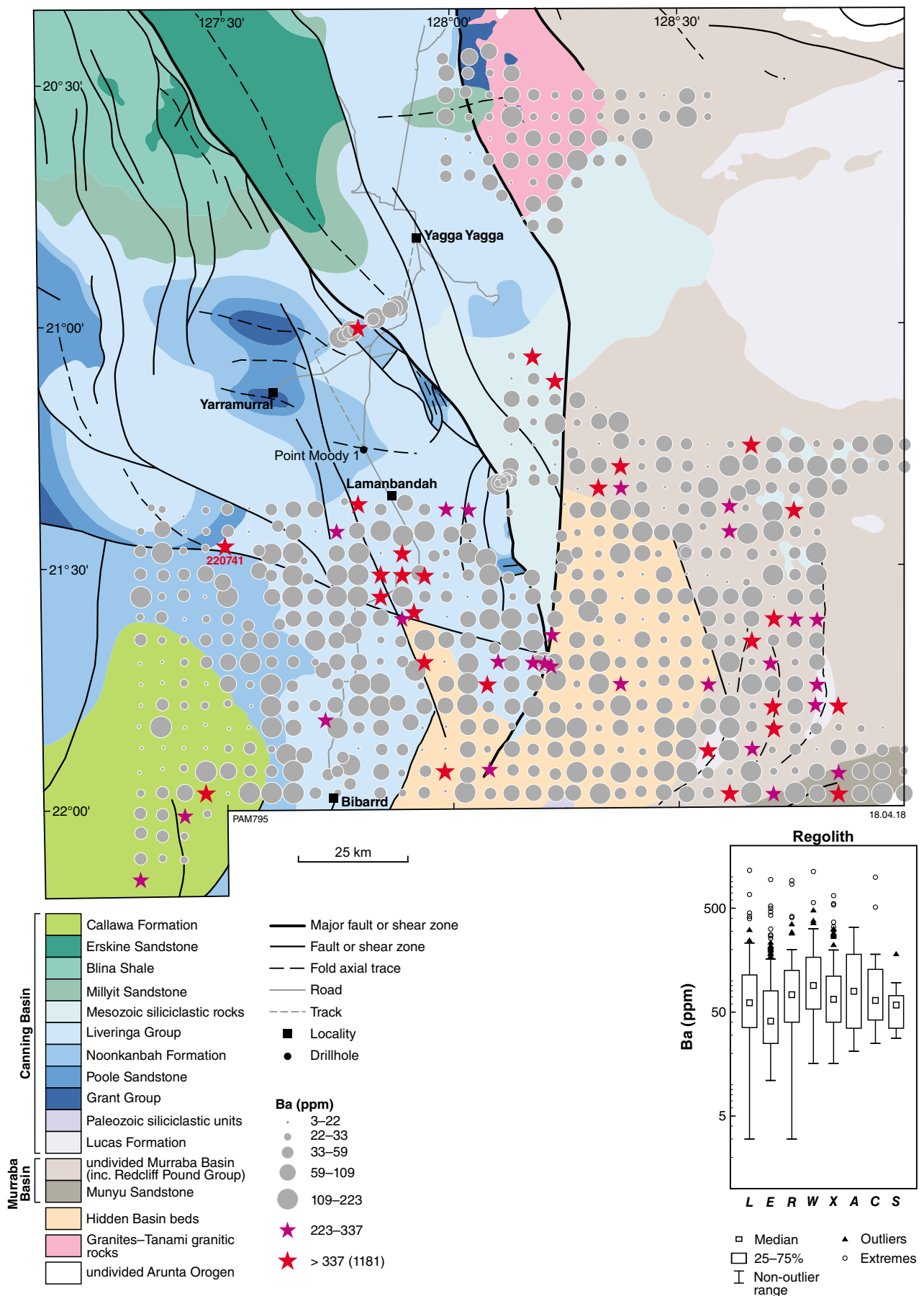


Figure B24. Bubble plots for lithophile elements shown against 1:500 000-scale interpreted bedrock geology and structures (GSWA, 2016): a) Ba (ppm)

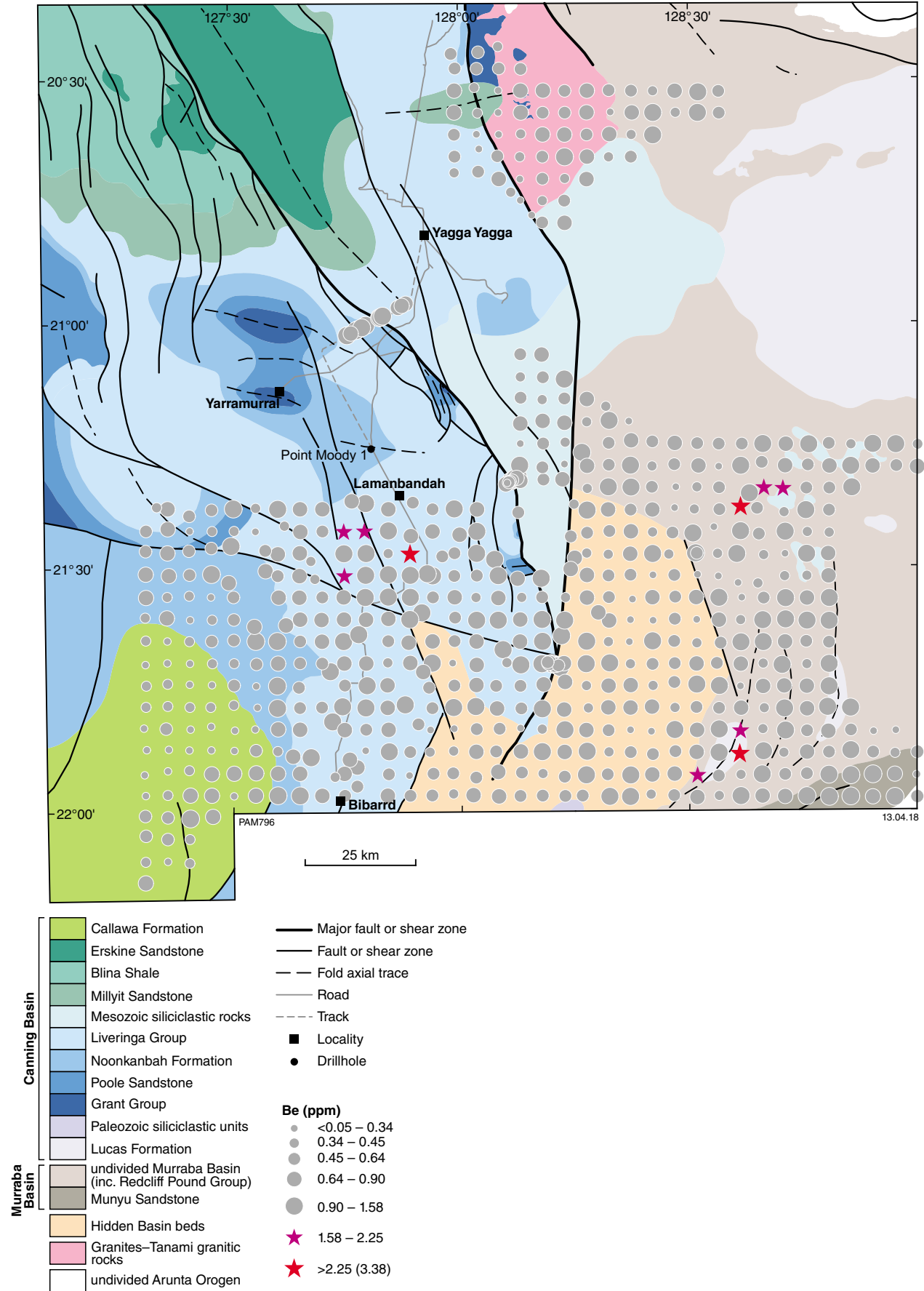


Figure B24b. Be (ppm)

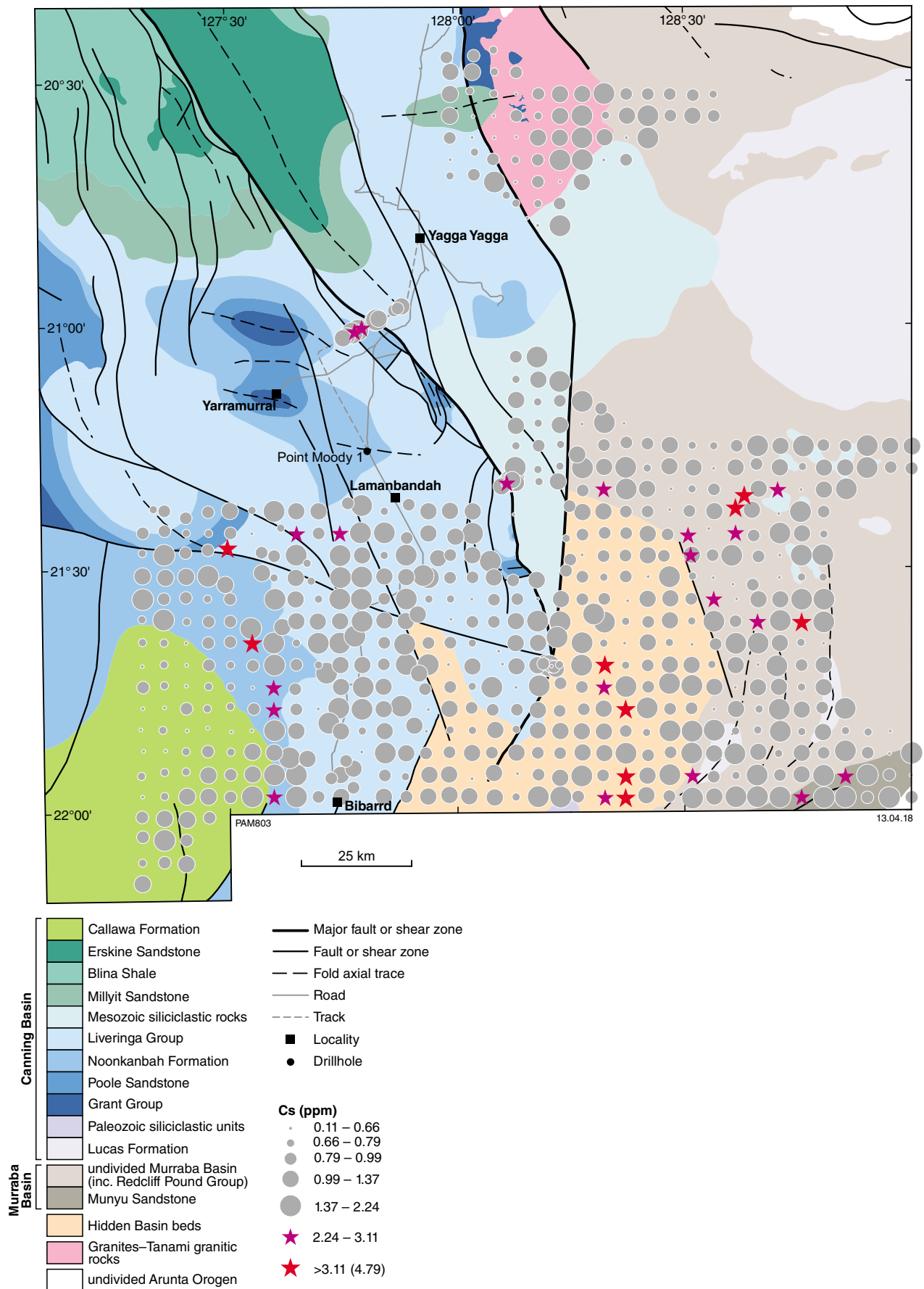
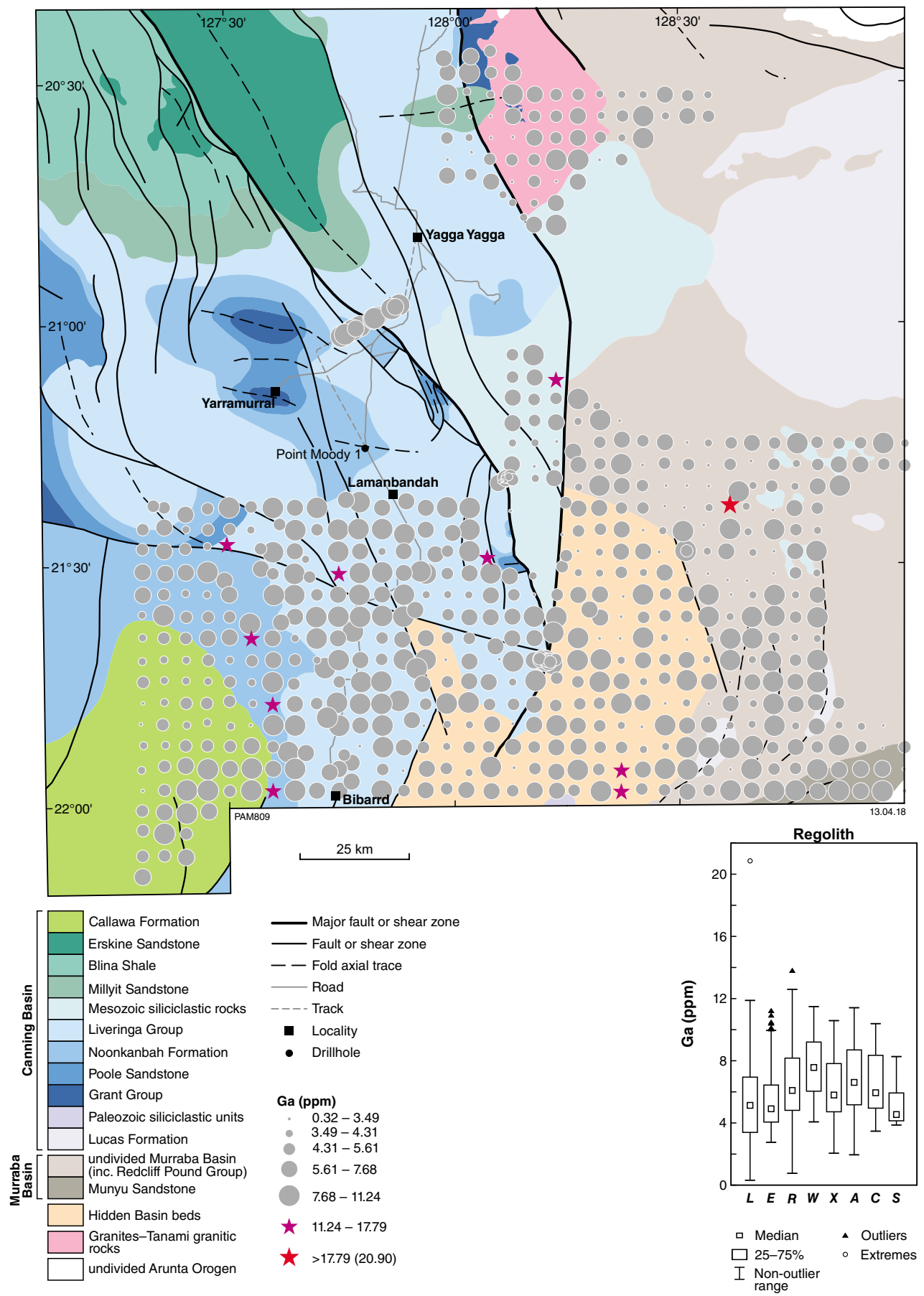


Figure B24c. Cs (ppm)



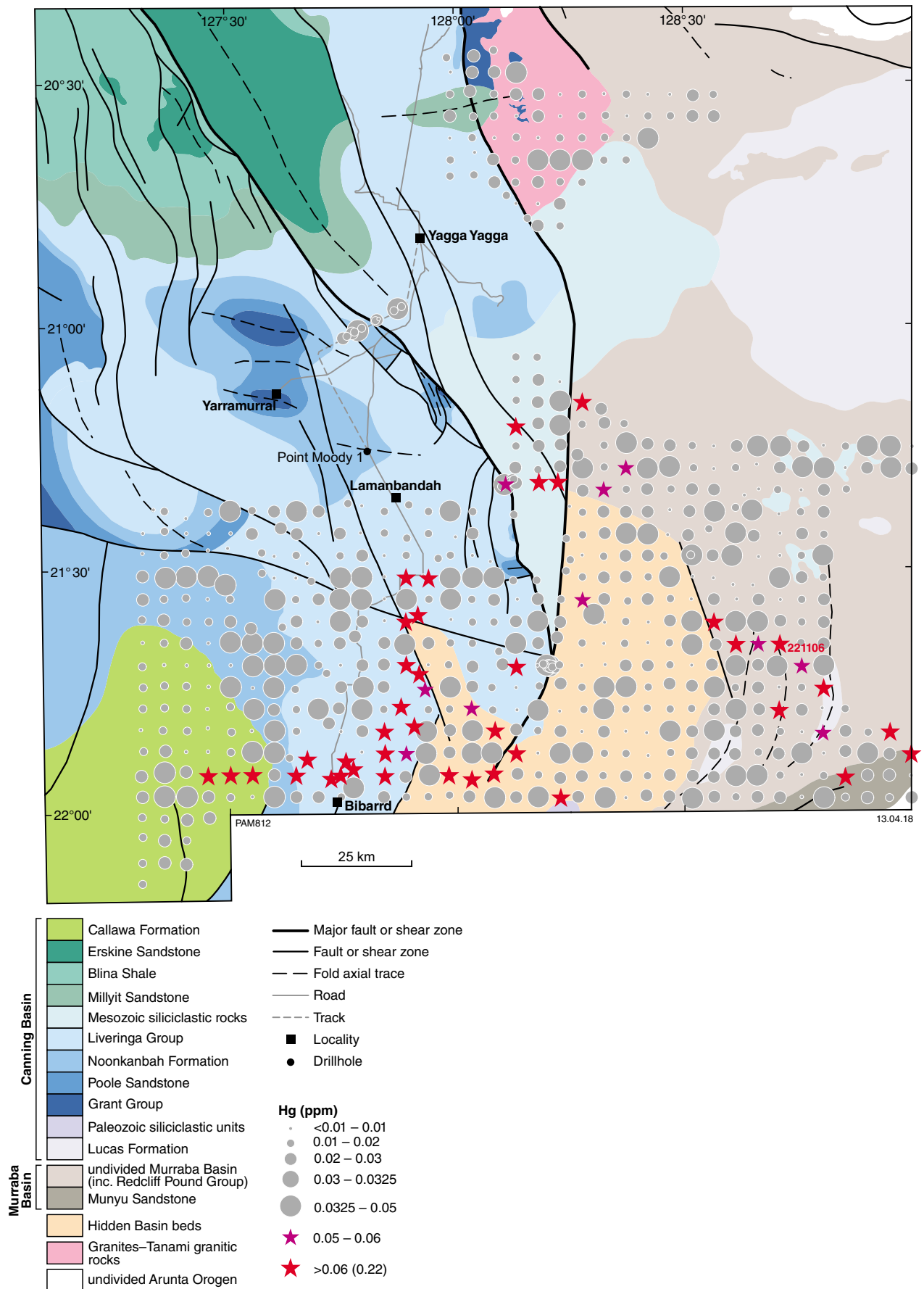


Figure B24e. Hg (ppm)

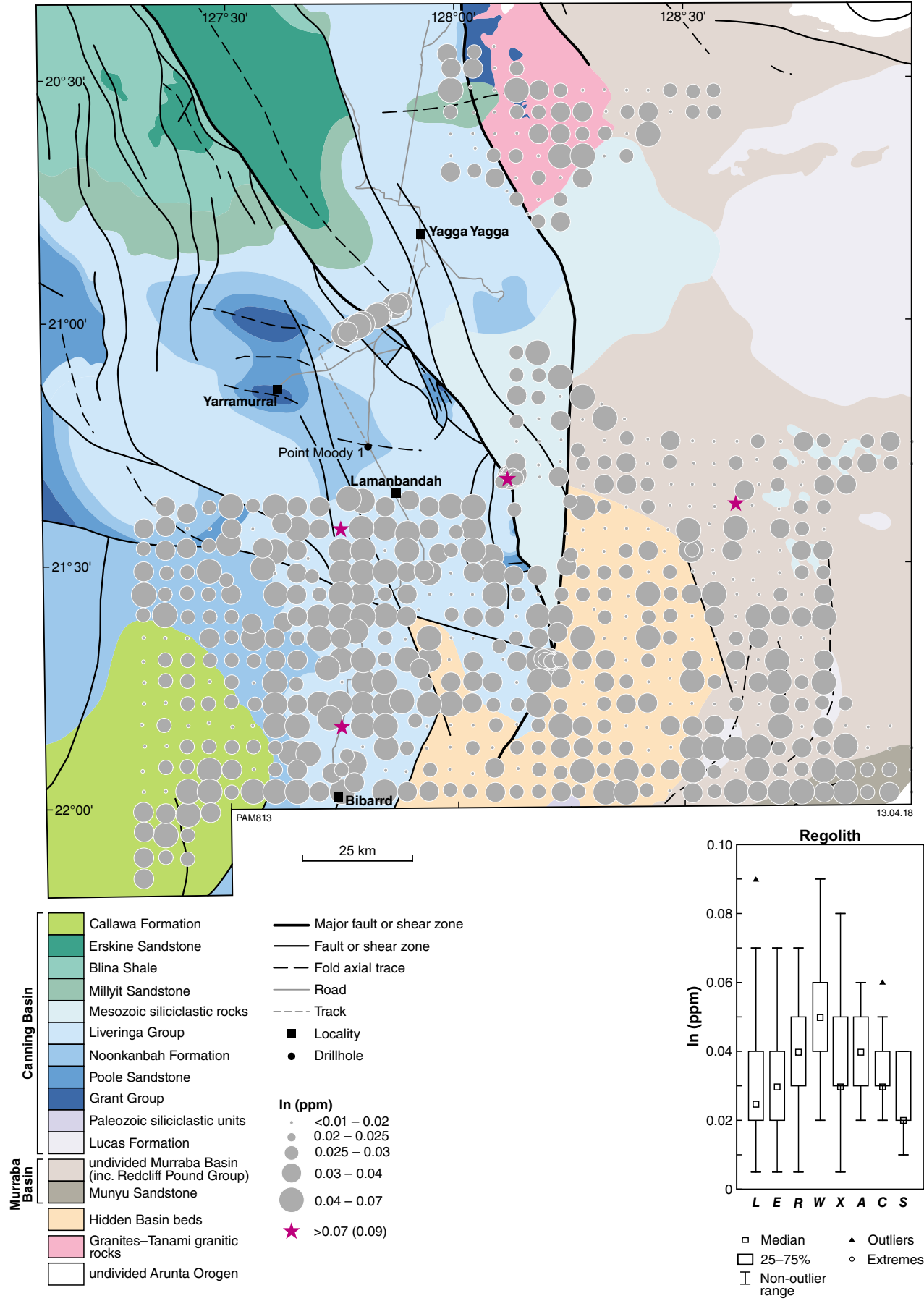


Figure B24f. In (ppm)

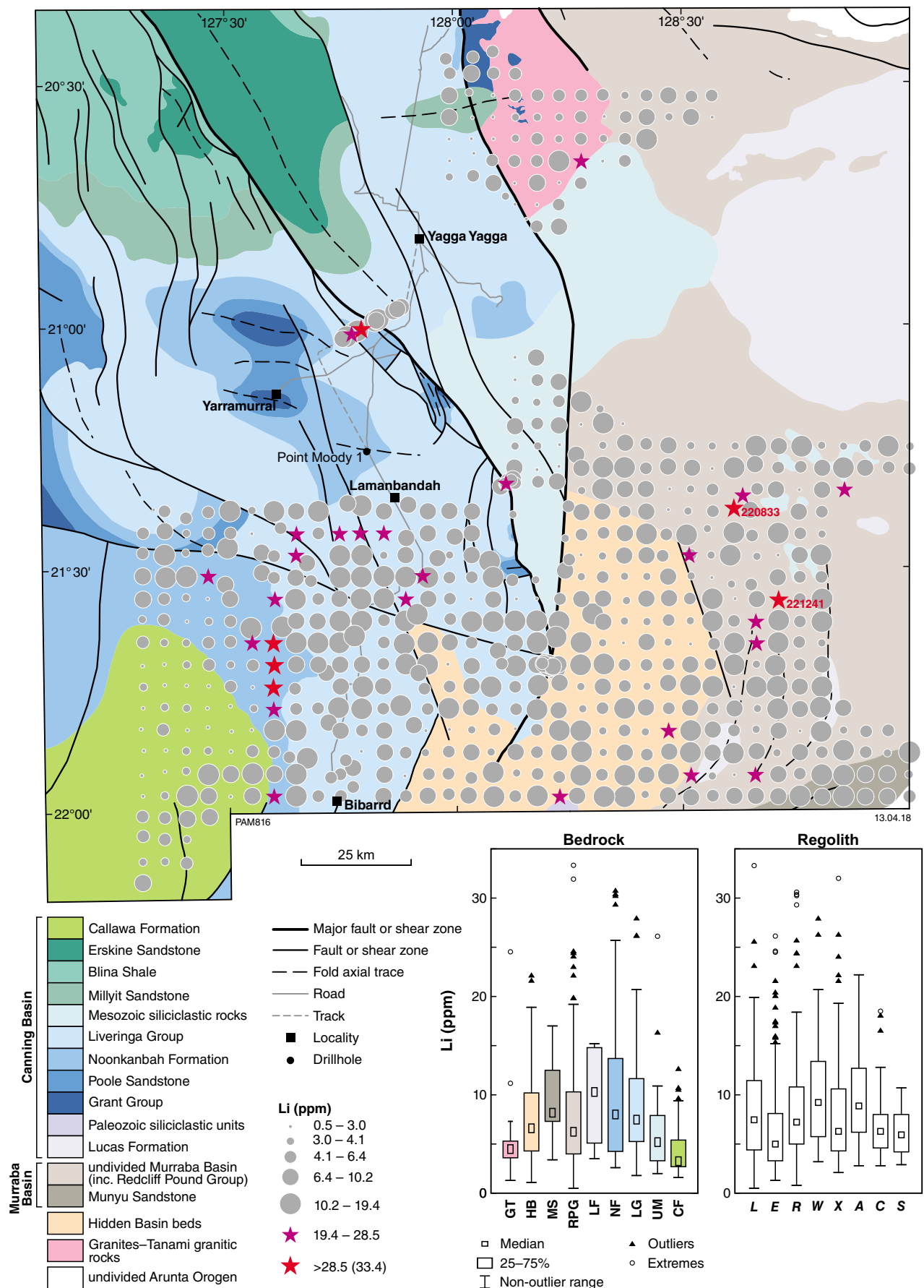
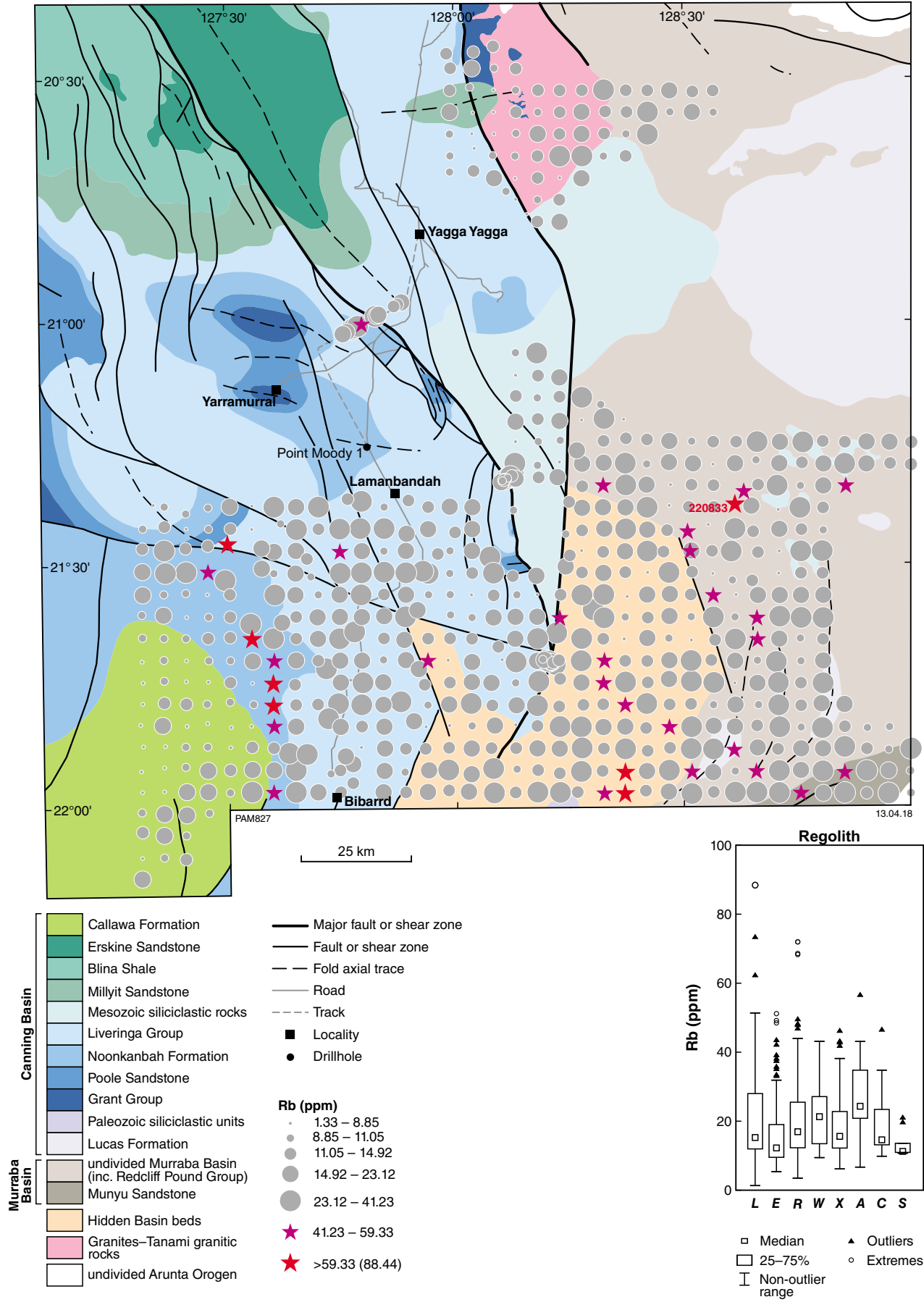


Figure B24g. Li (ppm)



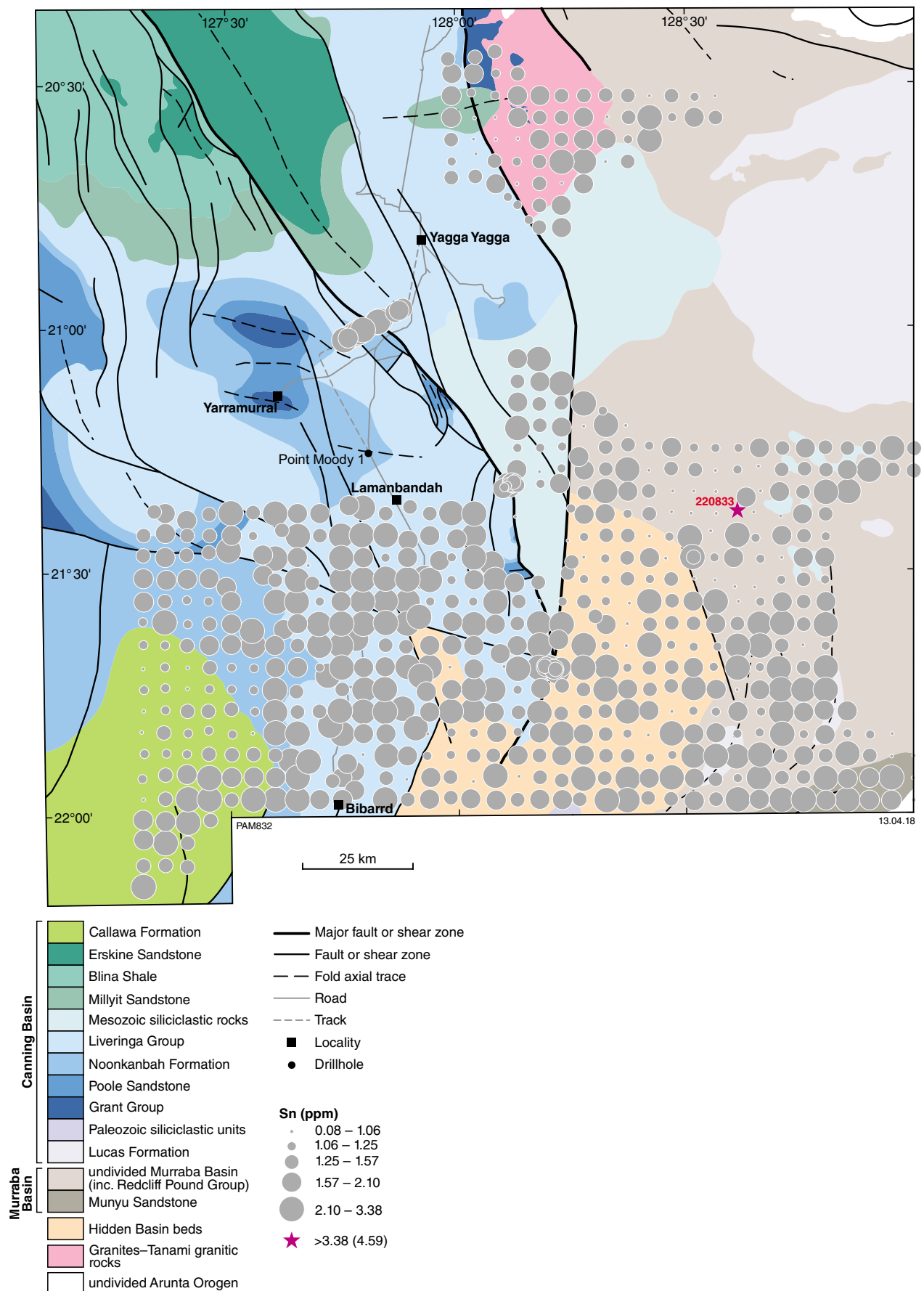


Figure B24i. Sn (ppm)

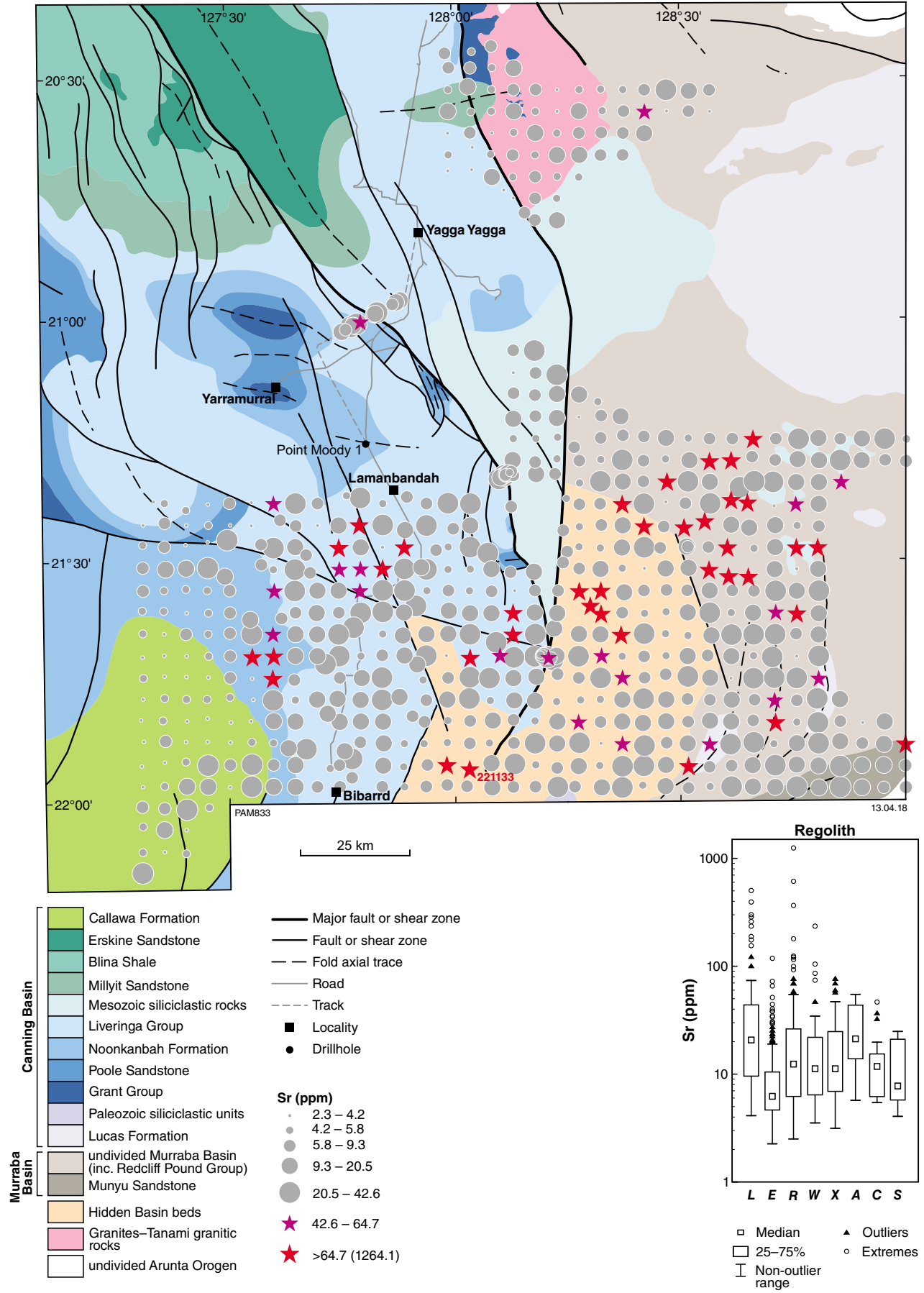


Figure B24j. Sr (ppm)

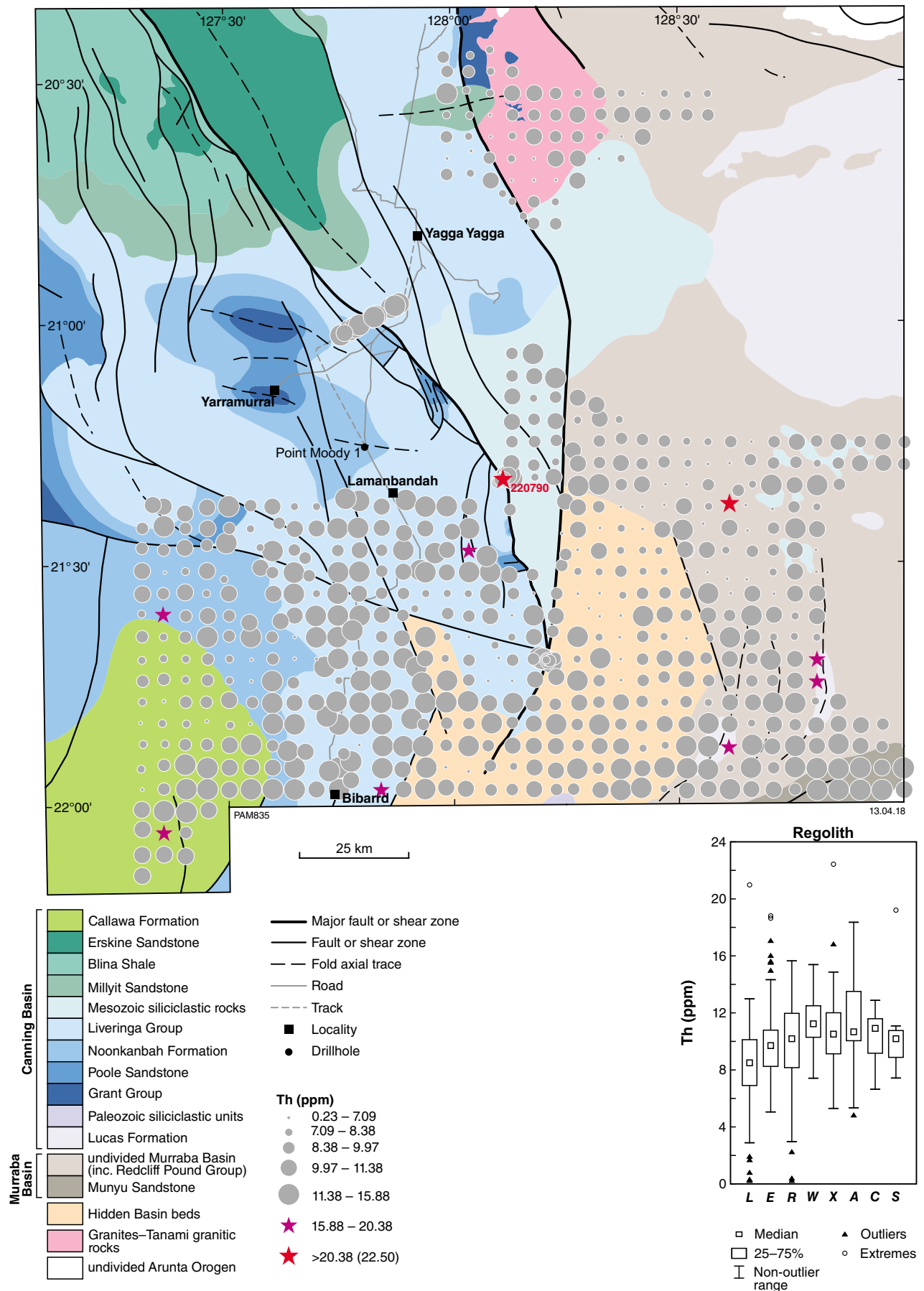


Figure B24k. Th (ppm)

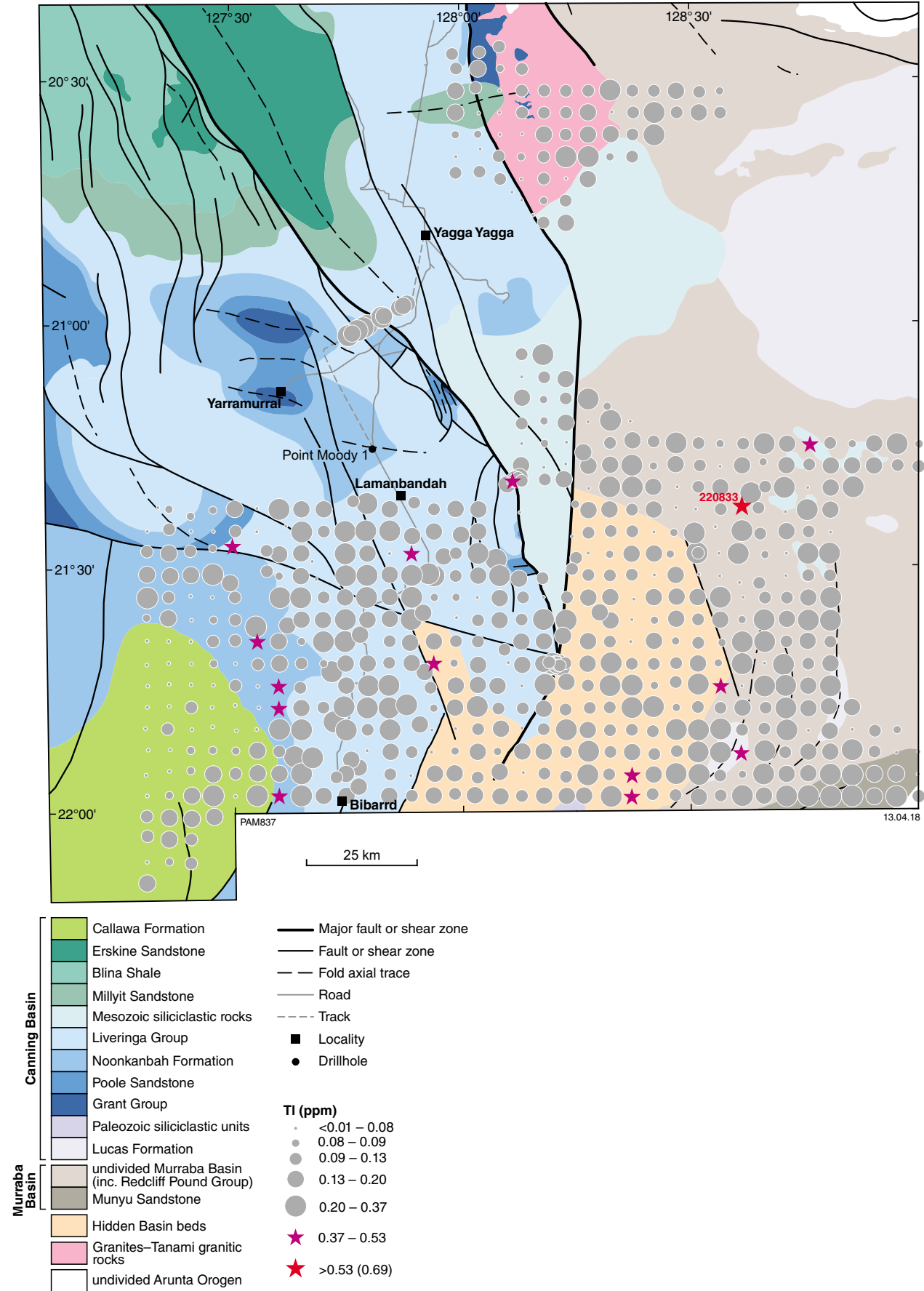


Figure B24I. Tl (ppm)

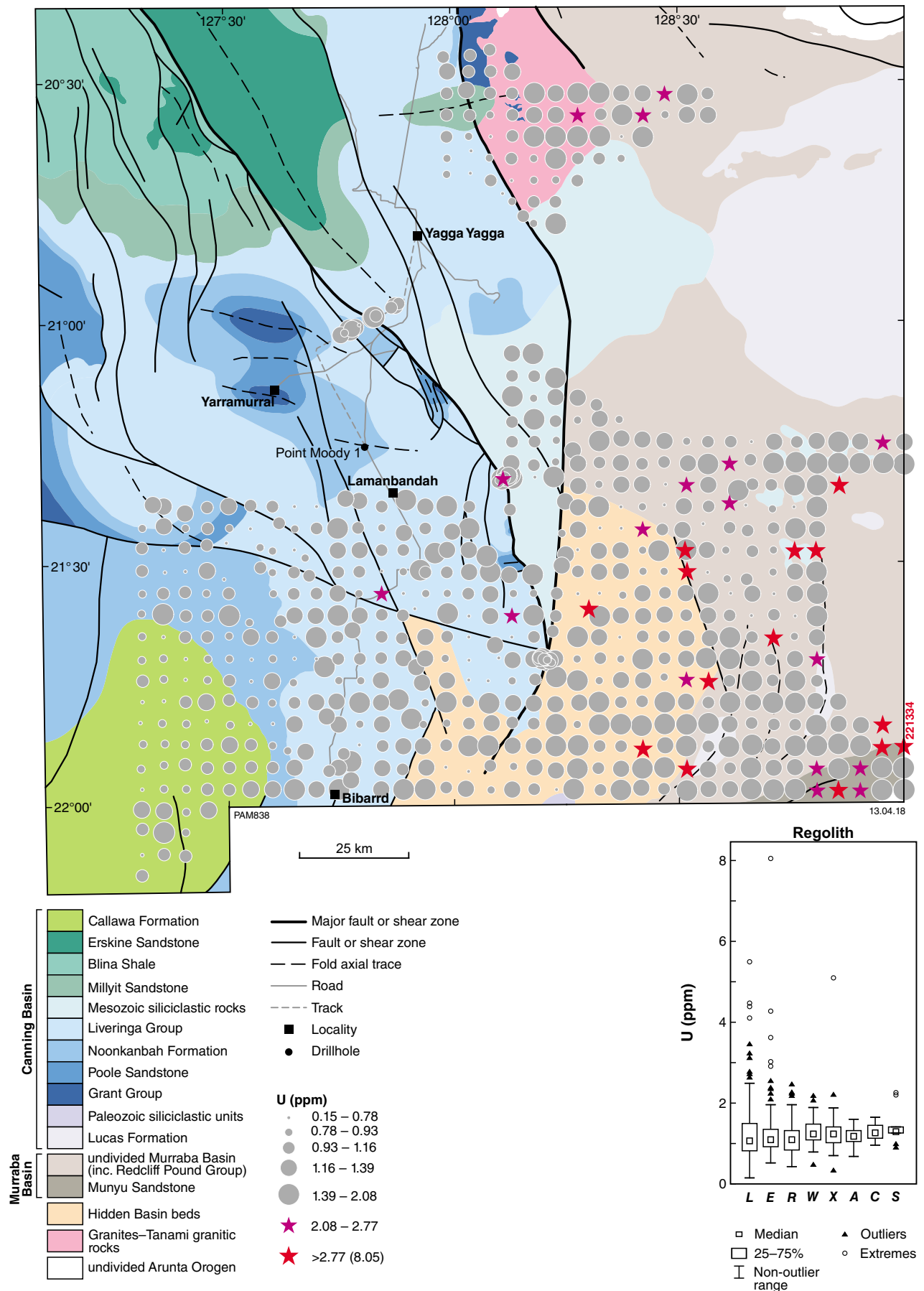


Figure B24m. U (ppm)

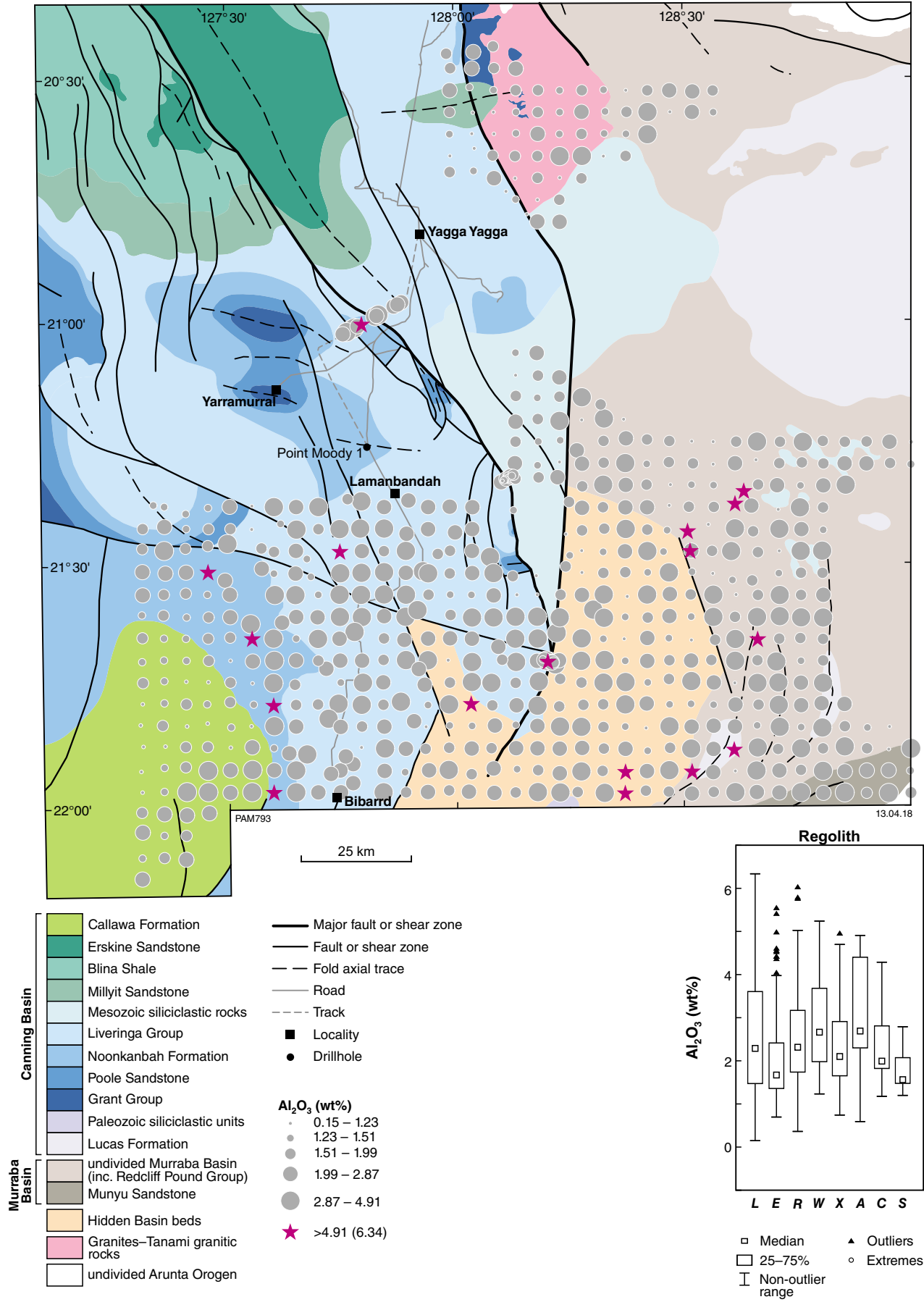


Figure B25. Bubble plots for major elements shown against 1:500 000-scale interpreted bedrock geology and structures (GSWA, 2016): a) Al_2O_3 (wt%)

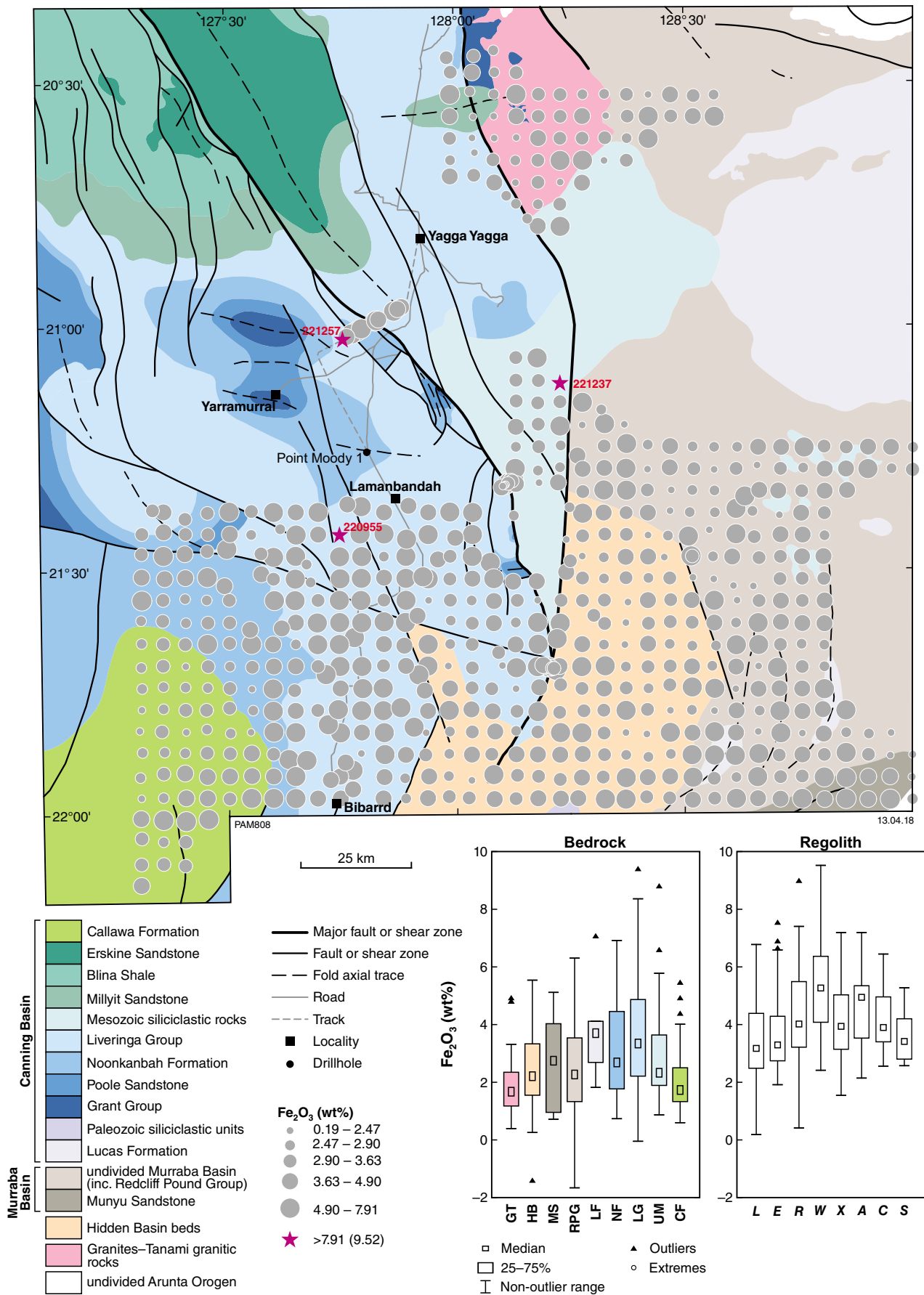
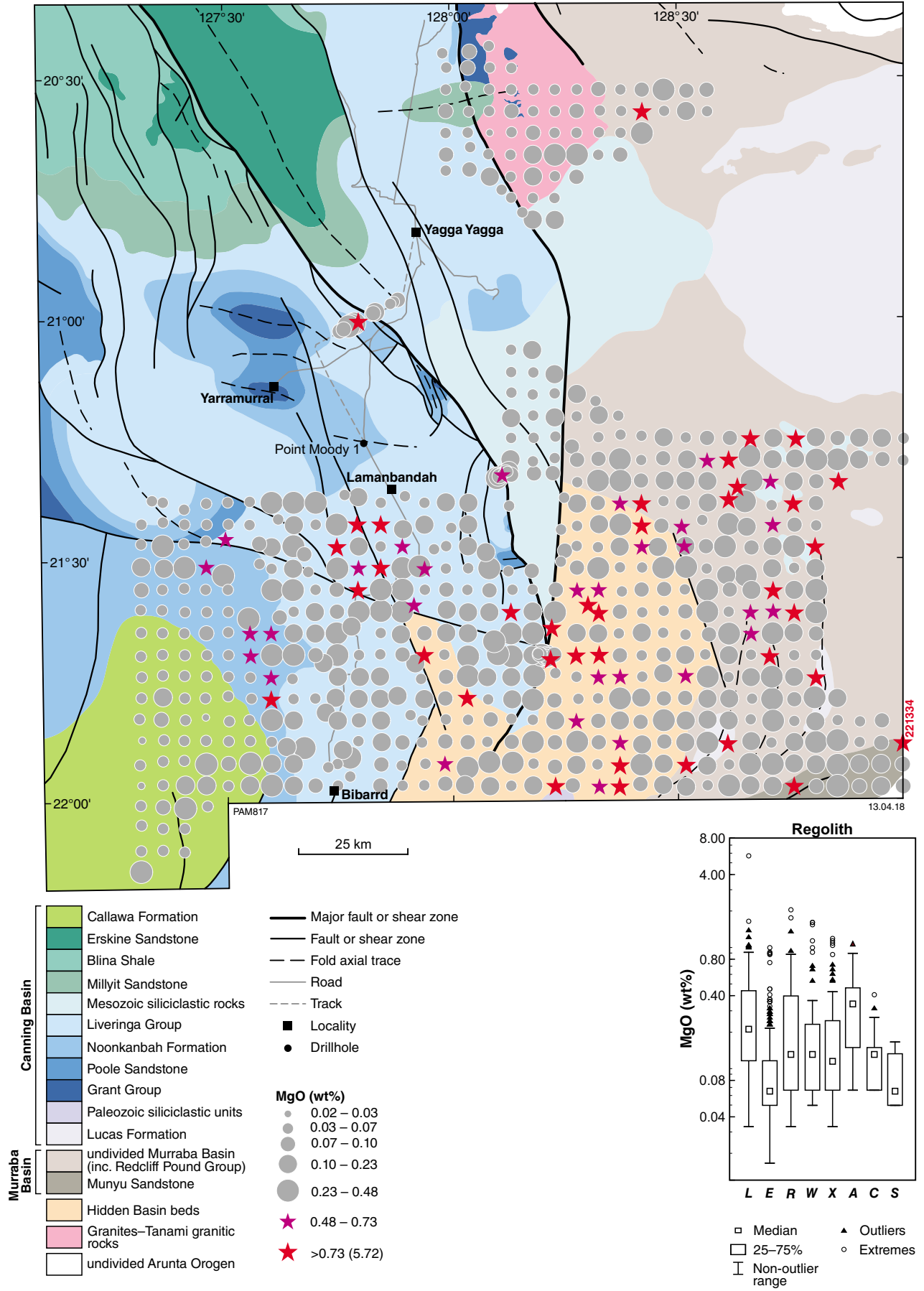


Figure B25b. Fe_2O_3 (wt%)



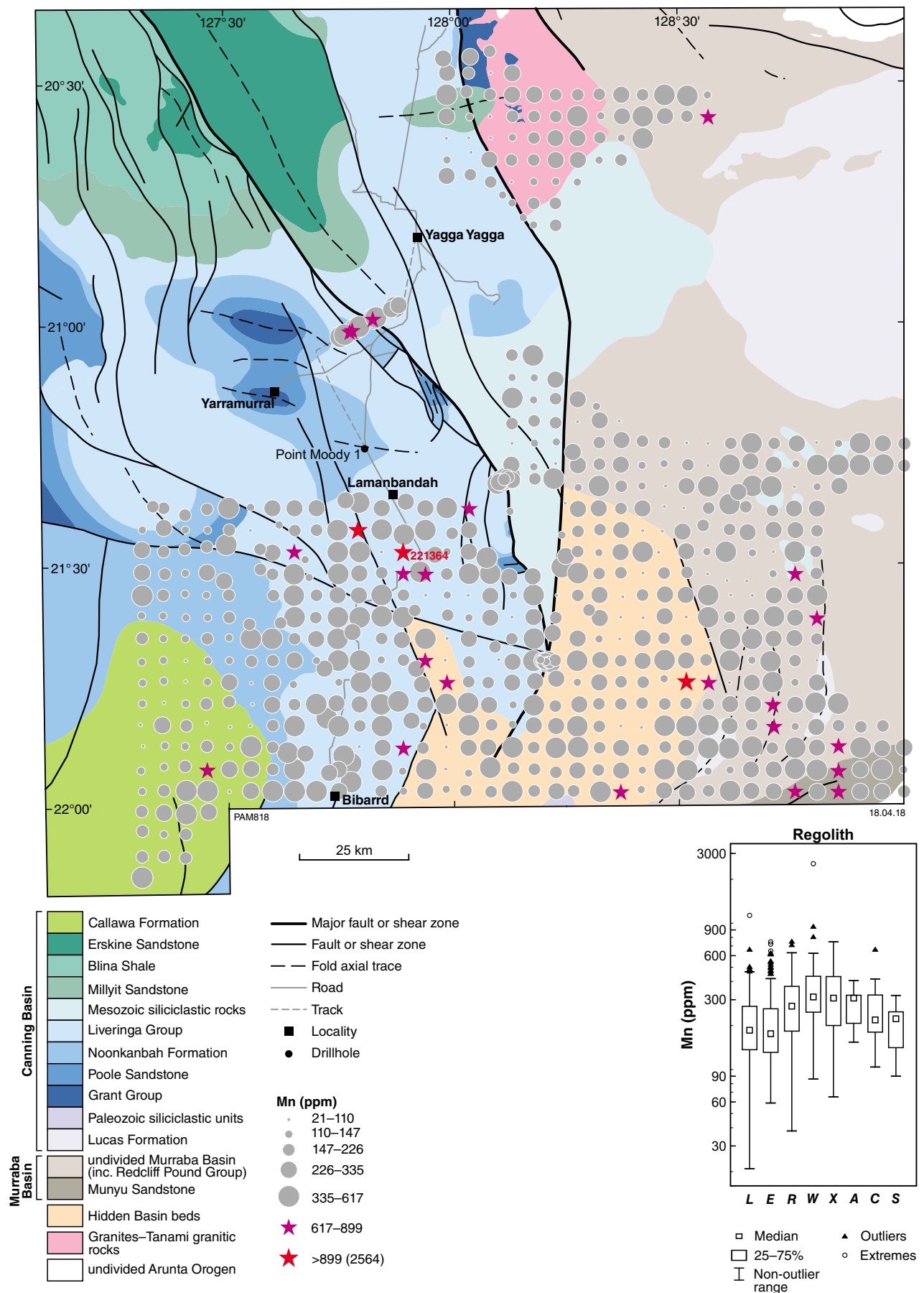


Figure B25d. Mn (ppm)

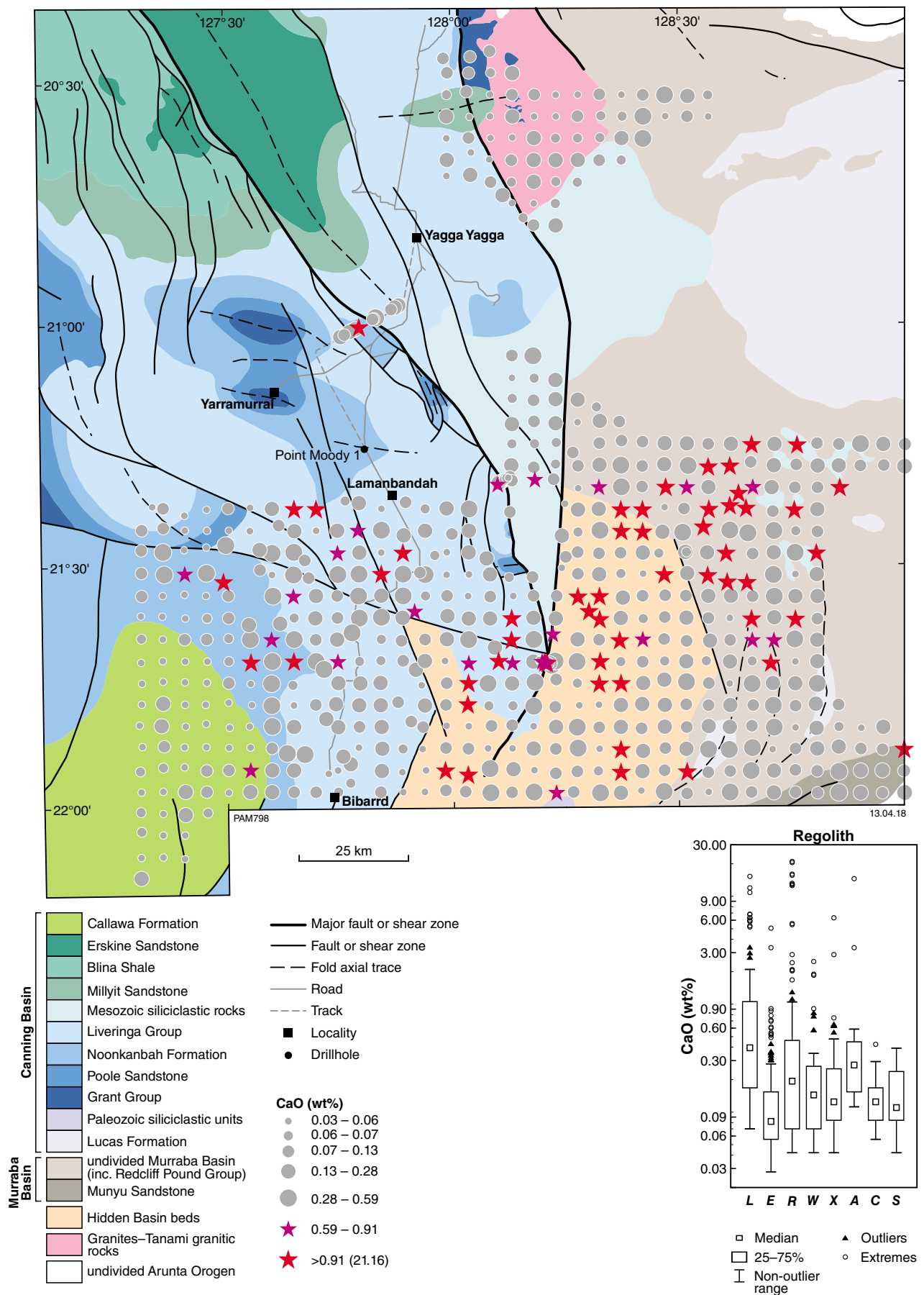
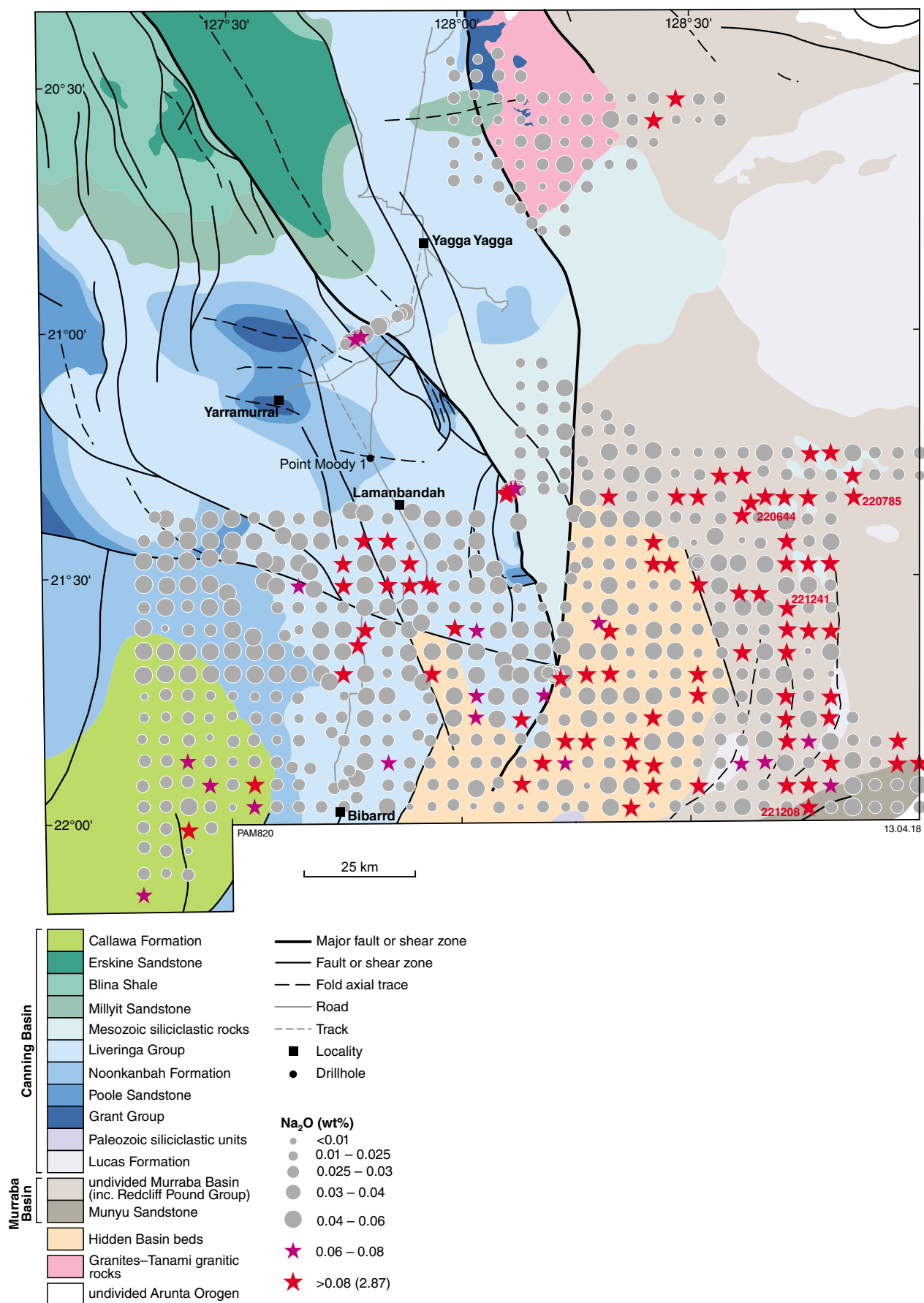
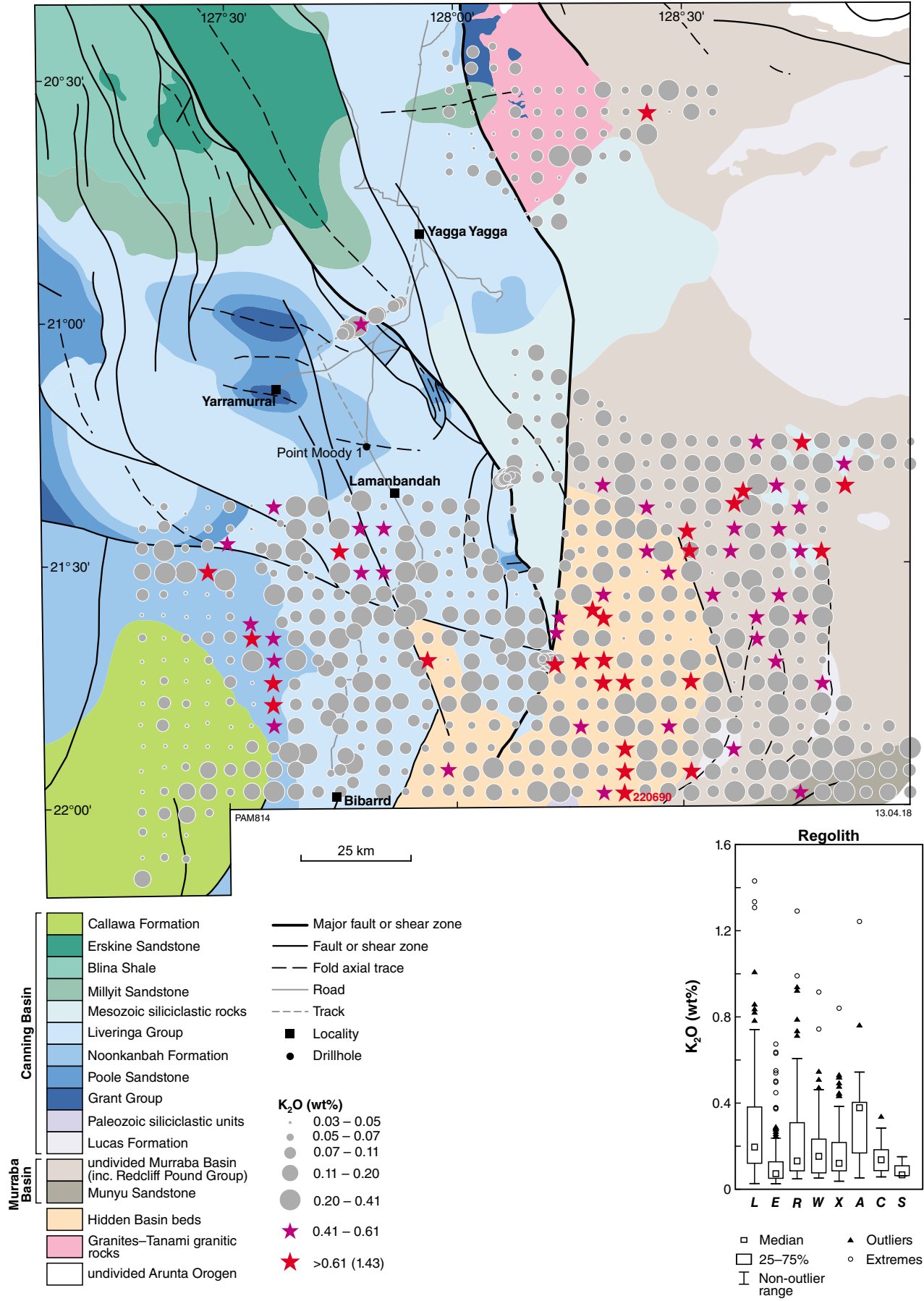


Figure B25e. CaO (wt%)

Figure B25f. Na₂O (wt%)



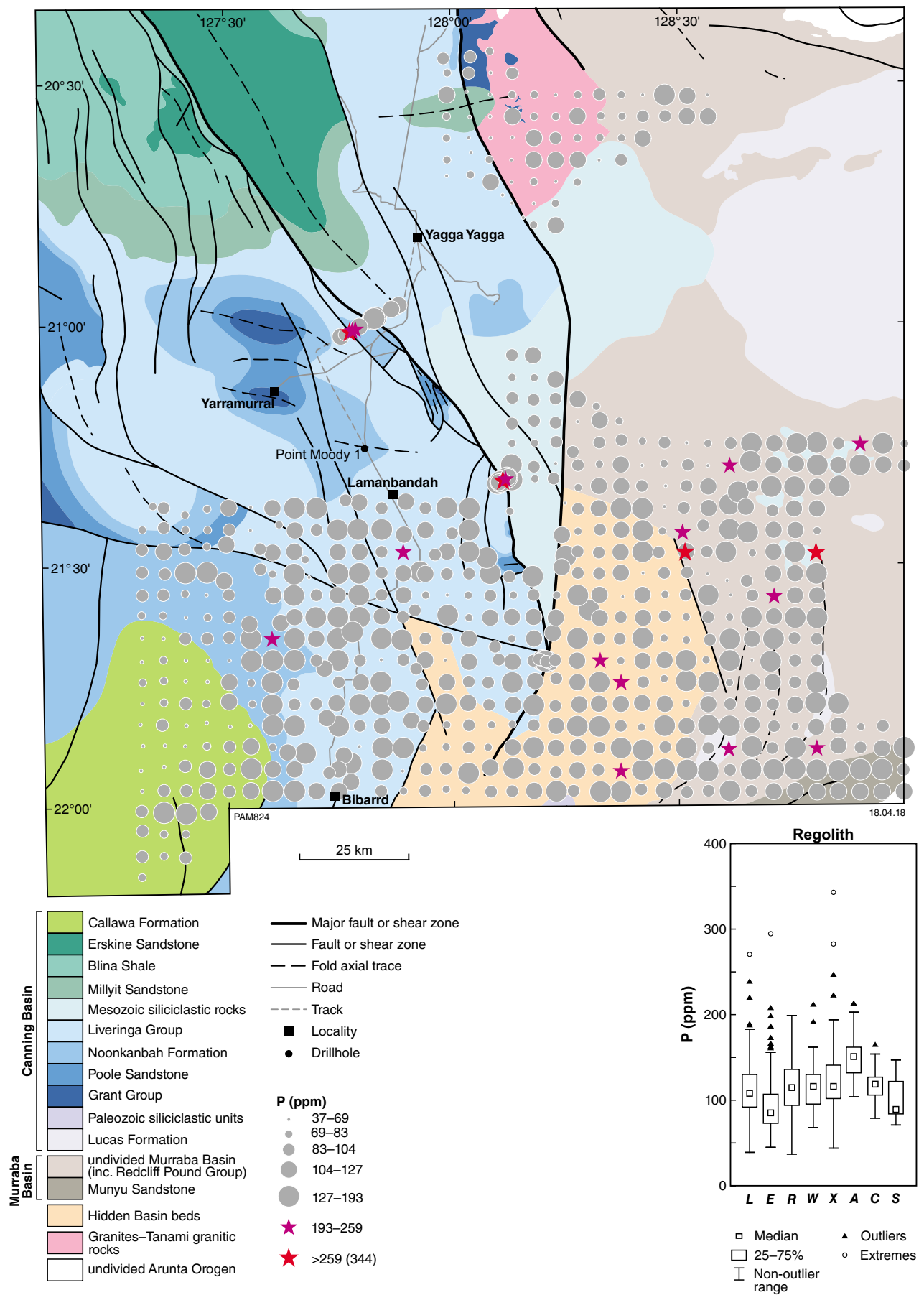
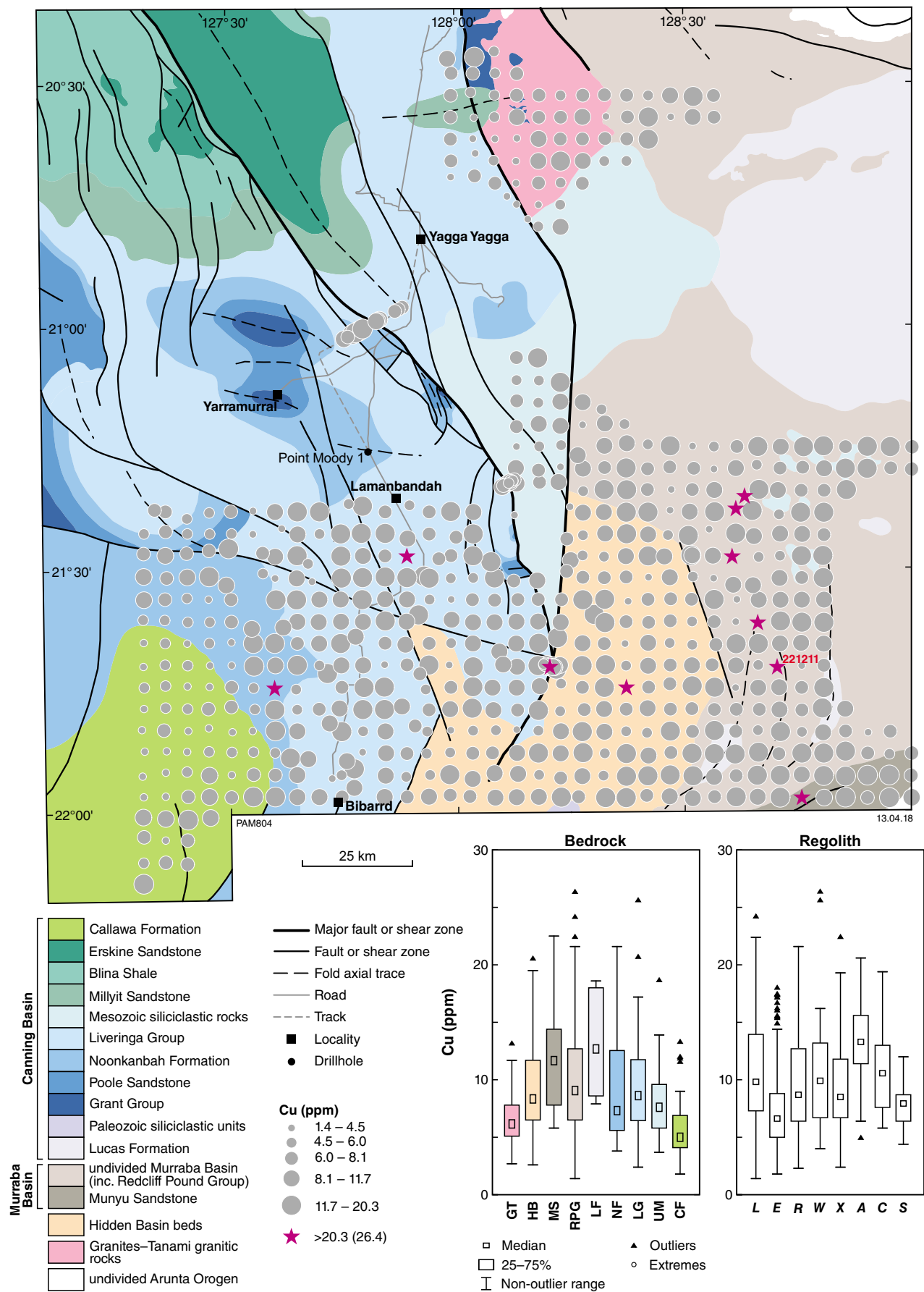


Figure B25h. P (ppm)



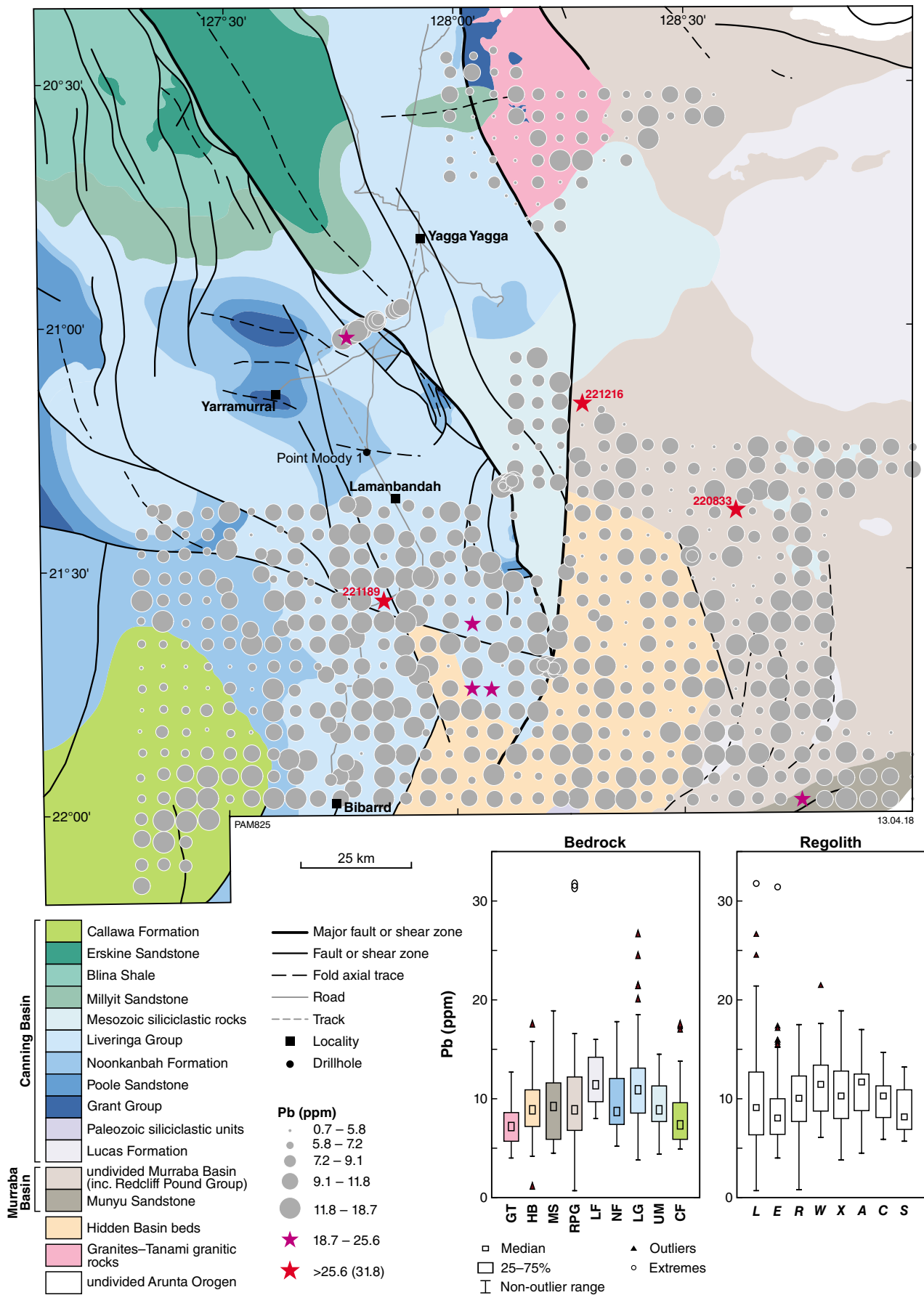


Figure B26b. Pb (ppm)

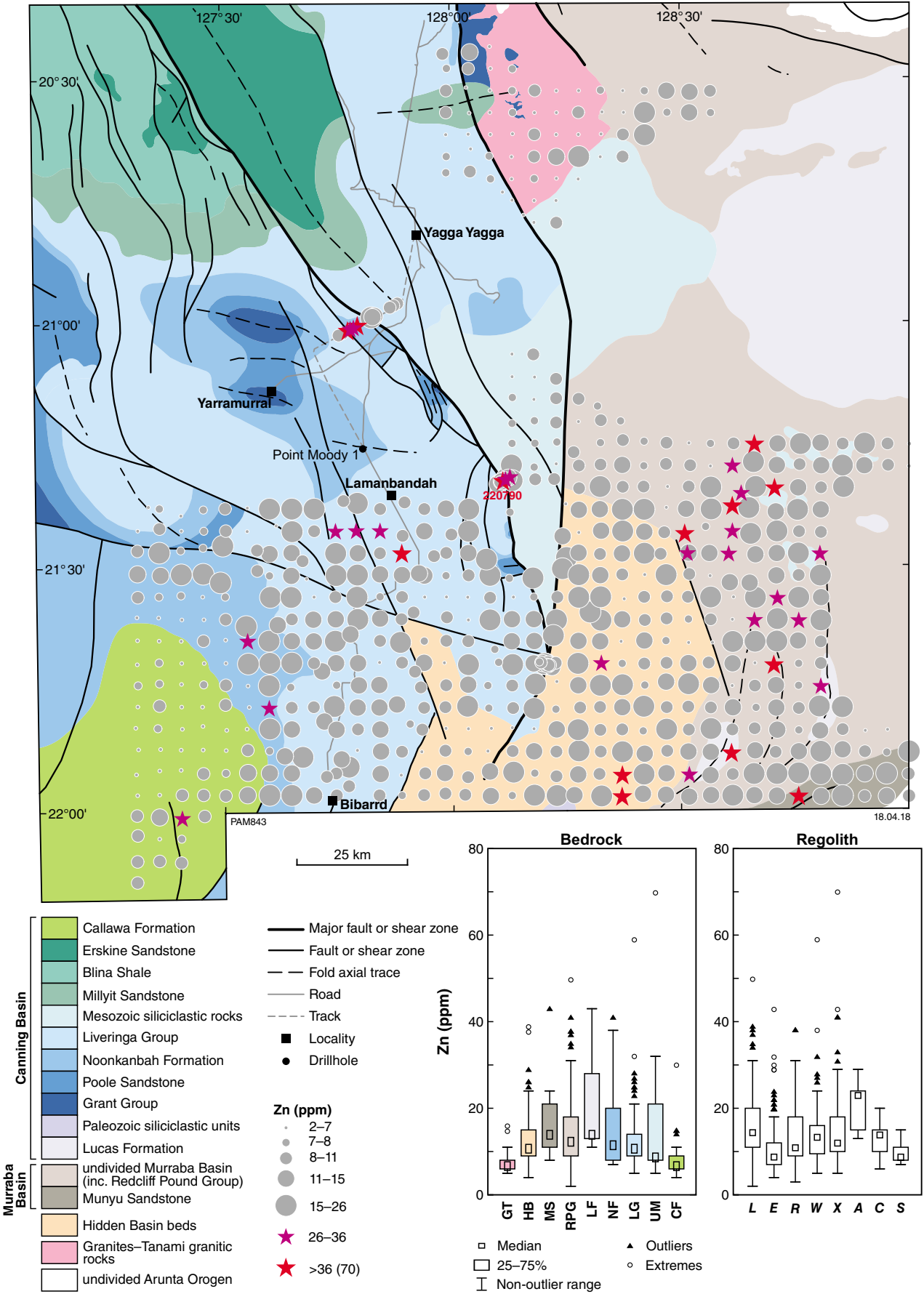


Figure B26c. Zn (ppm)

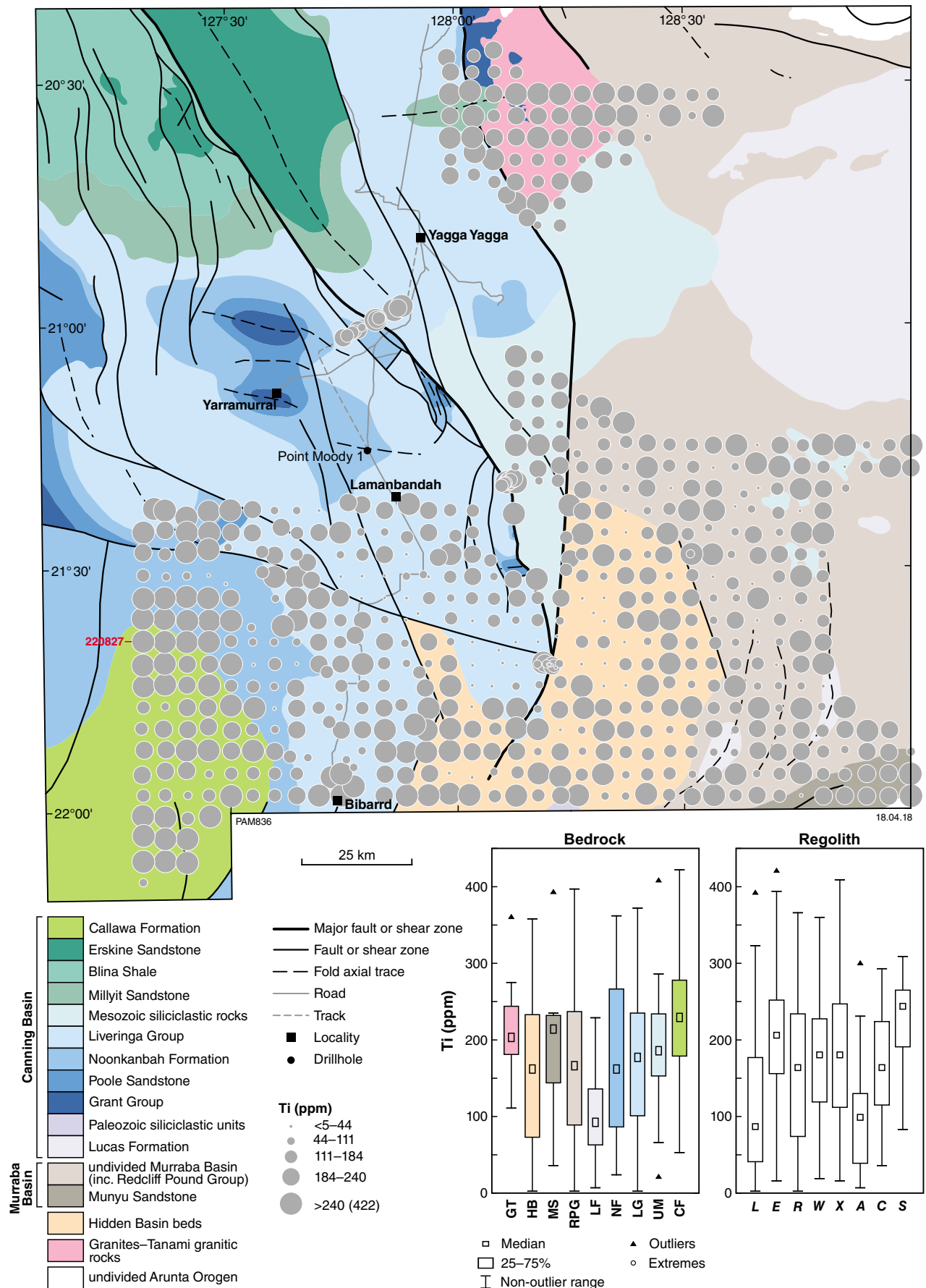


Figure B27. Bubble plots for high field strength elements (HFSE) shown against 1:500 000-scale interpreted bedrock geology and structures (GSWA, 2016): a) Ti (ppm). Data for Ta not shown as all data are censored

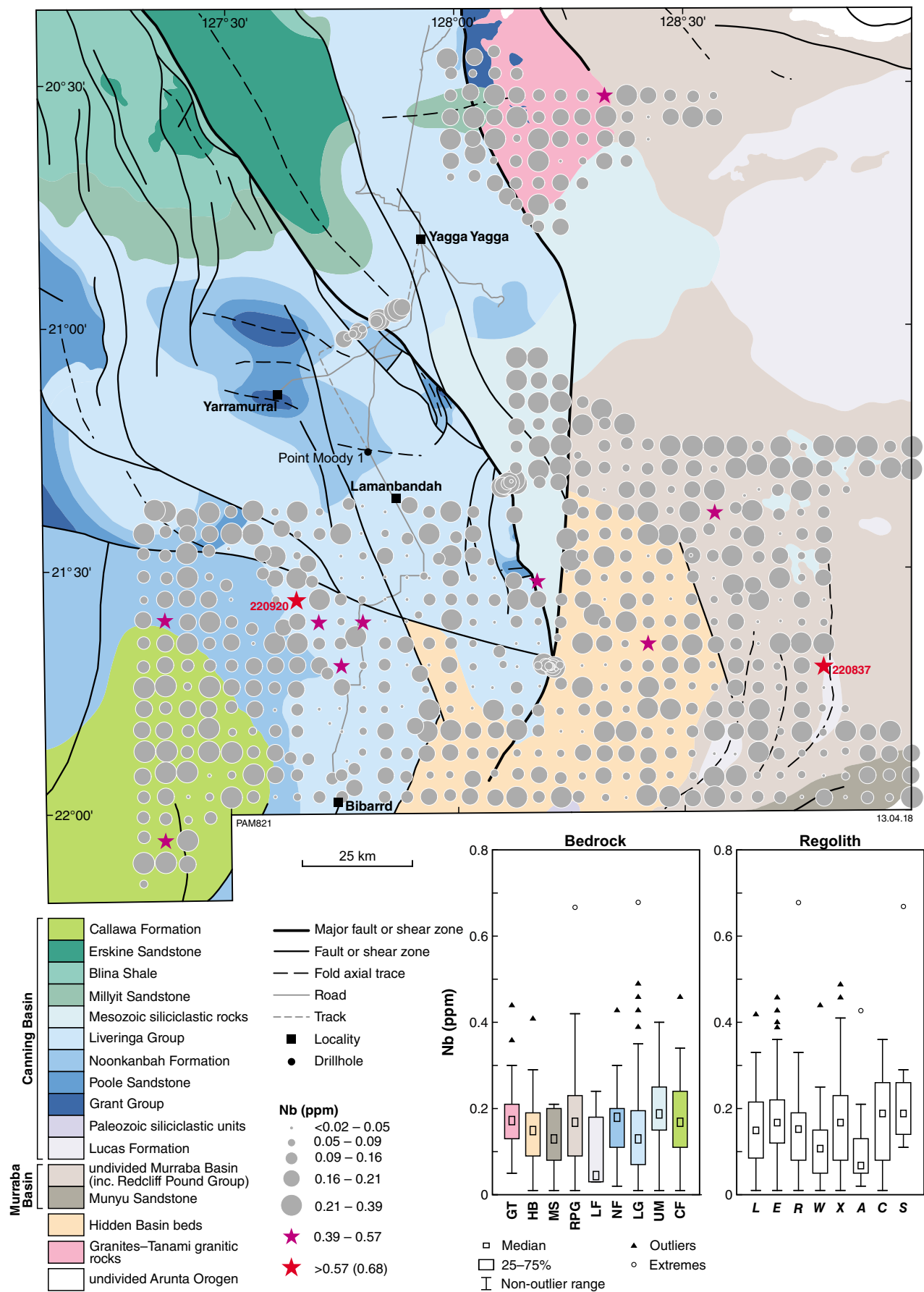
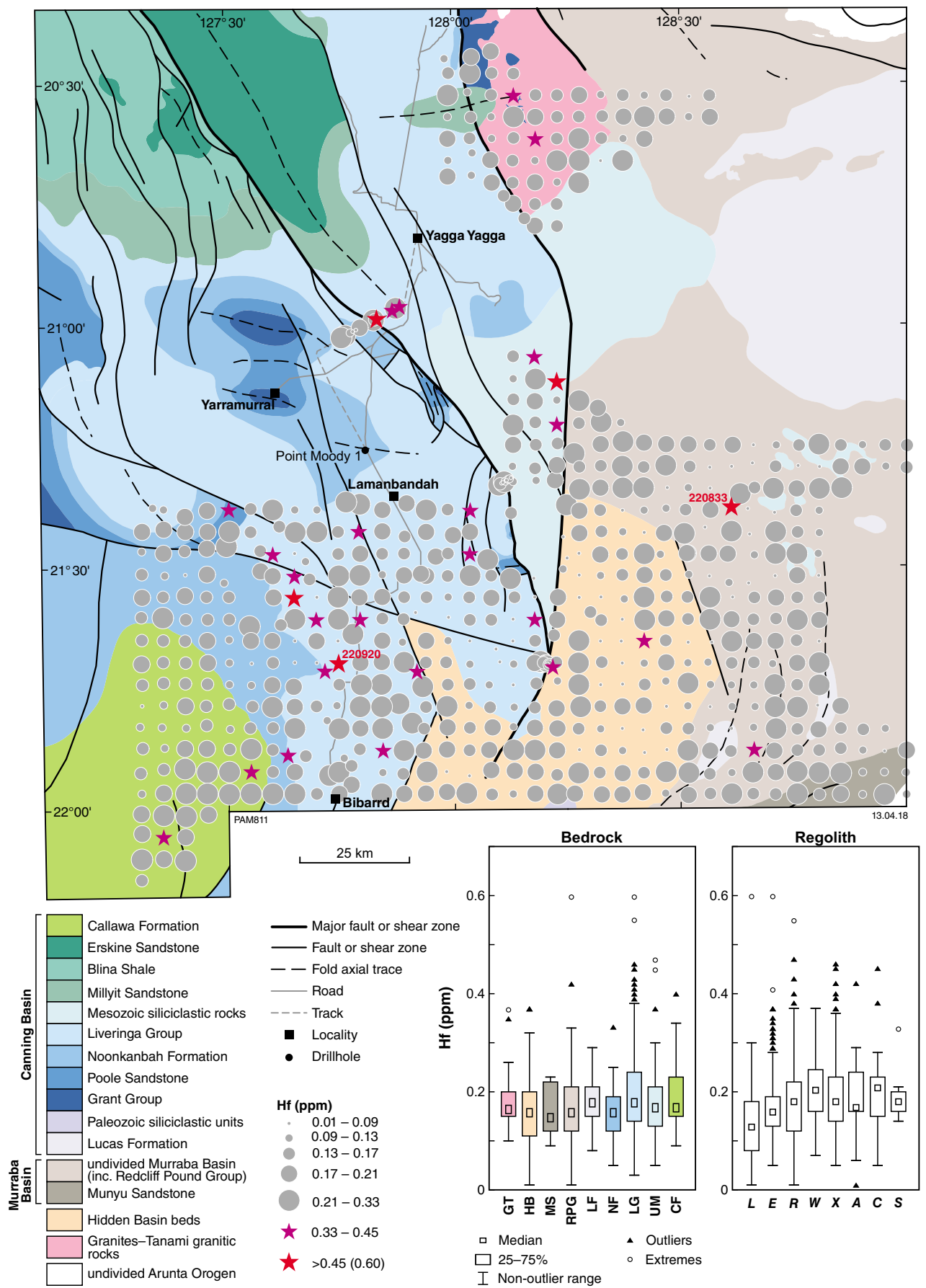


Figure B27b. Nb (ppm)



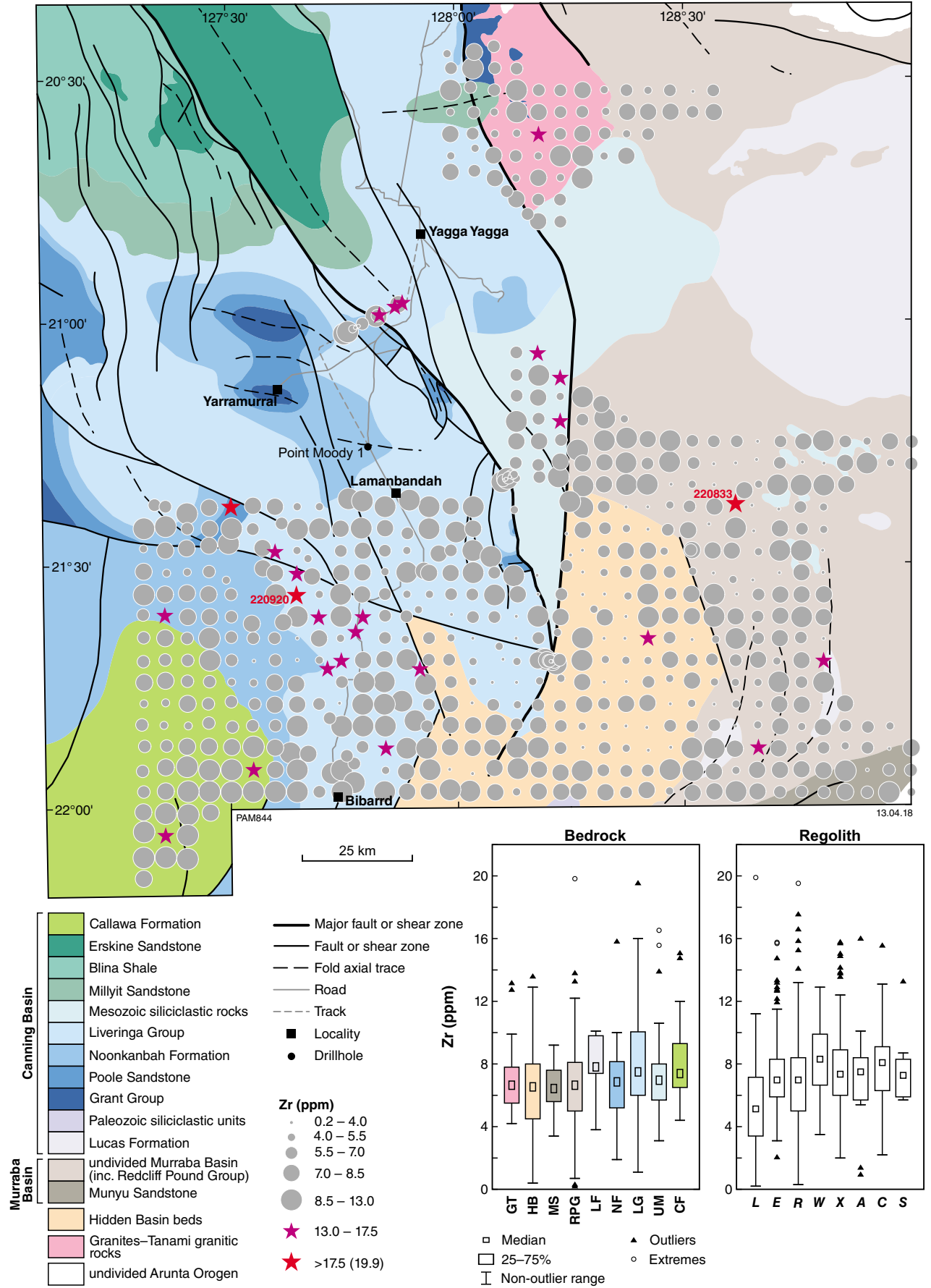
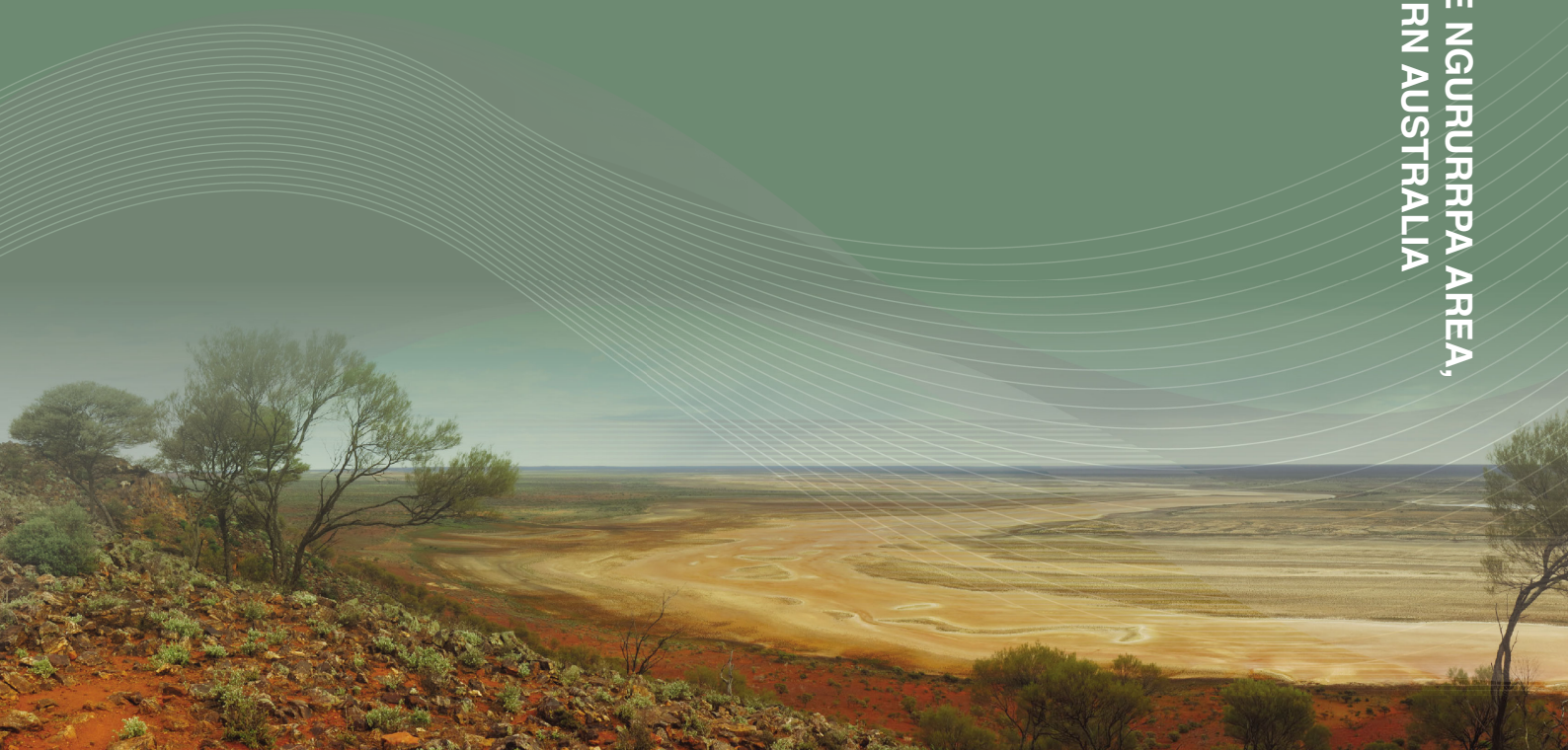


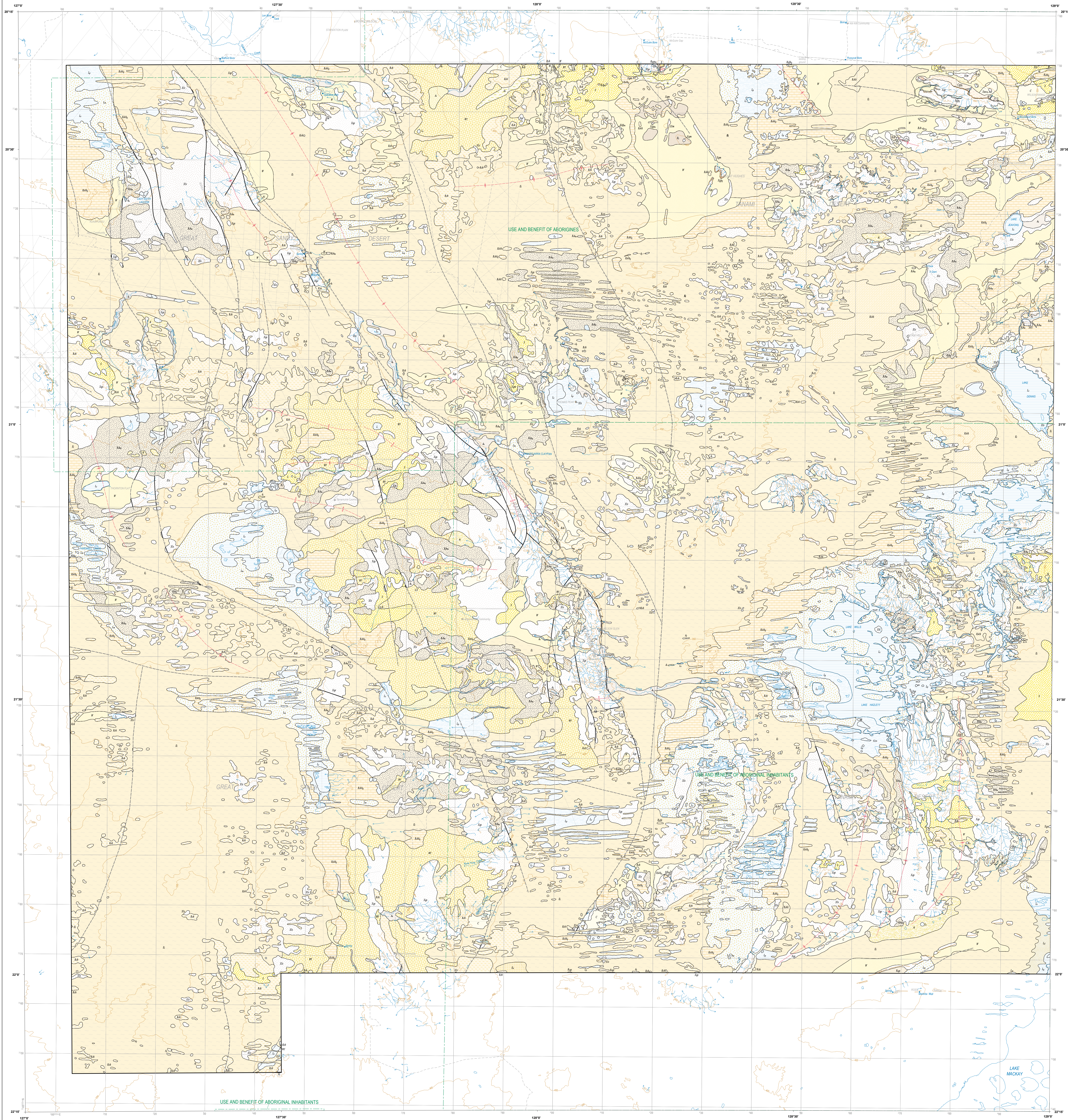
Figure B27d. Zr (ppm)

This Record is published in digital format (PDF) and is available as a free download from the DMIRS website at
<www.dmp.wa.gov.au/GSWApublications>.

Further details of geological products produced by the Geological Survey of Western Australia can be obtained by contacting:

Information Centre
Department of Mines, Industry Regulation and Safety
100 Plain Street
EAST PERTH WESTERN AUSTRALIA 6004
Phone: +61 8 9222 3459 Fax: +61 8 9222 3444
www.dmp.wa.gov.au/GSWApublications

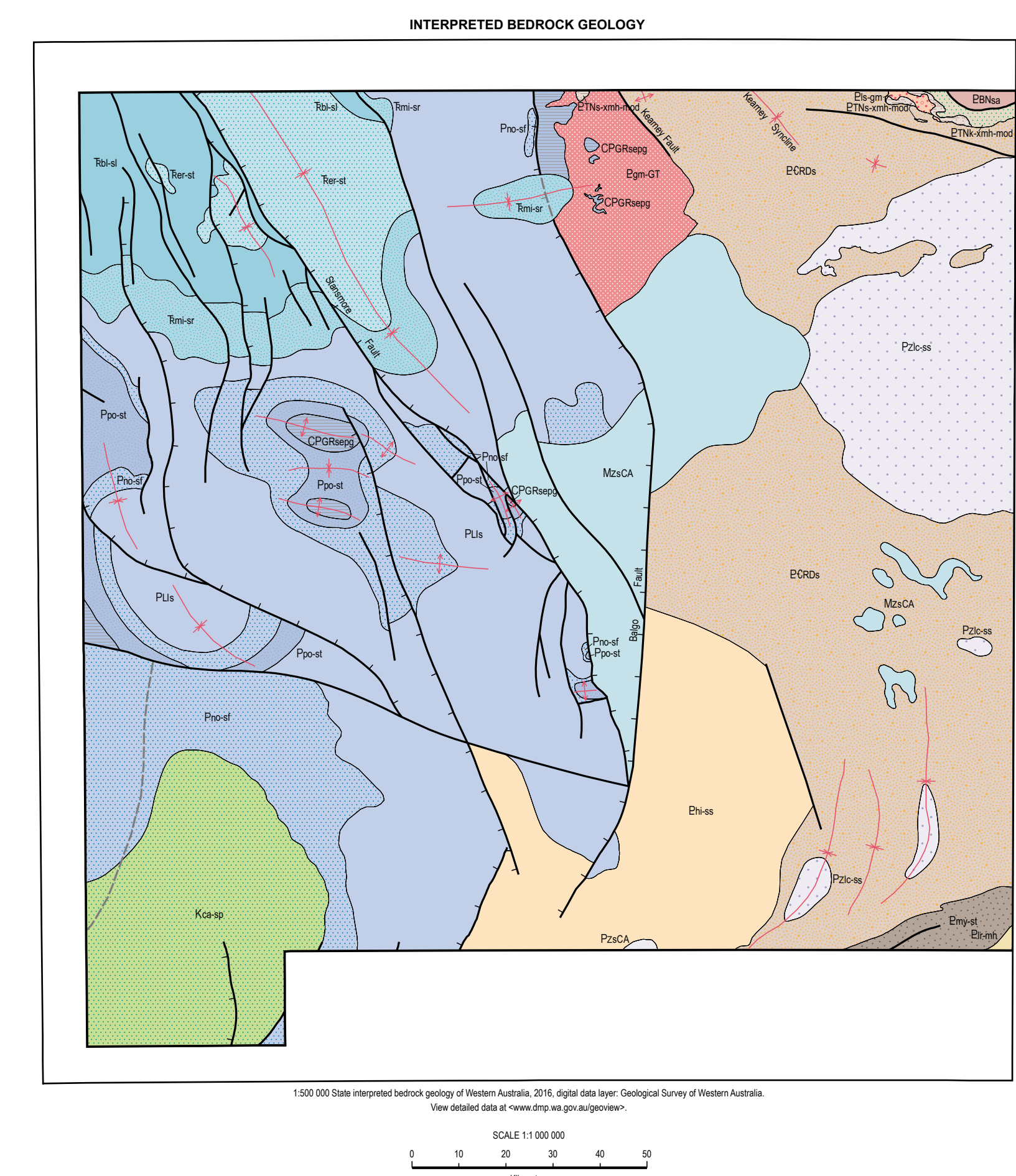




- DEPOSITIONAL REGIME**
- Alluvial units**
- C Colluvium derived from different rock types, includes gravel, sand, silt and clay
 - 17 Fungus-like clay, silt, and sand in alluvial deposits
 - 12b Quartzitic sand, silt, and gravel in alluvial deposits, derived from granitic rocks
- Sheetwash units**
- 19 Clay, silt, and sand in sheetwash fans
 - 17 Clay, silt, and sand with abundant fungoid pits
- Alluvial units**
- 19 Clay, silt, and sand in drainage depressions
 - 19a Sand, silt, and clay in alluvial drainage depressions, clays, and ephemeral floodplain lakes, low-lying areas with internal drainage
 - 19b Superficial channel commonly terminating in a sheetwash cone, ephemeral
 - 19c Clay, silt, sand, and gravel in alluvial fans
 - 19d Sand, silt, and clay in localized depressions with eolian sandpan
- Lacustrine units**
- 19 Lake and lacustrine deposits, undifferentiated
 - 19a Sand, silt, and gravel in dunes adjacent to and within playa lakes
 - 19b Silt, sand, and gravel in high-lying fans adjacent to playa lakes
 - 19c Freshwater lake
 - 19d Mixed dune, eolian, and alluvial deposits, typically adjacent to playa lakes
 - 19e Saline and gypsumiferous evaporite, clay, silt, and sand in playa deposits
 - 19f Saline lake, rimmed by evaporite gypsum and carbonate deposits
- Eolian units**
- 19 Unconsolidated to consolidated, quartz-dominated eolian sand in longitudinal dunes
 - 19a Not like dune
- Residual unit**
- 19 Residual and eolian sand with minor silt and clay, low vegetation, dunes locally common

- RESIDUAL REGIME**
- Residual or residual units**
- 19a Quartzitic sand, silt, and clay, derived from weathered monzogranite and monzonite and metasedimentary equivalents, localized outcrops of weathered bedrock
 - 19b In situ weathered sedimentary rocks, quartzitic
 - 19c Fungus-like deposit, massive to blocky, derived from metasedimentary rocks, includes iron-cemented reworked products
 - 19d Fungus-like deposit, massive to blocky, derived from monzogranite and monzonite, and metasedimentary equivalents, includes iron-cemented reworked products
 - 19e Fungus-like deposit and non-cemented products derived from sedimentary rocks
 - 19f Dolerite, containing magnetitiferous, residual in place
 - 19g Calcic, undifferentiated
 - 19h Groundwater calcic, locally forms low mounds, nodular to massive, commonly with alternating layers of carbonate and dolomite
 - 19i Siliceous, residual or siliceous dolomite
 - 19j Residual sand, locally iron-rich and silty, may contain fungoid pits and nodules

- EXPOSED REGIME**
- 19a Granitic rocks
 - 19b Monzogranite and monzonite, metasedimentary
 - 19c Carbonate-rich sedimentary rocks
 - 19d Metasedimentary rock, undifferentiated
 - 19e Sedimentary rock with locally derived calcium
 - 19f Volcanic rock, undifferentiated
 - 19g Mafic volcanic rocks, basalt
 - 19h Quartz-rich metasedimentary rock with locally derived calcium
 - 19i Quartz-rich sedimentary rock with locally derived calcium



- Geological boundary**
- 19a Colluvium Formation
 - 19b Fungus-like Formation
 - 19c Sheetwash Formation
 - 19d Alluvial Formation
 - 19e Lacustrine Formation
 - 19f Eolian Formation
 - 19g Residual Formation
 - 19h Exposed Formation
 - 19i Metasedimentary Formation
 - 19j Volcanic Formation
 - 19k Mafic Formation
 - 19l Quartz-rich Formation
 - 19m Quartz-rich Formation

